AD NUMBER

AD097150

NEW LIMITATION CHANGE

TO

Approved for public release, distribution unlimited

FROM

Distribution authorized to U.S. Gov't. agencies and their contractors; Administrative/Operational Use; AUG 1956. Other requests shall be referred to Wright Air Development Center, Wright-Patterson AFB, OH 45433.

AUTHORITY

AFAL ltr, 19 Jul 1972

PROCEEDINGS OF THE OSU-WADC RADOME SYMPOSIUM

THOMAS E. TICE

ROBERT FOUTY

OHIO STATE UNIVERSITY

AUGUST 1956

WRIGHT AIR DEVELOPMENT CENTER

WADC TECHNICAL REPORT 56-393
VOL. I
ASTIA DOCUMENT No. AD 97150

PROCEEDINGS OF THE OSU-WADC RADOME SYMPOSIUM

THOMAS E. TICE
ROBERT FOUTY

OHIO STATE UNIVERSITY

AUGUST 1956

ELECTRONIC COMPONENTS LABORATORY
CONTRACT No. AF 33(616)-3212
PROJECT No. 4158

WRIGHT AIR DEVELOPMENT CENTER
AIR RESEARCH AND DEVELOPMENT COMMAND
UNITED STATES AIR FORCE
WRIGHT-PATTERSON AIR FORCE BASE, OHIO

Composer Litho & Prtg. Co., Springfield, O.
500 - October 1956

FOREWORD

This report was prepared by Dr. Thomas E. Tice and Mr. Robert Fouty of the Ohio State University, Columbus, Ohio, on Air Force Contract No. AF 33(616)-3212, under Task No. 41547 of Project No. 4158, "Radome Techniques and Components." The work was administered under the direction of the Electronic Components Laboratory, Directorate of Research, Wright Air Development Center, with Lt. William Croswell and Mr. Fred H. Behrens acting as task engineers.

ABSTRACT

This report is one of four containing the papers submitted for the 1956 Radome Symposium held at the Ohio State University, Columbus, Ohio. The papers contain technical information pertaining to the design, fabrication, and testing of radomes for ground and airborne use.

PUBLICATION REVIEW

The publication of this report does not constitute approval by the Air Force of the findings or the conclusions contained therein. It is published only for the exchange and stimulation of ideas.

FOR THE COMMANDER:

for FRED C. SCHMIDT, JR.
Lt. Colonel, USAF
Chief, Electronic
Components Laboratory
Directorate of Research

TABLE OF CONTENTS

VOL. I

LARGE GROUND RADOMES

RADOME GOALS

RADOME TEST METHODS

A POLARIZING, REINFORCED, BROAD-BAND ANISOTROPIC PANEL

H. S. Kirschbaum
Antenna Laboratory
Department of Electrical Engineering
The Ohio State University

INTRODUCTION

The panel to be described below, while not originally intended for radome use, might nevertheless be of interest in radomes for the following reasons:

a. The panel can be used in its present form to obtain circular polarization over a broad-band of frequencies.

b. The metallic sheets could serve as reinforcing for the panel.

c. The combination of anisotropic dielectric with the metallic sheets might, through modificaton of the present panel, effect an improvement in the transmission parameters of the panel.

The panel consists of an anisotropic dielectric with ϵ_y in the y direction greater than ϵ_x in the x direction, propagation through the panel being in the Z direction. At intervals along the y axis there are imbedded in the panel metallic sheets whose planes are parallel to the X-Z plane. A y oriented linearly polarized wave is not affected by the metallic sheets, its propagation constant in the panel being determined ϵ_y and ω. An X oriented linearly polarized wave has a propagation constant in the panel which is affected by the metallic sheets as well as by ϵ_x and ω. The X oriented wave, while in the panel, is in effect in a wave guide whose cut-off wave length is twice the electrical distance between metallic sheets. Because of this and because $\epsilon_y > \epsilon_x$ the curves of propagation constants vs frequency are very nearly parallel to each other over a broad band of frequencies. By properly choosing the panel thickness a differential phase shift of 90° can be obtained for the x and y oriented waves. If a wave linearly polarized at an angle of approximately 45° with respect to the y axis is incident normally upon the panel, a circularly polarized wave will be transmitted through the panel.

Manuscript released by the editor 24 July 1956 for publication as a WADC Technical Report.

ANALYSIS

Figure 1 shows the important dimensions of the panel and in addition shows a plane linearly polarized wave incident upon one face of the panel. This wave has electric field components E_x and E_y both being equal in magnitude and in time phase with each other. Ideally these two components should be transmitted with no attenuation, but with a 90° differential phase shift in time between the emerging fields.

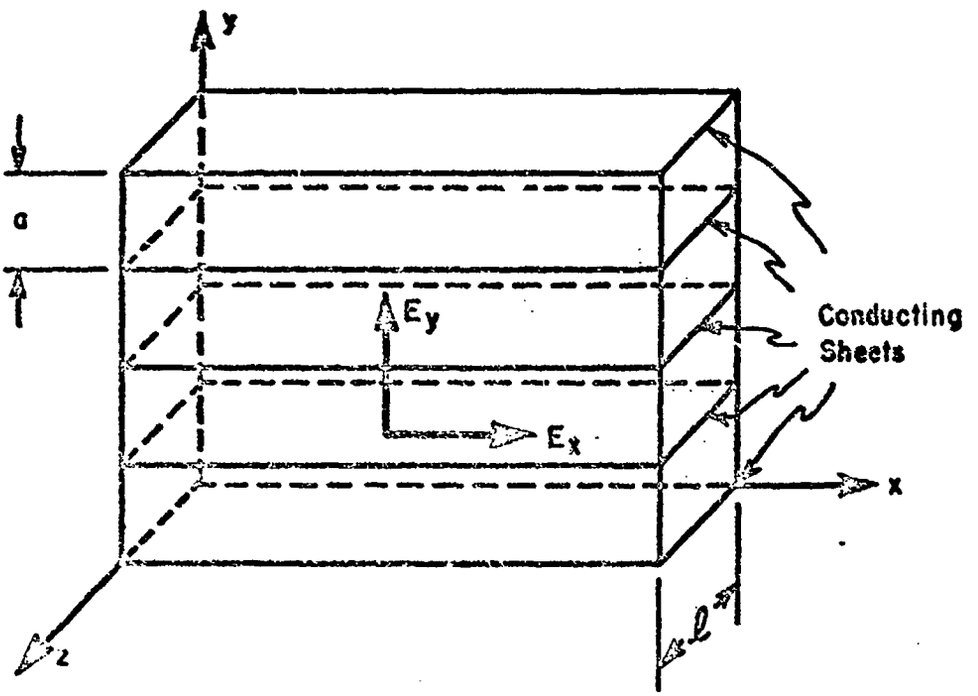

Fig. 1.

Figure 2 shows the phase constants for the x and y polarized waves. The frequency ω_o is that frequency at which the slopes of the two curves are equal. This is taken as the center of a frequency band over which the differential phase constant is very nearly constant. The phase constants are given by

$$\beta_y = \frac{2\pi}{\lambda}\sqrt{k_y} \qquad (1)$$

$$\beta_x = \frac{2\pi}{\lambda}\sqrt{k_x - \left(\frac{\lambda}{2a}\right)^2} \qquad (2)$$

where λ is the free space wave length of the wave. Letting λ_o denote the free space wavelength at the center frequency ω_o then,

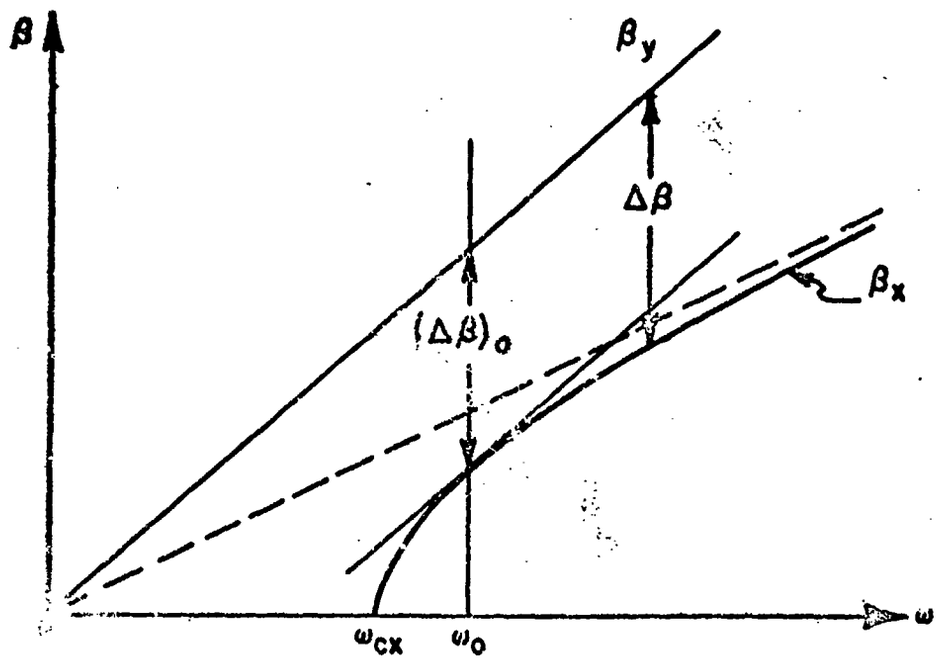

Fig. 2.

$$\lambda_o = 2a\sqrt{k_x\left(1 - \frac{k_x}{k_y}\right)} \tag{3}$$

At this wavelength the differential phase constant $(\Delta\beta)_o$ is,

$$(\Delta\beta)_o = \frac{\pi}{a}\sqrt{\frac{k_y - k_x}{k_x}} \tag{4}$$

In order to achieve a 90° differential phase shift at the wave length λ_o it is necessary to choose ℓ so that $\ell\,(\Delta\beta)_o = \pi/2$. When this is do

$$\ell = \frac{a\sqrt{k_x}}{2\sqrt{k_y - k_x}} \tag{5}$$

In order to have good transmission through the panel it is necessary to match the two free space regions separated by the panel from each other. For the y component this can be done at the center frequency by making $\beta_{yo}\, \ell = n\pi$ where n is an integer. When this is done,

$$\ell = \frac{n\,\lambda_o}{2\sqrt{k_y}} \tag{6}$$

For the x component at center frequency, the guide impedance in the panel is set equal to that of free space. Upon doing this,

$$\lambda_o = 2a\sqrt{(k_x - 1)} \tag{7}$$

The four conditions set forth in equations 3, 5, 6 and 7 when solved for a, ℓ, k_x and k_y yield,

$$k_x = \frac{2n}{2n - 1} \tag{8}$$

$$k_y = k_x^2 \tag{9}$$

$$a = \frac{\lambda_o}{2\sqrt{k_x - 1}} \tag{10}$$

$$\ell = \frac{n\,\lambda_o}{2\,k_x} \tag{11}$$

For example at $\lambda_o = 3.00$ cm if n = 3 there results,

$k_x = 1.20$ $\qquad$ a = 3.35 cm, (= 1.32 inches)

$k_y = 1.44$ $\qquad$ ℓ = 3.75 cm, (= 1.477 inches)

Figure 3 shows the calculated axial ratio for this panel over a band of frequencies from to mc.

EXPERIMENTAL RESULTS

Using polystyrene and polyfoam it was not possible to construct an artificial anisotropic dielectric with the above relative dielectric constants. Instead a panel was constructed using an anisotropic dielectric having the

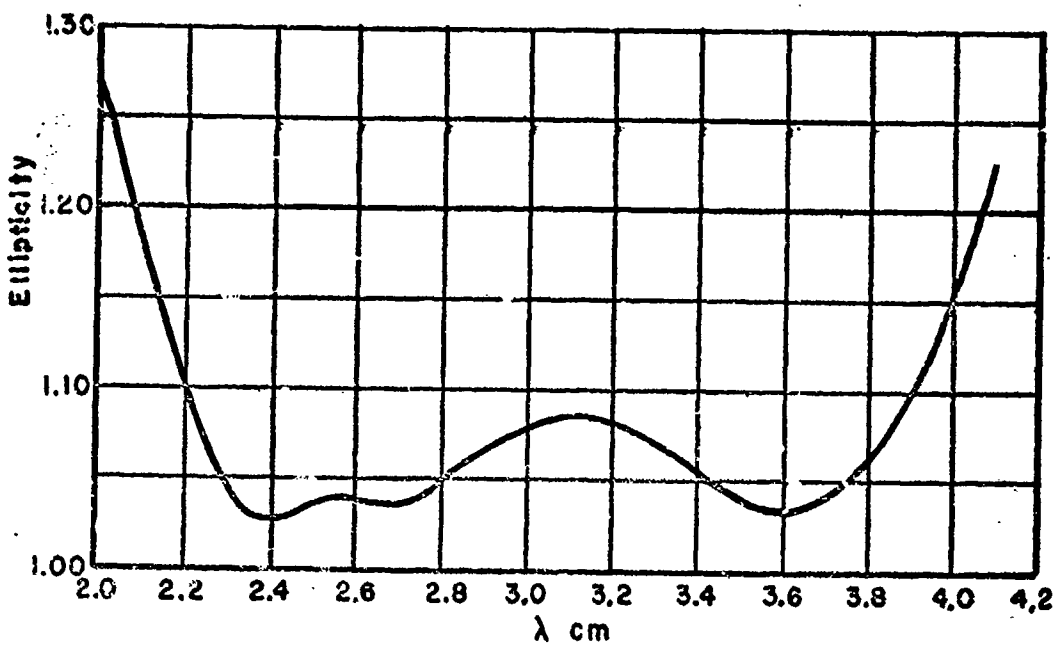
1.30
1.20
1.10
1.00
Ellipticity
2.0
2.2
2.4
2.6
2.8
3.0
3.2
3.4
3.6
3.8
4.0
4.2
λ cm

Figure 3

maximum ratio k_y/k_x obtainable from polystyrene and polyfoam. This panel, the dimensions of which are tabulated in Table I, is shown in figure 4.

Table I

Dimensions of Experimental Panel

$k_y = 1.795$	$a = 2.64$ cm	$\lambda_o = 2.70$ cm
$k_x = 1.470$	$f = 2.59$ cm	

The experimental and calculated performance of this panel is shown in figure 5 where the wave incident upon the panel emanates from a 4" x 4" horn place several inches from the panel. The horn was loaded with absorbing material to absorb any cross polarized reflection from the window. These tests were made with the wave normally incident upon the horn.

Transmission coefficients have been calculated for this panel at 8.80 kmc. They are 1.00 for both the y polarized and x polarized waves, both waves being normally incident on the panel. Transmission coefficients were measured for angles of incidence up to 30° as shown in figure 6. It was not possible to go beyond this since the panel was too small. The transmission coefficients slightly in excess of unity are caused by a focusing effect of the panel. The rays emanate from some point on the throat of the horn and are refracted toward the normal in the panel. After emerging from the panel, they appear to emanate from a "virtual" source somewhat closer to the panel than the actual source.

CONCLUSIONS

This panel, which contains metallic sheets as an integral part of the panel, offers some interesting possibilities for possible radome use. Further analysis and experimental work will have to be done in order to achieve those transmission properties which are desirable for radomes.

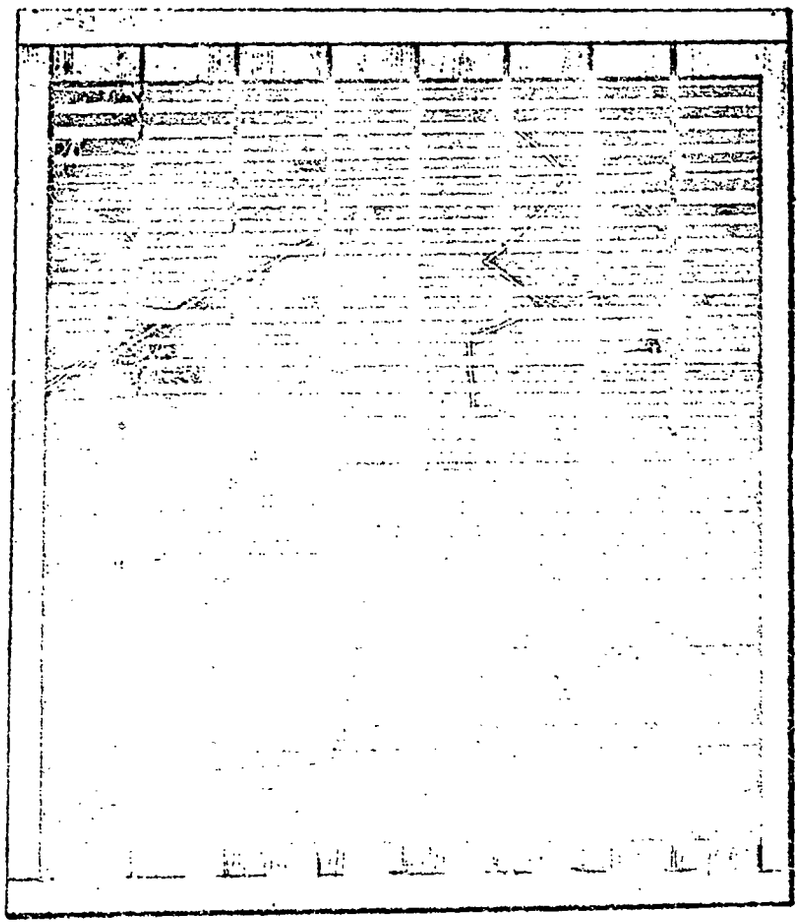

Figure 4

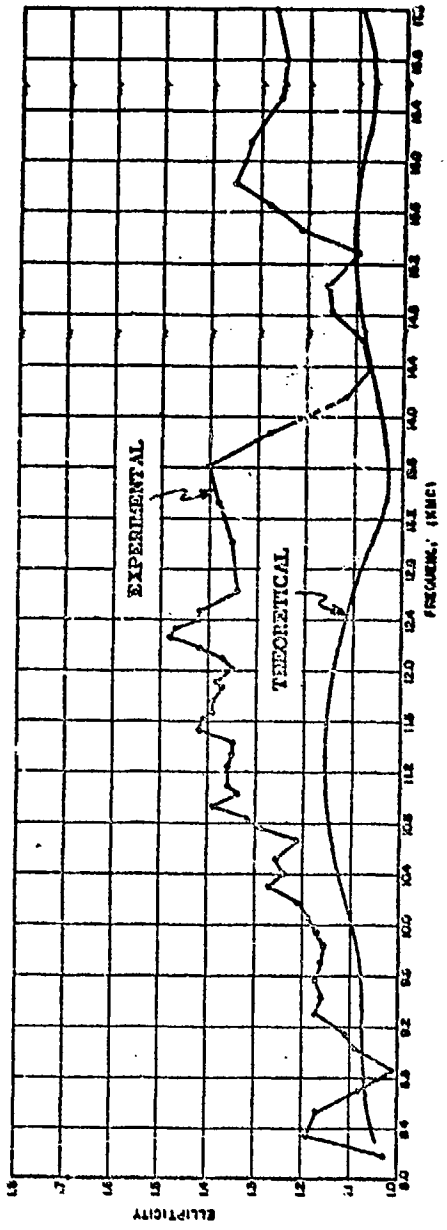

FIG. 5

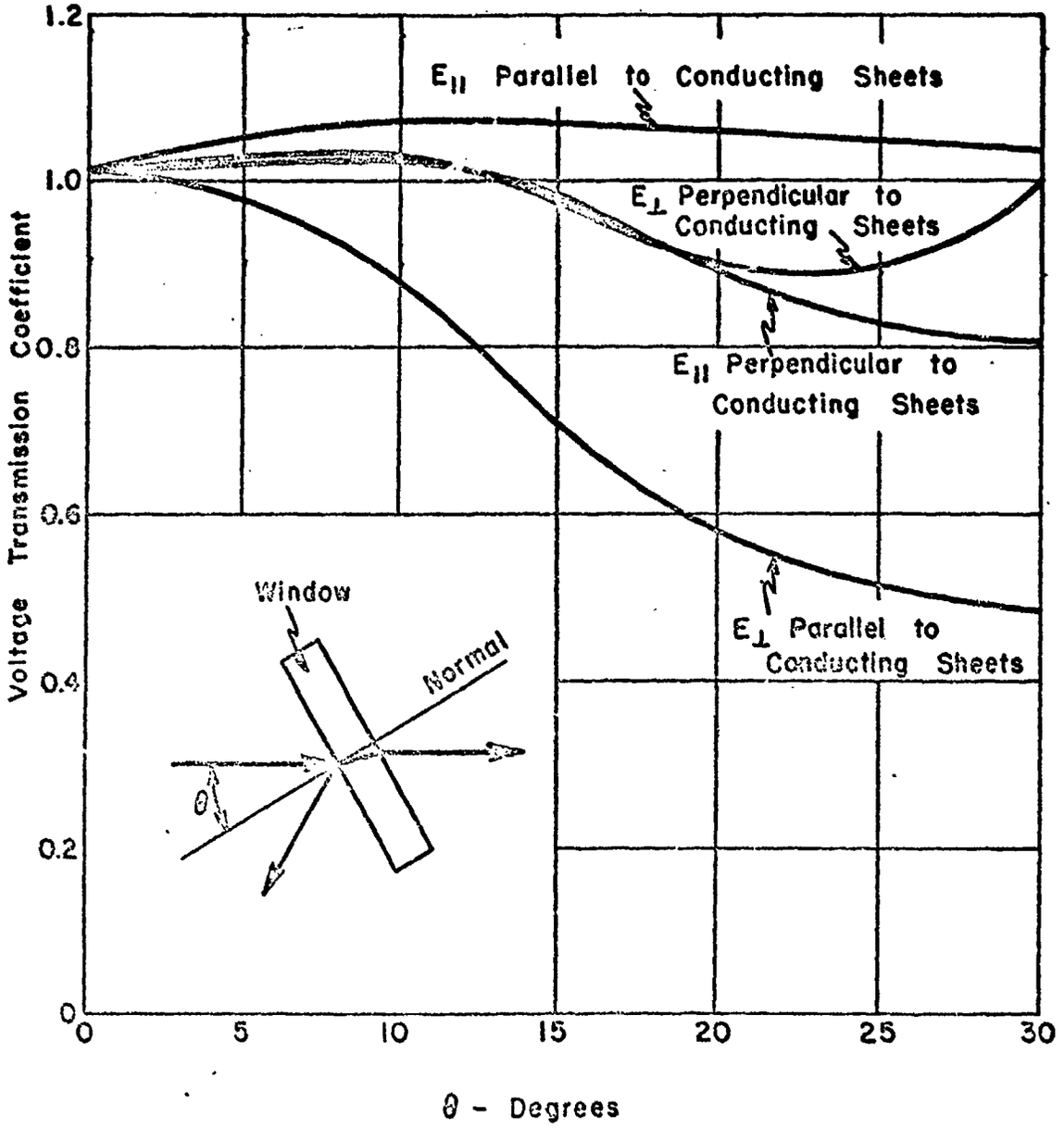
1.2
1.0
0.8
0.6
0.4
0.2
0
Voltage Transmission Coefficient
E|| Parallel to Conducting Sheets
E⊥ Perpendicular to Conducting Sheets
E|| Perpendicular to Conducting Sheets
E⊥ Parallel to Conducting Sheets
Window
Normal
θ
0
5
10
15
20
25
30
θ - Degrees

Figure 6

THE DIELECTRIC TENSOR OF ALTERNATING-LAYER MATERIAL WITH APPLICATION TO HONEYCOMB AND BROADBAND RADOMES

Jack Kotik

TECHNICAL RESEARCH GROUP

§1. Dielectric honeycomb material has attracted radome fabricators because of its high strength-weight ratios (in sandwich form). Rational design of such radomes requires that the effect of honeycomb on microwaves be calculable. If the ratio of cell size to wavelength is small enough, the honeycomb will act as a homogeneous anisotropic material. We shall calculate its constitutive tensors $\tilde{\mu}$, $\tilde{\epsilon}$.

We first calculate the constitutive tensors of alternating-layer medium, which is shown in Fig. 1.

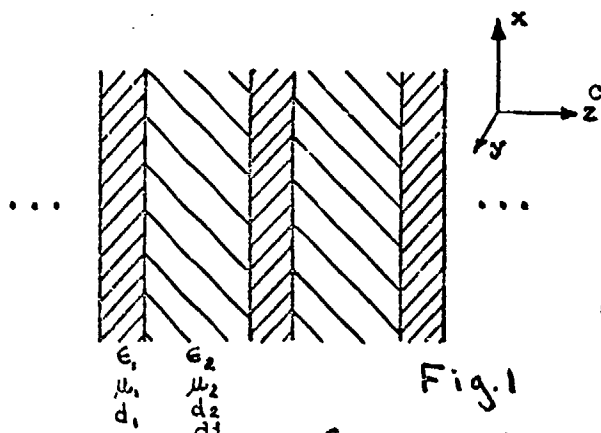

Fig. 1

Static (long-wavelength) considerations indicate that

$$\epsilon_\tau = f_1\epsilon_1 + f_2\epsilon_2 \qquad 1.1$$

$$\epsilon_\sigma^{-1} = f_1\epsilon_1^{-1} + f_2\epsilon_2^{-1} \qquad 1.2$$

where $f_i = \frac{d_i}{d_1 + d_2}$, ϵ_τ is the dielectric constant for $\vec{E}$ parallel to the z-axis and ϵ_σ is the dielectric constant for $\vec{E}$ normal to the z-axis. The direction of propagation is quite immaterial, so that in the coordinate system of Figure 1, the elements of $\tilde{\epsilon}$ are $\epsilon_{xx} = \epsilon_{yy} = \epsilon_\tau$, $\epsilon_{zz} = \epsilon_\sigma$, and the other elements vanish. The results for $\tilde{\mu}$ are completely similar. Formulas 1.1, 1.2 are essentially the formulas for condensers in parallel and in series. This rapid derivation gives results which can be obtained in a more rigorous manner, as in QSR No. 1 on AF33(616)-2973.

§2. Honeycomb can be analyzed by dissection. Invoking symmetry we may take as a unit cell the following:

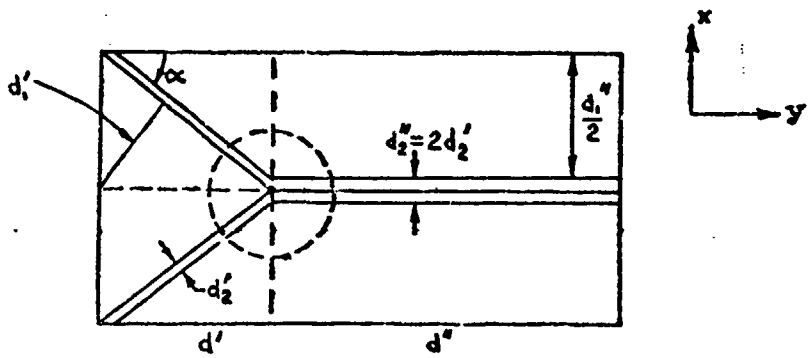

Subcells $'$, $''$ will be in parallel (series) for $\vec{E}$ parallel to x,z (y). Cell $''$ is alternating-layer material, and hence ϵ_x, ϵ_y, ϵ_z are given in terms of 1.1, 1.2. Observing that the $'$ cell may itself be bisected, and that the result is almost a unit cell (although not a natural one) of alternating-layer material, we have

2.1 $$\epsilon'_x = \epsilon'_\sigma \cos^2\alpha + \epsilon'_\pi \sin^2\alpha$$

2.2 $$\epsilon'_y = \epsilon'_\sigma \sin^2\alpha + \epsilon'_\pi \cos^2\alpha$$

2.3 $$\epsilon'_z = \epsilon'_\pi$$

where ϵ'_π , ϵ'_σ are determined from 1.1, 1.2 using the geometry of the preceeding figure. The quantities α, d_1' , d', d'' depend on the details of the circled region and details of the cell boundaries, but for ordinary honeycomb in which $d_2'' \ll d_1''$ the uncertainty is small. The subcells are combined to give

2.4 $$\epsilon_x = f' \epsilon'_x + f'' \epsilon''_x$$

2.5 $$\epsilon_y^{-1} = f' \epsilon'^{-1}_y + f'' \epsilon''^{-1}_y$$

2.6. $$\epsilon_z = f' \epsilon'_z + f'' \epsilon''_z, \text{ where}$$

$$f','' = \frac{d',''}{d' + d''}$$

This analysis is rough but may be expected to be rather accurate for $d_2'' \ll d_1''$; naturally it is most accurate when $\lambda \gg d_1''$.

Measurements at WADC on a sample having $\epsilon_1 = 1$, $\epsilon_2 = 4\ (1 + .014j\ )$ yielded $\epsilon_x = 1.10$, $\epsilon_y = 1.15$, $\epsilon_z = 1.20$. There is generally some uncertainty regarding d_2' , d_2'' because of the way in which the fiberglass is impregnated with resin. However, the value of d_2' was believed to lie in the range .005" -

.008". Theory yields the following values:

d_2'	ϵ_x	ϵ_y	ϵ_z
.006"	1.097	1.135	1.184
.0065"	1.104	1.147	1.198
.007"	1.111	1.158	1.213

The values for $d_2' = .0065"$ agree very well with the measured values. Additional information may be found in QSR No. 1 on AF33(616)-2973. Formulas for transmission through anisotropic multilayers may be found in the report, "The Propagation of Electromagnetic Waves Through Anisotropic Multilayers" by S. Cutler, AF19(604)-1307.

Alternating-layer material, in which one layer is thin (say .010" - .020") and made of fiberglass and the other is thicker (say .050" - .100") and made of foam, has been used in the construction of wideband radomes. Our previous results can be used to obtain a simple analysis of such radomes. In the frequency band for which both layers are thin this radome wall is simply a slab of homogeneous anisotropic material with $\tilde{\mu} = 1$ and $\tilde{\epsilon}$ given by 1.1, 1.2. For instance, if $d_1 = .050"$, $\epsilon_1 = 1.07$, $d_2 = .010"$, $\epsilon_2 = 4$ we have

$$\epsilon_x = \epsilon_y = \epsilon_T = 1.558$$

$$\epsilon_z = \epsilon_s = 1.219$$

We see that the high transmission in the low-frequency band is due to low dielectric constant rather than any "tuning" effect associated with the multilayer, and that a transmission calculation based on $\tilde{\epsilon}$ is simpler than the conventional calculation.

Redheffer has also investigated a slab of alternating-layer material (with layers parallel to the slab boundaries), from a different point of view, and found that it is equivalent to a homogeneous isotropic slab having $\tilde{\mu} \neq 1$ and a different thickness. This result is surprising but correct and merely indicates that the "natural" equivalent of alternating-layer medium is anisotropic, as in Section 1. "Natural" means that thickness and the property $\mu = 1$ are preserved. The situation may be cogently formulated via the following equivalence:

An anisotropic slab with thickness d and

$$\tilde{\epsilon} = \begin{Vmatrix} \epsilon_x & 0 & 0 \\ 0 & \epsilon_y & 0 \\ 0 & 0 & \epsilon_z \end{Vmatrix}, \quad \tilde{\mu} = \begin{Vmatrix} \mu_x & 0 & 0 \\ 0 & \mu_y & 0 \\ 0 & 0 & \mu_z \end{Vmatrix}$$

where $\epsilon_x = \epsilon_y$, $\mu_x = \mu_y$, has the same (complex) transmission coefficient at $\perp$-pol. (all θ and ω) as the isotropic slab having

(I) $\underline{\epsilon} = \gamma_\perp \epsilon_x$, $\underline{\mu} = \gamma_\perp \mu_x$, $\underline{d} = d/\gamma_\perp$

and the same (complex) transmission coefficient at Π-pol. (all θ and ω) as the isotropic slab having

(II) $\underline{\epsilon} = \gamma_\parallel \epsilon_x$, $\underline{\mu} = \gamma_\parallel \mu_x$, $\underline{d} = d/\gamma_\parallel$

where $\gamma_\perp = \sqrt{\frac{\mu_z}{\mu_x}}$, $\gamma_\parallel = \sqrt{\frac{\epsilon_z}{\epsilon_x}}$. Hence a polarization-independent equivalence is possible only for those special media having $\gamma_\perp = \gamma_\parallel$ or $\tilde{\epsilon} = \underline{a}\tilde{\mu}$, where $\underline{a}$ is a scalar.

STREAMLINED LENS-RADOMES

Alan F. Kay

TECHNICAL RESEARCH GROUP

The conventional antenna used with a radome is a paraboloidal dish and feed. The feed serves as a source of spherical waves and the dish focuses or collimates this energy into locally plane waves which travel out into space. The function of the radome in this process is to act as if it were not there. A focusing element of another type occasionally used instead of the dish is a dielectric lens. At the same time the lens action of radomes with intentional or unintentional tapers has frequently been observed. It seems natural to ask if it is not possible to combine the function of the dieleetric housing, the radome, and the antenna focusing element into a single unit, a "lens-radome".

In a certain sense, "lens-radomes" have been used before. Any time a dielectric lens is used in a flush mounted application or without a radome, the focusing and housing functions are being performed by a single component. But such applications are not the ones in which radomes have difficult problems. For one thing, until now lens-radomes have not been streamlined. Their exterior surfaces have been flat, almost flat, or at most, spherical.

An example of the latter, which we will refer to a number of times again, is the Luneberg lens. Let me recall (Slide 1) that a Luneberg lens is a spherically symmetric lens whose index of refraction (which is the square root of the relative dielectric constant) varies radially from a maximum of $\sqrt{2}$ at the center to a value unity on the outer surface following the law $n^2 = 2 - (r/a)^2$, where a is the radius. On the basis of geometrical optics, a point source placed on the surface of the Luneberg lens focuses into a plane collimated beam. Because of the spherical symmetry, the beam will scan throughout all space without distortion if the source traverses the surface of the lens appropriately.

Lunebergs have been built and tested at many laboratories and have been found to operate well in the microwave range up to frequencies above X band. Some of you who have had so little luck with geometrical optics in radome error analysis, may be skeptical of a purely optical design working so well in this case. A proof that geometrical and physical optics are quite accurate for the Luneberg lens has been obtained by Henry Jasik, who in his doctoral thesis at P.I.B. gave an exact electromagnetic solution of radiation from both a dipole and an omnidirectional source on the surface of a Luneberg lens. Jasik compared this solution with the physical optics solution and found no practical difference for the main lobe and the first side lobes for the case of a lens as small as 2 1/2 wavelengths in diameter. Unlike conventional radomes a Luneberg lens has a slowly varying refractive index. There are no index discontinuities and the maximum index value is relatively small.

The reason I have spent a little time talking about the Luneberg lens is that I want to describe today designs for streamlined lens-radomes of which the Luneberg lens is a special non-streamlined-case. Before doing so, I would like to discuss briefly the preliminary considerations which led us to this design. To begin with, our ultimate goal has been an axially symmetric dielectric lens-radome, with fineness ratios as high as 3 to 1, capable of scanning to $\pm 45^{\circ}$, and usable in applications where there are weight, strength, thermal and erosion problems, as well as electrical transmission and boresighting requirements.

Certain theoretical considerations, as well as the weight of experience, shows that only the Luneberg lens and certain modifications of the Luneberg which are also spherically symmetrical can achieve perfect focusing for a range of scan angles. We thus consider designs which focus approximately throughout a scanning range. We have restricted our attention primarily to a two dimensional analysis in the plane of the feed offset. Considerations under this two dimensional restriction are sufficient to show that most design approaches are unsatisfactory. A number of design procedures were considered at first. These utilized homogeneous, multilayered, and continuously varying indices. The continuously varying indices included radial variation, linear variation both axial and transverse, and combinations of all of these. In every case, a particular type of index variation was considered first, then some criterion of focusing and scanning was employed such as two or three point correction or the Abbé sine condition, and then the ray paths were determined. Let me call this the "analytical" approach. These attempts were abandoned for one or more of the following reasons: inadequate streamlining, computational complexity, inadequate scanning range, or impractical index values.

The design which has proved most successful and which I shall discuss today reverses the analysis procedure. We start by choosing a field of curves which, if they were rays, would mean good focusing and scanning properties. Then we "synthesize" a variable refractive index such that the rays associated with this index are the chosen curves. We thereby realize the desirable focusing and scanning properties.

Let me illustrate this method with an example (Slide 2). Suppose we would like the outer surface of the lens-radome to be an ellipse given by equation (1) where the source, or feed phase center, is at the point (-1,0). Observe that for A sufficiently large, the fineness ratio is as large as you please. Now we want a family of rays which focus and imply some scanning ability. We choose the family of ellipses specified by a parameter t in equation (2), where θ is the angle that the ray makes with the axis at the source. These curves were chosen for a number of reasons:

(1) they focus, that is they all start from the axial feed point and emerge at the outer surface of the lens parallel to the axis.

(2) they satisfy the Abbé sine condition. This condition

implies that when the feed point is moved off the axis for a short distance the beam will scan and the lens will continue to focus, not only those rays in the plane shown, but also the rays leaving the source and entering the lens in all directions in space.

3) When A = 1, this design reduces to the ordinary Luneberg lens. By taking A larger than 1, we are thus, in a way, "pushing out" the Luneberg lens, proceeding from the known to the unknown - and since A is arbitrary - with as big a jump as we care to take.

Now how do we determine a refractive index variation which actually makes the curves of equation (2) into rays? We have the differential equation (3) of a ray in a continuously varying medium, which says that the ray's curvature $\varkappa$ equals the dot product of the unit normal to the ray $\bar{n}$ and the gradient of the logarithm of the refractive index. This equation is a direct consequence of the eikonal equation (4) for the wave fronts, ψ = constant. The eikonal equation may be derived as the asymptotic solution of Maxwell's equations for the phase of the field as $\lambda \to 0$. Both of these derivations are given in Silver's antenna book. From the equations of the rays we can find expressions for their unit normals and their curvature. In an analysis design one would have the index and a desire to find the ray paths. Here we have the ray paths and desire the index n(x,y). This requires solving a first order partial differential equation - which can be done by the following method. We first find the orthogonal trajectories of the rays; these are the wave fronts. This can be done by numerically integrating the first order ordinary differential equation (5), or by the simple graphical means of starting at a point on the outer lens surface and, with the aid of triangles, tracing by eye a curve which intersects each successive ray at right angles. The graphical method has been quick, simple, and accurate for this problem.

Now if s is arc length along a particular wave front, then the ray equation may be integrated to yield equation (6). Upon substitution for curvature and changing the integration variable to t, we obtain (7) in which the integrand is a function of t alone by substitution of φ from the solution of (5). In the Luneberg case (A = 1), these integrals may be found explicitly and we "rediscover" the Luneberg index variation. For the case A > 1, a numerical solution is required. Again a graphical procedure works well. We take a pair of dividers with a fixed small spacing Δ s, and lay off a series of equidistant points, say 1,2,..., j, on the wave front, the first point being at the outer surface. Then by the trapezoidal rule, applied to (6), the value of log n at the j-th point is found from equation (8) where $\varkappa_i$ is obtained by interpolation, from the values of curvature of the rays near the ith point. n_0 is an arbitrary initial value of n (one of the nice points in this method is that the index on the outer surface is arbitrary). In this way, we determine n on each wave front and repeating for all the wave fronts we have n at a set of points covering the whole lens. By interpolation we determine contours

of constant index n, the "isofracts". This method was tested with the Luneberg lens, (case A = 1 in equation (2), and it gave the Luneberg index variation with an accuracy in n of ± .005 or better.

The results of this method for the case A = 2 are shown in Slide 4. Eight rays, fourteen wave fronts, and the isofracts in steps of .02 from 1.00 to 1.38 are shown. The lower half of the lens is symmetrical and is not shown.

As an illustration of a more streamlined case, rather than choose a larger value of A, we decided to employ a more practical, ogival outershape (Slide 5). Here the equation of the outer surface is given by (9). The equations of the rays are shown in (10). The case $n_o = 1$, is shown in Slide 6.

Since in actual fabrication the outer surface would probably be taken along the n = 1.02 isofract, the overall fineness ratio of such a lens radome would be about 2:1. If the index of the outer surface n_o is chosen greater than unity, then a refraction will take place at the boundary which must be accounted for in the equations for the rays. While our method still applies in principal, difficulty is experienced near the nose and a situation prevails which may be summarized as follows. In view of the requirements of focusing, the Abbé sine condition, and a large fineness ratio, if we ask for an index at the outer surface of $n_o = 1.2$ or greater, then the thickness through which an index appreciably greater than unity prevails, turns out to be so thin that it seems just as satisfactory and much simpler to work with an n_o = unity design to begin with and then add a thin high index layer to the outer surface. The error introduced thereby may be partially compensated for later.

Let us turn now to some practical considerations. How would one make such a variable index lens? To answer this question we examine the technology developed for the Luneberg and other variable index lenses. Let us consider a lens suitable for X band or lower frequencies. It has been found satisfactory to approximate the index gradient by ten homogeneous layers with index of refraction starting at 1.02 and increasing in steps of .04 with a tolerance of ± .01 or perhaps ± .02. Loss tangent must be less than .01 but dimensional tolerances are half the thickness of the layer and are no problem at all. Luneberg lenses are now available commercially from at least three places: Emerson and Cummings, Delaware Research and Development Corporation, and Scientific Associates, Inc. Their methods of manufacture differ. The layers may be machined or molded in matched dies. They may be made of polyfoam of various densities, perhaps loaded with conducting particles, or of a ceramic foam. They may be artificial dielectric.

All these techniques apply equally well to the streamlined lens-radomes. As an illustration of cost, it is estimated that a single experimental model of either the blunt or streamlined shape, held to tolerances and made by machining would cost $7,000. If matched dies were used, the cost would be much higher, especially since the layers are not spherical.

Two practical problems are transmission loss and weight. Table II shows the estimated maximum transverse diameter in wavelengths for a streamlined lens-radome for a 3 db and a 1 db maximum transmission loss for three typical materials. Table II also gives the weight of the lens-radome for two diameters and the same materials. The data indicates that loaded materials are likely to be far too lossy but that unloaded materials may be too heavy. Or, alternatively, a small lens-radome should have no loss or weight problem, but a large lens-radome would probably require an unusually low loss, light weight foam to be feasible. The ceramic foam, of course, has a thermal advantage, and it has been suggested that at least the outer shell might be made of ceramic for this reason.

Feeding the lens is another problem. Table III shows the maximum feed aperture diameter versus the lens radius. This data is based on physical optics and the Raleigh criterion.

The Abbé sine condition does not guarantee a large amount of scanning. How do these lenses behave off axis? Can they scan to 45°? To answer these questions, ripple tank model studies were made for TRG by H. D. Rix of the Pennsylvania State University Physics Department. To make the models we machined flat plexiglass stock on one side to a thickness predetermined so that when these models sat on the plate glass bottom of the ripple tank, and water covered them to the right depth, the velocity of 12 cps ripples over any point on the lens relative to that over "deep water" equaled the design refractive index of the lens at that point. The ripples were photographed by transmitted light, focused by the ripples themselves and frozen by a stroboscopic chopper driven synchronously with the source oscillator.

As a test of the validity of the ripple tank analogy for this particular problem, a 10 inch diameter model of a Luneberg lens was made and tested. Slide 8 shows the results with a point source. The emergent wave front is plane but with an amplitude oscillation having a 1λ period and believed to be an inherent diffraction effect. Slides 9 and 10 show a line source. The fine focusing properties of the Luneberg lens are clearly brought out.

One of the drawbacks of the ripple tank method is that attenuation can not be properly modeled. The ripple attenuation always exceeds that of a low loss dielectric especially when the index is high. Values above 1.5 can not be realized on the present Penn State ripple tank for this reason. In order to minimize this effect the streamlined models were made smaller, 10 cms. in transverse diameter.

Another difficulty is that the optical index of refraction of the plexiglass and the water differ so that over the non-flat portion of the lens, optical refraction errors distort the outlines of the lens and the wave fronts above. The ripples themselves distort smooth curves such as the lens boundary or machining lines so that their images appear cycloidal.

The next two slides show the blunt and streamlined lens-radomes, each 5λ in transverse diameter. At normal incidence focusing is as good as the Luneberg lens. The amplitude oscillations of period 1λ are still present in the emergent wave front. The next slide shows a tolerance study. The wave fronts behind are the ones on the previous slide. Those slightly ahead were photographed in a double exposure when the water depth was increased .17 mms so that the indices are related as shown. The next two slides show the blunt and streamlined lenses with the point source at about 30° off axis. The streamlined case is shown again in the next slide as a double exposure. The circular wave fronts of the source alone are shown superposed. The next slide shows the streamlined lens at 40° off axis. Definite beam deterioration is noticeable.

A line source properly models an incident field on reception. But since antenna feeds are not isotropic, a point source does not model the antenna properly on transmission. For this reason the line source photographs shown next are perhaps of more interest. We have the blunt lens at 0°, 15°, 30°, 40°, 50°, and 60° incidence, and the streamlined lens at 0°, 15° and 30°, incidence. Although we observe that the scanning range appears to be at least $\pm 30^{\circ}$, this study is still in progress and definite conclusions can not be stated at this time.

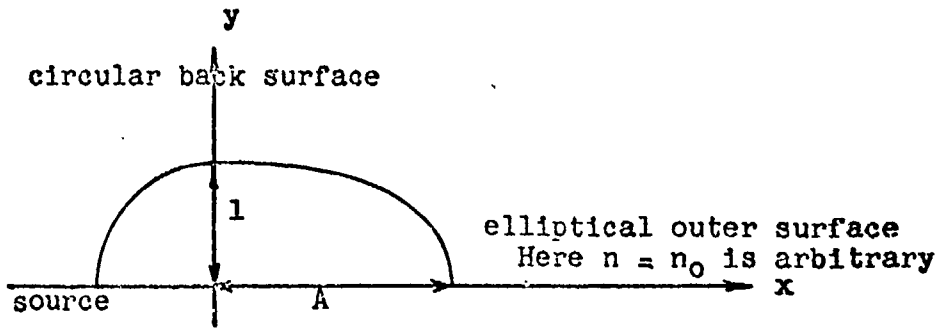

(1) $\left(\frac{x}{A}\right)^2 + y^2 = 1$

(2) $x = a \cos t + b \sin t + c$

$y = d \sin t \qquad 0 < t < \pi/2$

where

$a = (1 - A)\cdot\cos\theta - A \qquad b = \cos\theta$

$c = (A - 1)\cdot\cos\theta \qquad d = \sin\theta$

(3) $\mathcal{K} = \bar{n}\,\nabla \log n \qquad n = n(x,y)$

(4) $|\nabla \psi|^2 = n^2$

(5) $$\frac{d\theta}{dt} = -\frac{y_t^2 + x_t^2}{y_t y_\theta + x_t x_\theta}$$

(6) $$\log n = \int \chi \, \partial s$$

(7) $$n(x,y) = n_o \exp \int_t^{\infty} \frac{(y_t x_{tt} - x_t y_{tt})(x_\theta y_t - y_\theta x_t)dt}{(x_t^2 + y_t^2)(y_t y_\theta + x_t x_\theta)}$$

(8) $$\log n_j = \log n_o + \Delta s \left(\sum_{i=2}^{j-1} \chi_i + \frac{\chi_o + \chi_j}{2} \right)$$

(9) $$M(x^2 + y^2) + Nx + Py + Q = 0$$

where $M = b_o + (a_o - c_o) \tan \varphi$

$N = (b_o^2 + c_o^2 - a_o^2) \tan\varphi - 2a_o b_o$

$P = 2b_o(c_o - a_o) \tan\varphi + a_o^2 - b_o^2 + c_o^2 - 2a_o c_o$

$Q = a_o c_o (a_o - c_o) - c_o b_o^2 \tan\varphi + 2a_o b_o c_o - b_o c_o^2$

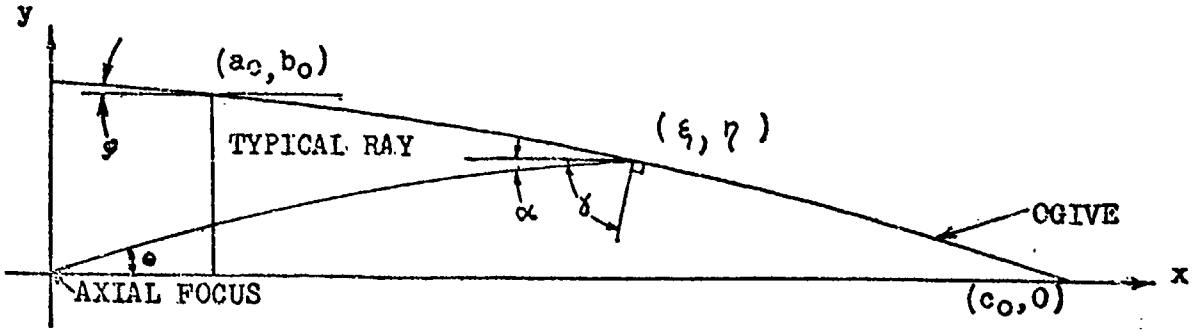

(10) $$Ax^2 + By^2 + Cx + Dy = 0$$

where $A = -\eta^2 \tan\theta$ $\qquad C = 2\xi\eta^2 \tan\theta$

$B = -2\xi\eta - \xi^2 \tan\theta$ $\qquad D = -2\xi\eta^2$

Table II

Material	Maximum diameter in wavelengths		Weight, lbs	
	for 3db loss	for 1db loss	diameter 5 inches	diameter 30 inches
1) Polystyrene foam	444	148	.89	193
2) Loaded polyfoam	6.3	2.1	.22	48.4
3) Ceramic foam	133	44	.71	154

Table III

Lens Radius in Wavelengths	Maximum Feed Diameter in Wavelengths (Raleigh Criterion)	
	$\lambda/8$	$\lambda/16$
3	.58	.33
4.8	.845	.483
6	1.0	.58
10	1.45	.87
18	2.16	1.34
30	3.0	1.92
50	4.1	2.68

LUNEBERG LENS SIMULATION IN A RIPPLE TANK

N. L. Walbridge and L. A. Woodward
University of Vermont

(Sponsored by the Office of Naval Research)

During the past four years a group at the University of Vermont Physics and Electrical Engineering Departments have developed the ripple tank as a quantitative tool. By optical means, using a coincidence of two line images from certain sections of neighboring waves, amplitudes of small ripples within a 30 d.b. intensity range are measured with accuracies approaching two percent.

In the Proceedings of 1955 we reported briefly on the use of the ripple tank. Index simulation is accomplished by thin layers of water over blocks of transparent material. The reduced speed of ripples in shallow water produces shorter wavelengths and the effects of refraction.

We have now extended the range of index values to more than two, corresponding to dielectric constants over four. The attenuation due to absorption is larger than for the case of radar, and it also increases faster with index. This should not, however, prevent the successful simulation of many radar actions.

A recent application has been the simulation of the Luneberg lens in which the dielectric of a sphere must vary as $(2-r^2)$ from the center out to the surface where $r = 1$. For the ripple tank a circular disk about eight wavelengths in

diameter was machined down to a dome-like shape so that the depth of water over any point was such as to give an index value according to the above definition.

Figure 1 is a representation of the radiation produced by this disk lens with a point source on the rim. The absorption through the center part of the lens is seen to have reduced the power in the center of the beam. The phase fronts, however, are substantially straight lines. This particular simulation is not perfect, due in part to the difficulty of machining the slight change in cut over the surface of the disk.

In order to avoid the effect of the larger absorption through the center of the lens, and also to conform with actual radar practice, the point source was replaced by a directed beam. This was given by a sectoral horn simulation, with a half-power beam width of 26°.

The effective or virtual center of this primary radiation was some distance from the rim of the lens, that is, it was outside the focus. The resulting radiation is seen in Figure 2. Something of an image is produced a short distance from the lens, toward which the emergent waves first converge and from which they then diverge.

In order to move back the focal point from the rim of the lens to the position of the feed pattern source, that is, to reduce the refracting power of the lens, the index was reduced over the entire disk. This was accomplished by raising

the water level slightly by adding a measured amount of water to the tank. This was only one arbitrary, but a very convenient, way of decreasing the index at every point. Since this is a departure from the theoretical index distribution of the Luneberg lens, there are probably many other distributions which would be usable. The most desirable one would probably be obtained only by experiment.

Figure 3 shows the main lobe of the radiation produced after several trials of adding slight amounts of water. It consists of practically "plane" waves. The beam shape is smooth, similar to that from a small reflector, and has a half-power beam width of the order of six degrees.

The next point considered was the fact that any radar lens of this type has to be constructed of shells of chosen thickness and appropriate dielectric to approximate as closely as possible the theoretical variation. We then simulated such lenses by machining disks to various discreet levels. Choice of index steps was arbitrary and the number of such steps was varied from five to ten.

The result of one such adaptation is shown in Figure 4, with hardly any basis for choosing between this and the preceding figure. Only five steps of index variation and corresponding thickness of rings (instead of shells) were used.

Curves of the radiation pattern above and also for three other slightly different water levels over this five-step lens

are plotted in Figure 5. All intensity values were normalized to the same maximum value. These were measured at a radial distance of twelve or more wavelengths from the lens, which may, perhaps, be considered as in far field.

All of these curves show the same general smooth shape, with half-power beam widths from 5.8° to 7.0°. These seem to show that a satisfactory beam may be produced by a smaller number of shells of discreet dielectric values than might be supposed. Also, the assortment of dielectric constants required may not be critical. Those most available could be selected and the thicknesses determined accordingly. In these examples given here no measurements of the index values were made. More work would relate beam shape and width to specific and practical designs of such lenses.

Side lobes with these small aperture lens simulations are very low. Measurements have not yet been made on them, but they seem to be of the order of 20 d.b. down from the peak intensity.

Another project for investigation is illustrated in Figure 6. By inserting a simulated section of a radome wall into a beam, the boresight shift caused thereby can be measured to perhaps a half mil. By varying the angle of incidence a curve could be obtained giving the boresight shift at all aspects of a given radome shape with a specified antenna location. Other curves would show the effect of wall thickness and dielectric consta since these can be simulated

over sufficiently wide ranges. The probability seems good that a combination of these parameters can be found that will produce a boresight shift constant over the angle of look.

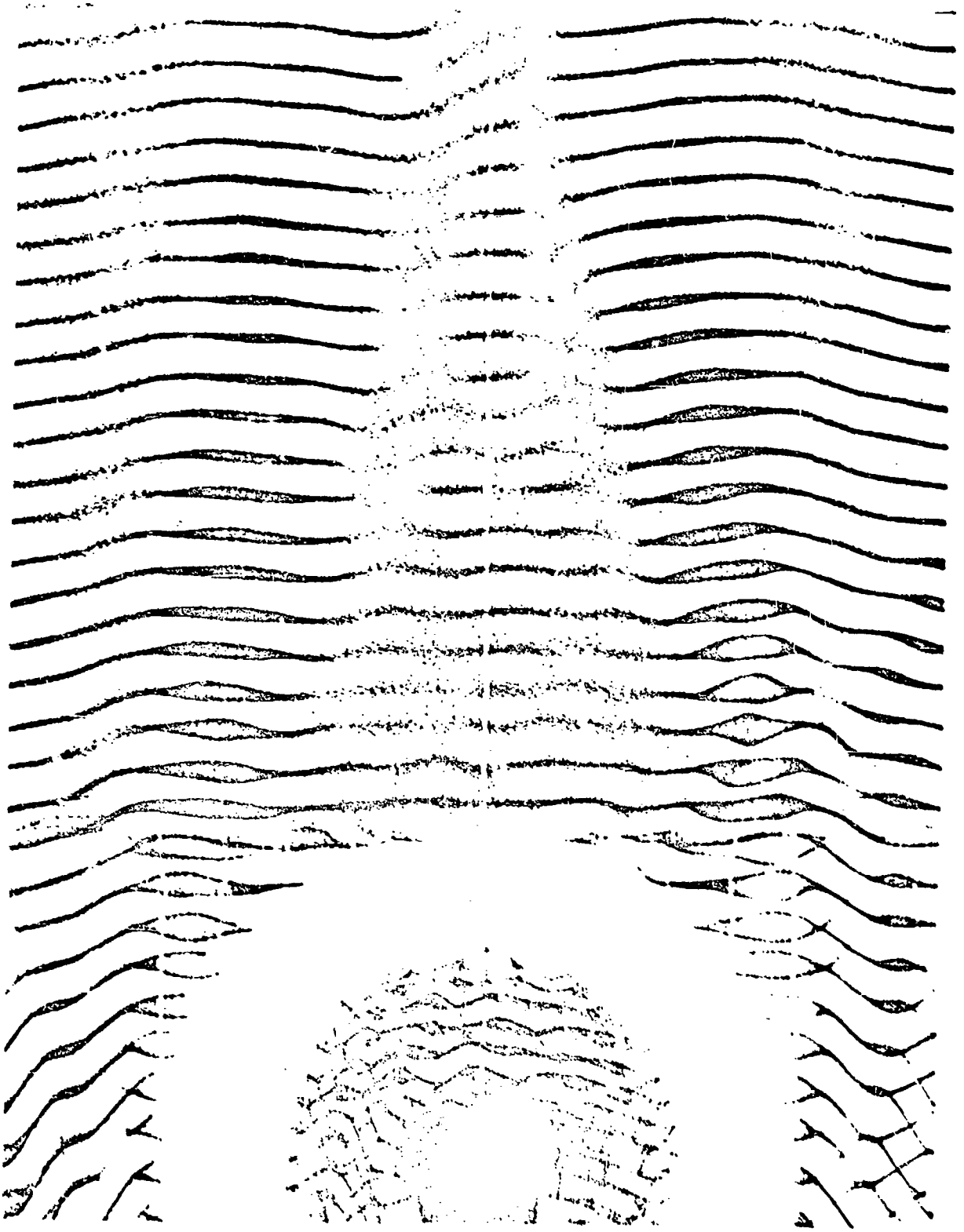

Fig. 1. Luneberg Lens Simulated by Machined Contour under Water.

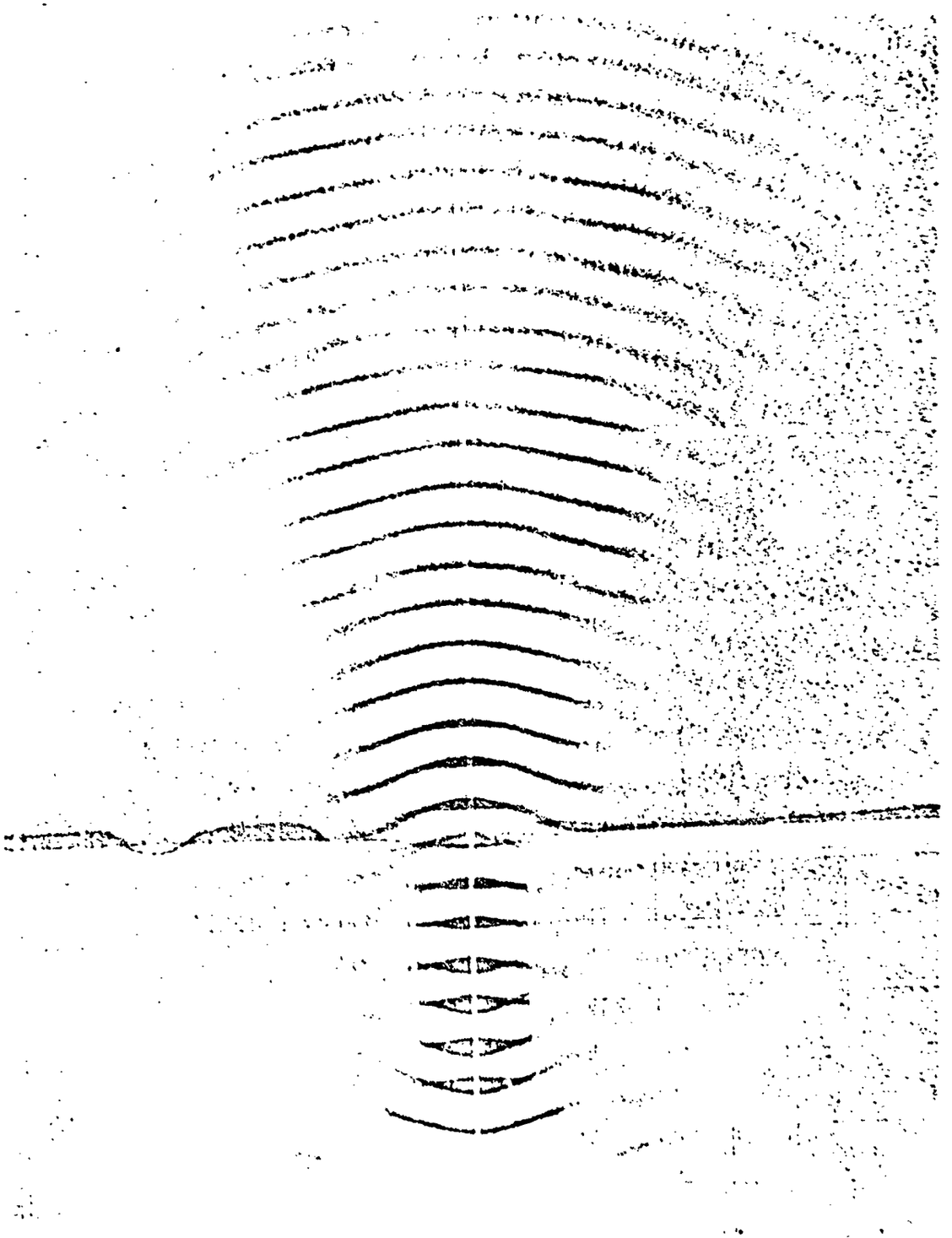

Fig. 2. Luneberg Lens with Horn Feed, Center of Feed Some Distance from Lens.

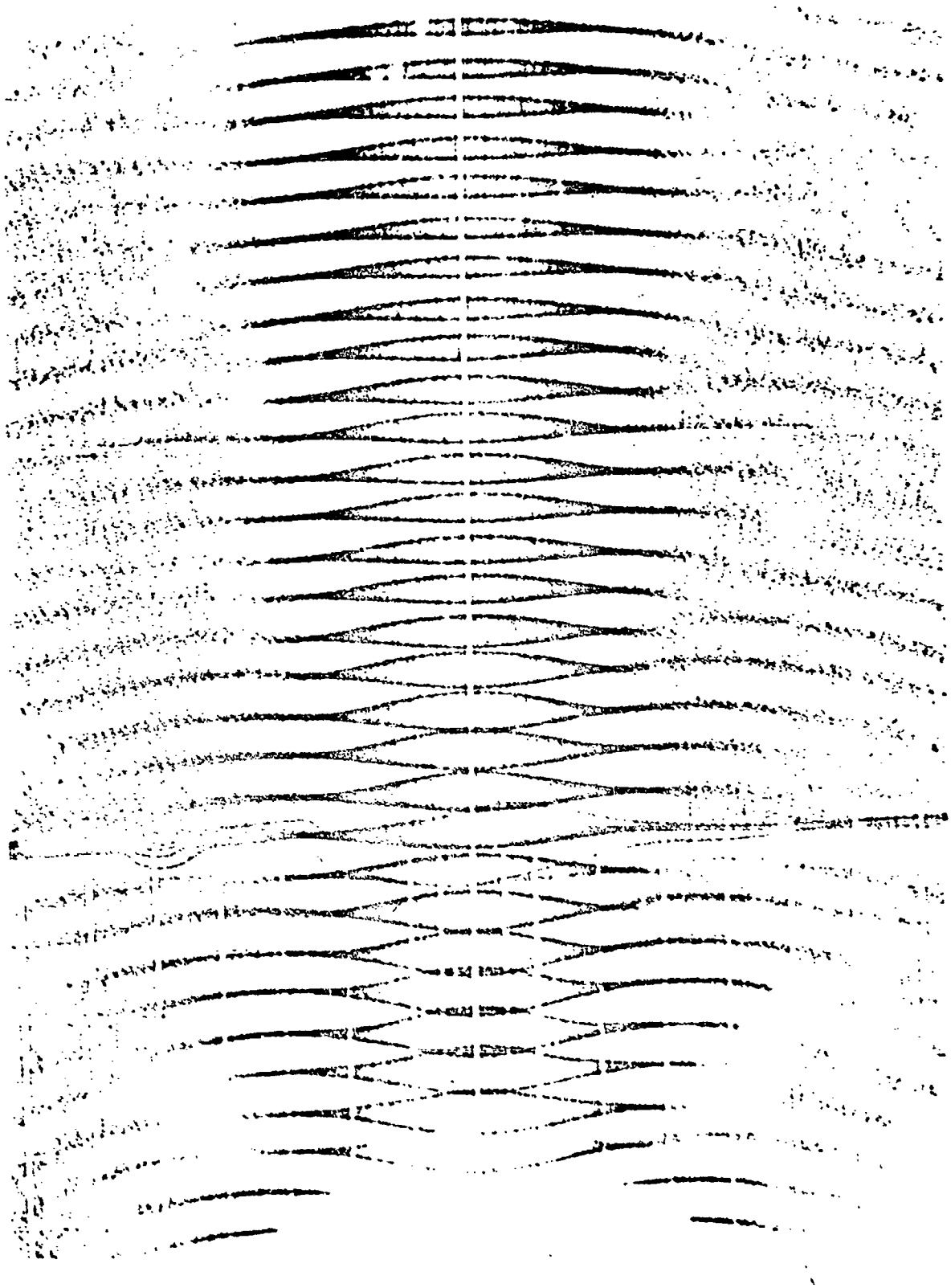

Fig. 3. Same as Fig. 2, with Index at All Points Reduced Slightly.

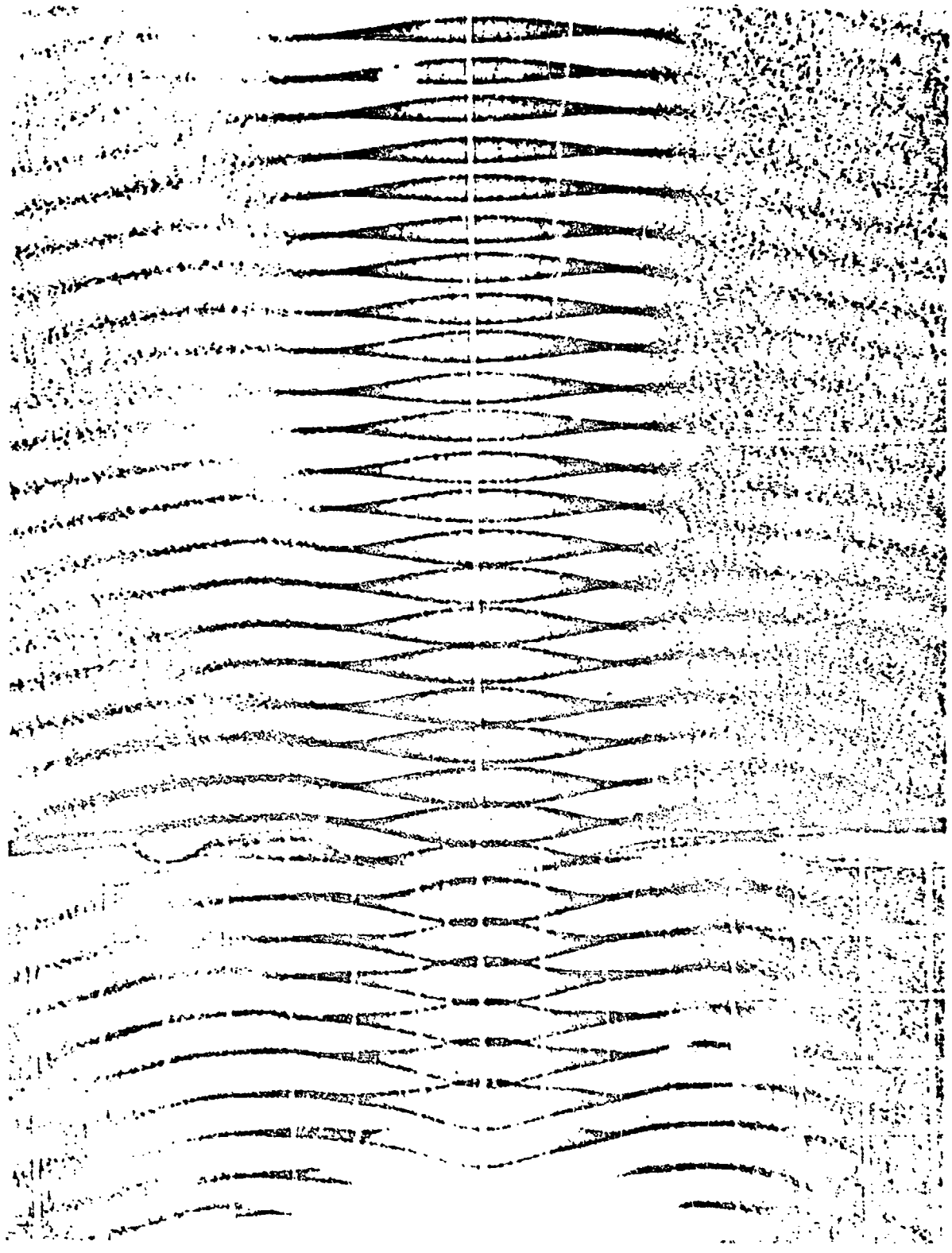

Fig. 4. Modified Luneberg Lens Consisting of Five Shells.
(Cf. Fig. 3)

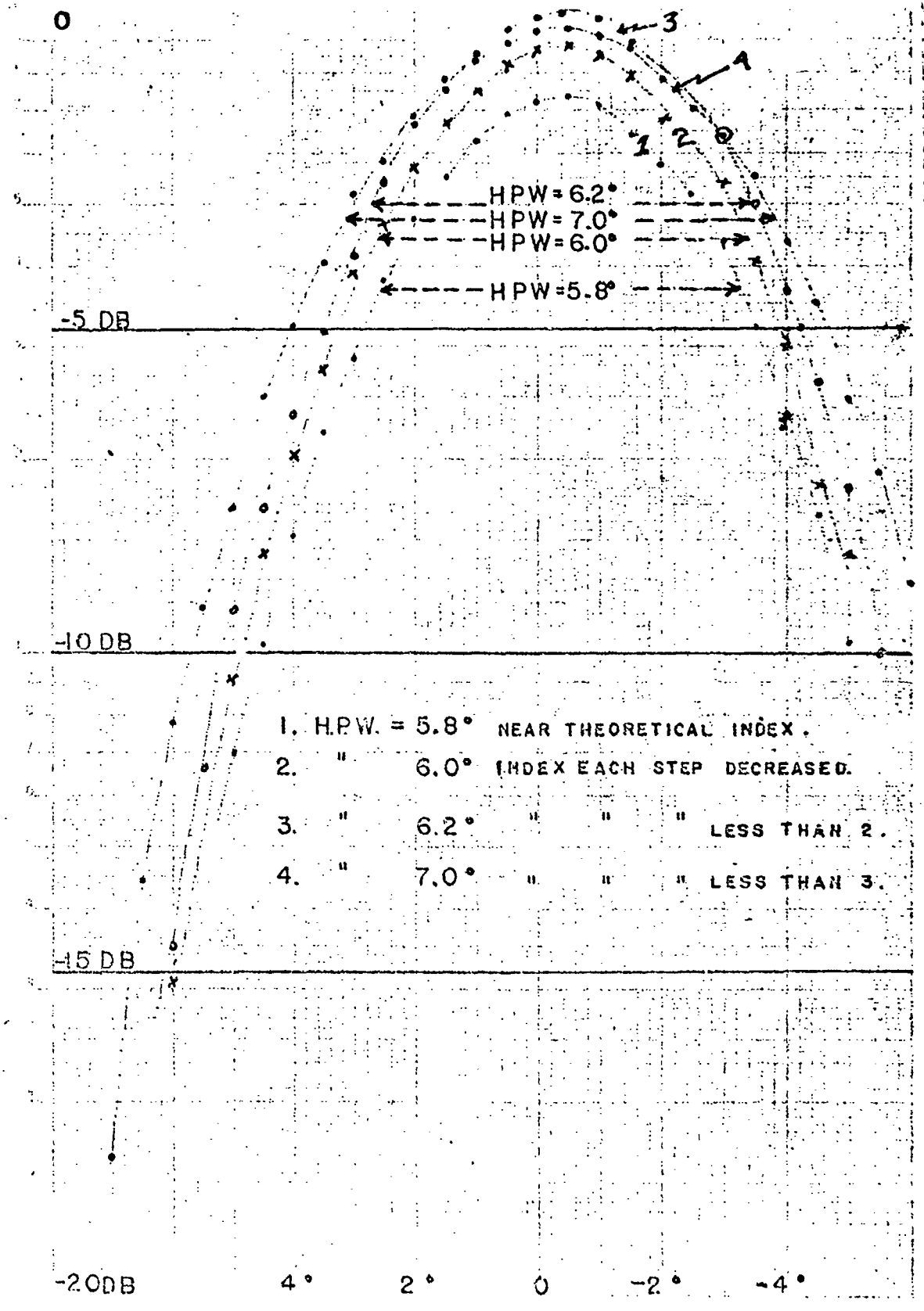

Fig. 5. Curves of Pattern in Fig. 4 with Three Other Index Variations over Same Lens.

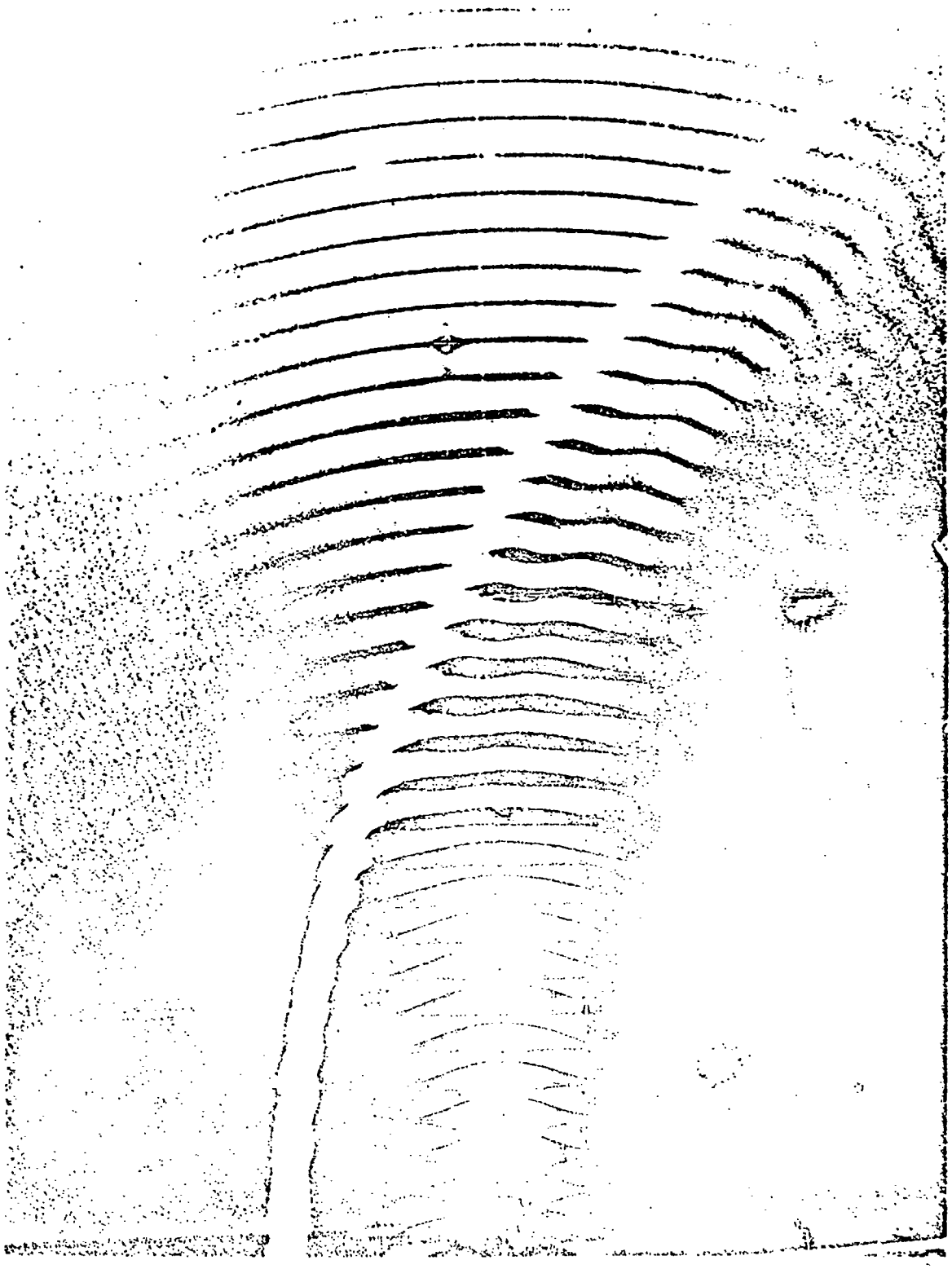

Fig. 6. Boresight Shift Due to Section of Radome Wall Can Be Measured.

BORESIGHT PREDICTION TECHNIQUE

Paul I. Pressel
Aerophysics Departments
Goodyear Aircraft Corporation
Akron, Ohio

This paper covers a simple procedure by which the boresight error characteristics of figure-of-revolution radomes can be easily estimated. The method to be outlined will permit a rapid evaluation of the general configuration and magnitude of the boresight error characteristics of such radomes, without recourse to elaborate computational procedures.

Major efforts during the past few years have been directed at improving methods for predicting the boresight errors caused by radomes. As more refinements have been introduced, the computational procedures have increased in complexity. Some of the latest, and perhaps most elaborate, techniques require high-speed computers, with very large data-handling and storage capacities (such as the IBM 704), if the computations are to be carried out economically. Adequate computational facilities may not always be available, and it is not always possible to devote the necessary time to programming, which is quite complex.

For the purpose of this discussion, the boresight error will be defined as the tilt in average phase front induced by the radome wall, as illustrated in Figure 1. Actually, in a conically scanning system, boresight is defined as the angular shift of the cross-over, which to a first and generally fairly good approximation is the same as the beam refraction in the offset plane caused by the radome at the particular offset (or look) angle in question. The radome wall structure will be assumed to have fairly uniform transmission over the range of incidence angles encountered between the rays from the dish and the normals to the radome wall, so that pattern distortion due to poor transmission can be ignored. A collimated beam will be postulated with a plane phase front normal to the rays emanating from the dish as shown in Figure 1. During passage through the radome wall, the rays will undergo varying amounts of insertion phase (defined as phase retardation in excess of that incurred in travelling through an equal thickness of air at the given angle of incidence). The slope of a line drawn as a best fit through the various amounts of insertion phase undergone by the different rays, with respect to the phase front of the undistorted beam,

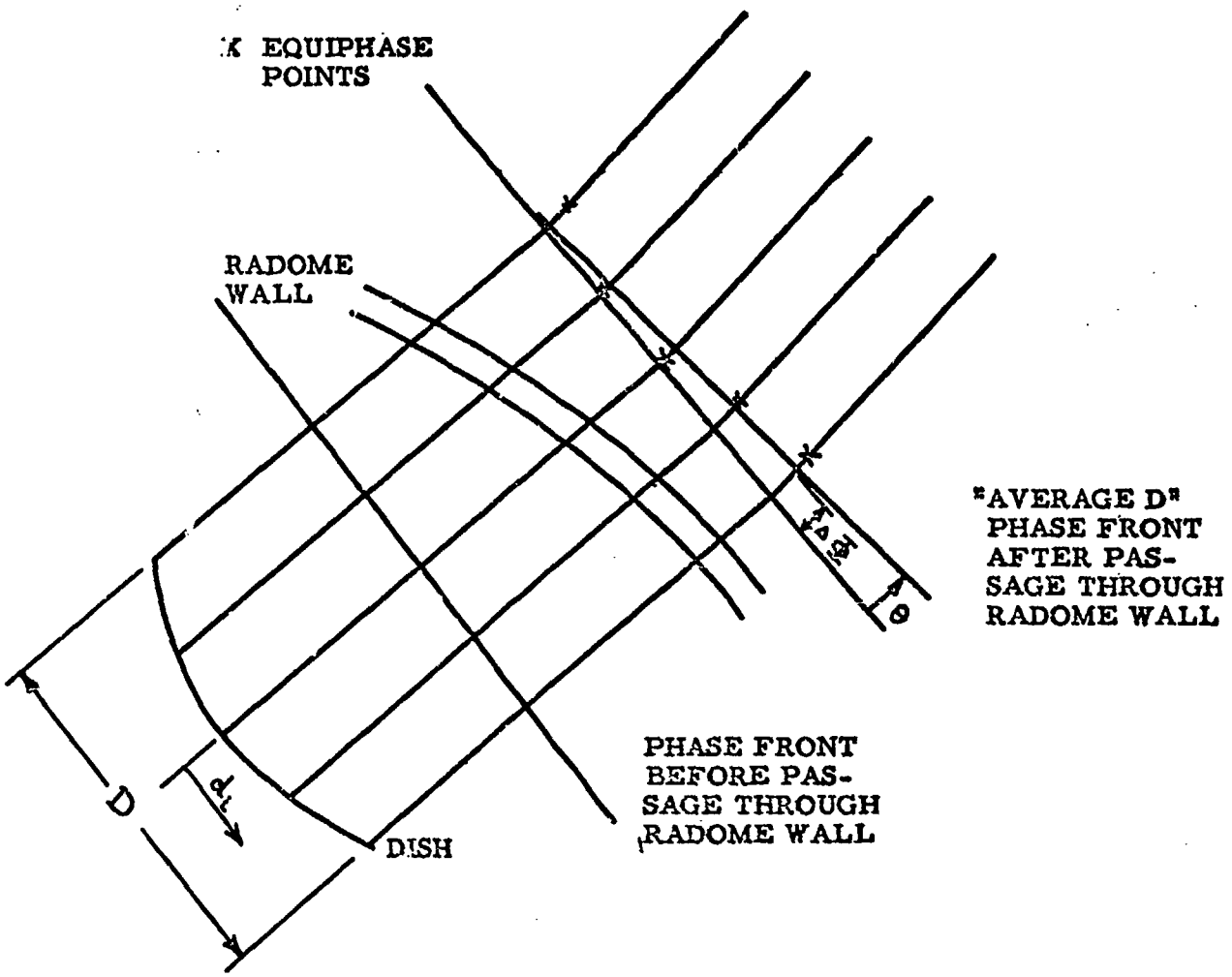

Figure 1 - Equivalent Effect of Radome Wall Structure on Beam

will define the boresight error. In Figure 1 the boresight error in radians will be defined as:

$$\theta \cong \frac{\Delta\Phi}{D} = \frac{\Sigma w_i \Phi_i d_i - \frac{(\Sigma w_i \Phi_i)(\Sigma w_i d_i)}{w_i}}{\Sigma w_i d_i^2 - \frac{(\Sigma w_i d_i)^2}{w_i}} .$$

where w_i = weighting factor for the i-th ray,

Φ_i = insertion phase undergone by the i-th ray,

d_i = distance in electrical degrees of the i-th ray from the central ray.

Only rays lying in the offset plane passing through the radome axis are assumed to contribute to the boresight error. Finally, it will be assumed that the radome is substantially a figure-of-revolution, that the antenna beam is symmetrical, and that the dish and radome are at least 10λ in diameter.

In Figure 1 five rays are shown emanating from the dish: the central ray, the 3-db down rays, and the edge rays. The central ray does not contribute to the slope of the new phase front, providing the other rays are symmetrically located with respect to it. With four rays, satisfactory results have been achieved for wall structures which may vary gradually in thickness. Sharp narrow discontinuities in the form of ring compensators result in less reliable results. Presumably better predictions can be achieved with a larger number of rays, but since the intent is to achieve a rapid survey of the characteristics, the increase in labor would defeat the purpose. On the other hand, it will be shown that tolerable results can be achieved with only the two edge rays.

Each ray is treated as if it were a plane wave impinging on an infinite plane sheet having the identical wall construction as that existing at the intersection between the ray and the radome wall, and at the same angle of incidence. Although the expressions for the insertion phase introduced by multiple-layer walls are quite lengthy and complex, it is possible to determine the insertion phase rapidly by applying Smith Chart techniques to the transmission line analogy of the multi-layered wall. O. J. Snow showed some years ago that this could be done to establish the transmission characteristics of multi-layered

flat panels.[1] More recently Dr. H. F. Mathis, at Goodyear Aircraft Corporation, has shown that this technique can be extended to determine the insertion phase characteristics of such panels.[2] The graphical construction requires only four straight lines and one arc of circle per layer and a few simple calculations, which can be readily carried out with the aid of a slide-rule. The insertion phase of a single ray passing through a three-layer sandwich can be computed in about twenty minutes, without the benefit of any specially prepared charts. However, if a large number of points are going to be considered it is expeditious to prepare curves or tables of normalized impedance and propagation functions for the various layers over the range of incidence angles to be encountered.

After the insertion phase undergone by each ray has been computed, the slope of the phase front is established by calculating the slope of the best fit straight line passing through the varying amounts of phase retardation. A refinement can be introduced by weighting the contributions of the various rays according to the energy distribution across the dish. If only the two edge rays are used, the slope of the straight line passing through the insertion phase undergone by these two rays is used. In all these cases, it is implied that, to a first approximation, the insertion phase varies uniformly across the beam.

The degree of success that can be achieved with this method will be illustrated in the following examples, in which the predicted boresight errors of a radome, with this technique, are compared with the measured results. The calculations were carried out at five offset angles for four and for two rays. Figure 2 shows the results obtained for perpendicular polarization. The solid line is the measured boresight error characteristic; the dashed curve is based on four rays with weighting for energy distribution; the dotted curve is for four rays using uniform weighting; and the dash-dotted curve is based on the two ray prediction. In general there is good agreement between the over-all envelopes of the predicted and measured curves. At maximum error, the predictions do not exceed the measured results by more than 50%. As might be expected, the two-ray approximation shows less correlation with the measured results than do the more elaborate calculations. Figure 3 shows somewhat similar results for parallel polarization. In general, less correlation has been found for parallel polarization. The greater variations between predicted and measured values are believed to be due to the fact that contributions from off-axis regions are neglected. These same discrepancies have been noted before in more elaborate

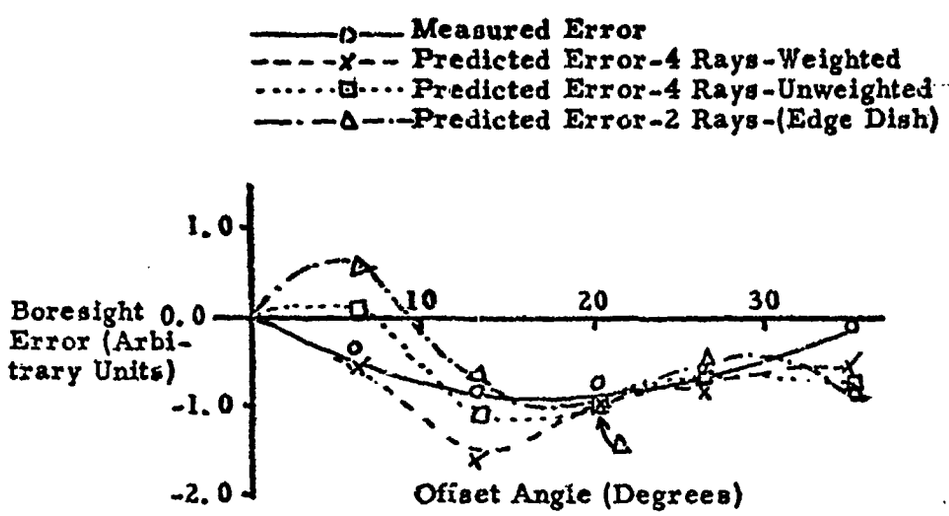

Figure 2 - Measured and Predicted Errors of Uncompensated Radome - Perpendicular Polarization

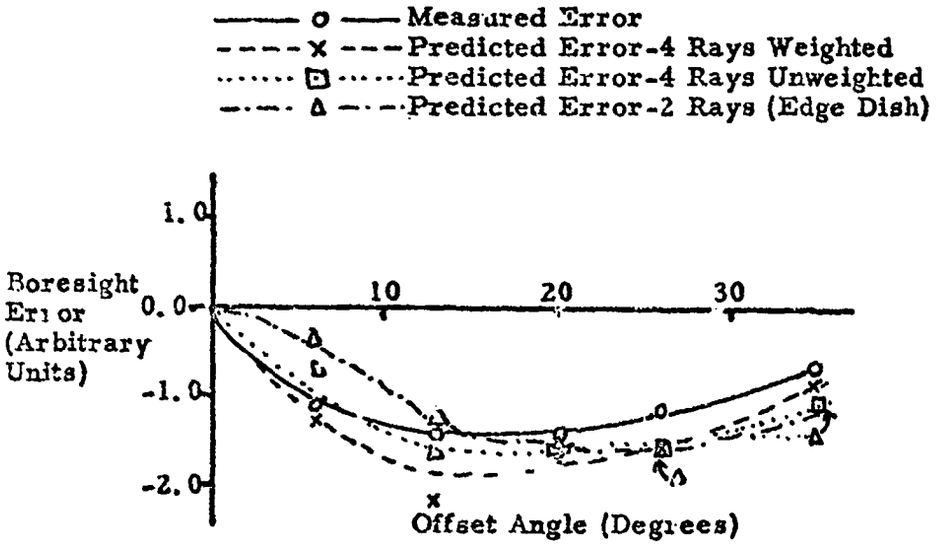

Figure 3 - Measured and Predicted Errors of Uncompensated Radome - Parallel Polarization

computations for the parallel polarization case. Off-axis contributions due to perpendicular polarization presumably cancel out in their effect on boresight because of symmetry. However, for parallel polarization, they probably tend to add and contribute to the over-all effect on boresight error. Note that not too much emphasis should be placed on the results obtained for a single offset angle, which can be distorted considerably.

The technique was next applied to a more severe case. With four rays, the calculations were carried out on the same radome compensated by means of a compensating ring. At all but two offset angles, the compensating ring lay in the path of one or two rays, and was accordingly taken into account. In those cases where the ring lay between two rays, an additional ray was introduced through the ring to make some allowance for its effect, and the effect of the central ray was also taken into account. As shown in Figure 4 for perpendicular polarization, the compensating effect is somewhat evident but the correlation between the predicted and measured results is not so good, as was found previously. In the case of parallel polarization, Figure 5, the lack of agreement is even worse, but the compensating effect is still present. It is believed that to account properly for the effects of sharp discontinuities such as these compensators, more rays should be used in the computational process.

On the basis of these results, it appears that, in general, for a surface of revolution radome, with a wall construction which does not include sharp discontinuities, a fairly reliable estimate of the over-all boresight error characteristic can be obtained, particularly for perpendicular polarization, which generally has the worst characteristics. A four-ray analysis yields good results, and a creditable performance can be achieved using the edge rays only.

One particular advantage of this method is that it permits a rapid evaluation of the characteristics of asymmetrical sandwiches for which tables and charts are not usually available. This method is also useful in rapidly determining the relative effects of wall tapers and other variations in construction. Of particular interest is the fact that in carrying out the graphical analysis, it is possible to acquire an understanding of the manner in which changes in wall structure parameters affect the behaviour of the beam.

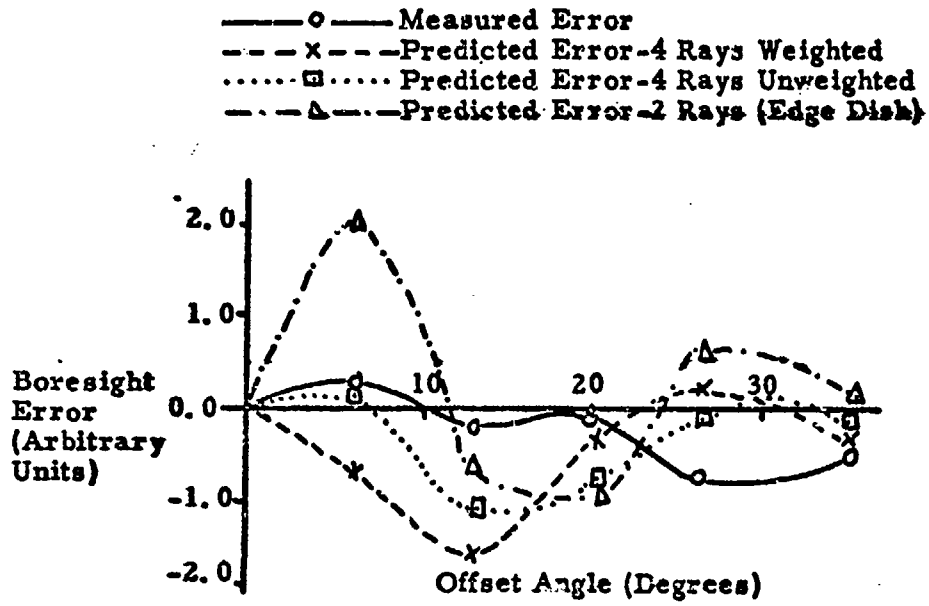

Figure 4 - Measured and Predicted Errors of Compensated Radome - Perpendicular Polarization

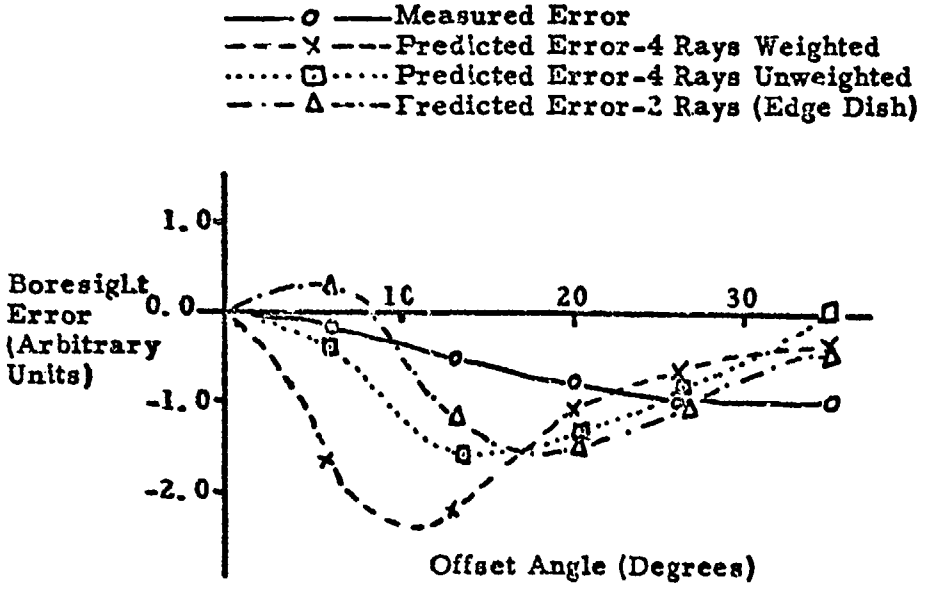

Figure 5 - Measured and Predicted Errors of Compensated Radome - Parallel Polarization

REFERENCES

(1) O. J. Snow, "Report on Applications of the Impedance Concept to Radome Wall Design", Aeronautical and Electrical Laboratory, U. S. Naval Air Development Center, Johnsville, Pa., Report No. NADC-EL-52196; April 1953.

(2) H. F. Mathis, "Transmission Characteristics of Sandwiches", IRE Transactions on Microwave Theory and Techniques, Vol. MTT-3 pp 57-58, October 1955.

BUCKLING CRITERIA FOR SANDWICH SHELLS

by

W. Zophres
Zenith Aircraft
Gardena, Calif.

Sandwich structures subjected to loadings that cause instability have been observed to fail as a result of either:

a) over-all buckling, where there is no separation of the faces from the core (quasi-Euler mode), or
b) local instability, commonly referred to as wrinkling, where the faces tend to separate from the core.

In this paper, a brief summary of the elastic stability of long circular sandwich cylinders under axial compression, bending, torsion and uniform external pressure, is given. The buckling of conical shells is briefly mentioned and an expression for predicting wrinkling stresses is recommended.

When computing buckling stresses of sandwich structures, over-all buckling as well as wrinkling should be considered, with the lesser of the two determining the mode of buckling.

(I) OVER-ALL BUCKLING

(A) Axial Compressive Buckling of Circular Sandwich Cylinders.

The over-all buckling stress of a "long" (length/diameter >1) sandwich cylinder in axial compression is given approximately by (from ref. (1))

$$(1) \qquad (\sigma_{cr})_f = .4 K_c \frac{E_f (c+t)}{R\sqrt{\lambda_f}} \quad *$$

where

$K_c = 1 - .15H$ when $H \leq .98$ (sandwich strong in shear)

$K_c = \frac{.834}{H}$ when $H \geq .98$ (sandwich weak in shear)

and the remaining symbols are as defined under Notation.

* In ref. (1), the buckling coefficient K_c was minimized by taking $\lambda_f = .91$. Here λ_f was retained as such in the minimization, which will explain the slight difference in form of eq. (1) and the results reported in ref. (1).

Equation (1) is based on large deflection theory* with the faces assumed to act as membranes, i.e., the bending stiffness about their own middle surface is neglected. The membrane assumption is conservative and is a commonly used one in sandwich structures. The deflection function used to obtain eq. (1) was not complete, only a diamond shape wave pattern was considered. When the results leading to eq. (1) are reduced to the homogeneous, isotropic, thin-walled cylinder, the resulting buckling stress is

$$(2) \qquad \sigma_{cr} = .242 \frac{E\bar{t}}{R} \qquad \left(\begin{matrix}\bar{t} = \text{wall thickness} \\ \nu = .3\end{matrix}\right)$$

Kempner, ref. (2), used a more complete deflection function and was able to obtain for the homogeneous, isotropic, thin-walled cylinder the expression

$$(3) \qquad \sigma_{cr} = .182 \frac{E\bar{t}}{R} \quad **$$

If the ratio of (3) to (2), which is approximately equal to .75, is applied to eq. (1), the result is

$$(1a) \qquad (\sigma_{cr})_f = .3 K_c \frac{E_f (c+\bar{t})}{R\sqrt{\lambda_f}}$$

It is interesting to note that the experimental buckling stresses reported in ref. (1) are equal to or greater than the theoretical stresses obtained from eq. (1a) (these experiments were performed on curved sandwich plates which were designed in such a way as to include at least one ideal buckle).

Equation (1) applies to an isortopic sandwich cylinder. The corresponding buckling equation for the orthotropic cylinder (like a honeycomb core-glass fiber face sandwich) is much more complicated and has not as yet been minimized. Equation (1) (also 1a), however, may still be used to obtain estimates for the buckling of orthotropic sandwich cylinders, provided the lesser of the two

* The large deflection theory was successfully used for the axial compressive buckling of homogeneous, isotropic, thin-walled cylinders to explain discrepancies between experiments and the classical small deflection theory.

** The classical small deflection theory for the same case yields $\sigma_{cr} = .6 \frac{E\bar{t}}{R}$

transverse core shear moduli is used and the 0° or 90° warp direction of the faces ($E_c = E_{90}$) is oriented parallel to the cylinder axis. A slight reduction in E_c may be necessary to compensate for the smallness of the face shear modulus (this statement is based on what is already known from the orthotropic flat plate theory).

(B) Pure Bending Buckling of Circular Sandwich Cylinders

A complete theoretical solution for this type of buckling has not been obtained yet. An expression is available for bending buckling of a sandwich cylinder that is weak in shear ($H \geq .9B$). For this case, it was found, ref. (3), that the critical bending stress is equal to the axial compressive buckling stress of a sandwich cylinder weak in shear, namely

$$(4) \qquad (\sigma_{cr})_f = \frac{G_c (c+t)^2}{2tc}$$

This expression is eq (1) with $K_c = .834/H$. Physically, this critical stress is associated with shear instability in the core and is characteristic of most sandwich buckling problems when the sandwich construction is exhibiting large shear deformations. This equation says that the critical load is equal to the transverse shear stiffness of the sandwich.

Limited bending buckling tests performed by Gerard, ref. (4), on sandwich cylinders weak in shear (aluminum alloy faces - cellular cellulose acetate core) indicate that the experimental buckling stress is on the average 32 per cent higher that the theoretical value obtained from eq. (4). Tests were also conducted on cylinders having aluminum alloy faces and end grain balsa wood core. The results, however, showed the experimental stresses to be approximately four times less than the theoretical values. This was attributed to either a poor bond or to some other mode of buckling.

(C) Torsional Buckling of Circular Sandwich Cylinders

The over-all buckling stress of a sandwich cylinder in torsion is given by (from ref. (5))

$$(5) \qquad (\tau_{cr})_f = K_T \frac{E_f (c+2t)}{R}$$

where K_T for a long, isotropic cylinder, where the faces are considered as membranes, may be obtained from fig. (1). For the buckling coefficients of finite cylinders, and for the case where the faces are not treated as membranes, the curves in ref. (5) may be consulted. In ref. (5), the buckling of the orthotropic cylinder is also treated, however lengthy computations are necessary to minimize K_T.

No experimental confirmation of the theory has as yet been published.

(D) Buckling of Circular Sandwich Cylinders Under Uniform External Pressure

The uniform external pressure under which a long sandwich cylinder will buckle is given by the expression (from ref. (6))

$$q_{cR} = \alpha \frac{3 E_f t (c+t)^2}{2 R^3 \lambda_f} \tag{6}$$

where

$$\alpha = \frac{\left(1 + \frac{b}{a}\right)^3}{4\left(1+\frac{b^2}{a^2}\right)\left[1 + \frac{2 E_f t (c+t)}{G_{R\theta} a b \lambda_f}\right]}$$

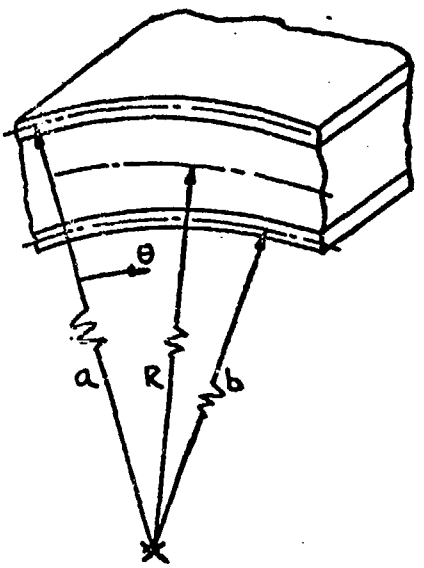

$G_{R\theta}$ = shear modulus in R-θ plane
a and b are as shown on the sketch

In eq. (6) the faces of the sandwich are assumed to act as membranes.

Some preliminary computations indicate that for long, thin-walled, sandwich cylinders that are strong in shear, the factor α is very close to unity.

If $\alpha = 1$, eq. (6) is in the same form as the buckling expression of a long homogeneous cylinder ($I_s = t(c+t)^2/2$ for a sandwich construction).

For the effects of finite length and the non-membrane action of the faces on the buckling pressure of sandwich cylinders, refs. (7) and (8) may be consulted.

No experimental results are available to substantiate the theory.

(E) Buckling of Circular Cylinders Under Combined Axial Compression, Bending and Torsion

The buckling of isotropic sandwich cylinders under combined axial compression, bending and torsion loads has been investigated theoretically in ref. (9). Minimizations, however, were carried out only for the special case of sandwich

constructions weak in shear (large shear deformations in the core). It was found that, for this case, the interaction equation is of the form

$$(R_T)^2 + R_c + R_B = 1 \tag{7}$$

where the R's are the usual stress ratios. For example, R_c is the ratio of applied axial compressive stress to the buckling axial compressive stress, when all other stresses are absent. Since for sandwich constructions weak in shear the buckling load is equal to the transverse shear stiffness,

$$R_T = \frac{T/2\pi R^2}{(c+t)^2 G_c/c}$$

$$R_c = \frac{N}{(c+t)^2 G_c/c} \tag{8}$$

$$R_B = \frac{2MRt/I}{(c+t)^2 G_c/c}$$

where

T = applied torsional moment, in-lb.
M = applied bending moment, in-lb.
N = applied axial compressive load, lb/in.
I = moment of inertia of sandwich cylinder with respect to its diameter, $in.^4$

(F) Buckling of Conical Shells Under External Pressure

No work of this nature has as yet been done for sandwich cones. Recently, Bijlaard, ref. (10), suggested an approximate method for computing critical pressures of homogeneous, isotropic, conical shells. The method consists

essentially in replacing the cone by an equivalent cylinder of radius R (see fig. (2)) and a length

$$\ell_{eq.} = \left(\frac{r_1 + 1.2 r_2}{2.2 r_2}\right)\ell \tag{9}$$

where r_1, r_2 and ℓ are as shown in fig. (2).

As a first approximation, the same approach may be used for sandwich cones. It should be noted here, however, that the above reasoning could not be applied to eq. (6), since that equation is for the infinitely long cylinder. Instead, the results of ref. (8), where a finite sandwich cylinder is considered, should be used.

(II) WRINKLING OF SANDWICH FACES

The wrinkling type of instability of the sandwich faces has received considerable attention, both experimentally and theoretically. The solution that seems most promising at the present, and one that is fairly simple to use, is that of Goodier and Hsu, ref (11). By assuming nonsinusoidal modes of buckling, they were able to obtain wrinkling stresses of half the magnitude obtained in previous investigations. The critical wrinkling stress in the sandwich faces is given by

$$\left(\sigma_{\omega,cr}\right)_f = \frac{E_f E_c t^2}{2 G_c \lambda_f c^2}\left(-1 + \sqrt{1 + \frac{2 G_c^2 \lambda_f c^3}{E_f E_c t^3}}\right) \tag{10}$$

where E_c is the Young's modulus normal to the plane of the sandwich, and the other symbols are as defined under Notation.

Equation (10) was obtained considering a flat plate in edgewise compression. As an estimate to wrinkling stresses of sandwich cylinders it will be assumed that eq. (10) applies to curved surfaces under compressive or torsion loads.

(III) NOTATION

c = core thickness, in.
t = thickness of one face, in.
R = radius of cylinder to mid-plane of sandwich, in.
E_f = Young's modulus of face material, p.s.i.
G_c = transverse shear modulus of core, p.s.i.
ν_f = Poisson's ratio of face material
$\lambda_f = 1 - \nu_f^2$

$$S = \frac{ctE_f}{2\lambda_f(c+2t)RG_c}$$

$$H = \frac{2ctE_f}{3\sqrt{\lambda_f}(c+t)RG_c} \left(= \frac{4\sqrt{\lambda_f}(c+2t)}{3(c+t)} S \right)$$

Other symbols are defined as they appear in the report. The subscript f is here used to identify quantities associated with the faces of the sandwich.

(IV) REFERENCES

1. March, H. W. and Kuenzi, E. W., "Buckling of Cylinders of Sandwich Construction in Axial Compression", Forest Products Laboratory Report No. 1830, 1952.

2. Kempner, J., "Postbuckling Behavior of Axially Compressed Circular Cylindrical Shells", Journal of The Aeronautical Sciences, May 1954.

3. Wang, C. T. and Sullivan, D. P., "Buckling of Sandwich Cylinders Under Bending and Combined Bending and Axial Compression", Journal of the Aeronautical Sciences, July 1952.

4. Gerard, G., "Bending Tests of Thin-Walled Sandwich Cylinders", Journal of the Aeronautical Sciences, September 1953.

5. March, H. W. and Kuenzi, E. W., "Buckling of Sandwich Cylinders in Torsion", Forest Products Laboratory Report No. 1840, 1953.

6. Raville, M. E., "Analysis of Long Cylinders of Sandwich Construction Under Uniform External Lateral Pressure", Forest Products Laboratory Report No. 1844, 1954.

7. Raville, M. E., "Supplement to Analysis of Long Cylinders of Sandwich Construction Under Uniform External Lateral Pressure, Facings of Moderate and Unequal Thicknesses", Forest Products Laboratory Report No. 1844-A, 1955.

8. Raville, M. E., "Buckling of Sandwich Cylinders of Finite Length Under Uniform External Lateral Pressure", Forest Products Laboratory Report No. 1844-B, 1955.

9. Wang, C. T., Vaccaro, R. J., and De Santo, D. F., "Buckling of Sandwich Cylinders Under Combined Compression, Torsion, and Bending Loads", Journal of Applied Mechanics, September 1955.

10. Bijlaard, P. P., "Critical External Pressure of Conical Shells that are Simply Supported at the Edges", Bell Aircraft Corporation Report 02-941-027, 1953.

11. Goodier, J. N. and Hsu, C. S., "Nonsinusoidal Buckling Modes of Sandwich Plates", Journal of the Aeronautical Sciences, August 1954.

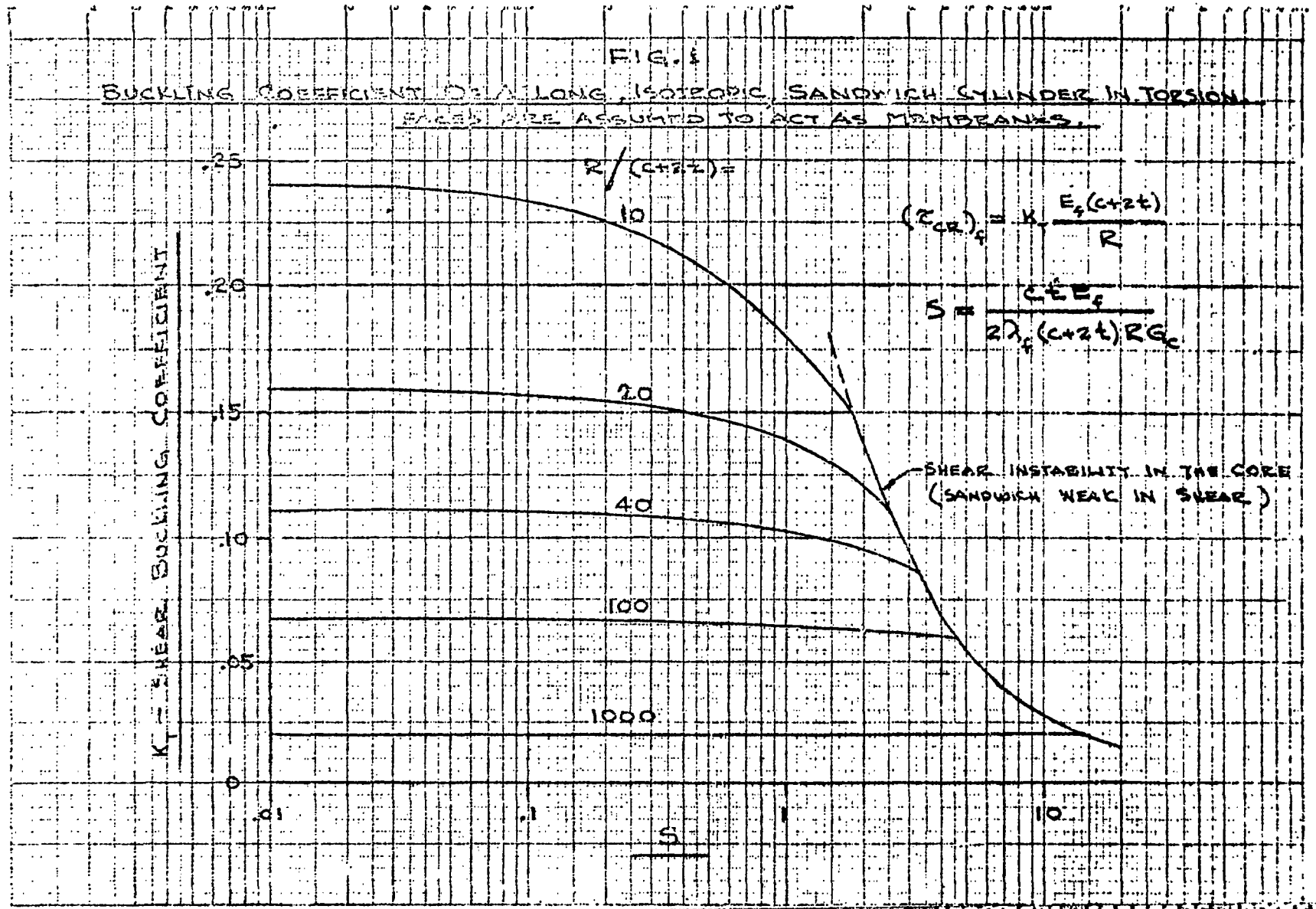
FIG. 5
BUCKLING COEFFICIENT OF A LONG, ISOTROPIC SANDWICH CYLINDER IN TORSION.
FACES ARE ASSUMED TO ACT AS MEMBRANES.
K_T = SHEAR BUCKLING COEFFICIENT
R/(c+2t) =
10
20
40
100
1000
$(\tau_{cr})_f = K_T \frac{E_f(c+2t)}{R}$
$S = \frac{c\,t\,E_f}{2\lambda_f(c+2t)RG_c}$
SHEAR INSTABILITY IN THE CORE
(SANDWICH WEAK IN SHEAR)
.25
.20
.15
.10
.05
0
.01
.1
1
10
S

FIG. 2

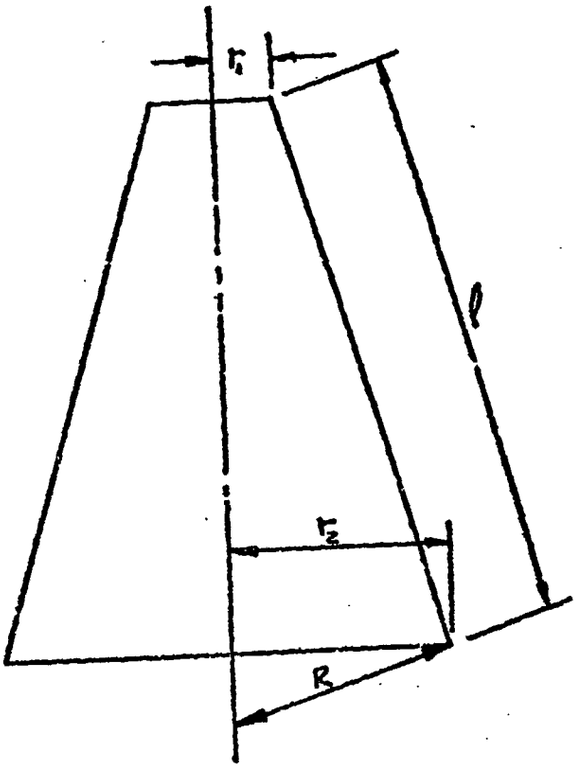

A DESIGN NOTE ON HONEYCOMB SANDWICH CONSTRUCTION

by Melvin Mark
Raytheon Manufacturing Company
Wayland, Massachusetts

A common radome material is the plastic sandwich type structure composed of two faces or skins of dense material separated by and bonded to a honeycomb core (see Figure 1). The question often arises of how to calculate the elastic and thermal properties of such a section. Simple methods for estimating the moment of inertia of a sandwich beam, its associated modulus of elasticity, and the thermal conductivity value should be very useful in preliminary design work.

Elastic Beam Properties

Consider first the problem of estimating the moment of inertia and the associated modulus of elasticity for a sandwich beam construction. A first approximation would be to assume only the skins contribute to the moment of inertia, that they are held apart a distance equal to the core thickness, and that they develop their full modulus of elasticity. To check this simplified analysis, four sample sandwich materials with different skin and core thicknesses were tested as beams and their deflections measured under load.

The four sample beams were of constant cross section, simply supported, with a concentrated load applied at the center of the span. For these conditions, the ratio of load W to mid-span deflection d can be written (Reference 1)

$$\frac{W}{d} = \frac{48\,E\,b\,t\,c}{L^3}\left(t + \frac{c}{2}\right) \qquad (1)$$

where E is the modulus of elasticity of the skin material, L is the span length of the beam, and the other symbols are defined as shown in Figure 1. The sample beams were five inches wide with thirty inches between supports; skin and core thicknesses were as given in Table I. The skin material was made of combinations of 181 and 113 glass fabric with 114 finish, impregnated with polyester resin (Selectron 5003). The core was 1/4 inch cell size polyester fiberglass honeycomb with a density of approximately eight pounds per cubic foot. The skins were bonded to the core with polyester resin. All samples were cured at room temperature. A flexural modulus of elasticity of 3.4×10^6 psi (obtained by experimental measurement) was used for the skin material.

For each sample beam, mid-span deflections were measured with a dial indicator over a range of loads from three to thirty pounds. A plot of load versus deflection could then be made and the slope (load-deflection ratio) determined for each sample. These plots were linear for all samples with data scatter less than 5 percent. A comparison of the results of the calculations using equation (1) and the test measurements are given in Table I.

Table I illustrates that the simplified approach of calculating the moment of inertia for a sandwich beam by neglecting the core and assuming the skins develop their full modulus of elasticity gives answers that are within 10 percent of the measured results. This simplified analysis should be applicable to all long sandwich type beams in bending where the skin thickness is small ($t < 1/5\ c$) compared to the thickness of the core and where the core is sufficiently strong in shear to prevent collapsing of the two skins.

Thermal Conductivity

An expression for the equivalent thermal conductivity k of a sandwich honeycomb such as shown in Figure 1 can be written

$$\frac{(2t + c)}{k} = \frac{2t}{k_s} + \frac{1}{C} \qquad (2)$$

where k_s is the thermal conductivity of the skin material, C is the conductance associated with the core, and the other symbols are as previously defined. If C in equation (2) is considered to be made up of conduction through the solid part of the honeycomb and convection through the air cell of the honeycomb, the following can be written:

$$C = \frac{xh}{2} + (1-x)\frac{k_c}{c} \qquad (3)$$

where h is the film coefficient for the honeycomb air cell, k_c is the thermal conductivity of the core material, and x is that fraction of the core area that is air.

The first term in equation (3) represents the heat transfer through the air cell. When such an air space forms part of a wall construction, an additional resistance to heat flow is introduced at each added surface. Because of the difference in temperature on the two sides of the air space, some degree of air movement is set up within the space unless the space is unusually narrow. Heat is transferred across the space by convection currents and by radiation. The resistance of the air space is, therefore,

approximately the sum of the two individual surface resistances h, or 2/h. Consequently, the term xh/2 appears in equation (3) for that fraction of core area that is air.

The value to use for h in equation (3) could be expected to lie between two limiting values. The lower limit would be the h value equivalent to the conductivity of an air space equal to the core thickness. The upper limit would be the equivalent value obtained for an air space infinite in two dimensions, but of thickness equal to the core thickness (reference 2). The true value for the h would be greater than the value for the lower limit as air movement is present, yet less than the upper limit since the air space is of finite dimensions. Consequently, an average value of the two limits appears reasonable for an approximate answer.

An experimental determination was made* of the thermal conductivity for two honeycomb sandwich samples. The samples had .034 inch skins made of combinations of 181 and 112 glass fabric with Garan finish, impregnated with polyester resin (BRS 142). Sample A had a four-pound per cubic foot nylon phenolic honeycomb core .309 inches thick, sample B a six-pound per cubic foot CTL (glass fabric) phenolic honeycomb core .311 inches thick. Both cores had 1/4 inch cell size honeycomb and were bonded to the skins with epoxy resin. The thermal conductivity of the skin material k_s was taken as 2 BTU/hr-sq.ft.-°F/in., the value for the core material k_c, 1.5 BTU/hr-sq.ft.-°F/in. The cross sectional core area for sample A was 94.5 percent air, 5.5 percent solid material; for sample B, 93.5 percent air, 6.5 percent solid. Substituting in equations (2) and (3), the values shown in Table II are obtained; the experimentally measured values are given also.

Since the thermal conductivity values used for the skin material and core were approximate values (± 15 percent) and the value for h is an approximation, as explained, the excellent agreement shown in Table II should not at present be taken as an indication of the accuracy of the method. However, it does substantiate the method as a good approximation, the accuracy of which can be fully established when more experimental evidence is available. Moreover, from Tables I and II it can be seen both the k approximation and that for the elastic beam properties are of sufficient accuracy for preliminary design work when honeycomb sandwich construction is employed.

* Using standard apparatus at the Massachusetts Institute of Technology.

References

1. Mark, M., "Moments of Inertia and Deflection of Plastic Sandwich Beams", Modern Plastics, Vol. 32, No. 7, 1955, p. 146.

2. Rowley, F. B. and Algren, A. B., "Thermal Resistance of Air Spaces", A.S.H.V.E. Transactions, Vol. 35, 1929, p. 165.

TABLE I

Sample	Thickness, in. Core	Skin	Load - Deflection Ratio, lb/in. Measured	Calculated
I	0.204	0.029	21.8	23.4
II	0.228	0.022	20.5	20.6
III	0.275	0.014	17.4	17.5
IV	0.180	0.029	19.6	18.0

TABLE II

Sample	Temperature °F	Thermal Conductivity, k, BTU/hr.-sq.ft.-°F per inch Measured	Calculated
A	61°F	0.463	0.45
A	114°F	0.486	0.50
A	150°F	0.509	0.53
B	63°F	0.493	0.46
B	107°F	0.512	0.51
B	140°F	0.538	0.54

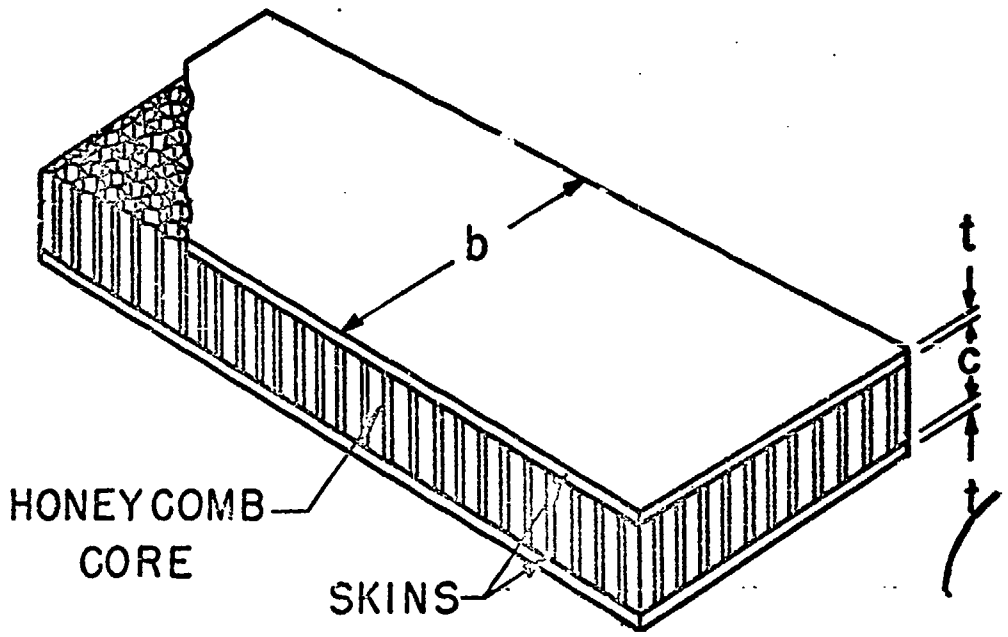

FIGURE 1

HONEYCOMB SANDWICH

PHOTOGRAPHS OF SOME EFFECTS ON RAIN DROPS OF SHOCK WAVES PRODUCED BY 60-CALIBER AND 20-MM PROJECTILES

F. C. P. Seidl

BOEING AIRPLANE COMPANY

I. Abstract

Projectiles from a 60-caliber and a 20-mm gun were fired through simulated rain drops of diameters 1.7 ± 0.3mm. The projectile velocities were varied from 1900 ft/sec to 4060 ft/sec and in certain cases the intensities of the bow shock waves could be estimated. Motion-picture sequences of the interactions of the projectiles and rain drops were taken by a Fastax high-speed camera setup. Times between successive photographs were approximately 150 microseconds. The impacts of the low shock waves were seen to jar and distort the rain drops which always broke up some 600 to 4000 microseconds later. The times required for breakup seemed to depend upon the shock wave intensity. In cases requiring times of the order of 4000 microseconds, blasts of debris and gaseous explosion products from the gun muzzle may have contributed to the breakup.

II. Introduction

While evaluating the problem of the rain erosion of radomes and leading edges of a supersonic aircraft, the following question arose: What happens to a typical rain drop when struck by the bow shock wave generated by the nose of a supersonic aircraft or by a prong extending out ahead of the nose? The experiment described herein was designed in an attempt to answer this question.

III. Experimental Method

A simple expedience for examining the effects of shock waves on rain drops was to photograph progressively the motion of a projectile and its associated shock waves through simulated rain drops. The production of rain drops of any desired size was merely a matter of choosing a proper orifice from which water could fall. The intensity of the bow shock waves could be controlled by varying the speed of the projectile and the shape of its nose. A high-speed Fastax motion-picture camera (see Reference 1) was available for photographing the rain drops before and after impact with a bow shock wave. Unfortunately, the camera was not sufficiently fast to stop the motion of the projectiles and to define the shock fronts; although the presence of these can be recognized by their blurred images.

The projectiles were fired from either a 60-caliber or 20-mm gun through the rain drops into a revetment (see Figure 1). For measuring projectile speeds two screens were situated some 8 ft beyond the point of intersection of the rain-drop stream and the line of fire. Each screen was a one-foot square wooden frame strung with fine copper wires which had to be replaced after each shot. The time required for each projectile to traverse the distance between the successive screens was measured by a crystal-controlled chronometer.

The optical system (see Figure 2) consisted of the following elements mounted in a line: (1) A zirconium low-voltage arc light (Sylvania C-100) located 60 inches from a first collimating lens, (2) A pair of 6-inch diameter converging lenses mounted 30 inches apart and (3) A 16-mm Fastax high-speed camera (see Reference 1) situated 60 inches from the second lens. The arc was at the focus of the first lens which formed a region of collimated light. The second lens collected this light and focused it on the camera's iris diaphragm which was set at f/22. The rain fell through the region of collimated light between the two lenses. Both the drops and the projectiles appeared on the photographs as shadows. Actually, the drops were dark because they refracted light out of the camera. On the other hand, the projectiles formed true shadows by intercepting the light. Moreover, the photographed sizes of the rain drops and the projectiles were independent of their distances from the camera.

The Fastax camera (see Reference 1) exposed a continuously moving film. The shutter action was produced by a high-speed rotating parallel-sided prism. The latter was synchronized by gears with the moving film. Electric power for operating the camera was obtained from a booster circuit (see References 1 and 2). In order to gain a rapid acceleration of both the rotating prism and the film reels, the booster circuit supplied power at 300 volts for the first 100 milliseconds of operation, at 290 volts during the second 100 milliseconds and at 280 volts for the remainder of a run. In typical operation only the final 20 feet of a 100-foot reel of film was moving at the maximum speed of 8000 frames per second. The exposure time was equal to the reciprocal of the product of the number of frames per second and 5.6. The firing of the gun was always delayed 0.6 seconds after starting the camera in order to allow it to approach full speed. Finally, Super XX 16-mm film or its equivalent was used in all runs.

The artificial rain drops were produced by the breakup of a fine stream of water emerging from a single 0.035-inch hole drilled at the end of a pipe which was joined to a 50-gallon drum. The latter was supported so that the 0.035-inch hole was 10 feet directly above the point of intersection of the line of fire and the optical axis of the camera. In falling the stream broke up into cigar-shaped slugs of water, each of which formed into a spherical drop. This fact and the relation between droplet diameter and orifice diameter has been explained by Lord Rayleigh (see Reference 3).

The water stream and droplets fell through a 4-inch tube which acted as a wind shield. The simulated rain appeared on the photographs as spherical drops about 1.7 ± 0.3 mm in diameter (see Table I). An indication of the horizontal and vertical separations between drops can be seen in the photographs. Usually, the drops landed within a horizontal circle of 2-inch diameter. By running the film through a motion-picture projector, the

larger drops were seen to fall faster than the smaller ones, as was expected.

Three types of projectiles were used; see Figure 3. Two of the three types were fired in an unrifled 60-caliber gun. The lack of spin permitted these projectiles to tumble; however, as may be seen from the photographs, when the projectile was traversing the rain, the tumbling had not yet become appreciable. Of the 60-caliber projectiles, one type was a right circular cylinder of diameter 0.599 inches and of one-inch length, the other type had a conical nose of 60° full apex angle. The 60-degree cone was chosen because data were available on the shock fronts produced by such projectiles. The third type of projectile was from a standard 20-mm shell. The 20-mm projectiles were rifled but this did not seem to modify appreciably their bow shock waves; for photographs of 2-pound spinning projectiles in motion see Reference 4.

IV. Experimental Procedure

Each firing of a projectile through simulated rain was carried out according to the following program:

(1) The Fastax camera was loaded with 100 feet of Super XX 16-mm film.

(2) The bearings of the rotating parts of the camera were lubricated with special oil.

(3) The light source and the chronograph were turned on.

(4) The simulated rain was allowed to fall.

(5) The camera was started simultaneously with a time-delay device, which some 0.6 seconds later, fired the gun.

(6) The reading of the chronometer was recorded and this was the time required for the projectile to traverse the ten feet between the wooden screens.

V. Results

Twenty-one motion-picture sequences were obtained each showing the effects of firing a projectile through simulated rain. Of these, ten were taken of 60-caliber conical-nose projectiles whose speeds ranged from 2460 ft/sec to 4060 ft/sec. Six of the shots were with 20-mm projectiles which travelled at 2660 ± 40 ft/sec. Five shots were made using bluff cylindrical 60-caliber cylinders travelling about 1900 ± 100 ft/sec; chronologically, these were the first shots fired, but they are mentioned last because their speed measurements were unsatisfactory. Finally, one sequence was taken of a conical-nose projectile fired without any rain. Because of an improved setup, there was less horizontal spreading of the rain drops in the shots using the conical-nose projectiles and the 20-mm ammunition.

All projectiles were fired at supersonic speeds and any rain drop not having experienced a direct impact with a projectile was subject to a series of effects as follows:

(1) Impact of the bow shock wave that originated from the region near the nose of the supersonic projectile.

(2) The Prandtl-Meyer expansion waves that arose mainly from the shoulder region of the projectile.

(3) Impacts from secondary shock waves which originated from the rear of the projectile and from its turbulent wake.

(4) The debris and gases from the propelling explosion came last.

The strength of the bow shock wave can be estimated for the conical-nose projectiles (see Table II). The other effects were relatively weak except for the debris and gases from the propelling blast. The place of entry of this last effect could be seen in the photographs under consideration.

The results which were evident from the motion-picture sequences are given below:

(1) Nowhere was there evidence that rain drops were immediately broken up by the impacts of the bow shock waves. Apparently there were several cases where, through a direct hit with a projectile, rain drops were instantly broken up into a fine spray. Dark smudges or dark clouds in certain pictures can be explained as due to the refraction effects of a great many tiny liquid droplets and not by regions of high water vapor content or of possible air-density changes (see Section VI, C).

(2) The rain drops were jarred and immediately deformed by a bow shock wave. In many instances the drops broke up before the blast of debris and gases from the gun muzzle swept by. The time required for drop breakup depended upon the strength of the shock wave, but was never less than about 600 microseconds (μsec). Drops further away from the line of fire took longer to break up. Those drops which were situated closest to the line of fire of the bluff-nose cylindrical projectiles broke up first (e.g., 600 μsec in shot 19); here each of the bluff-nose projectiles produced a strong local bow shock which may have been stronger in the vicinity of the nose than for other types of projectiles, but whose intensity certainly fell off more rapidly with distance from the line of fire.

(3) It was found that the exposure times were 20 to 27 μsec and the times between successive frames were 115 to 160 μsec. The exposure times and the inter-frame periods were calculated from (a) Blurs in the images of projectiles and their associated shock fronts, and (b) The change in projectile positions between successive frames. The operation of the camera was such that the inter-frame period was equal to 5.6 times the exposure time.

TABLE I CHARACTERISTICS OF NATURALLY OCCURRING PRECIPITATION*

(Air Density as at 0°C and 740 mm Press.)

Popular Name	Precipitation Intensity mm/hr	Precipitation Intensity in/hr	Droplet Diam. mm	Velocity of Fall Rates Meters per sec.	Milligrams of liquid water per cu meter of air	Grains of Liquid Water per cu ft of air
Clear	0.00	--	--	--	0.00	--
Fog	Trace	--	-.01	0.003	6.0	0.002
Mist	0.05	0.002	0.10	0.25	55.5	0.024
Drizzle	0.25	0.01	0.20	0.75	92.6	0.04
Light Rain	1.00	0.04	0.45	2.00	138.9	0.06
Moderate Rain	4.00	0.16	1.0	4.00	277.8	0.12
Heavy Rain	15.00	0.59	1.5	5.00	833.3	0.365
Excessive Rain	40.0	1.6	2.1	6.00	1851.9	0.81
Cloud-burst	100 to 1000	4.0 to 40.0	3.0	7.00	4000 to 35000	1.75 to 15.30

* F. A. Berry, Jr., E. Bollay and N. R. Beers, Handbook of Meteorology, McGraw Hill (1945).

TABLE II SHOCK-FRONT ANGLES AND PRESSURE STEPS IN THE CASE OF 60-DEGREE APEX ANGLE CONES FIRED AT VARIOUS SPEEDS

Shot Number	Projectile Speed	Mach Number	Angle between conical part of bow shock front & line of fire*	Pressure ratio across the true conical part of the shock front**
	ft/sec	M	Degrees	P_1/P_o
1	4060	3.64	38.0	5.63
2	3690	3.29	38.8	4.76
3	3140	2.80	41.3	3.80
4	2910	2.60	42.3	3.42
6	2730	2.44	43.3	3.14
8	2510	2.24	45.5	2.78

* Cf. Fig. 11, p. 467, J. W. Maccoll, Proc. Roy. Soc. A, vol. 159, p. 459 (April 1937).

**Interpolated from the results of Table II, p. 285, G. I. Taylor and J. W. Maccoll, Proc. Roy. Soc. A, vol. 139, p. 278 (Feb. 1933).

(4) Not later than 2500 to 4000 μsec after the passage of a projectile, the rain drops always had broken up if initially they were within about 2 1/2 inches of the line of fire at the moment of firing. The ultimate breakup times were clustered about 2500 μsec in the cases of 20-mm shots and were nearer to 4000 μsec for 60-caliber conical-nose projectiles. However, before the elapse of 4000 μsec the drops had been overtaken by the blast of gaseous explosion products and there was some question as to the contribution of the latter to the breakup.

VI. Discussion

A. Shock Waves Produced by the Projectiles

The three types of projectiles were fired at supersonic speeds and any projectile travelling through air faster than the speed of sound produces a bow shock wave (see Reference 5). The surface of this shock wave is approximately conical and symmetric relative to the line of fire. The apex of the cone lies near the nose of the projectile and may be either just a little ahead of the nose or attached to it depending upon both the shape of the latter and the ratio of projectile speed to the speed of sound. The forward-most portion of the shock wave is its apex; from here the shock front bends back away from the direction of motion. In fact, the faster the projectile is moving, the more acutely its shock front bends back.

The shock wave separates one region of constant pressure, P_0, density and air velocity lying ahead of it from another region of relatively constant pressure, P_1, density and air velocity lying behind. In the cases which concern the projectiles fired against rain, the thicknesses of the transition regions were of the order of 10^{-3} to 10^{-4} cm (see References 6 and 7); i.e., the shock-wave thicknesses were much less than the diameters of naturally occurring rain drops (see Table I).

Of the three types of projectiles, the bluff-nose cylindrical ones produced bow shock waves which were the most intense (i.e., P_1/P_0 was largest) in regions very close to the nose; but in these cases the intensities fell off more rapidly with distance away from the line of fire (see Reference 8). On the other hand, most was known about the intensities of the shock waves produced by the conical-nose projectiles; values are given in Table II for both the pressure change across a bow shock front and its inclination as a function of projectile speed. These values are good for regions near the nose and had been obtained theoretically and had been checked by measurements (see References 9 and 10). Finally, the 20-mm projectiles were available for firing and offered a variation of type of bow shock which might be more comparable to that formed by the nose of a supersonic aircraft.

In the case of actual projectiles (see References 8 and 11), the pressure ratio P_1/P_0 always tends to fall off with increasing distance from the flow axis (i.e., the line of fire). In particular, it was found that (see Reference 11), for a 60° conical-nose projectile, the pressure ratio P_1/P_0 falls to roughly 0.7 of the values given in Table II at a point distant some 4R from the flow axis; R denotes the

cross-sectional radius of the projectile. A decrease in slope of the shock front relative to the direction of motion is another manifestation of the decrease in shock intensity with increased distance away from the flow axis. In the case of a full 60° conical-nose projectile, the decrease in shock slope is gradual and does not become very appreciable at regions closer than 4R to the flow axis (see References 9 and 11).

Shadow photographs of projectiles and their shock waves have been taken by the Ballistic Research Laboratory, Aberdeen, Md. One such photograph shows the shock waves produced by a 155-mm projectile travelling at a speed of Mach 2.479 (see Reference 12) and very little decrease in the slope of the bow shock front is evident out to 8R. However, this photograph is not directly applicable to those projectiles which were fired through the rain drops because it shows a more "streamlined" projectile and the nature of flow around a supersonic projectile is such that any abrupt changes in shape create secondary effects which cause the bow shock wave to fall off more rapidly.

B. Period of Small Surface-Tension Oscillations

The theory of small surface-tension oscillations of a liquid drop about a spherical form has been worked out by Lord Rayleigh (see Reference 13). The shape of the surface of the oscillating drop can be expressed as a superposition of several harmonically time-dependent deformations each characterized by a particular Legendre polynomial. The most important mode of oscillation occurs for the Legendre polynomial of order $n = 2$; this means that the drop configuration oscillates between a dumbbell shape and a flattened sphere, where the flattened regions are slightly concave. Values of the period of oscillation for $n = 2$ are set out in Table III.

TABLE III SMALL SURFACE-TENSION OSCILLATIONS

Diameter of Water Drop mm	Period of Oscillation T μsec
1.0	2900
1.5	5300
2.0	8200

It is interesting to note that the observed times between a typical impact of a bow shock wave with a rain drop and drop breakup are of the same magnitudes as the time required by a small surface-oscillation to change a sphere into either the slightly dumbbell-type configuration or into a flattened sphere; i.e., for water drops whose sizes are the same as in the simulated rain, $(1/4)T$ equals 1000 μsec to 4000 μsec. Moreover, in certain motion-picture sequences rain drops having been struck by a bow shock wave appeared to grow into flattened spheres and ultimately into a short of doughnut-shaped objects before breaking up.

In at least one case (see shot No. 20), a drop of rain having absorbed energy from the impact of a shock wave changed into a dumbbell shape before breaking up. However, since the theory of surface-tension oscillations only applies to small oscillations, it cannot be concluded without further consideration that the shock-wave impacts excited surface oscillations in the rain drops and that these oscillations were of sufficient amplitudes to break up the drops.

The time of transit of a compression wave through the body of a typical rain drop should have been

$$(1.7 \text{ mm})/v = 1.2 \text{ μsec},$$

where v denotes the velocity of sound in liquid water (v = 4750 ft/sec). The fact that the drop breakup times were some thousands of times greater than 1.2 μsec is further evidence that the breakup mechanism is related to a surface effect.

C. Interpretation of Dark Clouds on Some Pictures

In certain photographs a dark cloud suddenly appeared and slowly dissipated. Such clouds always formed adjacent to the blurred image of a projectile and in a region which previously had contained a rain drop. In all cases it was possible to associate the formation of one of these clouds with a direct impact of a projectile and a rain drop. However, the transformation of a rain drop of 1.7-mm diameter into a cloud some hundreds of times larger in area was surprising and, consequently, some explanation was sought.

Suppose that in the optical setup depicted in Figure 2, there was a local anomaly in the refractive index throughout some region of the order of a cubic inch in size and which was located somewhere between the two collimating lenses. Let the anomalous refractive index be denoted by $n + \Delta n$ compared to an index equal to n everywhere else. Light which passed in and out of the anomalous region would be refracted so that it no longer would be brought to a focus at the center of the iris diaphragm of the camera. According to the laws of refraction, it can be shown that the light which passed through the anomalous region would be focused on a point that is at a distance δ from the optical axis of the camera. The magnitude of δ is given by the following relation:

$$\delta(\text{inches}) = 60\,\epsilon;$$
$$\epsilon \cong (\Delta n/n)\tan\phi;$$

here ϕ denotes the angle between the incident ray and a normal to the surface of the anomalous region. If the diameter of the camera aperture were 0.1 inches, then a value of Δn equal to or greater than $(0.05/60)\cot\phi = 0.000833\cot\phi$ would be necessary to reflect light out of the camera.

The difference between the refractive index of water and air is 0.333. Since this is the equivalent Δn for a rain drop, the latter would refract light out of the camera for all angles of incidence down to $\phi = \text{arc cot}\,(0.333/0.000833) = 0.1°$ and this effect must have been responsible for making the rain drops appear as little dark circles.

On the other hand, water vapor has a refractive index of 1.00025 compared to n = 1.00029 for air. In order for water vapor to refract light out of the camera, the following relation must be satisfied:

$$60 \times (1.00029 - 1.00025) \tan \phi \gtrsim 0.05 \text{ inches}$$

or

$$87^\circ \lesssim \phi < 90^\circ.$$

Physically this means that, even if a region were to be 100% water, only a portion of its periphery corresponding to $87^\circ \lesssim \phi < 90^\circ$ would be able to refract light out of the camera.

Thus, the dark clouds which appeared on certain photographs must be due to sizeable variations in refractive index such as can be attributed to liquid water itself. Consequently, these clouds are indications that a rain drop is atomized into liquid spray by impact with a supersonic projectile.

VII. Acknowledgment

The cooperation of the following persons is gratefully acknowledged. The Fastax camera equipment was supplied and set up by George Hays of the Boeing Airplane Company Power Plant Unit. During most of the runs the camera was operated by either W. Tribou or H. Tacker. The guns were set up and fired under the direction of Andy Duzsik, Bomber Weapons Unit.

REFERENCES

(1) Bulletin on Fastax High-Speed Motion Picture Cameras, Wollensak Optical Co., Rochester 21, New York.

(2) Model J-410 Fastax Control Unit ("The Goose"); Instruction Book No. 1262, Industrial Timer Corporation (Oct. 15, 1948).

(3) J. W. Strutt (Lord Rayleigh), Theory of Sound, Dover (1945) vol. II, p. 362.

(4) J. W. Maccoll, Proc. Roy. Soc. A, Vol. 159, p. 459 (April 1, 1937).

(5) R. Courant and K. O. Friedrichs, Supersonic Flow and Shock Waves, Interscience (1948).

(6) H. W. Liepmann, A. Roshko and S. Dhawan, On Reflection of Shock Waves from Boundary Layers, NACA Report 1100 (1952).

(7) A. E. Puckett and H. J. Stewart, Quar. of Appl. Math., vol. VII, p. 457 (Jan. 1950).

(8) J. H. Clegg and W. E. Bergdolt, Jour. of Appl. Phys., vol. 24, p. 1389 (Nov. 1953).

(9) G. I. Taylor and J. W. Maccoll, Proc. Roy. Soc. A, vol. 139, p. 278 (Feb. 1933).

(10) J. W. Maccoll, Proc. Roy. Soc. A, vol. 159, p. 459 (April 1937).

(11) F. D. Bennett, W. C. Carter and V. E. Bergdolt, Jour. Appl. Phys., vol. 23, p. 453 (April 1952).

(12) T. von Karman, Jour. of the Aeronaut. Scies., vol. 14, p. 373 (July 1947).

(13) See page 373 of Reference (3) or H. Lamb, Hydrodynamics, Dover (1945), p. 475.

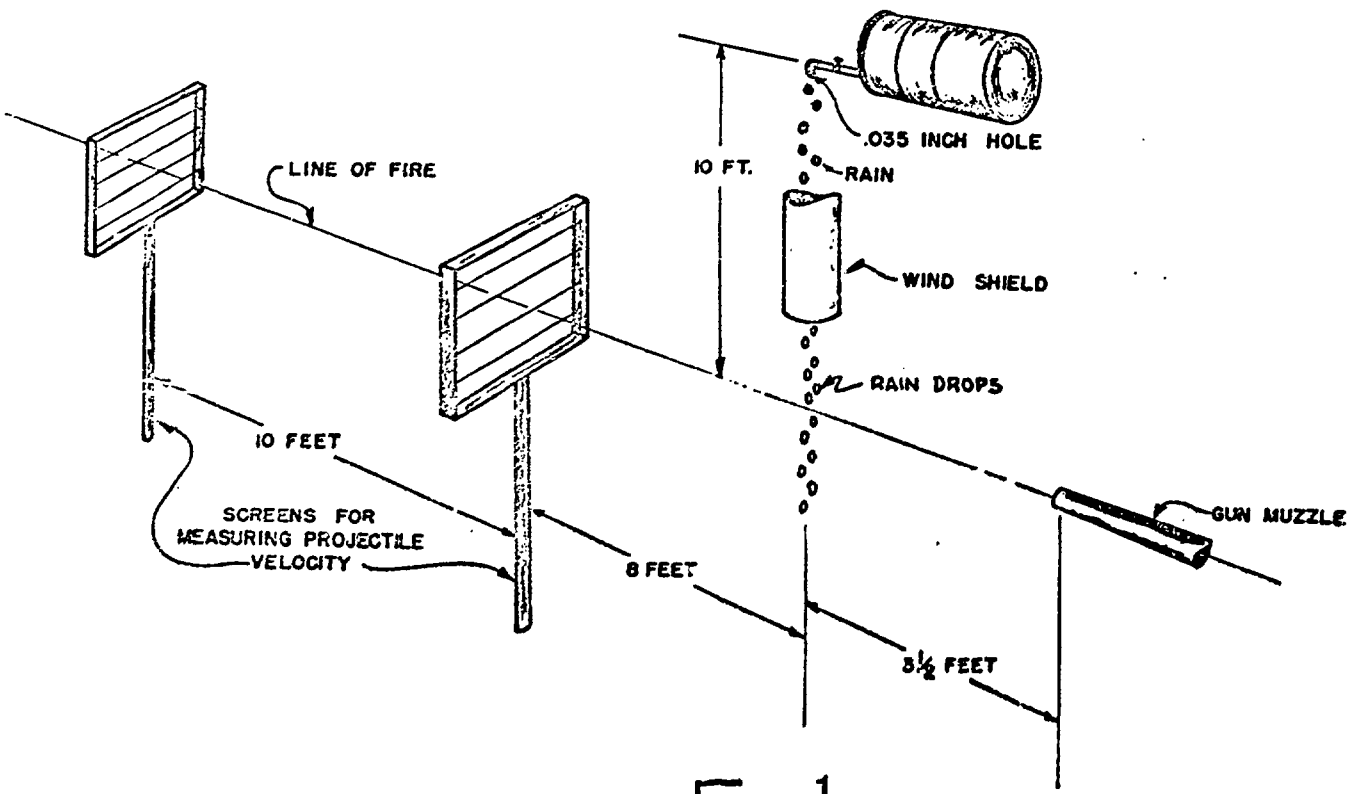

Fig. 1

ARRANGEMENT FOR STUDYING EFFECTS OF PROJECTILE SHOCK WAVES ON RAIN DROPS

(VIEW ALONG LINE OF FIRE)

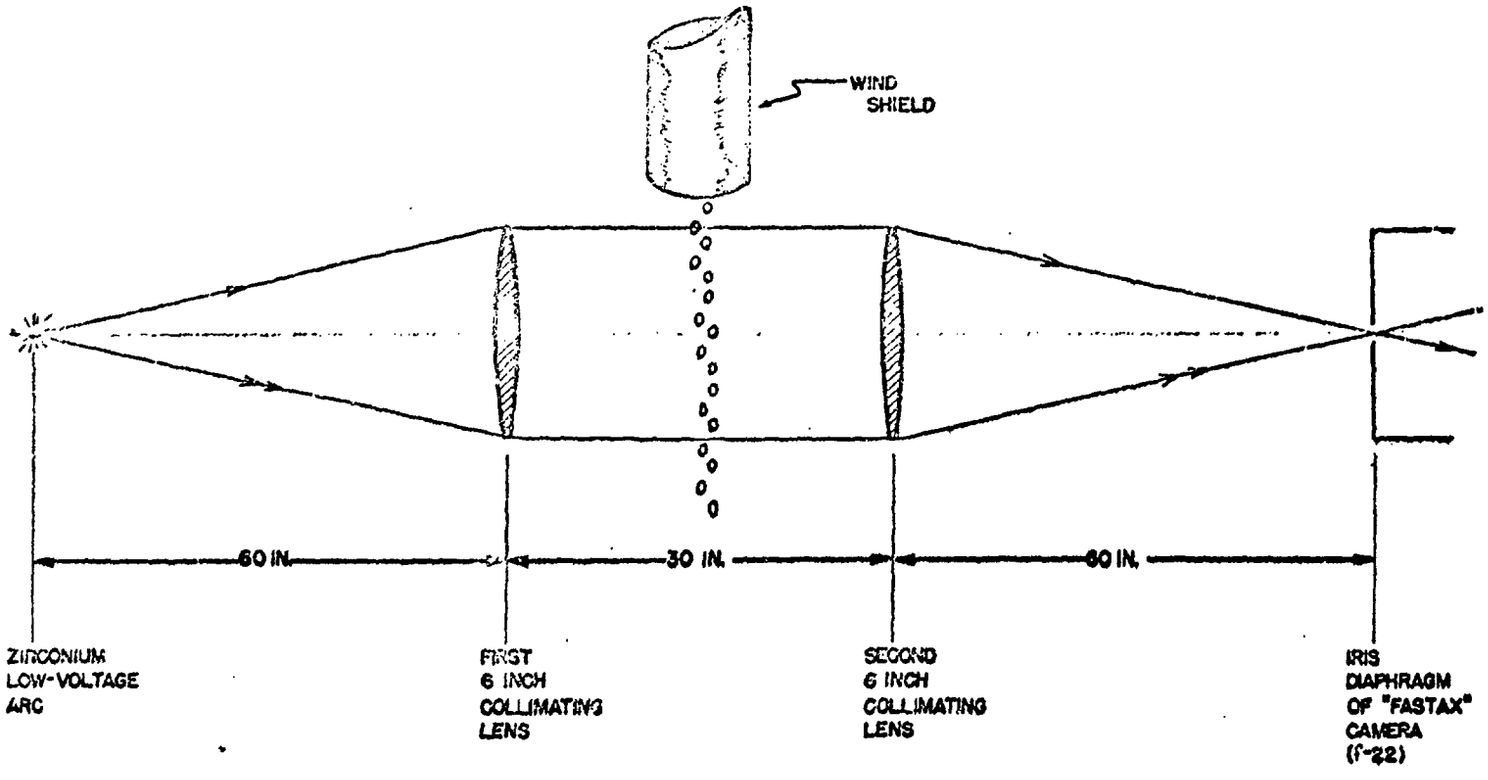

FIG. 2

ARRANGEMENT FOR STUDYING EFFECTS OF PROJECTILE SHOCK WAVES ON RAIN DROPS

(VIEW ALONG AXIS OF CAMERA)

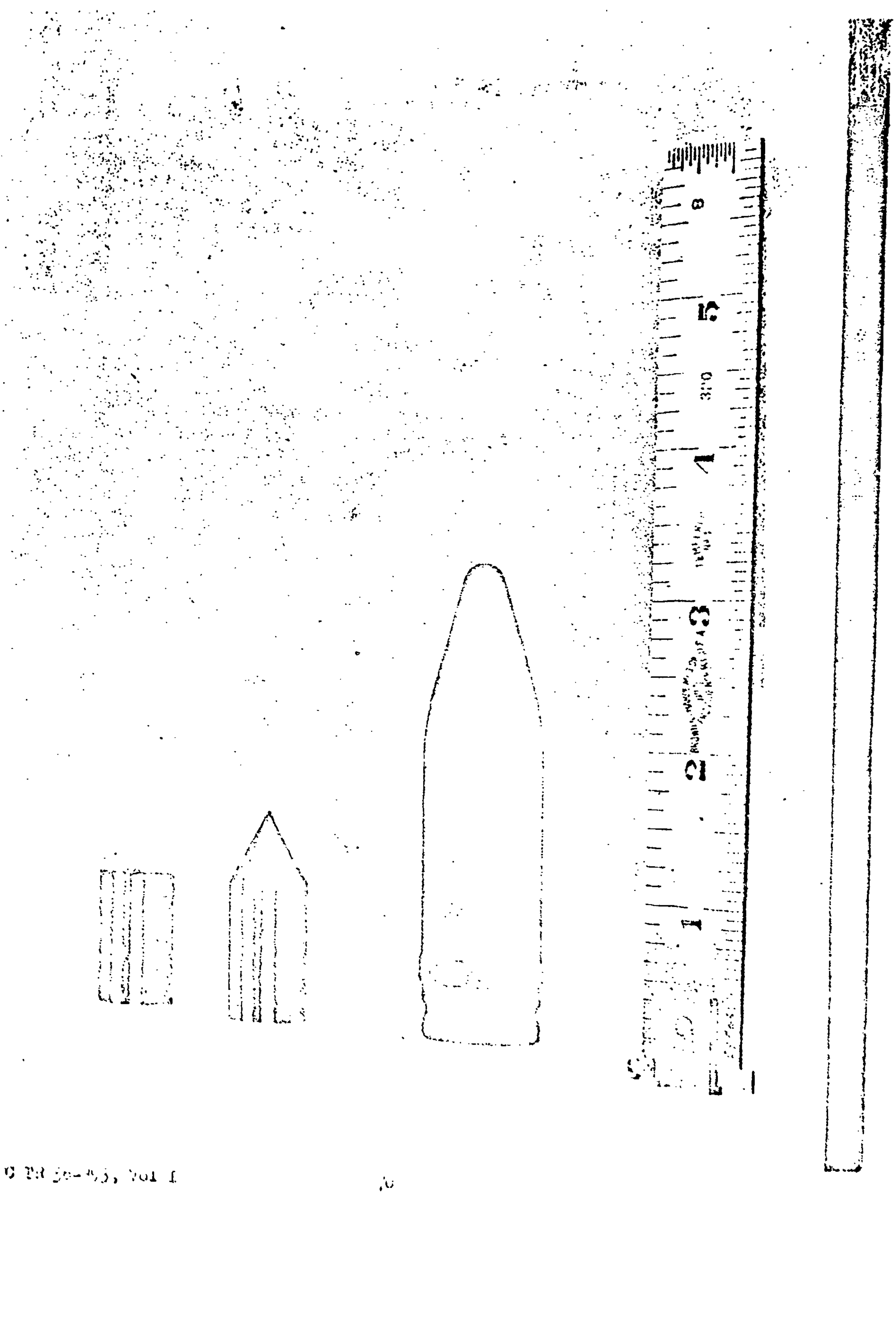

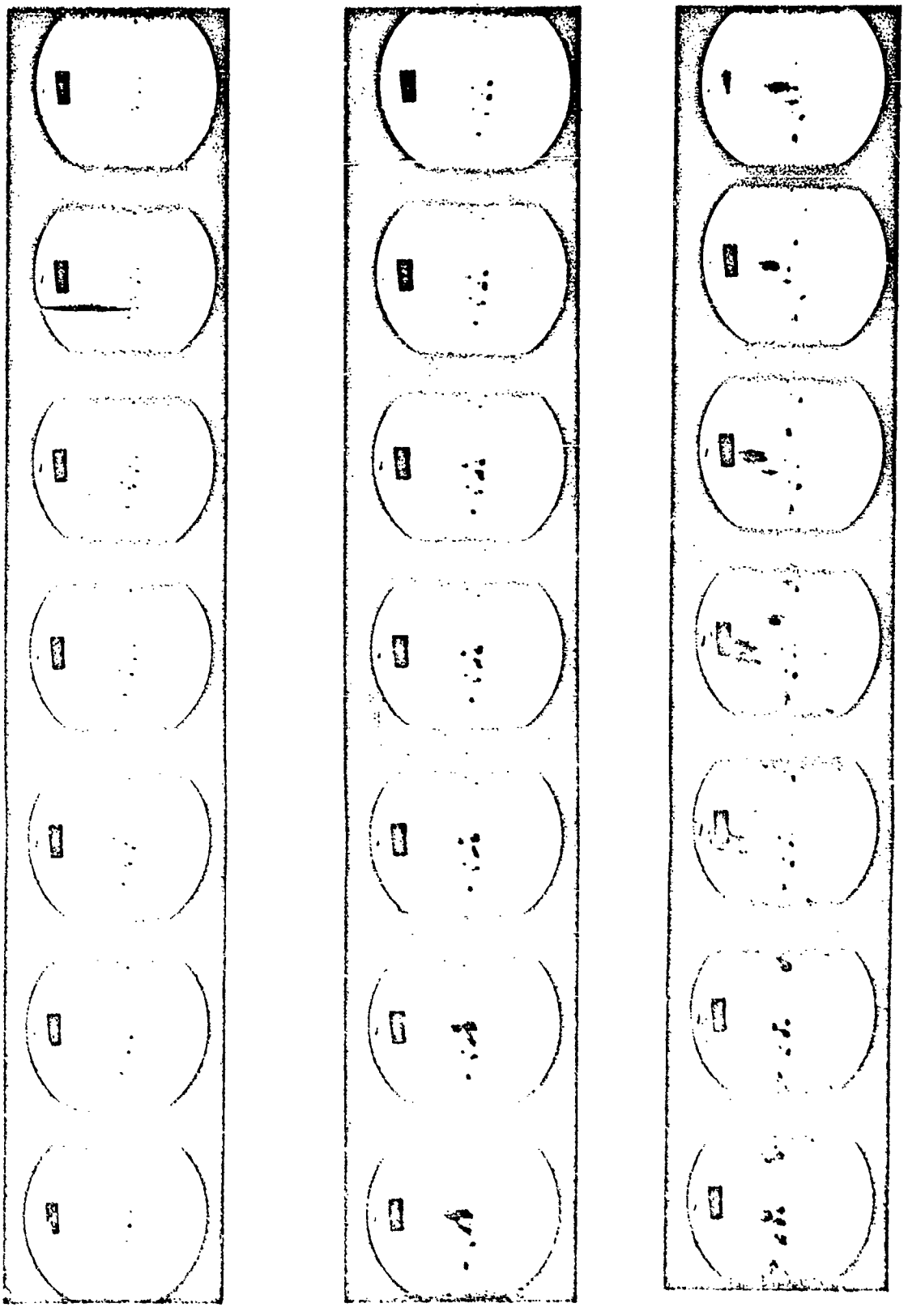

Shot No. 1. [illegible] Projectile 60-Caliber with 60° Nose Angle and 4000 ft/sec

[illegible] projectile [illegible]-caliber with 60° Full Arex Angle
[illegible] ft/sec

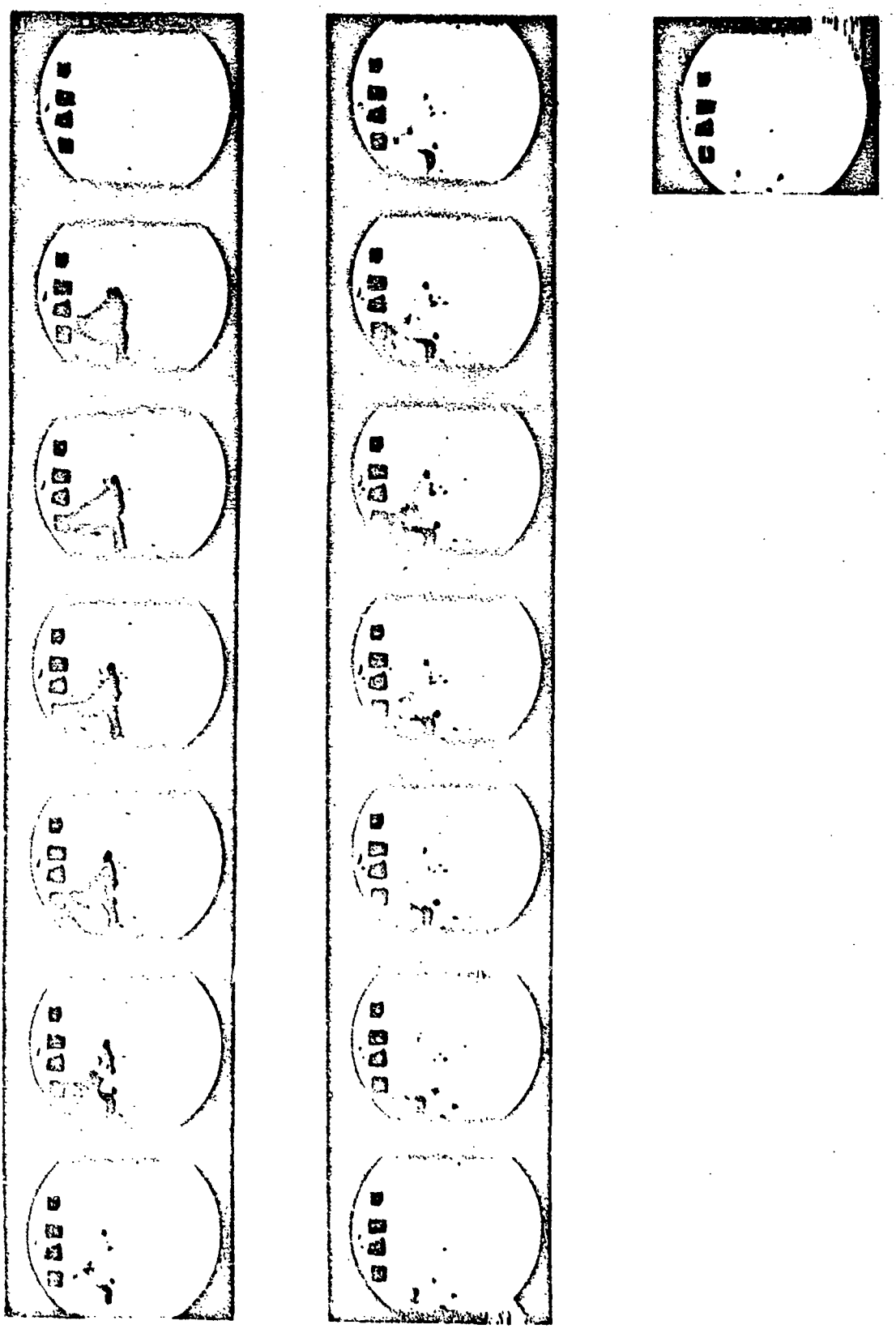

Shot No. 4. Conical-Nose Projectile 60-Caliber with 60° Full Apex Angle Speed 2910 ft/sec

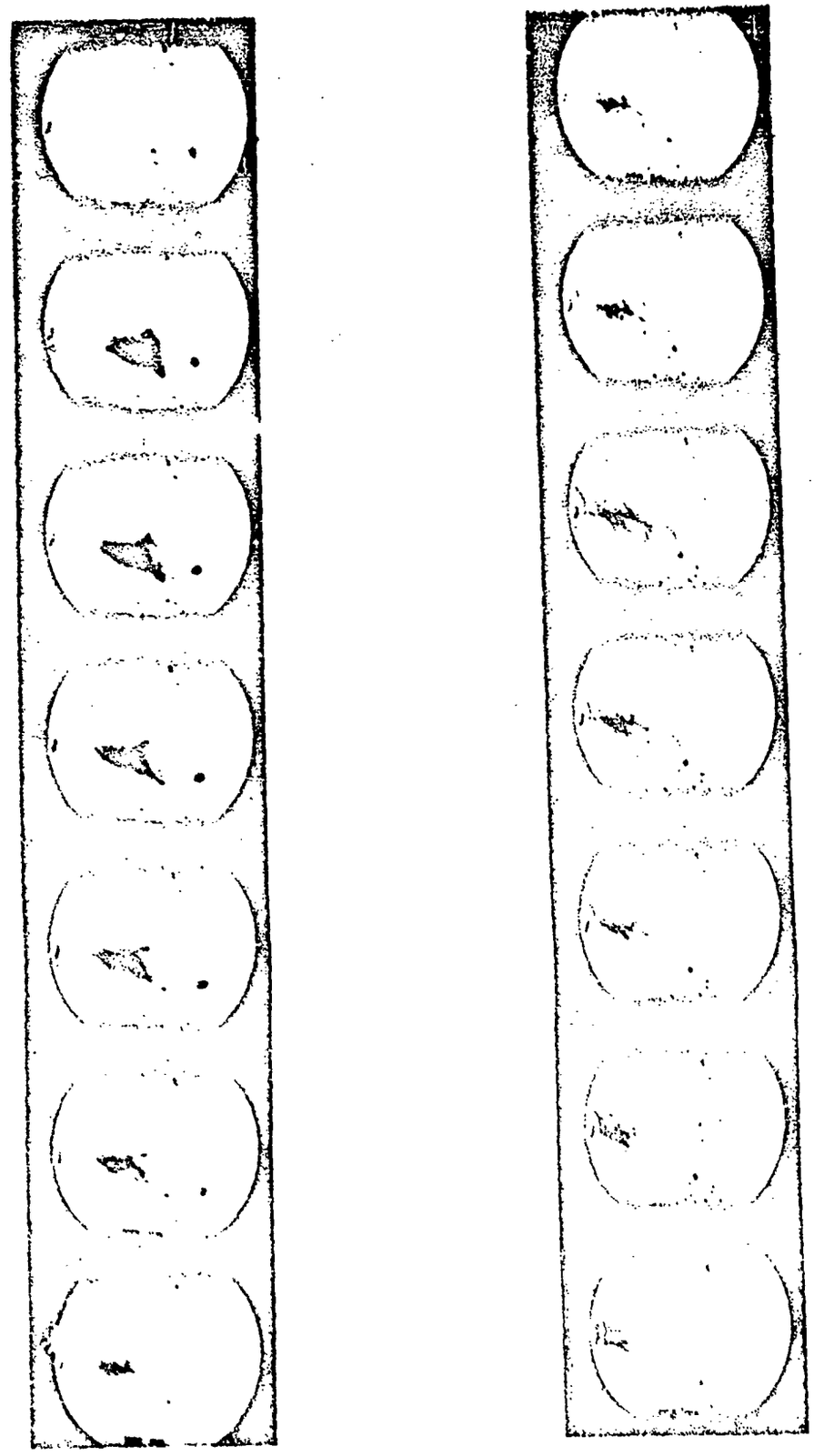

Shot No. 6. Conical-Ogive Projectile 60-Caliber with [illegible] Full Apex Angle
[illegible] Ft/sec

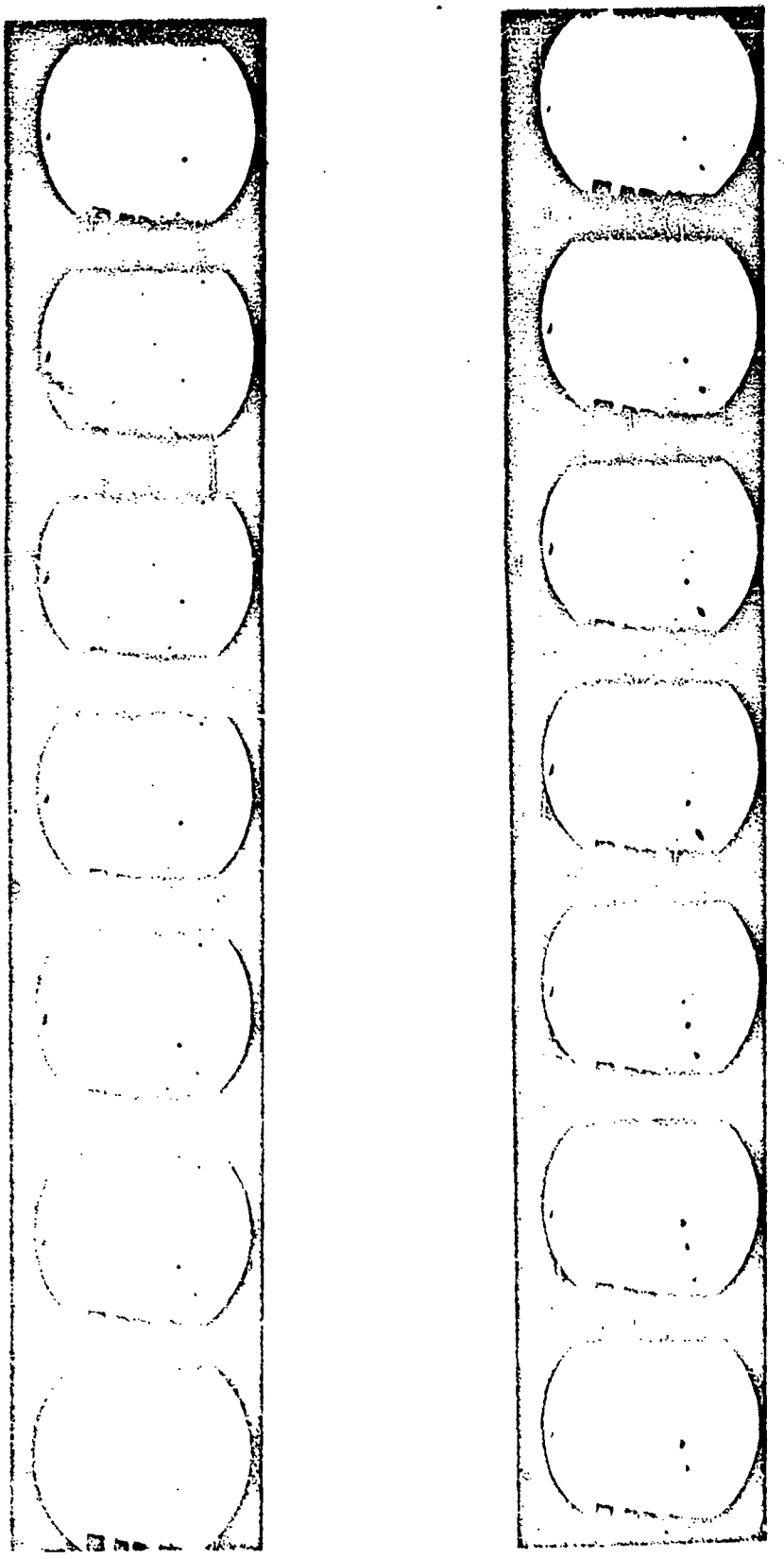

Shot No. 8. Conical-Base Projectile 60-Caliber with 60° Full Apex Angle
Velocity 2510 ft/sec

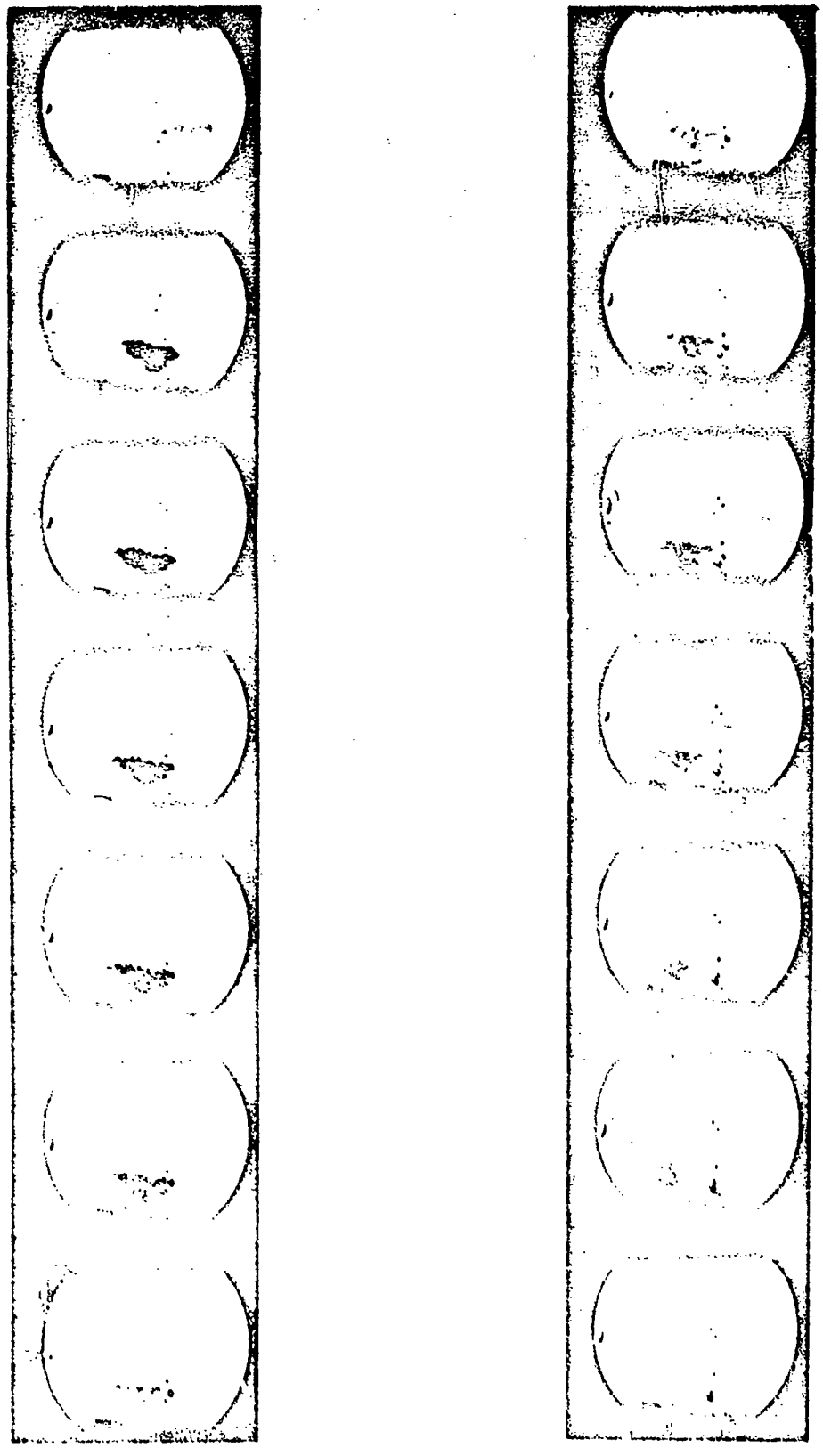

Shot No. 10. Conical-Nose Projectile 60-Caliber with 60° Full Apex Angle
Speed 2680 ft/sec

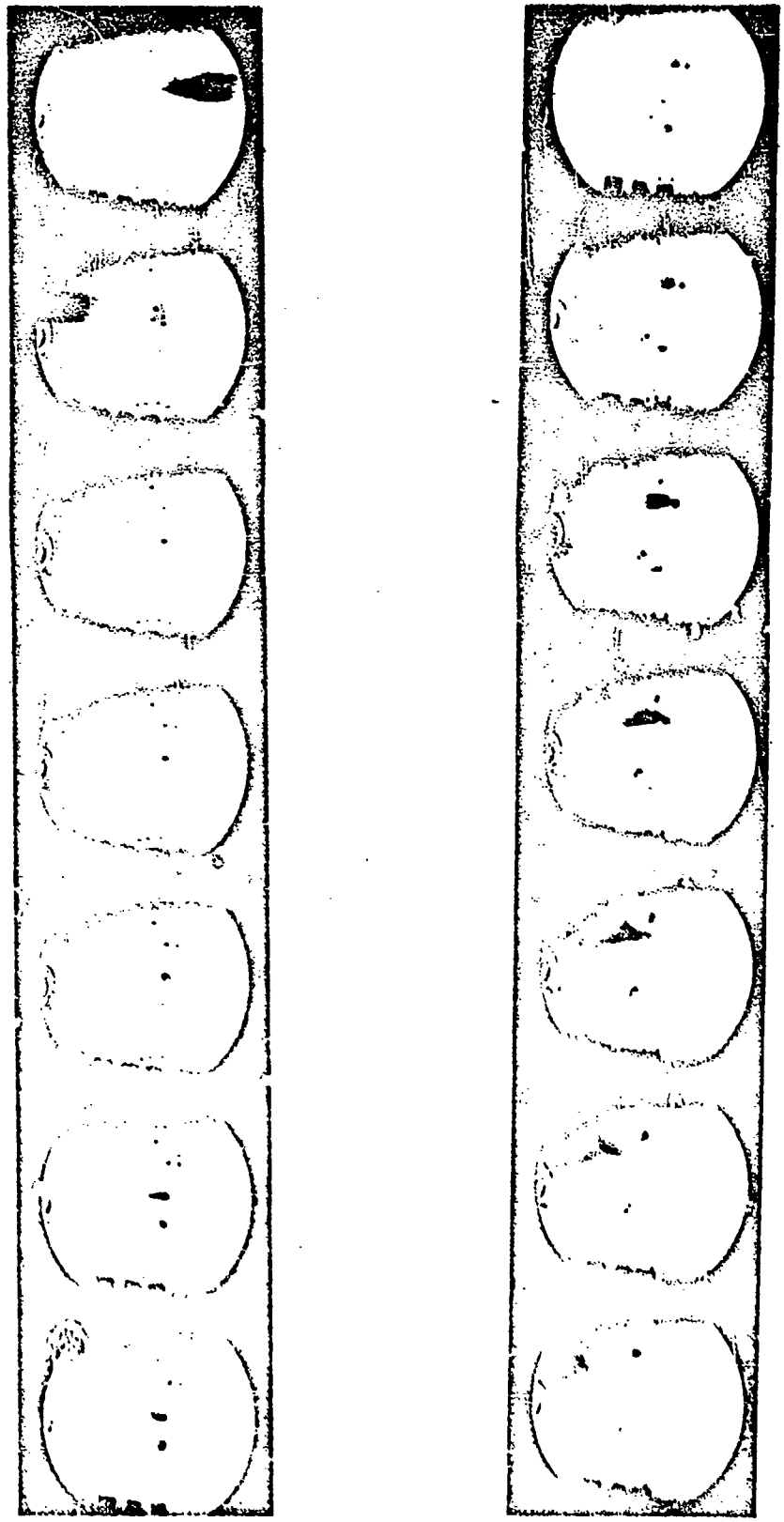

Shot No. 14. 20-mm Projectile, Speed 2660 ft/sec

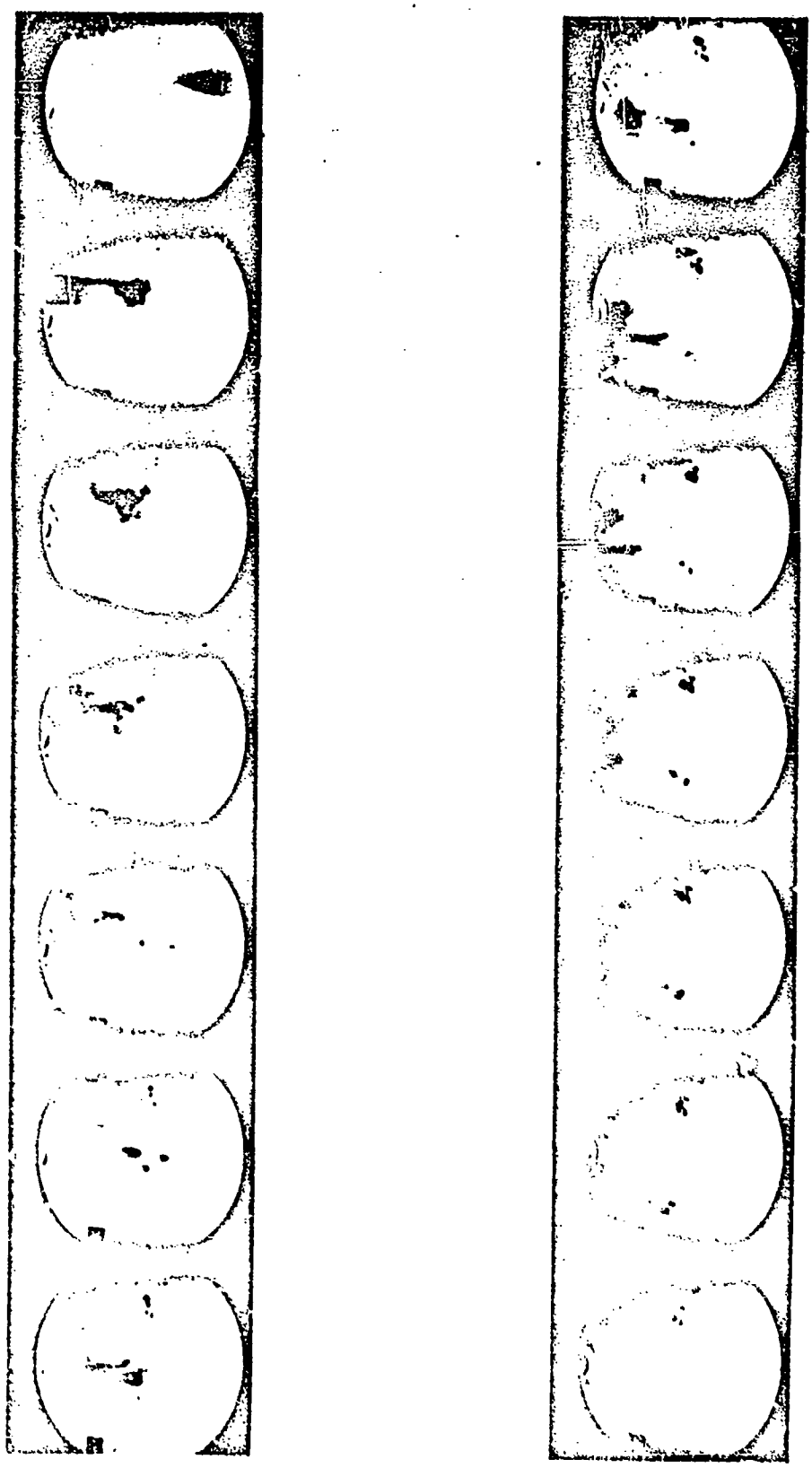

Shot No. 15. 30-mm Projectile, Speed 2720 ft/sec
Vol. I

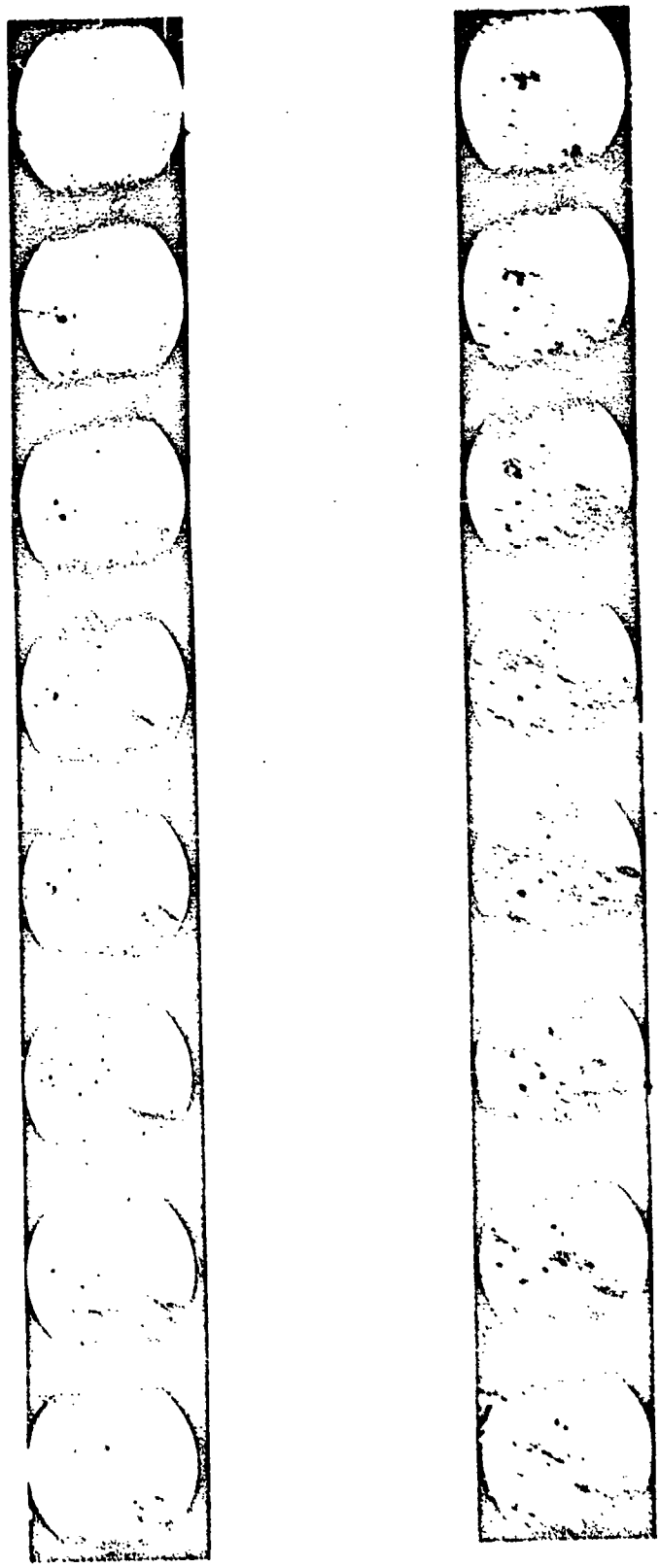

Shot No. 19. Fluff-Nose Cylindrical 60-Caliber, Speed 1900 ± 100 ft/sec

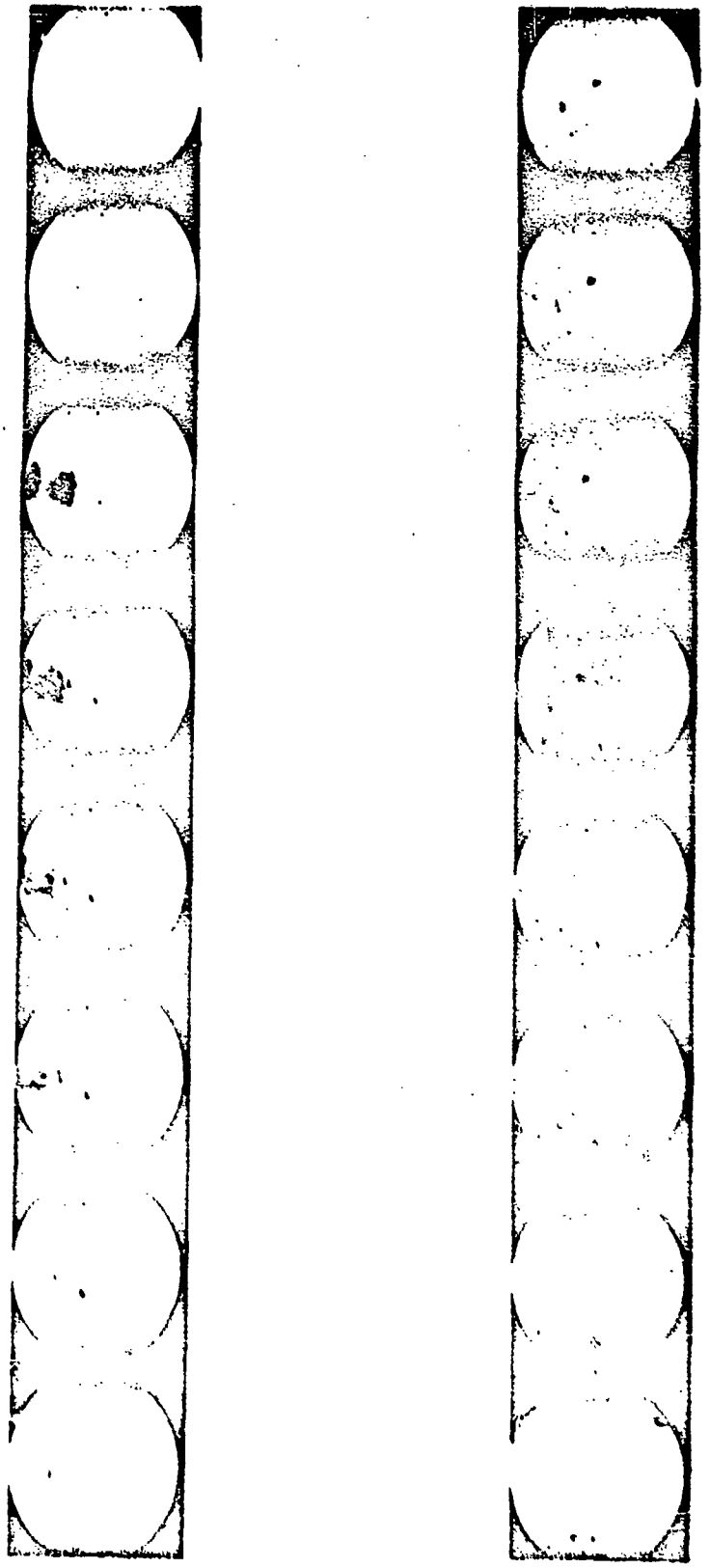

Shot No. 20. Bluff-Nose Cylindrical 60-Caliber, Speed 1900 ± 100 ft/sec

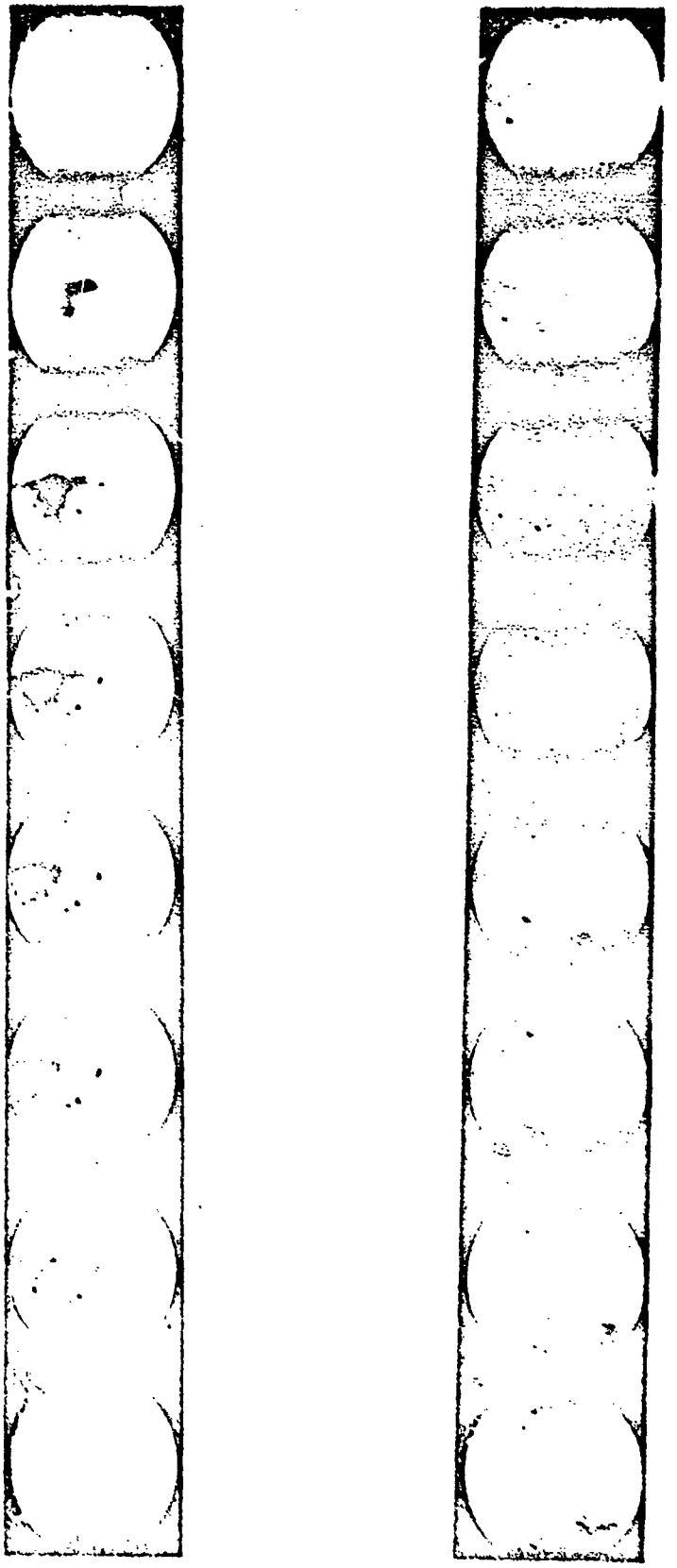

Shot No. 21. Bluff-Nose Cylindrical 60-Caliber, Speed 1900 ± 100 ft/sec

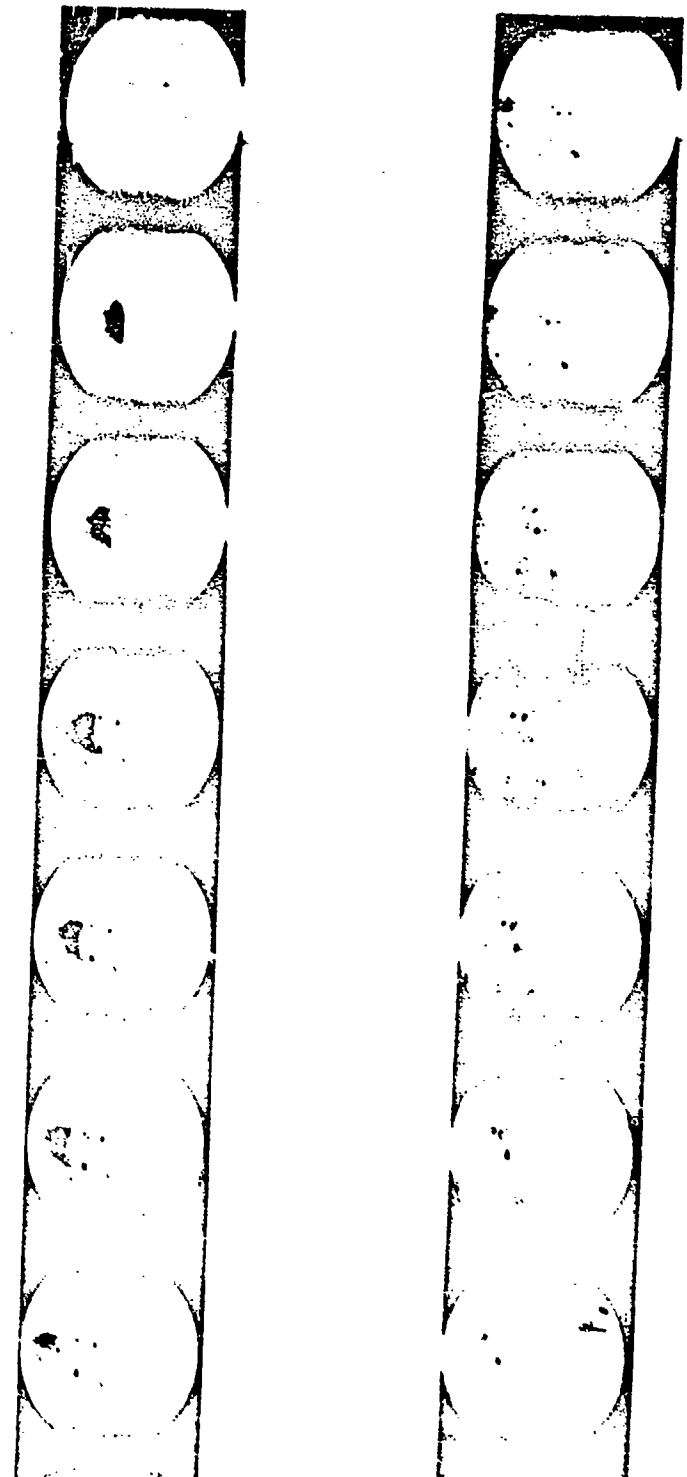

Shot No. 22. Bluff-Nose Cylindrical 60-Caliber, Speed 1900 ± 100 ft/sec

THREE DIMENSIONAL ERROR PREDICTION

George M. Hahn and Edmund J. Pinney*
Dalmo Victor Company, San Carlos, California

I. INTRODUCTION

In a previous paper[1] presented by members of this organization, a number of methods for theoretically predicting the change in boresight due to the presence of the radome were described. One of the methods, referred to in the reference as "Scattering Technique", will be discussed in some detail in the present paper.

The basic idea of this method is to regard the radome as a perturbation source, determine the electromagnetic fields due to this source and then combine them with the fields due to the antenna without the presence of the radome. It is then possible to determine the boresight shift by comparing the two field configurations. The electromagnetic formulation is of necessity fully three-dimensional; none of the usual optic or plane wave approximations are made, and flat panel transmission and reflection coefficients are not employed.

II. DERIVATION OF THE BASIC INTEGRAL EQUATION

Maxwell's Equations for electromagnetic fields in a dielectric of volume V, and whose time variation is of the form $e^{-j\omega t}$, are:

$$\bar{D}=\epsilon\bar{E} \qquad \bar{B}=\mu\bar{H}$$

$$\nabla\times\bar{E}-j\omega\mu\bar{H}=0 \qquad \nabla\times\bar{H}+j\omega\epsilon\bar{E}=0 \qquad (1)$$

$$\nabla\cdot\bar{E}=0 \qquad \nabla\cdot\bar{H}=0$$

where all symbols have their usual meaning.

Similar equations hold in free space, if ϵ and μ are replaced by ϵ_0 and μ_0 respectively.

According to Stratton[2], the electromagnetic fields in this problem are the same as those that would be generated if no dielectric were present at all, but instead a distribution of virtual currents and charges. Let J be the virtual current distribution inside V, σ the virtual surface charge on S, the surface bounding the volume V and K the virtual surface current distribution on S. Here

---

* Department of Mathematics, University of California, Berkeley, Calif.

1. Damonte, Hahn and Gunter, "Error Prediction Methods", Proceedings of the Radome Symposium, Vol. III, June 1955
2. J. A. Stratton, "Electromagnetic Theory", McGraw Hill Co., 1941

$$J = -j\omega\left(\frac{\epsilon\mu}{\mu_0} - \epsilon_0\right)\bar{E} \tag{2}$$

while σ and $\bar{K}$ are determined from the boundary conditions on S. The scalar and vector potentials can then be written:

$$\phi_p(P) = \frac{1}{\epsilon_0}\int_S \sigma(Q)\,\frac{e^{-jk_0R}}{4\pi R}\,dS \tag{3}$$

$$\bar{A}_p(P) = \mu_0\int_V J(Q)\,\frac{e^{-jk_0R}}{4\pi R}\,dV + \mu_0\int_S \bar{K}(Q)\,\frac{e^{-jk_0R}}{4\pi R}\,dS$$

where P and Q represent field and source points respectively and

$$k_0 = \omega\sqrt{\mu_0\epsilon_0} \tag{4}$$

The subscript p indicates that we are referring to the perturbation fields; these can be calculated from the perturbation potentials in the usual manner.

For the case $\mu = \mu_0$, one finds for the electric field:

$$\bar{E}_p(P) = (K-1)\left[k_0^2\int_V \bar{E}(Q)\,\frac{e^{-jk_0R}}{4\pi R}\,dV - \int_S \bar{n}\cdot\bar{E}(Q)\,\nabla\frac{e^{-jk_0R}}{4\pi R}\,dS\right] \tag{5}$$

with $K = \epsilon/\epsilon_0$, $\bar{E}(Q)$ the total electric field, and $\bar{n}$ the outward normal to S. Equation (5) is an integral equation relating the perturbation fields to the antenna fields and the physical properties of the radome. Since $\bar{E}(Q) = \bar{E}_p(Q) + \bar{E}_0(Q)$ the equation must be used for two separate calculations:

a) determination of $\bar{E}(Q)$, i.e. the effect of the presence of the radome on the field in the volume occupied by the radome itself,

b) calculation of $\bar{E}_p(P)$, i.e. the far field effects of the perturbation sources.

For the latter calculation, the following approximation is usually made:

Let O be some convenient origin in or near V and let $\bar{r} = \bar{m}r$ be the vector from O to P, $\bar{m}$ being a unit vector. If $\bar{q}$ denotes the vector from O to the point of integration, Q, then:

$$R = r - \bar{m}\cdot\bar{q} + O(1/R) \tag{6}$$

Retaining only the first two terms, equation (5) reduces to:

$$E_p(P) \cong -(K^2-K_o^2)\frac{e^{jk_o r}}{4\pi r}\,\bar{m}\times\left(\bar{m}\times\int_v \bar{E}(Q)\,e^{-jk_o \bar{m}\cdot\bar{q}}\,dV\right) \qquad (7)$$

III. TECHNIQUES OF SOLVING THE INTEGRAL EQUATION

It is clear that one cannot hope to obtain solutions in closed form to equation (5) or to equation (7). The starting data are the measured fields $(\bar{E}_o)$ in numerical form. While it would be possible to fit these data in some polynomial approximation, the complicated geometry of most radomes would still prevent one from exactly solving the equations.

Numerical methods must therefore be resorted to, and three different methods were considered by the authors.

a) The Grid Method:

Suppose $\bar{F}_p(P)$ denotes an approximation to $\bar{E}_p(P)$ then $\bar{F}(P) = \bar{E}_o P + \bar{F}_p(P)$ is an approximation to $\bar{E}(P)$

It is then possible to define an error term

$$\varepsilon = \int_V \bar{R}(Q)\cdot\bar{R}^*(Q)\,dV \qquad (8)$$

where the $\bar{R}$'s are defined in such a manner that they vanish when $\bar{F}(P) = \bar{E}(P)$. The radome volume is now covered by a grid of N points sufficiently close together; the approximation $F_p(P)$ is assumed as due to contribution from the N points:

$$\bar{F}_p(P) = \sum_{n=1}^{N} a_n \zeta(P) \qquad (9)$$

The error term then becomes

$$\varepsilon = \sum_{m=1}^{N}\sum_{n=1}^{N} R_{mn}\,a_m\,a_n^* \qquad (10)$$

which is minimized by equating the $\frac{\partial \varepsilon}{\partial a_n}$ and $\frac{\partial \varepsilon}{\partial a_n^*}$ to zero for $n = 1 \cdots N$. This gives N linear equations in the N complex a_n's; solving these the results are then substituted into (9) and $\bar{F}_p(P)$ is obtained.

b) Stationary Phase Approximation

The method to be outlined here depends on the fact that the integrals in the integral equation have integrands involving the product of $\frac{e^{jk_o R}}{4\pi R}$ and the internal electric field. Now if the internal

electric field behaves locally like a plane wave, it contains a factor e^{jkx}, where x is the coordinate in the direction of the wave. The two exponential factors are responsible for the change in phase as the point of integration moves about in the dielectric shell.

Now consider a straight line drawn outward from the point of observation $R=0$. Suppose for simplicity that $x=0$ when $R=0$. Then on this line the ratio R/x remains constant, and the exponential argument $jk_0x + jkx$ increases linearly as R increases. However on some lines the factor of proportionality is zero, so the phase remains constant. These are all the lines lying on a cone (which might be called the "cone of stationary phase") with axis parallel to the direction of propagation of the interior electric field, and elements inclined to the axis at an angle equal to the compliment of the critical angle for the dielectric. On one side of this cone the phase increases as R increases, and on the other side the phase decreases as R increases. The contributions to the integral from the region near the cone add together and reinforce each other. The contributions from the region well away from the cone have a tendency toward mutual cancellation.

The idea then is to approximate the dielectric sheet locally by a flat sheet which fits as closely as possible to the curve of intersection of the cone of stationary phase and the surface of the dielectric sheet, and to evaluate the integrals in the integral equation for that flat sheet, and on the basis of the assumption that the electric field is essentially plane in the region of importance in the integral. This is probably not a bad assumption because the cone of stationary phase occupies only a limited region near the point of observation.

This gives rise to what may be considered merely a flat plate theory. However, it is not the usual sort of flat plate theory. In the usual flat plate theory the dielectric shell is approximated by a flat plate whose two sides are tangent to the shell in the local region of interest. In that theory the plate is held fixed in the determination of the field at all points of the local region. In the present theory, on the other hand, the orientation and thickness of the fitting flat plate change from point to point, and depend on other properties of the shell than its thickness alone. This may be expected to give a more accurate theory than the usual flat plate theory.

c) Lumped Fields Method:

Another approach is to divide up the radome into a number of circular disks of the order of a wavelength in diameter. The point is to "lump" the local behavior of the electric field in each disk in a way one can handle, and then to use the basic integral

equation to tie together the fields in the different disks. To do this one must first express the electric field throughout each disk in terms of the field at the center. Certain assumptions are required to do this. One may assume that the internal field in the disk is approximated by two plane waves whose directions of propagation may be set at will, but may, in particular, be given the directions that the internal waves in a flat sheet would take when acted upon by the local magnetic field considered as a plane wave. If that is done, one can apply a good deal of plane sheet theory to simplify calculations of the local fields.

It is then possible to calculate the total field at the center of each disk by integrating over each disk and then summing over all the disks. The problem then reduces to a set of linear equations in the unknown fields at the centers of the disks. Rather than attempt to solve these directly, one can again resort to a least squares and successive approximation theory, as described in Paragraph III a).

The three methods just discussed are all of considerable complexity. The grid method, to provide sufficient accuracy, requires an excessively large number of points taken. As a result, the storage requirements exceed the capacities of available computing machines. The stationary phase method is hampered by the difficulty of fitting the sheets to the cones of stationary phase. This process proved so difficult that the approach was abandoned completely. The lumped field technique looks the most promising of the three.

It should be pointed out that the existence of a unique, bounded solution to equations (5) and (7) is by no means obvious. The existence of the singularity in the term $\frac{e^{ikR}}{R}$ makes the question non-elementary, from a mathematical point of view. However, the results mentioned in the following paragraph tend to show that such a solution does exist, a condition which one would expect from the physics of the situation.

IV. RESULTS

To test the possibility of a successive approximations scheme as suggested in paragraphs III a) and c) above, the following experiment was carried out. A cylindrical polystirene (ϵ=2.5) ring, large compared to the wave length was placed in front of a parabolic reflector transmitting at X-band. The resulting pattern was measured in the E plane of the antenna. Three points of the pattern were then computed using the iterative scheme outlined in III c), on the basis of one plane wave only and then for the next two higher approximations. In each case the higher order approximations were successively closer to the measured values than the low order approximations.

At the present time computations are being carried out at WADC to test the method on a radome; unfortunately no results have become available as of the date of this paper.

The authors would like to thank Mr A. Gaetano for making the measurements, and Dr. C. B. Barker and his group at Hughes Aircraft Company for making available a considerable amount of antenna and radome data. The work was performed under Contract AF 33(616)-2524 with WADC.

RADOME RAIN EROSION TESTING
BY MEANS OF SUPERSONIC SLEDS

M/R 16-875 May 1956

Prepared by

RAYTHEON MANUFACTURING COMPANY
MISSILE SYSTEMS DIVISION
Bedford, Massachusetts

for

THE OHIO STATE UNIVERSITY
WRIGHT AIR DEVELOPMENT CENTER
RADOME SYMPOSIUM
Columbus, Ohio
June 4, 5, and 6, 1956

Prepared by:
Chester L. Smith

ABSTRACT

A method is presented of determining the sled travel in a known artificial rain field required to obtain the same erosion damage (if any) encountered by a missile in free flight in any given natural rain. The conditions of test and the mathematics of simulation are discussed. Methods used to determine the "worst case" of erosion, which is used to determine the maximum sled travel, are shown, and methods of rain field sampling to obtain droplet size, distribution, and rainfall rate are given.

1. INTRODUCTION

The severe damage sometimes suffered by flying in weather conditions where the air is full of particles poses a problem in the design of any moving vehicle. Three types of airborne particles are known to cause damage. (1) rain, (2) hail and (3) sand. This discussion will be confined to the case of rain except for some general comments on the relative importance of the other two particle classes.

In order to obtain specific information about the relative rain erosion resistance of various radome materials three main attacks on the problem have been made by various laboratories: (1) Whirling Arm [2,6] (2) Flight in natural rain [6] and (3) Ballistic test in spray field. [2] The whirling arm technique, as it is currently performed, is good subsonically. The flight through natural rainfall by an aircraft carrying samples is a dangerous operation and the results, while demonstrating the existence of erosion, are not quantitative, since radar studies have shown natural rains to be non-homogeneous. The ballistic method is good for supersonic uses, provided that a correlation between natural rains and the spray field can be given. The small size of the test specimen and the few impacts made with droplets in this method make an interpretation of the integrated effect very difficult.

A fourth method, pioneered by Dittmann [2] and others at Convair is the supersonic sled. A full size article, say a radome, is mounted on a rocket propelled sled similar to those used for other captive high speed tests and fired through a spray field at a speed near Mach 2. The problem is to correlate the sled test with an equivalent natural rainfall. Since neither the particle distribution in the spray field nor the time velocity history of the sled run are precisely the same as the quantities of a free firing in natural rain, some means of relating them must be found in order to interpret the results.

2. METHOD OF TEST

2.1 The Sled

The test vehicle is a two-unit sled arranged as shown in Figure 1. The purpose of the two-unit sled instead of one large one is that it behaves very much like a two stage rocket. By keeping the frontal area of the booster unit the same as the main sled the drag is essentially the same as a single sled. Both units carry seven JATO motors and shortly after a speed of Mach 1 (booster burnout) is reached, the booster disconnects. The main sled now fires and accelerates to a speed in the vicinity of Mach 2.0 which is maintained until the spray field has been passed. A water brake is used to stop the main sled. Aerodynamic drag, coupled with a lower velocity, is expected to slow the booster before it reaches the water. It is equipped with a water brake scoop to bring it to a full stop short of the main sled.

2.2 The Spray Field

The spray field occupies the 2100 feet of track where the sled speed is maximum.

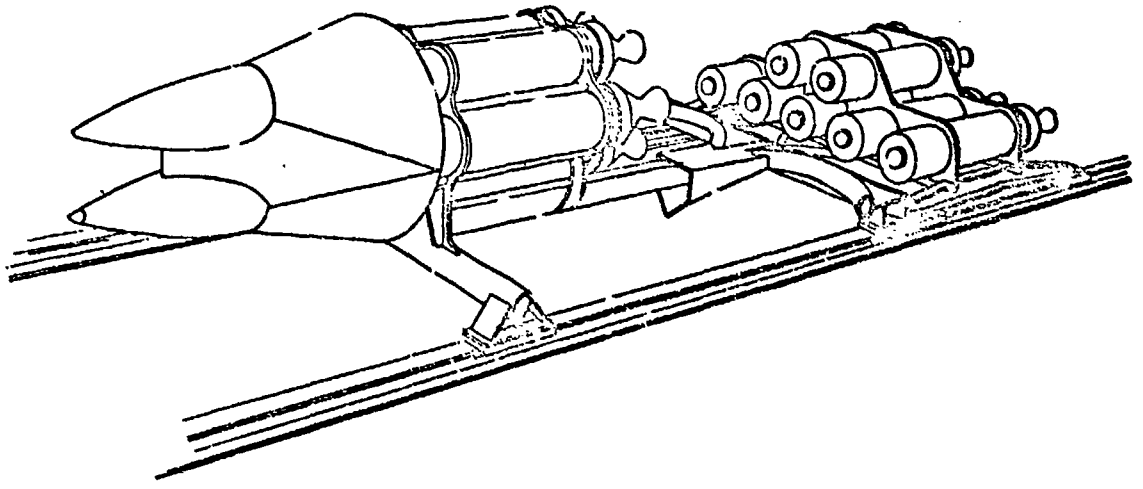

Figure 1 - Test Sled and Booster Combination

The nozzles used are the Spraying System (O. (Chicago, Ill.) Vee Jet 1/4 U 8050. Since the erosion effect is proportional to some positive power greater than unity of the particle diameter, the more-erosive larger droplets make possible some saving in the number of sled runs needed in any given simulated rain rate. The highest equivalent rain fall rate (5 in./hr) is obtained with a pressure of 4.5 psig and a symmetrical separation of 18 feet. Nozzles are directed upwards 50°, and are located six feet apart along the length of the spray field in pairs as indicated in Figure 2.

2.3 Drop Size Distribution

The method of measuring the distribution of water throughout the range of drop size consisted of capturing the drops in oil pans and measuring them visually. First the drops were captured in an oil pan which had two kinds of oil in it, see Figure 3.

The two kinds of oil do not mix readily so the drops which fell into the motor oil descended slowly and rested on top of the silicon oil. The captured

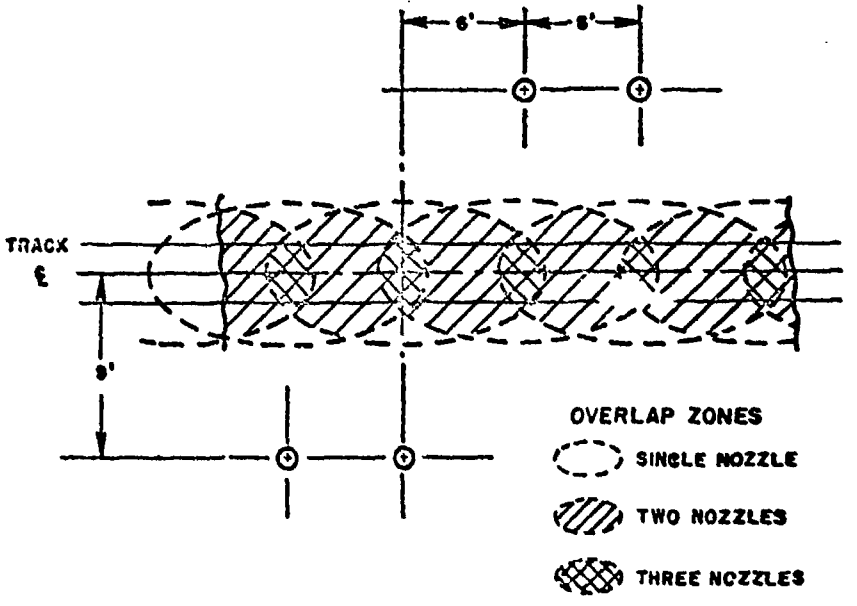

Figure 2 - Spray Nozzle Deployment

Figure 3 - Oil Pan Detail

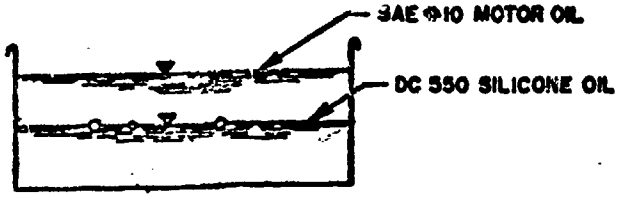

drops were then photographed 1:1. The droplets can be preserved for several days before the oils begin to mix or appreciable water absorption takes place. The photos were made immediately after droplet capture. Comparison with photographs of drops in air showed that the shape was not distorted sufficiently to cause appreciable error.

Reading the negatives was performed by measuring each droplet with a comparator. This method proved to be tedious. While a scanning counter exists the negatives were not suitable for its use. It was found that certain persons could, after some practice, estimate the drops in each group very accurately. In a trial of this method one girl was able to reduce the time required to read a photograph from 5 hours (two people) to 24 minutes (two people). The estimated count never varied more than 1% from the actual and the error in the value of d_o was 0.03 mm.

After the drop count had been made for each station these readings were correlated with measurements of rain rate as made with gauges. It was found that the variation of the median drop diameter with rain rate was comparatively small. The drop diameters are principally a function of the nozzle pressure, not rain rate. Some apparent increase in size was noted: however, the best explanation of this is that the spray is not horizontally uniform with respect to size distribution, but the larger droplets tend to appear in the edges. Since this is also the triple overlap region the empirical formula is good only for the nozzle arrangement used in the tests.

2.4 The Rain Rate

2.4.1 Rain Rate Measurement

A system of rain gauges similar to that shown in Figure 4 were used to measure the rain rate. Several determinations were made for each set of field conditions and the results averaged.

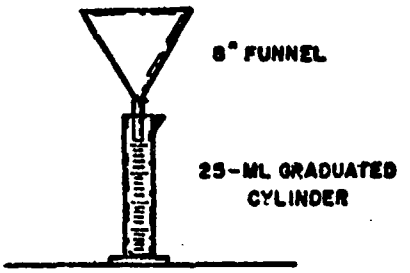

Figure 4 - Rain Gauge

Measurements made with a row of gauges spaced 18 inches apart down the field at the anticipated center line of the radome showed the rain not only to be heavy at all stations but also to have a high variation. The range of rates for the spacing and arrangement shown in Figure 2 was 3.82 to 8.68 inches per hour. The rms value of I was 5.05 in. /hr. The correlation of I with d_o was found to be:

$$*d_o = 1.56\, I^{.145}$$

where d_o is in. mm

I is rain rate in. /hr

The small value of the exponent of I indicates that drop size growth with increasing rain rate is small. In natural rainfall the corresponding exponent is in the neighborhood of 0.20 to 0.30 with a few observers [1] reporting numbers up to 0.37 and 0.40.

$*d_o$ = the drop diameter which divides the amount of water into two equal portions.

3. THEORY

3.1 The Radar Limitation

The criteria for establishing the equivalent rainfall conditions in the tests may be derived from the limitations imposed upon the radar guidance system by the rain itself. It is obvious that some rainfalls which have a finite probability of occurring, can be sufficiently severe as to completely neutralize any weapon system that depends upon electromagnetic radiation in the microwave region or higher.

The range to lock-on is given by:

$$R = C \left[\frac{\sigma P \lambda^2 G_1(\phi, \vartheta) G_2(\phi, \theta)}{L^2} \right]^{1/4} \qquad (1)$$

where C = constant relating to system of measurement (i.e. km, stat. mi., naut. mi., etc.)

P = Power transmitted

σ = radar cross-section of target

λ = wavelength

$G(\phi, \theta)$ = The gain function antenna system

L = Path loss

The path L is governed by the maximum allowable two-way path attenuation which will permit a reliable lock-on. If this is assumed to be 3 db above the ambient noise level, then R_{LO} can be determined for given values of the other variables.

Where scattering or absorptive particles are present in the volume between the radar and the target, the lock-on range is reduced to the point where the signal returned is detectable 3 db above the ambient noise level. The formula:

$$a = \frac{10\, I}{\lambda^2 L} \qquad (2)$$

where I = rain rate in. /hr
λ = wavelength
L = path length mi
a = db/mile

$$f_m < \dot{\psi}_p < f_T \quad . \tag{7}$$

The remaining factor is the attenuation caused by absorption and scattering. The attenuation effect for λ = 3 cm is shown in Figure 5.

Where the relative velocity of target and radar is zero, the Doppler frequency drops to zero and both effects must be considered. A condition such as this occurs if the target orbits around the radar location, or if the target and airborne radar move at the same velocity, as in a tail chase.

3.2 Erosion Factor

It has been shown by Marshall and Palmer [4] that the drop size distribution of most natural rainfalls can be represented by

$$N = N_o e^{-\Lambda d} \tag{8}$$

where N = number of drops in group d + δd

N_o = number of drops in group d = 0

Λ = function of the rain rate I.

Treating Λ as a constant (i.e. I = constant)

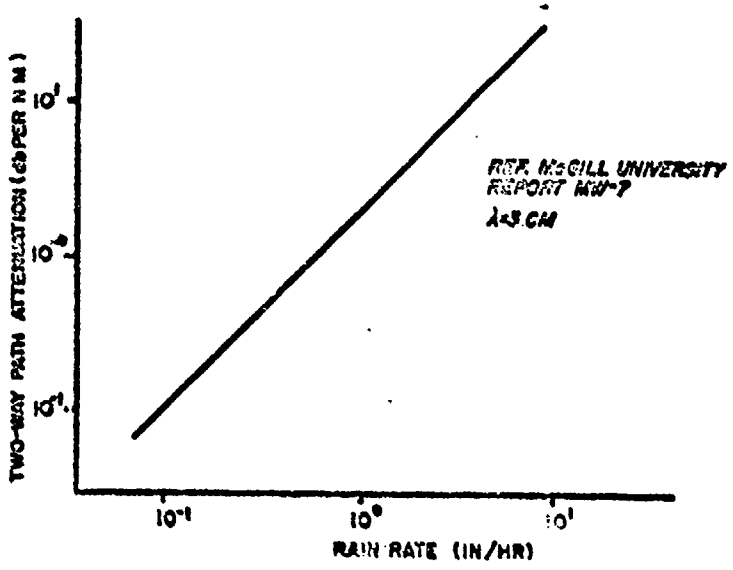

Figure 5 - Attenuation vs Rain Rate

The impact stress is proportional to the square root of the mass

$$p = \sqrt{m} = cd^{3/2} \tag{9}$$

Experimental results to date indicate that Equation 9 probably holds, or at least that the exponent 3/2 is a first approximation. Letting the exponent be k for purposes of theory, the erosion caused by the i^{th} group is:

$$E_i = N_i d_i^k \tag{10}$$

With the definitions given in equation 8 the total erosion factor (E_I) due to droplet size distribution is:

$$E_I = \int_0^\infty Nd^k \, \delta d^k = N_o \int_0^\infty e^{-\Lambda d} \, \delta d \tag{11}$$

which is readily integrated as:

$$E_I = \frac{N_o \, \Gamma(k+1)}{\Lambda^{k+1}} \tag{12}$$

That the erosion rate goes up enormously with increasing velocity has been established in sample tests by the Cornell Aeronautical Laboratory, [6] Convair [2] and others

$$R_E \propto V^b \tag{13}$$

The value of b has been determined from data published by Convair and is found to range between 3.5 and 8 for supposedly identical rain conditions. Probably the variation could be accounted for in the sizes of particles encountered. Let b be a constant and,

$$R_E = KV^b \tag{14}$$

The component of V effective in erosion is normal to the radome surface. From Figure 6 it can be seen that

$$R_E = KV_N^b = KV^b \cos^b \theta \tag{15}$$

The appearance of K is incidental in this discussion since we are concerned with the relative erosive abilities of two different drop distributions. The constant K may be omitted since it is divided out later in the analysis.

It has been shown by Atlas [1] that

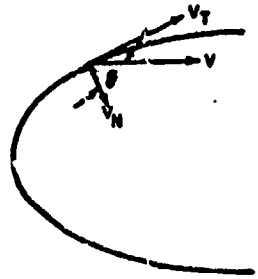

Figure 6 - Effect of Angle of Incidence on Rain Erosion

$$\Lambda = 3.75\, d_o \tag{16}$$

and that d_o is related to rain intensity by:

$$d_o = 1.79\, I^{0.21} \text{ where I is in in./hr} \tag{17}$$

and d_o in. mm

The value of N_o in the Marshall and Palmer treatment is invarient with rain rate. While this may be a justifiable simplification for meterological purposes, closer examination of the data used shows that their equation fails to describe the numbers of smaller drops present. This is no criticism of the meterologists because they themselves point out this limitation. The difficulty comes in trying to correlate artificial rains where the drop distribution is quite different.

Both natural rainfall and artificial rain field droplet distribution can be described by:

$$N = e^{-\sum_{n=o}^{\infty} a_n d^n} = \prod_{n=o}^{\infty} e^{-a_n d^n} \tag{18}$$

The erosion integral, in general terms, is:

$$E_I = \int_0^{\infty} \prod_{n=o}^{\infty} e^{-a_n d^n}\, d^k\, dd \tag{19}$$

unless K is a positive integer or zero the form is not readily integrated. However for practical purposes where N vs d has been experimentally found, the value of E_I may be obtained graphically by:

$$E_I \approx \sum N_i d_i^k \tag{20}$$

At the stagnation point $\theta = 0$ and $R_E = K_V^b$ and the impact is less everywhere else. It has been shown by Wetterborg[7] et al that aerodynamic

considerations reduce the value of V_N below that given by equation 15. However, at the higher velocities the effect is less important and, considering the inexact state of rain erosion knowledge, probably can be neglected until some of the grosser aspects of the problem have been examined in more detail. Aerodynamics may affect the results if the velocity ratio between the sled speed and the free flight condition is not close to unity.

3.3 The Sled Simulation

The total erosion experienced by a radome traveling at a speed, V, through a rainfall, I, in a period of time, $t_2 - t_1$, is given by:

$$E = K \left[\int_{t_1}^{t_2} V_N^b \, dt \right] \int_0^\infty e^{-\sum_{n=0}^{\infty} a_n d^n} \, d^k \, dd \tag{21}$$

The equation holds equally whether the radome is mounted on a free flying vehicle, or on a captive one like a sled. The object of the tests is to establish a valid estimate of the damage caused by certain natural rainfall. With this in view, it is necessary only to write a ratio between the natural and artificial erosion integrals.

$$\nu = \frac{K_m \int_{\text{missile}}^{\Delta t} V_N^b \, dt \int_0^\infty \left(\prod_{n=0}^{n=\infty} e^{-a_n d^n} \right) d^k \, dd \quad \text{(Nat. Rain)}}{K_s \int_{\text{Sled}}^{\Delta t} V_N^b \, dt \int_0^\infty \left(\prod_{n=0}^{\infty} e^{-a_n d^n} \right) d^k \, dd \quad \text{(Art. Rain)}} \tag{22}$$

ν = number of sled runs required to simulate any given missile flight situation.

Since the material object is identical in both cases and the aerodynamics are similar if the speeds are nearly the same then:

$$K_m \approx K_s$$

and letting the velocity factor be denoted by E_v.

equation 22 becomes:

$$\nu = \frac{E_v E_I \text{ (Missile)}}{E_v E_I \text{ (Sled)}} \tag{23}$$

The existence of a maximum ν depends on the flight history of the missile and upon the foreshortening of its range by rainfall intensity. Except where the limitation is severe the curve of V vs I is fairly constant after the maximum has been passed. The radar limitation is the stronger variable and the product of the two integrals tends to be nearly constant, or even to diminish despite the fact the rain intensity is increasing rapidly.

4. OTHER EROSION PROBLEMS

4.1 Snow Erosion

The apparent absence of snow erosion is evidently due to the small size of the erosive particle. While snow flakes may be quite large they consist of an airy lattice of individual crystals. Impact with such a structure would first collapse the lattice and then demolish the crystals. Current aircraft and missiles are not significantly affected, but when the relative energy of the individual crystals to the vehicle approaches the fatigue or impact breaking strength of the materials used, snow erosion will be noticeable.

4.2 Sand Erosion

Sand or soil particle erosion has occasionally been reported on military aircraft flying at comparatively low altitudes over desert terrain. The phenomenon is ordinarily confined geographically, but might also be expected over "Dust Bowl" areas. Since the particles must be carried by air currents, a definite gradation of size distribution can be expected with altitude. The criteria for deciding what particle spectra to anticipate at altitude during a sandstorm is insufficiently not known, and the question is presumably unanswerable at this time.

As far as a missile is concerned, materials which can withstand up to a minute of sand blast with medium particles at missile speed will probably be satisfactory for radomes and leading edges.

4.3 Hail Erosion

The occurence of hail in dangerous quantities is sufficiently low as to pose no problem in the control of damage to aircraft and missiles. However,

reports by NACA and the Military indicate that erosion and damage inflicted by hail when it does occur, is often sudden and severe.

Meteorological records are available for determining the sizes of hail which occur most frequently on the ground. For purposes of tests, these particles may be assumed to be airborne. Since an ice pellet, unlike a water drop, may be accelerated with an air blast, sample tests of the hail erosion-resistance in radomes and other materials are feasible.

4.4 Rain Erosion Simulation by Other Media

Conditions relating to Change of Erosion Medium.

A. Velocity Ratio

Since missile velocity increases with launch velocity, it becomes virtually impossible to simulate erosion for maximum-speed condition, due to the fact that the number of runs becomes prohibitively high. For speeds above M 3.5, an attractive possibility for reducing the cost of simulation is to use a higher-density liquid as the erosion agent.

The only high-density material which is a liquid at ordinary temperatures is mercury. If we stipulate that the relative kinetic energy contained by the drops shall be the same, and that whatever changes of state that take place shall be identical in kind and energy, then,

$$E_1 = E_2 \;\&\; \psi_1 = \psi_2 \tag{24}$$

where E is energy and ψ is the function of state of the two media.

For equal energy,

$$1/2\, m_{Hg}\, V_{Hg}^2 = 1/2\, m\, V_{H_2O}^2 \tag{25}$$

$$M_{Hg} = 13.546\, M_{H_2O}$$

$$V_{Hg} = \sqrt{\frac{\rho H_2O}{\rho Hg}}\, V_{H_2O} = 0.272\, V_{H_2O} \tag{26}$$

Where the test material is ceramic on plastic, mercury may be useable, but its action on metals and alloys should be investigated prior to test.

The curve in Figure 7 terminates about M 3.6 because of a change of state in mercury.

For any other pairs of media

$$V_1 = V_2 \sqrt{\frac{\rho_2}{\rho_1}} \tag{27}$$

B. Changes of State

In order to be certain that the changes of state in the collision are the same, it is necessary to investigate the changes of state that may occur in ordinary rain erosion at high speeds. The first law of thermodynamics states that:

$$JQ = E \tag{28}$$

Where J Joule's Equivalent
Q Quantity of Heat
E Energy of Impact

If the water is assumed to be liquid at the beginning of impact, and is allowed to achieve the vapor stage during impact, the Q term in equation

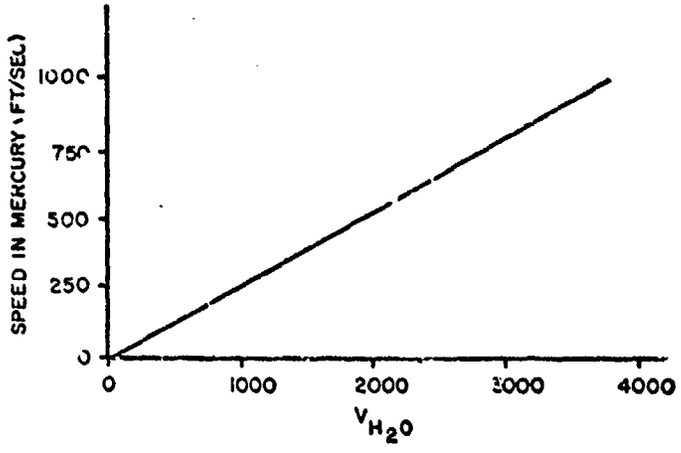

Figure 7 - Equivalent Test Speeds in Mercury (First Order Effects)

$$Q = Q_{liq.} + Q_L + Q_{vap} \tag{29}$$

If the particles were ice crystals, or hail stones, Q terms for the solid state and latent heat of fusion would be added to those for the liquid and vapor states.

$$Q = Q_{sol} + Q_F + Q_{liq.} + Q_V + Q_{vap} \tag{30}$$

Terms 1, 3, & 5 are all of the form

$$Q = \int_{T_a}^{T_b} c\,dT \tag{31}$$

where c is the specific heat and T_a T_b are the initial and final temperatures achieved within a given state.

It is interesting to compare graphically the mercury and water changes of state. Figure 8 shows the permutation of water states for various initial temperatures.

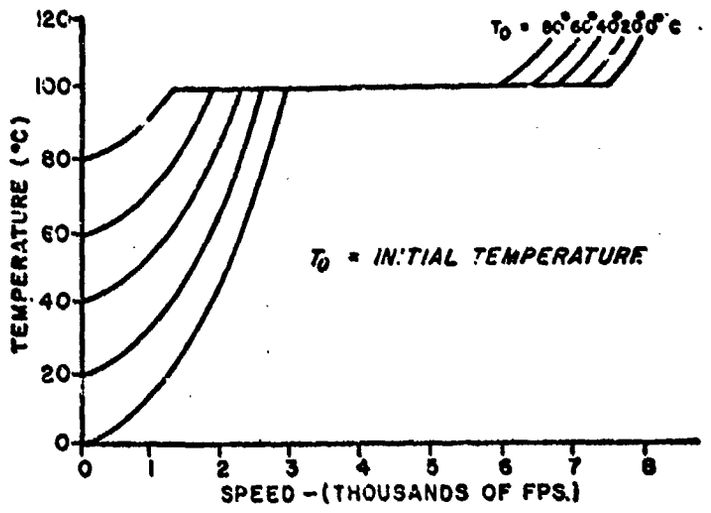

Figure 8 - Water Temperature After Impact

Sufficient energy is present to cause the water temperature to rise to the transition zone at a speed of about 3000 feet/sec no matter what the initial temperature was. If we avoid media conversion for transition zones, an upper limit near M 2.6 is imposed. Figure 9 shows the maximum range of liquid-to-vapor change in mercury. The low specific heat of mercury allows a rapid rise in temperature and the transition zone is reached by 1086 feet/sec.

Specific heat is in general a function of temperature, but in most instances may be taken as a constant throughout the temperature range of any given state, provided that additional states of freedom are not excited in the material. With this simplification and substitutuion from (30) into (29) we obtain an expression for the changes of state.

$$1/2\, mV^2 = J \left[(mc_{liq} (T_1 - T_o) + mq + mc_{v_{ap}} (T_2 - T_1) \right] \quad (32)$$

$$\frac{V^2}{2J} = \Delta T_{liq}\, c_{liq} + q + \Delta T_{vap} c_{vap} \quad (33)$$

q is the latent heat of fusion per unit mass. In using equation (33) it is necessary to take the right hand terms in sequence. That is, the

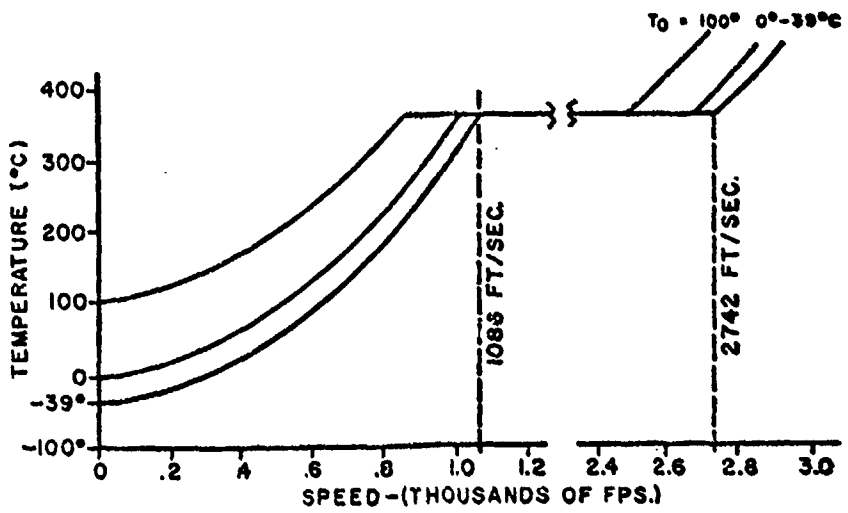

Figure 9 - Mercury Temperature After Impact

energy is first used to satisfy the initial term and the excess assigned to the second; then any excess of energy is then assigned to the last term. The final temperature may then be calculated. It is necessary to follow the same sequence as the physical-state transitions of the erosion medium. If a material is capable of additional degrees of freedom, additional terms reflecting the variation of c would be required.

If it is to be assumed that in both media, no part of the drop is vaporized before the whole mass, then the mercury is capable of simulating rain erosion up to the limit imposed by the water. Probably, however, this model is too simple to yield satisfactory solutions near the point where transition begins.

According to equations 27 and 33, the maximum equivalent speed for rain erosion which may be simulated up to the mercury transition zone is Mach 3.6 at sea level, but this assumes that all of the water remains liquid in the transition zone.

These considerations show that while the exact limits may not be prescribed at this time, the change of erosion media will not extend erosion measurement techniques much beyond Mach 3.

5. CONCLUSIONS

Current sled designs call for maximum speeds of about Mach 2. Assuming the restriction $K_m \approx K_s$, equation 22 can be used up to the transition zone of water (M 2.6). This means that erosion on a vehicle traveling M 2.5 can be simulated by using existing sled techniques. Since the condition of simulation does not hold for speed ratios greatly different than unity, special sleds capable of speeds of Mach 3, or above will be required if this manner of test is to be pursued for higher velocities. Such a sled might use a double or triple booster system and require 6 to 10 miles of track in order to get perhaps 2000 feet of useful rain field.

Generally, the current-type sleds will yield satisfactory results for missiles and aircraft in the speed range of M 1.5 to M 2.5. The time of flight at extreme speeds for aircraft must be prescribed in terms of radar limitations due to precipitation, fuel consumption, etc. in order to determine the number of sled runs required for a given simulation.

REFERENCES

1. D. Atlas Jour. Met. Vol 10 No. 6, Dec. 1953 pp 486-488
2. W. L. Dittmann, R. F. Holmes, E. T. Steeger et al. "A Study of Rain Erosion Testing Methods for Supersonic Speeds". WADC TR 53-173
3. Olive G. Engel, "Mechanism of Rain Erosion". WADC TR 53-192
4. J. S. Marshall and W. McK. Palmer. Jour. Met. Vol. 5, No. 4 Aug. 1948, pp 165-166.
5. McGill University. Stormy Weather Project, Report MW-7
6. N. E. Wahl, R. R. Lopp, et al. "A Study of the Rain Erosion of Plastics and Metals" WADC TR 53-185
7. G. P. Wetterburg, E. F. Pope & J. S. Murphy. "Raindrop Impingement on Various Bodies of Revolution at Sub and Supersonic Speeds". Vol I Proceedings of the Radome Symposium, page 1. Ohio State University June 1955.

LARGE RIGID RADOME DESIGN

By

Hadley F. Morrison

Zenith Aircraft
Gardena, Calif.

Introduction:

It is becoming increasingly apparent that the field of large ground radomes encompasses requirements for rigid radomes. Because of this need, additional emphasis is being placed on the research, development, and evaluation of large rigid ground radomes. It might even be stated that the requirement for mobility which previously restricted the use of rigid radomes is in some instances no longer a serious bar to the use of the rigid radome.

The foremost intent of any radome is to provide protection to the radar antenna with a minimum attendant loss of transmission efficiency. This concept is no less applicable to large ground radomes than it is to airborne radomes. The design variables may differ; however, the net desired result is essentially the same. The evolution of the large rigid radome from preliminary design to final fabrication and test is based upon this prime consideration of high transmission efficiency. However, there are other important design factors which oftentimes are overlooked or are unduly minimized. A successful radome will reflect an honest evaluation and resolution of these many design variables and factors. In fact, it is a design responsibility to insure that the radome complies with these many factors which will result in an optimum design.

Discussion:

Among the factors which dictate optimum design of large rigid ground radomes are: (1) transmission efficiency, (2) service environmental operating conditions, (3) structural integrity, (4) safety of personnel involved, (5) field erection, (6) service operating life, (7) operational maintenance, (8) manufacturing and fabrication, (9) mobility, and (10) unit cost.

The feasibility of designing and manufacturing large rigid ground radomes per the above factors has been demonstrated by the Zenith Plastics Company, as well as various other commercial firms and military research and development centers. The research and development program which resulted in delivery of such a radome (hereafter called the Rome Dome) to the U.S. Air Force was sponsored by the Rome Air Development Center. The general requirements were for an anti-iceable rigid radome which was to be mountable on existing arctic towers. This radome was to be the cover housing for radar set AN/FPS-4 or for radar set AN/TPS-1D. In addition, it was required that the radome be transportable in a C-119 type aircraft. Because the many design factors are so inter-related, it is not possible to discuss them as separate entities. Thus, no attempt is made in this brief discussion to adhere to any specific numerical order such as appeared in the introduction.

The optimum configuration and size of the Rome Dome were selected on the basis of providing a radome which would lend itself to simplicity of design and ease of sectionalizing, transport, and erection. In addition, the radome must provide adequate inside clearances for the assembly of the antenna, must provide clearance between the edge of the antenna and the surface of the radome, and must be mountable on existing arctic towers. The radome configuration finally selected (Figure I) has a hemispherical dome of 10-foot spherical radius which is tangent to and continuous with a 20-foot diameter, five-foot high vertical cylindrical base segment. The resulting height (less lightning rod) is 15 feet. The surface was divided into eight identical peel-shaped side panels of approximately 8' x 18' and one 6-foot diameter circular top cap panel. It is well to note that no particular difficulty has been encountered by the fabricator in handling these panels during test erections.

The selection of materials for the Rome Dome, as with any radome, was dependent upon the integration and assimilation of the many varied design and operating conditions. The basic structural material selected was fiberglass reinforced plastics. This choice was made because of its desirable electrical properties and because it is now a well established fact that fiberglass is relatively maintenance-free. More specifically, the requirements per specification were that it should be fiberglass fabric (not mat) with suitable resins. Because of the anti-icing requirements of the radome and the consequent heat requirements which under certain conditions would render radome skin temperatures above normal, it was decided to use Selectron 5016 resin in combination with types 120, 181, and 182 glass fabric, RS-49 Garan finish. This combination of fabric and resin is relatively economical, is easy to work with, and is structurally reliable at the design heat versus load conditions.

In order to fully appreciate the panel construction it is necessary to note that the anti-icing means selected as best for this job was the use of ducted heated air. In this particular application the heated air flows through passages or channels which are integral with the radome sandwich panel and are adjacent to the outer surface. The final panel construction selected for the transmission area is shown in Figure II. This type of fabrication currently known as the lost-wax process for radome construction is permitted under license from the Douglas Aircraft Company. The base of the side panels and the top cap panel being outside of the transmission area are respectively honeycomb sandwich construction and thin solid laminate construction as indicated in Figure III. All attach edges and field joints are built-up solid laminate. Typical construction of the vertical field joints is shown in Figure IV.

The final panel construction indicated in Figure II was that configuration deemed best from an electrical transmission standpoint which would still render the necessary structural properties and be functionally adequate from the anti-icing standpoint. Original electrical transmission target was 95%, which served as the basis for theoretical calculations resulting in the sandwich construction shown in Figure II. Recent tests indicate that a transmission efficiency in excess of 90% can be expected through the sandwich of the panels.

The vertical field joints of Figure IV are not desirable from an electrical transmission standpoint (60-70% predicted). Because of the low transmission inherent in this type of joint, studies are currently being directed toward a practical joint design which will allow a maximum transmission with a minimum pattern distortion.

The heat requirements were established by a conservative thermodynamic analysis based on data available at that time. This analysis indicated a net heat requirement of 480,000 BTU per hour. It has since become evident from additional data that the original concepts were probably over-conservative, and in future designs for anti-iceable rigid radomes the governing heat requirement criteria will be adjusted accordingly.

The anti-ice heating system designed for the Rome Dome consisted primarily of (1) an oil-fed burner which is to be located in the radar tower below the second floor, and (2) a circulating system for ducting the heated air to the radome panels and partial return for recirculation. The system is provided with controls for maintaining preset heated air temperature and has safety and limit switches. All exposed hot surfaces have been thermal insulated and moving parts have been provided with protective covers.

The requirement per specification was that this radome should be operable in tropical and desert locations as well as locations of extreme cold. Because of these requirements plus the fact that equipment within the radome should not be operated in ambient temperatures above 125°F, it was necessary to evaluate the potential temperatures within the radome. It was found that outside ambient air must be circulated through the radome walls (normally used for anti-icing air) in order to prevent the ambient air temperature in the radome chamber from exceeding 125°F. This fact was found to be applicable for both the extreme desert and tropical daytime conditions.

It goes without saying that the radome had to be structurally sound. A complete aerodynamic investigation was conducted to arrive at design pressure loads due to the 109-knot wind requirement. Thus with the configuration, loads, and design established a stress analysis was completed. This stress analysis revealed that certain portions of the radome side panels had negative margins of safety. However, in view of the conservative assumptions and method of analysis and of previous experience in radome design, it was the weighted engineering opinion that the radome would withstand the design loadings without failure. The validity of these assumptions and opinions was later substantiated with the successful completion of the static test.

The fabrication means and cost of fabrication are influential factors in making or breaking a radome design. These factors are too often overlooked in preliminary radome design and can result in a finalized production design which is not economically feasible to produce. The previously noted operational factors must in the final analysis be compatible with the means of construction. Among the most common differences existing between desired and practical application is the problem of close tolerances. It is definitely next to impossible to provide the theoretical close tolerances often requested. Or at best, it is not possible to consistently provide extreme close tolerances even with the most precision tooling. The net results often indicate that the closeness of tolerance originally requested was not mandatory for normal radome performance. Had these tolerances been less stringent and more practical, it would have been possible to produce a radome almost as operationally efficient and much more economically efficient. It can easily be seen that because of extreme close tolerances the cost of tooling rises, the actual cost of fabrication rises, the cost of quality control rises, and the rejection rate rises. In addition, all too often each acceptable radome produced has had to be a tailor-made and hand-fit operation. Thus the fabrication

and economical factors cannot be discarded in radome design. This becomes especially true when the radome fabricator operates as a subcontractor and must remain competitive with others in the industry.

Specifically, the Rome Dome was developed from a research and development contract which was to reflect a successful radome and in addition was to reflect the development of production tooling. The evaluation of the tooling problem resulted in the selection of molds of cast phenolic tooling resin. This is an economical approach which renders good results over an extended quantity of parts. In the event of high quantity production the molds can easily be duplicated in cast phenolic tooling resin or in permanent metal molds. The type of radome construction was not difficult considering its anti-iceable functional intent. The materials selected for radome construction were easily handled and the tolerances required of parts and tooling were reasonable. The geometry of the radome also lent itself to reduced economics because all eight of the side panels are identical units which can be produced from the same mold.

The requirement for shipping the radome in C-119 type aircraft was beneficial in that the maximum panel size allowed was a size that could be easily handled from an erection standpoint. The only tool required for erection other than the ordinary hand tools and a stepladder was a lighweight erection pole. This erection pole is placed in a tripod-like support position when the first side panel is erected. This pole can be left in position while most of the remaining panels and the top cap panel are installed. Thus the basically monocoque structure is quite stable during the rapid erection.

It is a matter of necessity in any research and development program that the end product has proven itself testwise. Test of the Rome Dome, contractual and otherwise, consisted of electrical panel transmission tests, anti-icing air flow tests, static tests, complete erection tests, and anti-ice air heating equipment tests. The above listed tests were successfully completed at the contractor's facility prior to delivery of the complete radome and related heating equipment to the Air Force. Among the contractor's final recommendations was the recommendation that the radome and related heating equipment be operated under the severe service environmental conditions for which it was designed. It is felt that such operation would be conclusive proof of the feasibility and practicality of this design and, in addition, would render operating data of invaluable nature.

Since the overall program of rigid and non-rigid radome development and use indicates a continued and expanded field of effort, the Zenith Plastics Company has been conducting preliminary design studies resulting in proposals of rigid radomes of varying sizes and functional use. By functional use I intend to convey anti-iceable and non-anti-iceable types.

In studying and proposing these different designs the same basic design criteria have been used that were used in the complete design and fabrication of the original Rome Dome. The exception to this is, of necessity, that more emphasis must be placed on the handling and erection of the larger rigid radomes. This is understandable when one considers that the panel size cannot increase due to shipping limitations; therefore, the quantity of panels for one installation increases approximately as the square of the diameter. As well, erection becomes more of a problem because of the increased distances above the base. In addition to the same basic design criteria, an emphasis has been placed on providing a radome which would tend to be inherently stable throughout the erection period.

The importance of this can be realized when one considers that longer periods of time are quite naturally required to erect the larger radomes. During these longer erection periods the chances of unfavorable or destructive winds arising become more pronounced.

The existing Rome Dome design portends a successful application of the lost-wax process panel construction for ducting heated air in anti-iceable applications. Therefore, a similar approach has been used in the study and proposal of a rigid radome of 55-foot diameter.

The main emphasis relative to rigid radomes seems to be currently pointed toward the non-anti-iceable type; the reason for this being that data compiled by Rome Air Development Center, Lincoln Laboratory, Cambridge Research Center, and others reflects little icing occurring on large radomes. Because of this emphasis, studies have been completed resulting in proposals for 20-foot diameter, 35-foot diameter, and 55-foot diameter solid laminate rigid radomes. In addition, a study is currently being conducted for a 110-foot diameter solid laminate rigid radome. That emphasis is being directed toward the non-anti-iceable type of rigid radome is perhaps timely because of the trend toward larger antenna design. It is easy to see how the complexities of design and manufacture are reduced in the solid laminate type radome.

An additional fact of relative importance in the successful development and design of the larger rigid radomes is the amount of capital expenditure required. It is easy to understand how the complexities of the structural problems are multiplied many times as the size of the radome increases. It is difficult for the low-overhead subcontractor to theoretically evaluate and solve the intricate problems associated with large rigid radome development. Therefore, firm design and development will of necessity be slow unless it is underwritten with firm financial assistance.

Conclusion:

In summary and conclusion, the facts orient themselves in the following manner. The feasibility and practicality of rigid radomes has been established and proven by various fabricators. This contractor has successfully demonstrated this with the Rome Dome, a 20-foot diameter anti-iceable rigid radome.

Because of a continuing and increased need for rigid radomes, further study and development is being accomplished. The successful optimum radome designs as a result of these studies and developments will equitably encompass the many important design variables and requirements.

In addition to proposals by other fabricators, this contractor having successfully completed the full design of a 20-foot diameter anti-iceable radome, has completed the preliminary design of a 55-foot diameter anti-iceable radome. Other preliminary designs completed or near completion are non-anti-iceable rigid radomes of 20-foot diameter, 35-foot diameter, 55-foot diameter, and 110-foot diameter. Future designs will cover radomes of 150-foot diameter and 200-foot diameter. In order to develop these larger radomes it will be necessary to conduct extensive research and development programs aimed at determining methods of structural analysis, determining the electrical effects of various types of joints, and determining the most efficient structural designs without the sacrifice of rapid means of erection.

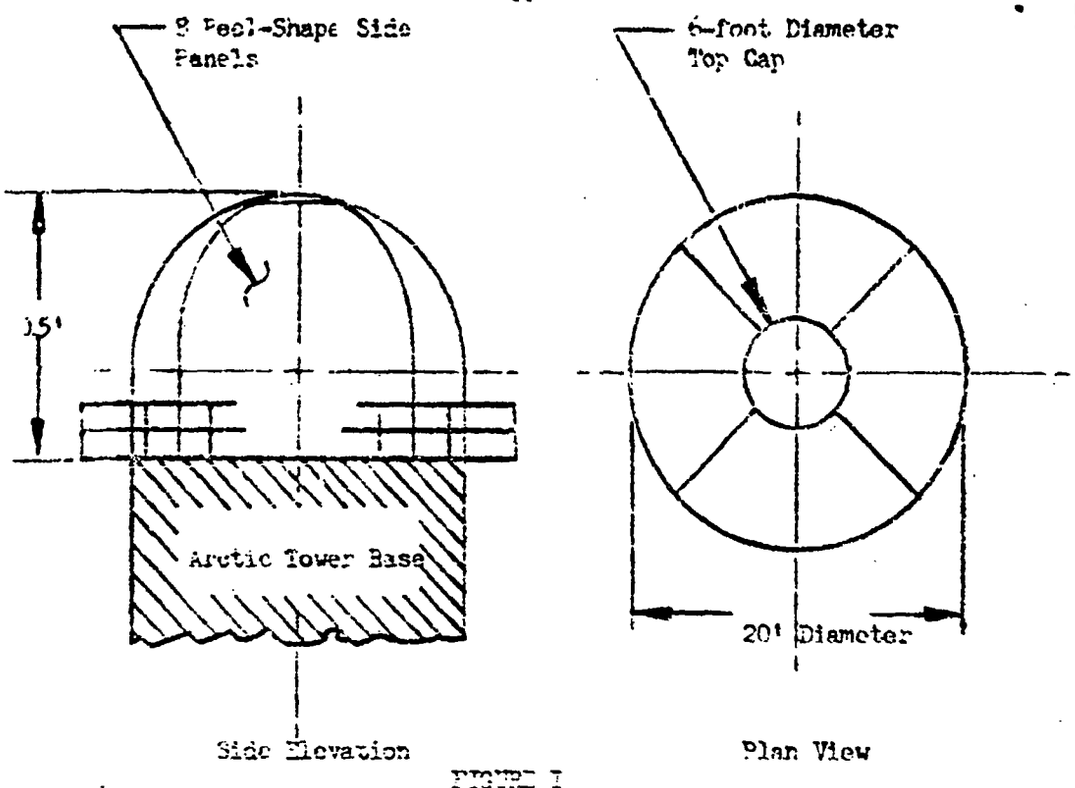

FIGURE I

RADOME CONFIGURATION

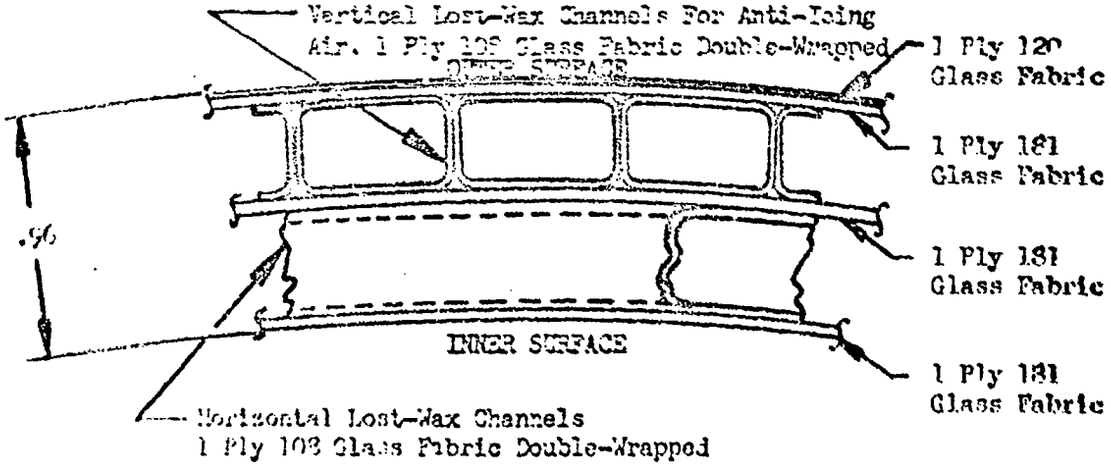

FIGURE II

SIDE PANEL CONSTRUCTION IN ANTI-ICED AREA

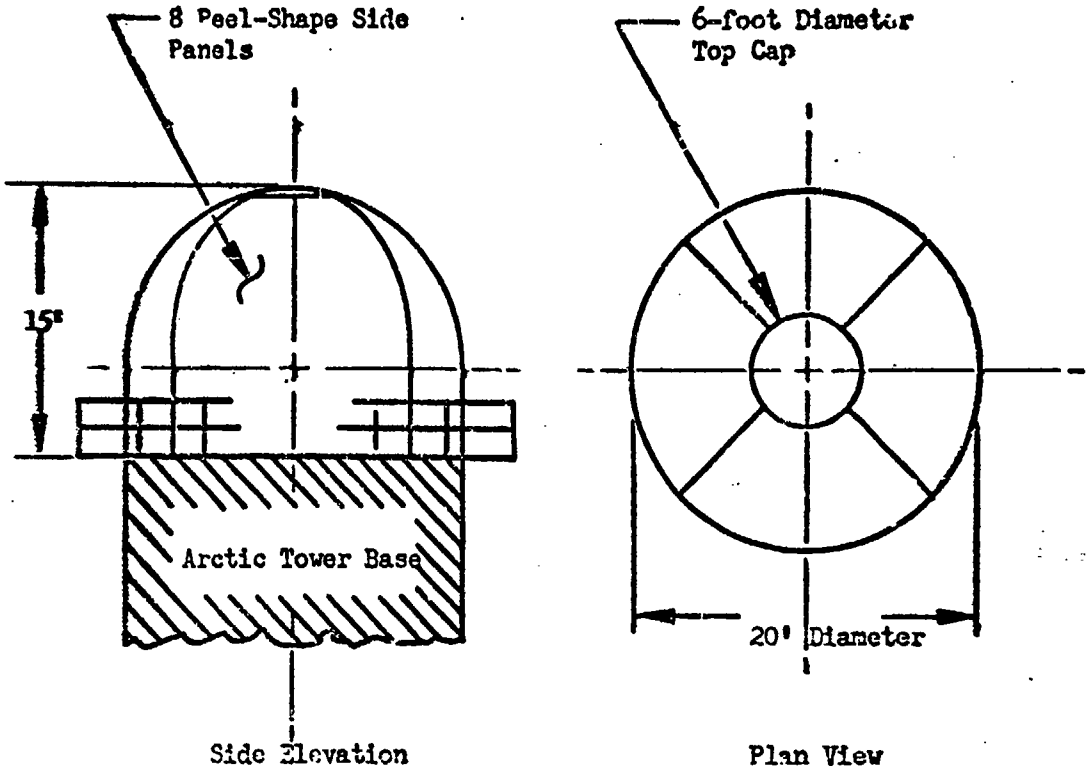

FIGURE I

RADOME CONFIGURATION

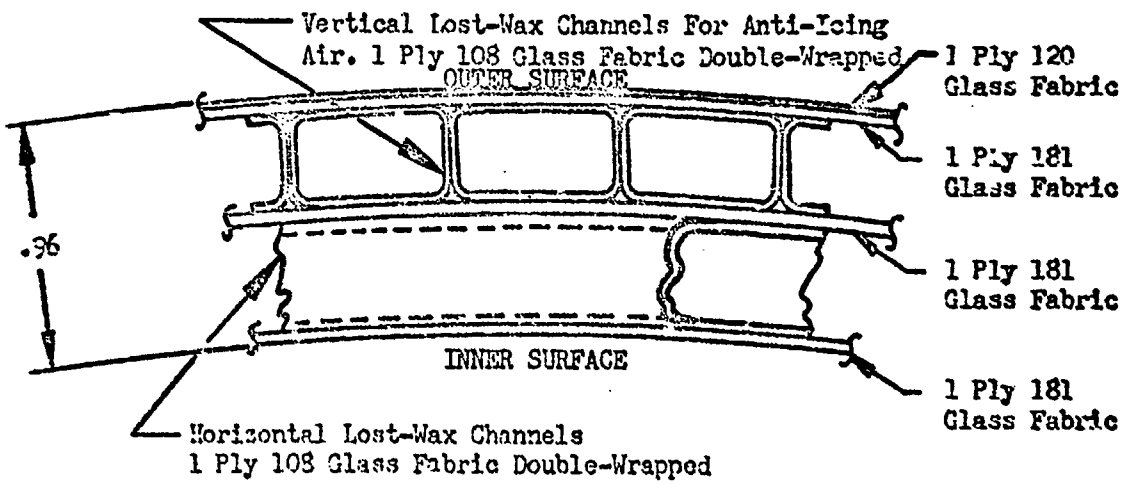

FIGURE II

SIDE PANEL CONSTRUCTION IN ANTI-ICED AREA

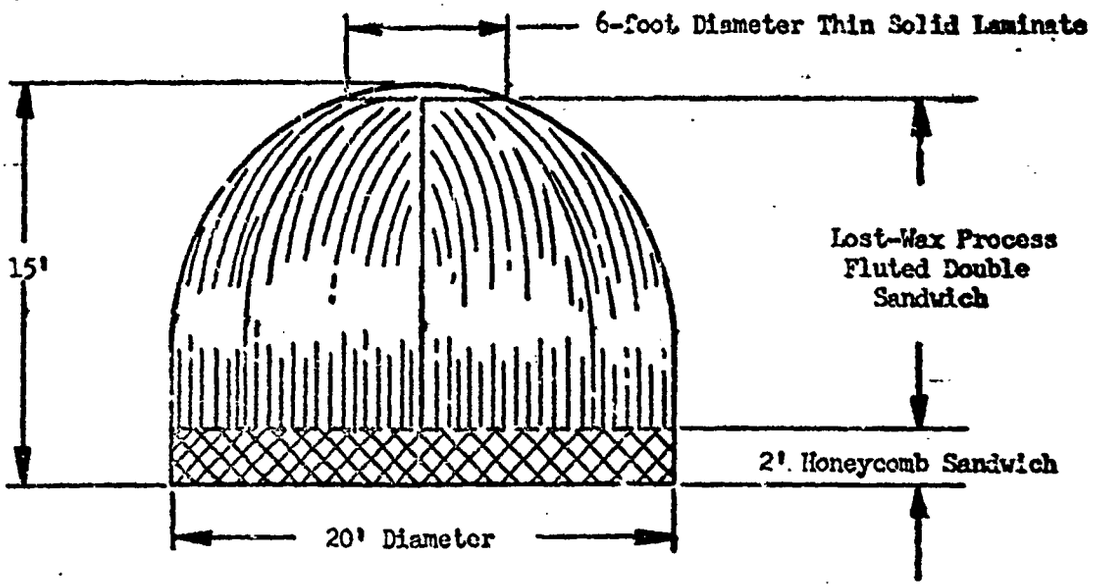

FIGURE III

AREAS OF BASICALLY DIFFERENT CONSTRUCTION

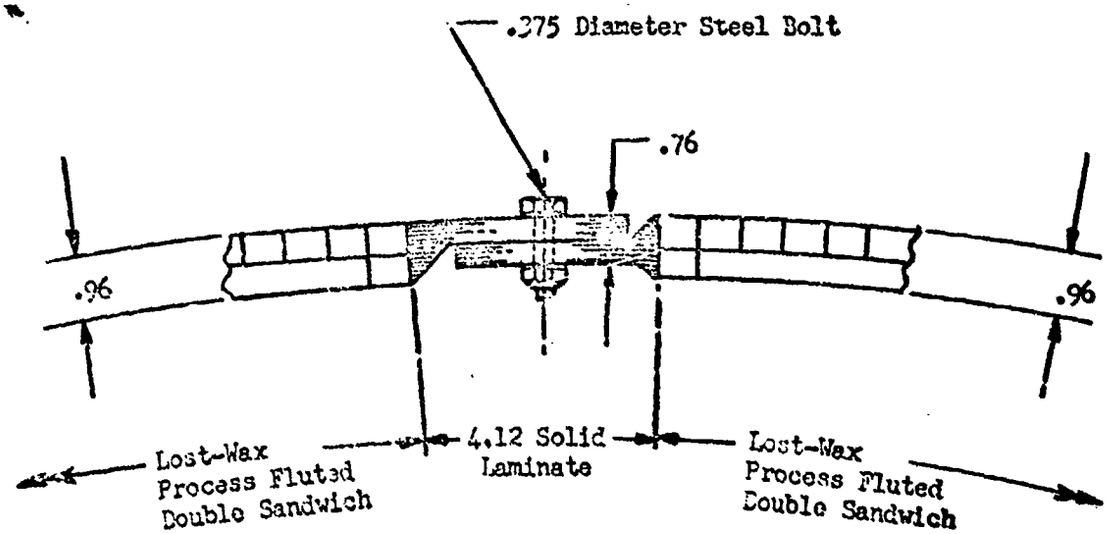

FIGURE IV

TYPICAL VERTICAL JOINT THROUGH TRANSMISSION AREA

LIGHTWEIGHT AIR SUPPORTED RADOME MATERIALS DEVELOPMENT

"DACRALON" PROOFED FABRIC

A paper
presented before
the

Ohio State University - Wright Air Development Center

RADOME SYMPOSIUM

June 4, 5, 6, 1956

Ohio State University, Columbus, Ohio

by

Lt. Donald E. Setter*
Rome Air Development Center
Griffiss Air Force Base
Rome, New York

*Presently with Phillips Chemical Co., Bartlesville, Oklahoma

LIGHTWEIGHT AIR SUPPORTED RADOME MATERIALS DEVELOPMENT

Lt. Donald E. Setter*
Rome Air Development Center

ACKNOWLEDGEMENT

The work on radome materials development mentioned here was accomplished principally through contract with DeBell and Richardson, Inc., Hazardville, Connecticut, where Mr. Mac Mead, Mr. Wayne Turner and Mr. Fred Wiley were responsible engineers. Some prior work with Cornell Aeronautical Laboratory and Mr. Walter Bird is significant and is mentioned for its background importance. This development was administered through the Materials and Miniaturization Engineering Section of the Rome Air Development Center where Mr. James L. Briggs and Mr. S. C. Nilo were cognizant engineers. The author was fortunate, serving as Project Officer, and it is with the kind permission of the aforementioned that I proceed.

INTRODUCTION

The purposes of this development was to improve the performance of air supported radomes, principally by lightweighting the current radome techniques that use rubberized fabrics. The benefits were to be (1) greater mobility for ground radar systems and (2) reduction of the overall cost of radomes thru use of less materials, less fabrication time, less effort in handling and installation, less maintenance and longer service life in such structures.

In order to accomplish these goals the following requirements would have to be realized.

(1) A yarn of higher tenacity or strength than those previously available was needed for the strength compared to weight necessary in lightweighting.
(2) A yarn of improved resistance to the elements was required.
(3) Proofing or rubber coating materials of greater weather resistance than those presently known were required.
(4) Proofing materials were needed that were capable of stronger joints than those attainable by present techniques and materials.
(5) Designs utilizing more economic engineering were also required.

*Presently with Phillips Chemical Co., Bartlesville, Oklahoma

These requirements and their engineering realization become the development contract undertaken by DeBell and Richardson, Inc., Hazardville, Connecticut on the 4th of January, 1954.

HISTORICAL BACKGROUND

The historical background for this development has a number of significant events, a few of which we might mention here. In 1946 the Air Defense Command and the Tactical Air Command imposed wind, temperature and ice loading requirements on radar systems that was about 400% of the design load for the antennas and pedestals. The need for environmental control was obvious.

Cornell Aeronautical Laboratory, Buffalo, New York, suggested to the Air Force in the fall of 1946 that an air supported radome could be used. Rubberized fabrics that were strong and flexible and fairly transparent to microwave energy at S and L band were to be fabricated into a truncated sphere that was internally inflated against external wind loads. A prototype structure, 50 feet in base diameter for the AN/CPS-6B Radar Set, was built by Cornell and erected in June, 1948 at Buffalo.

At the time of a demonstration, this prototype was damaged. It was repaired, re-erected and saw satisfactory service use for two years, which is fairly well for a prototype. The material used there was Fiberglas cloth proofed with Neoprene rubber. The need for improved materials arose early. Radomes using Fortisan rayon and Nylon in conjunction with Neoprene rubber were also proposed and these service tests items were manufactured. All were acceptable.

However, some shortcomings in performance were beginning to appear. Tear resistance was regarded as insufficient. Weathering had abominable effects on radomes in many cases. Materials were weakened at creases and folds. Artic use required a white structure. Radomes were heavy and bulky. Installation was not easy. In order to gain life against the elements in mid 1950, it was necessary to "beef up" the materials which detracted from reduced costs, improved electrical performance and related interests.

In 1951 Cornell undertook an Air Force contract to investigate improved materials for air supported radomes. Among the results there were two factors that were to be of great significance in the work that was to follow. It was learned that Hypalon synthetic rubber had promise for very good weather resistance, but it would require extensive development work before it could be commercially utilized in radome applications. Hypalon is a pigmented synthetic elastomer derived from chlorosulfonated polyethylene. The second factor was the possibility that the Dacron polyester type yarn could be made to have a rather high strength for its weight by hot-stretching or drawing the yarn. This high strength to weight ratio is important for lightweighting. But up until 1953 yarn drawing results had not been satisfactory. Any improved properties that were imparted to the yarn by drawing were lost in time recovery,

or by shrinkage at ordinary fabric processing temperatures.

Air supported radomes could, in 1953, be made from Neoprene proofed fabrics of Fiberglas, Fortisan rayon, Nylon or Dacron. In the proofed or rubberized form, all of these materials had a unit strength of about 10-12 pounds/inch for each ounce/square yard of material. Each ounce of weight per square yard represents about 1 mil of thickness. A fifty foot radome uses a fabric of about 35 ounces to the square yard and it weighs over a ton. Weather resistance was insufficient. However there were serviceable items placed in Air Force inventory, which no doubt has played some part in our national security. However, with an eye to further improvement, it appeared desirable to try to reduce costs and to improve electrical and physical performance for the long run by lightweighting and by improving weather resistance. This would result in simplified handling and installation, minimized maintenance, greatly extended service life, reduced costs in fabrication and materials as well as providing better electrical and tactical performance of radar systems.

DEVELOPMENT OF DACRALON

The word "Dacralon" has been used in referring to proofed fabrics consisting of Hypalon rubber and Dacron fabric as further explained here. The problems confronting the development of lightweight weather resistant materials for air supported radomes were primarily in the field of high polymer technology and utilization, and in the engineering design of such radome structures. Certain properties of high polymers and the techniques for their commercial processing as applied to synthetic fibers and elastomeric coatings became the main area for this development with DeBell and Richardson, Incorporated.

It appeared that continuous filament Dacron showed the most promise in high tenacity and weathering ability. The problem was how could the yarn be further drawn or stretched to permanently gain the desired tenacity in a stable form thru processes that were adaptable to commercial production. The Hypalon synthetic elastomer had indicated very good weather resistance in an advantageously pigmentable and curable rubber stock. The problem was to adapt Hypalon to this requirement, especially in regards to adhesion, cure and fire resistance thru processes adaptable to commercial or production coating of the Dacron fabric. Weaving was to be a problem for the fabric required a strength to weight ratio that was unheard of in the industry. Since the lightweight, proofed fabric for the development was to be about six ounces/square yard total weight, the Dacron base fabric was seen as weighing 2 1/2 to 3 ounces and pulling at least 160 pounds/inch in tension before break. Design considerations for such structures involving the correlation of fundamental properties with radome performance, the evaluation of rip resistance, the plying of fabrics, the reduction of calculated strength in weaving and coating operations became important areas of the development.

YARN -

First development efforts concerned the yarn. Initial experiments produced yarn tenacities over eight grams/denier whereas the yarn as purchased had a tenacity of around six. The yarns were drawn or hot-stretched at about 400-420 F by contacting a hot plate and then "heat-set" by remaining at some elevated temperature for varying lengths of time as an effort to anneal the yarn. Fortunately a valuable discovery came early in the development. As the extent of drawing or stretching is increased, the time of heat setting or annealing became less and less important in removing any induced or built-in mechanical stresses. At 15% or more drawing, the heat-setting time appeared to no longer affect the residual shrinkage. Once the drawing is beyond 10 percent, annealing time from next to nothing up to 45 seconds had little or no effect on residual shrinkage. This discovery helped pave the way towards commercial production, for processing time in annealing was practically eliminated. The small shrinkage problem was thus transferred from the yarn to the fabric where familiar pre-shrinking techniques could be applied.

The polyethylene terephthalate resin used to manufacture Dacron yarn is probably as pure as possible for the production melt spinning process. Even then, some impurities, gel spots or gas bubbles are present and these points of discontinuity become areas of stress concentration under filament tension. It is generally agreed that filament breakage occurs at points of stress concentration at a much lower overall strength value than can be attributed to inter- and intra-molecular forces. When flaws are oriented in the stress field as is the case in hot stretching or drawing, they are less likely to facilitate premature failure for some stress can now be transmitted around the oriented flaws.

In experiments that followed, it was indicated that the drawing contact time was not nearly as important as the temperature level or the extent of drawing. Apparently one must go far enough to pull the yarn right thru its old elastic boundaries into a new crystalline alignment to gain any significant benefit by drawing. It was also discovered that the permanence of the increase in tenacity was better with yarn that had been freshly melt spun or manufactured, than with old yarn from the same polyethylene terephthalate resin. It could be that some of the crystallinity induced into the filament in the original fiber forming process was slowly replaced in time by more amorphous areas with subsequently more elastic behavior, which lowered the modulus and had to be overcome in the stretch-drawing operation. Some re-orientation of polymer molecules and of crystallite areas were no doubt brought about by the stretching, but all of this gain could not apparently be retained by the extremely high viscosity at room temperature and the yarns lost some orientation in time. Most of the increased tenacity could be accounted for by the reduced crossed section of the drawn yarn with its lessened denier. Yarn breaking strength was generally improved somewhat by the stretching which would indicate some improvement in filament orientation. The contribution of stretching or drawing to crystallinity and the effect of this on tenacity and yarn strength was not fully determined for unfortunately, such an evaluation was beyond the scope of the immediate problem.

Another significant processing discovery was made wherein by raising the drawing temperatures to just under the melting range of the polymer, 475 F in this case, one could attain tenacities of nine and over at only 14% draft or draw. Tenacities of nine were attained also at 28% draft. So it was an important finding that as long as the extent of drawing was sufficient to gain some mechanical orientation, it was far easier to process the yarn nearer to its melting range in order to gain strength without inducing filament breakage.

First samples of woven fabric were rather loose, or were too tight and it appeared desirable to have a yarn of intermediate denier. The DuPont Company was approached to supply a yarn of 300 or 150 denier. Sixty pounds of 162 denier, 68 filament, Type 5100 Dacron yarn were obtained with a tenacity of 6.4 and 9% elongation. The somewhat different properties of this yarn was believed to be due to a greater amount of drawing of the yarn by DuPont in the filament manufacture. After some minor difficulties, this yarn showed great promise for its high strength to weight ratio, and it was decided to use this 160 denier material.

A difficulty arose in that the DuPont Company decided not to make the 160 denier yarn available as a commercial item at the time that materials were being procured for the fabrication of the prototype structure, in the fall of 1955. It was then necessary to revert to 220 denier yarn, in a slightly heavier weave to avoid having any part of the development not commercially available.

WEAVING -

In weaving there were many difficulties to overcome in using flat, low twist yarns in a loose, flat, lightweight fabric. Filament breakage, lack of sizings, uneven weaving and poor handling properties were eventually overcome much to the credit of Stern and Stern Textiles, Inc., Hornell, N. Y.

First fabrics of 47 x 47 count, 220 denier yarn come off the loom with snags and slubs as well as reed marks and wrinkles. Fabrics with a 2 x 2 taffeta weave construction were woven with more success, especially by weaving with dual warp yarns and weaving two picks in the shed, which involves the passage of two fill shuttles through the warp shed for each motion of the heddles. However, the resultant fabric was too loose or sleazy for the coating operation. A compromise 2 x 1 taffeta weave was not entirely satisfactory in the desired weight. The need for a 150 or 300 denier yarn, as mentioned before, became evident. But since the desired yarn could not be obtained for production weaving and coating, the 220 denier yarn was used in a fabric that had a breaking strength of about 450 lbs/inch and a weight of about seven ounces/square yard. This fabric met the light weight requirement. The fabric construction and weight could be modified to fit the strength requirement of its intended end use.

COATING -

The use of Hypalon was decided for it possessed the desired properties, especially weather resistance. Of first consideration in this area was the use of precoats for (1) possibly enabling easier handling, (2) promoting adhesion of coating and (3) possibly reducing moisture absorption.

Precoats of MDI (4, 4' - diisocyanatodiphenyl methane) were seen to promote adhesion of Hypalon to Dacron fabric, particularly in lap joints at elevated temperatures. Fabrics were precoated by slashing thru a 4% solution of MDI in toluene and then coating as soon as solvent was lost to avoid moisture pick-up by the MDI. The adhesion was satisfactory in that peel strengths of about 10 lbs/inch were seen in cemented lap joints while the adhesion and shear strength was greater than fabric strength for the light weight fabrics.

Initial elastomer formulations for the Hypalon coating stock were those recommended by the supplier. A two component system was used, one containing the ball milled dispersion of elastomer, stabilizers and solvent, while the second part contained vulcanization accelerators, curing agents, pigments, etc. in a compatable dispersion. Laboratory coating runs gave satisfactory results that led to production coating techniques. The optimum cure of Hypalon was determined by tensile tests on unsupported films of cured elastomer. Commercial coating techniques have been used throughout the development.

Curing presented many problems, for the residul shrinkage often caused puckering and wrinkling while most interleavening agents promoting blocking of the coating during cure. Surface stainings and off-colors were manifold. However, colors showed little change after considerable exposure in weatherometers. Some modifications of the coating were needed. The accelerator MBTS, mercaptobenzothiazyl disulfide, was replaced with double amounts of Thiuram M, tetramethylthiuram disulfide, to give a more controllable cure. Lead acetate, used for acid buffering in cure, was eliminated to improve whiteness. This reduced the pot life of the coating but to no major consequence. Flame resistance in heavier fabrics had to be improved thru the use of more antimony trioxide at the expense of some titania pigment.

Normal coating technology lead to the incorporation of the isocyanate adhesion promoting compounds into the coating material at least for the first pass of the coating application. An outgrowth of this modified first coat was the use of a latex or a solution of unpigmented Hypalon rubber and MDI in toluene to impregnate the fabric and fill the voids and interstices with elastomer in an effort to reduce moisture absorption without loss of adhesion and thus increase radar transmission under rain exposure conditions. Moisture absorptions was cut to 1% or less even with immersed, unsealed edges. Wet transmission at about 10,000 Megacycles per second was 97% minimum; then dry it was 99% in such a Dacralon proofed fabric.

The joint or seam cement formulation was modified to effect a faster, stronger cure. The Thiuram M and phthalic acid which had been recommended were replaced with Neoprene accelerator No. 22, (2 - mercaptoimidazoline) and with

DOTG Nicker (diorthotolyl quanidine). The coating dispersant was replaced with toluene solvent for a better cement. Tri basic lead maleate was the curing agent used to effect cross linking.

Two inch lap joints were cured in an oven for one hour at 250 F and generally had lap strength in excess of 200 lbs/inch. A loop of the coated, three ounce fabric usually broke at an area separated from the joint. A two hour cure enabled the joint to withstand four hours at 160 F under 120 lbs/inch load.

At this stage a significant achievement was noted since there had not previously been a cement available that would give satisfactory bonding of Hypalon coated surfaces especially at elevated temperatures. Joints had serrated edges with one inch deep V slots and the serrations were superposed to provide a continuous two inch lap joint.

Another significant discovery was that this proofed fabric, Dacralon, and its cement as developed, would lend itself to "heat sealing" techniques. Such a technique in proofed fabrics can save time and effort in fabrication, increase design latitudes and could allow new applications for the Dacralon proofed fabric. The Hypalon cement can be painted onto the surfaces to be joined and then allowed to air dry. Ten to fifteen minutes is generally sufficient for loss of solvent, however, satisfactory joints can be attained even if the "painted" surfaces are not joined for 72 hours. The surfaces are then sealed together with a hot iron. The joint at this stage is not completely cured, however, there is a high peel strength and the shear strength was seen to exceed 200 lbs/inch in a two inch serrated lap on a loop of five ounce fabric. The final and complete cure can be performed on the entire package in an oven.

TESTS AND DESIGN CONSIDERATIONS

Throughout this development numerous tests were performed to see what had been accomplished against specification requirements and for future guidance. Most tests were those common to the proofed fabrics trade and generally followed ASTM procedures. Strengths are reported on the ravelled strips and not by the grab method.

Burst tests are designed to give a strength figure for radome design. Fabric was clamped to a flat plate and inflated till it burst, providing a stress value according to the radius of curvature of the distorted fabric. Three ounce Dacron, coated with four ounces of Hypalon, (seven ounce Dacralon) was seen to have a burst strength of 120 lbs/inch and was regarded as satisfactory.

Weatherometers, sun lamps and natural weathering indicated that about three mils of Hypalon in a good coating was a minimum, for this permitted but a few percent loss of strength after extensive weathering.

Resistance to ripping in air supported structures is a valuable aspect, but it is difficult to accomplish and even more difficult to evaluate. Tongue and trapezoidal tear methods did not apply to biaxially stressed fabrics.

Puncture tests of samples stressed over a drum were difficult to correlate with radome performance. DeBell and Richardson conceived and built a device for applying a biaxial stress field that was not unlike a trampoline. In radomes of any size, a "test panel" can for some purposes be treated as a biaxially stressed, flat plate where the sample is progressively slit in the center until ripping ensues.

There arose in this regard a diametric situation where joint strength and rip resistance had requirements in opposite directions, since the ripping resistance in radomes seemed to require loose yarns of high strength that could move relative to one another, while the joints required extremely good adhesion of the yarns to coating. Since there was room for improvement in yarn strength and denier per end for each fabric, it appeared more logical to compensate for tearing characteristics through yarn strength and/or denier rather than sacrifice the unprecedented adhesion of coating and joints. Dacralon type fabrics performed better than Neoprene-Nylon on a given weight and construction basis.

The safety factors used in air supported radomes could be reduced from their value of about four or five, for the uncertainties in weathering effect and dead load fatigue could be greatly reduced in Dacralon fabrics.

Dacralon has an exceptional property in potential regard to accomodating stresses in a radome. The proof has an initially high modulus compared to related materials which gives its dimensional stability at normal conditions. Just above normal loads, Dacralon can yield elastically at medium stress levels to relieve stress concentrations. At higher loads the modulus is again high and continues high until break. The breaking strength is unprededented in materials of such light weight.

The unit strength of Dacralon proofed fabric is over 25 lbs/inch for each ounce of total weight as compared to about 12 for other types. In the bare uncoated fabric, there is breaking strength of about 65 lbs/inch for each ounce of fabric. Computing a cross-section and tensile from breaking strength, Dacralon has a tensile strength of over 25,000 psi even in thick samples. Twenty mil Dacralon pulls about 500 lbs/inch before breaking. Elongation is about 10-15%. Filaments of the hot stretched or drawn Dacron have a tensile strength of about 160,000, being considerably higher than most organics. Thus it is seen that Dacralon has an exceptionally high strength to weight ratio.

APPLICATIONS -

An extension of the work with DeBell and Richardson called for a prototype radome that would incorporate these improvements. It was decided to use a single ply Dacralon for this test structure with a crown of two ply Dacralon. The principal techniques of conventional radome design were utilized with those modifications necessary to adapt this new material to a prototype. This radome with 35 feet base diameter is now being fabricated by DeBell and Richardson, Inc. at Hazardville, Connecticut.

The heat sealing technique is being used in this fabrication. Each gore of fabric is being joined to the next by positioning and pressing together the lap with a hot iron on a contour form. The crown, crown plate, windows, etc. are being incorporated into the structure by similar techniques. The completed radome will then be cured as a whole in an oven to effect complete cure of the joints.

The Dacralon proofed fabric for the prototype weighs about 14 ounces/square yard. Such a Dacralon fabric is probably heavier than necessary for it would pull at least 450 pounds/inch before breaking. However, its use was considered expedient in this prototype for there could be further weight economics in subsequent items manufactured against specific end use requirements. Service life under normal conditions of five years minimum is anticipated. It is expected that the prototype fabrication will be completed for delivery to the Air Force this summer. A shipping container of heavier Dacralon material for the radome is also being fabricated.

Of concurrent interest in this regard, there was also developed through Rome Air Development Center by the B. F. Goodrich Company a radome maintenance coating using a modified, Hypalon based paint. The radome coating has been designated "Radolon" and is a blend of Hypalon and polyethylene in an air drying paint that can be brushed or sprayed. It is non-blocking, quick drying and can be made in a variety of permanent colors. It has excellent weather resistance, especially against ozone while samples are under stress. It has good shelf life and good adhesion to a variety of surfaces including laminar, reinforced plastics.

FURTHER USES FOR DACRALON

This Dacralon proofed fabric could lend itself to other designs and structures. Its use as a protective covering over framed structures of "geodesic" design might be interesting because of its strength and weathering ability as well as colorability and its fabrication techniques. The heat sealing technique of Dacralon could be utilized for fabricating a variety of air supported shapes and structures including inflated structural modules and large completed structures. Where necessary this technique might be used for on-the-spot fabrication of rather large structures where radiant energy of a variety of types including possibly infrared, microwave, gamma and beta energies might be used for curing the joint materials.

Radar antennas have been made of air inflated structures. Dacralon might be useable there for its high modulus, durability and fabrication techniques. Extremely high frequency radar, up to 30,000 megacycles per second, might use the Dacralon for its light weight or thinness, its dielectric properties, and moisture resistance. On the basis of preliminary tests, the dielectric constant for Dacralon approximates 3.5 and the loss tangent is about 0.02 at X band. Radar that requires minimum beam distortion and/or power reflection might possibly use Dacralon radomes.

There could be a variety of other applications that could benefit from the weather resistance, moisture proofness and light weight of Dacralon. Commercial tarpaulins and ice or wing covers might be possibilities. Portable housings, tents and shelters could be considered. Protective clothing might utilize the lightweight Dacralon for its resistance to moisture, acids and oxidising agents and its impermeability. Possible use in airships, fuel cells, materials packaging containers and life rafts may be realized. The yarn or fabric may well be used for reinforcings in various plastics and rubber products where its high modulus, moisture resistance and chemical resistance could be advantageous.

In conclusion, there has been developed a proofed fabric of outstanding strength to weight ratio, exceptional weather resistance, and which is capable of unique applications for its excellent joint strength and simplified fabrication techniques.

FUTURE TACTICAL BOMBER PROGRAM

V. Landis, Jr.

Douglas Aircraft Co.
Long Beach Division
Antenna Research & Development Laboratory

Your invitation to speak on our Tactical Bomber Program could not have been more fortunately timed. It arrived one day last spring when a group of us in the laboratories were discussing ways and means of solving some of the present and future problems facing us in radome design.

Today's answer to many of tomorrow's problems, whose sheer size and qualitative demands appear to elude human capacity seems destined to out-distance even the most starry-eyed prognostications.

So on this occasion it seems befitting that we extend our appreciation to the forward looking group of men who so wisely chose to establish so necessary a function as this annual radome symposium, allowing us to take a minute off from the hurly-burly of production and look to see what lies ahead. For like explorers, we must, at intervals climb the highest peaks to view the terrain ahead in order to spare ourselves the pain of coming up hard against unforseen problems and pitfalls.

As you may or may not know, we at the Long Beach Division of the Douglas Aircraft Company have thus far limited ourselves to the production of transport and troop carrying aircraft plus tactical bombers.

A tactical bomber may be defined as small or medium sized high speed aircraft with the capability of delivering a large pay load of destruction up to one thousand miles, at altitudes of 25 feet to 60,000 feet and return. It must carry communication, bombing, navigation, ILS, IFF, ECM (both passive and active), DF, IR, evasive maneuver, confusion repeating, rendezvous and computing equipments, plus many others almost too numerous to mention. It must have the speed of an interceptor and carry the bomb load of a B-36 in all weather; and it must be capable of being maintained and serviced in the front lines with a minimum of ground support equipment. To say the least, the tactical bomber is designed as an extremely versatile weapons system.

There are many problems ahead of us, but one of the foremost confronting Radome Designers and Engineers today is that of the extreme temperature increases on the radome, due to aerodynamic heating.

In our present program we are concerned with temperatures of 340°F at speeds of MACH 1.5 at sea level, to temperatures of 2,000°F at speeds of MACH 5.0 at 100,000 feet.

At speeds only slightly higher than MACH 3.5 (2700 MPH) it is no longer purely a problem of lacking knowledge for solutions, but we face a serious gap in our knowledge of the problems.

At higher temperatures and pressure, the air can be disassociated into separate gaseous components. At still higher figures electrons can be displaced and the air can become ionized. Some exploratory tests into this region have indicated chemical reactions as well as mechanical reactions.

On the urgent list to extend the bounds of our scientific knowledge are:

1. Fundamental studies of heat transfer both from gases to solids and within solids.

2. Studies of nuclear bond within solids

3. Studies of why the effects of temperature bring about the loss of structural strength.

A drastic change in the presently used radome materials and techniques is eminent in the immediate future to eliminate the existing design deficiencies of our future aircraft.

We have made some progress in the structural qualities of plastics, ceramics and silicons, some in fabrication techniques and others in basic radome design. However, a completely integrated solution to these many complex problems still eludes us.

It is no longer feasible to design a hemispherical radome, drill a few holes around the edges, fabricate an attach ring and mount it on the front of an aircraft. In many cases the radome is an integral part of the primary structure of the aircraft. As the speed requirements increase the radome becomes longer and smaller in diameter and angles of incidence jump from 0° to 50°, to 40° to 85°. Our structure people tell us it must be extremely thick to carry the loads. Our systems people say it must have 90° transmission and 3 MILS boresight error in order not to degrade system operation. Our aerodynamic people tell us the only place to obtain accurate air flow data is to put a pitot tube square in the center. Our operations analysis people tell us the pitot tube must have in-flight refueling capabilities, and the project people tell us it must be anti-iced to obtain all weather operation.

Our radomes must not only meet all these requirements, but because of thier missions they must be capable of withstanding nuclear radiation blasts up to 2000°F for 30 seconds and still not absorb enough heat to cause damage to the housed equipment rated at 180°F. This means a reflective coating. This coating must withstand rain and hail erosion at high speeds and temperatures and yet not affect transmission.

The radomes must be impervious to chemical reaction due to Jet fuel spillage. They must be capable of possibly flying through clouds of nitrous oxide and monatomic atmospheric oxygen that may be used for photography or ECM, without physical damage and they must withstand pressures subjected at altitudes of 100,000 feet and maintain a pressure seal.

The here-to relatively unimportant problem of radomes for flush mounted antennas looms up now as a new area for work. The problems of ionized air, heat and voltage breakdown at high altitudes can no longer be set aside.

These are but a few, but may suffice to indicate the trend that is so eminent in the growing magnitude of unsolved problems lying ahead.

So, today I would like to suggest some areas of serious deficiency that cry for action. There are several for us to choose from, but three command our instant attention. I speak of a looming shortage of usable radome material, a deficiency of technical manpower that is already with us and a growing dearth of new, basic knowledge.

Everyone of these in an essential ingredient of our success and each is sufficiently critical now to pose a threat for the future.

These problems are now sufficiently commanding to demand an ever increasing expenditure of time, manpower and dollars in research and development programs.

We must look ahead, recognize areas of both deficiency and plenty, then plan and act accordingly.

It is evident to all of us that there is a desperate need for trained Engineers and Physicists and especially those interested in this highly specialized field of radome design.

The dependence upon you and the others in kindred engineering and scientific fields is a very real and conscientious thing. In more ways than we readily realize, it is upon you, whom we rely, not only for our progress but for our protection.

There is more truth than fiction in the story of the devoted old lady who began her morning prayers with these words, "Give us this day our daily bread and enough Engineers and Scientists to keep us alive until tomorrow".

Whether we like it or not, we are in a race for technical supremacy with those who order the affairs of the Communistic states. The stake is frightening; it is the continued existence of the free world and perhaps man himself.

We are at the threshold; possibly across the threshold of another of the creative surges that have marked the great epochs in the history of man's progress. The circumstance is by no means of our contrivance alone. But while a little fatalism is not out of place, indeed it is essential. Our wine is from our own vines and to think otherwise would be folly. The challenge is clear, exhilarating and direct. We have little choice but to meet it head on and we must not fail in the opportunity it provides.

All in all, the picture is one of immense responsibility and great promises. Certainly a field which has come so far in so few years can be expected to meet the challenge with every success.

THE EFFECT OF COLLIMATION ERROR ON PROPORTIONAL NAVIGATIONAL SYSTEMS

D. Mayers

Hughes Aircraft Company

Proportional navigation is a guidance system which corrects to a collision course by attempting to make the vehicles rate of change of heading proportional to the rotation rate of the line of sight to the target. In mathematical notation, then

(1) $$\dot{\gamma} = \lambda\dot{\sigma}$$

γ and σ are, respectively, the angles which the vehicle's velocity vector and the line of sight from that vehicle to the target make with an arbitrary reference line in inertial space. $\dot{\gamma}$ and $\dot{\sigma}$ are the time rates of change of these angles. λ, often called the navigation constant, is simply a constant of proportionality.

When line of sight angle information is provided by a radar seeker, filtering of this information is used to smooth target noise. Typically, the system may resemble that provided by two simple lo-pass filters in series. In practice, then, the navigation equation looks like this

(2) $$\tau_1 \tau_2 \frac{d^2\dot{\gamma}}{dt^2} + (\tau_1 + \tau_2)\frac{d\dot{\gamma}}{dt} + \dot{\gamma} = \lambda\dot{\sigma}$$

τ_1 and τ_2 are the time constants of the two lo-pass filters. This equation can be recognized as a description of damped simple harmonic motion.

Radome, or more properly, collimation errors cause a displacement of the apparent line of sight from the true line of sight. If the component of this displacement in the direction of motion of the true line of sight is called η, then the effect of this error must be taken into account by adding $\lambda\dot{\eta}$ to the right hand side of Equation (2). Now the system is operating on an apparent line of sight motion, $\dot{\sigma}_A$.

(2a) $$\tau_1 \tau_2 \frac{d^2\dot{\gamma}}{dt^2} + (\tau_1 + \tau_2)\frac{d\dot{\gamma}}{dt} + \dot{\gamma} = \lambda(\dot{\sigma} + \dot{\eta}) = \lambda\dot{\sigma}_A$$

It is assumed that in the limited portion of the radome with which we are concerned the change of the collimation error, η, is linear with changes in the radar antenna offset angle from the vehicle's fore and aft axis. If this offset angle is called β, this statement of linearity may be written

(3) $$\dot{\eta} = k\dot{\beta}$$

The constant, K, is the collimation or radome boresight slope. It should be noted that K is positive for a change in apparent line of sight in the same direction as the change in offset angle which caused it.

To show how the collimation boresight error interacts with the vehicle's turning dynamics, some further substitutions must be made. First, the offset angle, β, may be written in terms of the angle, θ, which the vehicle axis makes with the original inertial reference line and the true line of sight σ. This can be done strictly only when the antenna axis is identical with the true line of sight. In practice, tracking errors are very small compared to offset angles and this simplification gives accurate results where K is of the order of 0.1 or less. With this understanding, then,

$$\dot{\beta} = \dot{\theta} - \dot{\sigma} \tag{4}$$

Here, again, $\dot{\beta}$ is positive if the offset angle is increasing. Substituting once more into Equation (2a)

$$\tau_1 \tau_2 \frac{d^2 \dot{\gamma}}{dt^2} + (\tau_1 + \tau_2) \frac{d\dot{\gamma}}{dt} + \dot{\gamma} = \lambda\dot{\sigma} + K\lambda\dot{\theta} - K\lambda\dot{\sigma} \tag{5}$$

$$= \lambda(1 - K)\,\dot{\sigma} + K\lambda\dot{\theta}$$

The axis of a turning vehicle is not in general coincident instantaneously with its velocity vector. The angular difference is called the angle of attack, α, and in general for smooth turning is in the same plane as the turning trajectory. One may describe this mathematically as follows:

$$\alpha = \theta - \gamma \tag{6}$$

or rearranging and differentiating with respect to time

$$\dot{\theta} = \dot{\alpha} + \dot{\gamma} \tag{6a}$$

The configuration of the vehicle determines the angle of attack necessary to cause a given turn rate. Thus it may be written

$$\alpha = \tau_S \dot{\gamma} \tag{7}$$

The constant of proportionality τ_S is called the vehicle's turning time constant. Substituting (7) and (6a) back into (5),

$$\tau_1 \tau_2 \frac{d^2 \dot{\gamma}}{dt^2} + (\tau_1 + \tau_2) \frac{d\dot{\gamma}}{dt} + \dot{\gamma} = \lambda (1 - K)\,\dot{\sigma} + K\lambda \left(\dot{\gamma} + \tau_S \frac{d\dot{\gamma}}{dt} \right) \tag{8}$$

or

$$(8a)\quad \tau_1 \tau_2 \frac{d^2 \dot{\gamma}}{dt^2} + (\tau_1 + \tau_2 - k\lambda\tau_S) \frac{d\dot{\gamma}}{dt} + (1 - k\lambda)\, \dot{\gamma}\,(1 - k)\, \dot{\sigma}$$

Equation (8a) is more complicated than Equation (2) but also describes damped simple harmonic motion. It can be seen that when a steady state condition is reached, i.e. the higher derivatives have vanished, the perturbed proportional navigation equation becomes

$$(9)\quad \dot{\gamma} = \frac{\lambda (1 - k)}{1 - k\lambda}\, \dot{\sigma}$$

It can be seen that if k becomes as large as $1/\lambda$, the system gain becomes infinite and further increases in k will actually cause acceleration in the wrong direction. This, then, describes one stability limit on collimation boresight slope i.e.

$$(10)\quad k\lambda < 1$$

In order that damped simple harmonic motion be in fact damped and therefore stable, the first order or damping term must be positive. Therefore, another condition for guidance stability in the presence of a boresight slope is derived by setting the first order term in (8a) equal to, or larger than zero, hence,

$$(11)\quad \tau_1 + \tau_2 - k\lambda\tau_S \geq 0$$

or

$$(11a)\quad k\lambda \leq \frac{\tau_1 + \tau_2}{\tau_S}$$

These equations describe then the maximum positive collimation boresight slope consistant with guidance stability.

Negative stability limits can be derived in many cases of interest by including in the guidance equation the vehicle's transient turn rate response to rudder signals. This response is in general of the form of another damped harmonic oscillator. If the resonant frequency of the vehicle's transient response is considerably larger than the tracking system resonant frequency, the following approximate negative stability criterion may be derived.

$$(12)\quad k\lambda > \frac{-2\zeta_o\, \omega_o \tau_1\, \tau_2}{\tau_2}$$

Here ω_o and ζ_o describe the resonant frequency and damping constant of the simple harmonic turn rate response, and τ_1, τ_2 and τ_S are as described before.

If the mathematical model of the guidance system is extended to include both the pitch and yaw planes of guidance it is found that similar stability criteria exist with regard to the component of collimation error which is at right angles to η . A collimation cross-talk slope k_x is described as follows:

$$\dot{\eta}_x - k_x \dot{\beta} \tag{13}$$

Here $\dot{\eta}_x$ is the apparent motion of the line of sight at right angles to the change in offset angle. In this two dimensional case the stability limits for crosstalk and boresight slopes are interdependent and a typical stability boundary diagram is shown in Figure II.

It should be noted, however, that the effect of collimation errors on guidance accuracy become pronounced long before the system becomes unstable. A typical curve of guidance miss due to scintillation noise as a function of positive boresight collimation slope alone is shown in Figure III.

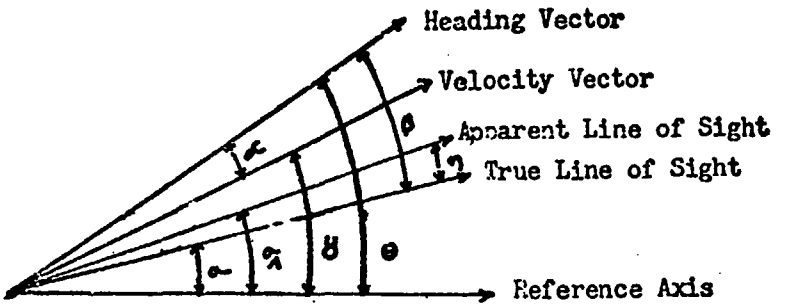

Figure 1

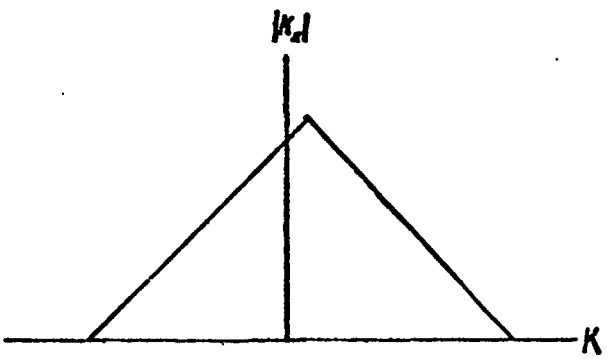

Figure 2

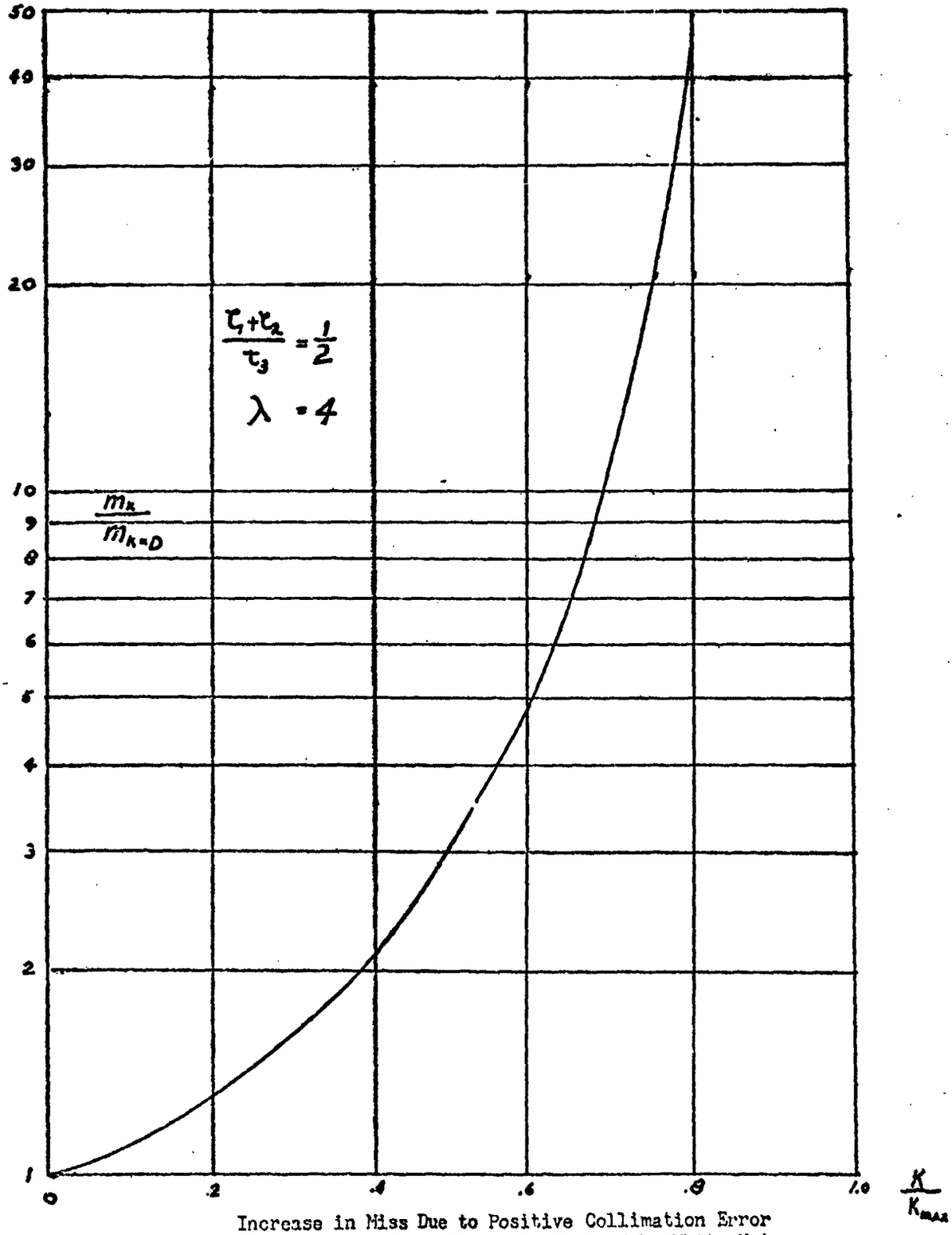

Increase in Miss Due to Positive Collimation Error
Slope when Guidance System is Excited by White Noise

Figure 3

DEVELOPMENT OF A VERY HIGH TEMPERATURE RADOME

By

Irving M. Ziff

Zenith Aircraft
Gardena, Calif.

With the conquest of 250°F to 350°F sandwich radomes within grasp, planning and investigation of the next thermal plateau had commenced at Zenith. While superficially looking over the avenues of attack, a very real obstacle was placed before us — an immediate need for a 500°F to 650°F radome able to withstand thermal shock to possibly 1500°F. The two materials available most closely approaching these requirements were Dow Corning's DC 2106 silicone laminating resin and Hexcel's CTL core. The CTL core is glass fabric base high temperature phenolic honeycomb and the DC 2106 laminating resin for the skins was preimpregnated onto fiberglass fabric. The sandwich construction was to be one-half-inch overall thickness with .410-inch thick core. The outside and inside skins were to be .060 and .030 inch, respectively. Several mechanical strength requirements that had been set forth were flexural skin stresses of 10,000 #/in^2 at 500°F after one-half-hour exposure at 500°F and a room temperature bending moment of 200 in-lb/in. width after a one-hour soak at 500°F. Of these requirements Zenith was only to perform the room temperature tests as a quality control measure.

A pre-production development program was started without delay. Autoclave molding with vacuum bags on the part in female tooling was the apparent approach. This was adopted after initial investigations and consultation with vendors. Beside the actual problems related to obtaining optimum properties from the constituents, the auxiliary materials for achieving the process had to be investigated. Release from the platens and molds was readily obtained with a thin coat of wax paste followed by a film of silicone release agent. Conversely, several investigations were necessary to find a releasing material for covering the top side of the lay-up. It was painfully discovered that cellophane and mylar would tend to fuse into the silicone skins at cure and postcure temperatures. Perforated teflon-impregnated glass fabric was finally accepted as the topside releasing agent. On top of this, industrial glass mat was used as a bleeder layer for achieving effective vacuum overall.

Polyvinyl alcohol was initially used both singly and doubly as the bagging material. Possible bag leakage necessitated a search for another bagging material. The outcome of this was the adoption of silicone rubber coated glass fabric. This was mechanically sealed to the mold using a gasket of high temperature zinc chromate.

Several combinations of flow and resin content in glass cloth preimpregnated with DC 2106 were tried. The combination that finally evolved as best suited to fulfill the molding requirements was a resin content of 34% to 38% and a flow of 14% to 16%. The flow is determined under 100 #/in^2 at 340°F. The volatile content to which this material is treated is below 1½%. The gel time of the resin under these conditions should be around 2½ minutes at 340°F.

In laying up the first test panels it was found that due to the bulk factor it was necessary to place the top skins in position when the build-up was level with the core. The bulk factor referred to is a ratio of the uncured to cured thickness. When the top skins were in place the build-up was completed. This gave a burying effect of the skins on the molded part, which became desirable as upon finishing the edges for attachments the danger of cutting through the top skins was lessened.

After testing the first sets of panels it was evident that an improvement of the core bond was necessary. Commercially available adhesives were avoided as their electrical properties as well as their ability to withstand the thermal shock were questionable. A core treatment was developed from which the flatwise tensile properties were improved as much as 65%. This treatment consists of etching the core in a 20% caustic soda solution for one-and-three-quarter minutes at 140°F. The core is immediately neutralized and rinsed in water. After complete drying of the core it is coated with silicone resin to the original density of 6.5 #/ft^3. Curing of this resin coat is critical, as too rapid a cure causes boiling of the toluene solvent which in turn causes a weakening bubbling effect.

Under pressure molding the dimpling of the skins between cell walls of the core was excessive. This was true even when molding pressures were reduced from 95 to 45 #/in^2. Another problem was filling of core cells with resin which drained from the skins. A novel idea of placing a precured ply of material one ply away from each side of the core was adopted. This, for the greatest part, eliminated dimpling as well as excessive flow of resin into the core. It was discovered that the secondary bond obtained to the precured ply was equal to a wet lay-up interlaminar bond. Initially the precured plies were cured between teflon sheets and then sanded. Sanding was later eliminated by curing between unimpregnated sheets of a fine glass fabric and tearing them away after cure.

Another very important factor is that upon completion of cure it was found necessary to maintain pressure until the temperature has been reduced to 150°F. Otherwise an unbonding or delamination of the skins is likely to occur. It may be noteworthy at this point to mention that silicone skins of this type are porous. This is probably advantageous as indications are that the CTL core gives off a degradation gas even though fully cured. In addition, any residual toluene would boil off at approximately 250°F. Either of these gases or a combination thereof could cause unbonding of the skins were they not porous.

At this stage tests were conducted on parts fabricated by the evolved process. These tests gave values equal to or exceeding the required bending moment. Values ranged from 200 in-lb to 250 in-lb/in. width. The process was then adopted for production fabrication of radomes. Production schedules were such that the time required for heating and cooling of the autoclave made it necessary to investigate the feasibility of vacuum bag molding. Investigations revealed that the use of augmented pressure was not necessary. A corollary advantage of the use of lower pressure vacuum bag techniques was the elimination of the need for precured plies. Production processes were finalized by adapting all the previously discussed developments using vacuum bag molding in conjunction with oven heating for cure. In addition, the construction was modified such that the inside and outside skin thicknesses were .050 and .040, respectively. Thus the meeting of production schedules was essentially accomplished without sacrificing surface conditions or structural integrity.

With radomes flowing off the production line research is far from complete. Evaluation of new materials is already in progress. Preliminary results obtained with a new silicone impregnated core material look very promising. Production problems such as warpage developed during cure and postcure are obstacles to overcome. Investigation of core bond improvement has barely been scratched, and a thorough investigation of the empirically derived flow-resin content-pressure relationship is imperative.

* * * * *

MATERIALS PROBLEMS IN AIRBORNE RADOMES DESIGNED FOR HIGH SPEEDS

by

R. A. Spurr, Senior Staff Chemist

and

G. D. Robertson, Head of Materials Application Section

Plastics Department
Research Laboratories
Hughes Aircraft Company
Culver City, California

I. INTRODUCTION

The task of choosing materials for radomes to be flown at supersonic speeds is a difficult one. Before the design of a radome can be started, it is nedessary that the designer have on hand adequate data concerning electrical and mechanical requirements. There is presently no simple line of reasoning by which he can proceed directly from this information to the selection of an appropriate material. The complexity of the problem is indicated by Figure 1. Because of the interrelation of the many factors involved, selection of an adequate material requires a careful balancing of a number of considerations and usually results in compromises in the degree to which each requirement is met. The choice is made more difficult by the lack of data on the performance of most materials under the conditions expected in flight.

It is the purpose of this paper to point out certain lines of inquiry which may be helpful in the selection of materials or in the development of new materials. It will not be possible in the time allotted for this paper to treat the problems involved in a comprehensive manner. Instead, after a brief discussion of some general considerations, a description will be given of experimental work being carried on at Hughes Aircraft Company with the aim of filling gaps in the existing information concerning properties of materials. Much of the work reported deals with the effects of aerodynamic heating, currently one of the important factors in radome design and material selection. Discussion of this topic will point out some of the interrelationships suggested by Figure 1.

II. EFFECTS OF AERODYNAMIC HEATING

A. General Considerations

Stagnation temperatures encountered at different altitudes and velocities are shown in Figure 2A. It should be noted that the temperatures of the boundary layer air and of the radome surface are generally lower than the stagnation temperature, as shown in Figure 2B.[1] The data plotted in Figure 2B are for operation under transient conditions at altitudes from 35,000 to 100,000 feet for an interceptor radome with a surface emissivity of 0.9; the indicated difference between the boundary layer and surface temperatures is due primarily to the loss of energy from the surface by radiation and by conduction through the radome. The bulk of the radome remains at temperatures considerably lower than the surface temperature. For these

reasons design considerations based on stagnation temperature alone are unnecessarily severe.

The important deleterious or potentially deleterious effects caused by heating fall roughly into two categories: reversible and irreversible. Reversible effects include variation of modulus, strength, and dielectric properties with temperature. Irreversible effects can occur in the following ways: 1. organic material in the radome may be oxidized; 2. material may be thermally degraded by nonoxidative processes; 3. absorbed moisture or contained gas may be rapidly expanded with the formation of blisters; 4. stresses set up by temperature gradients may cause delamination or crazing.

Estimation of the effect of temperature for both reversible and irreversible changes must include consideration of the length of time during which the material will be at high temperature. The shortness of some missile flights makes possible the use of materials which would degrade during long exposure to the peak temperatures encountered. For example, one material which loses strength and also begins to depolymerize at relatively low temperatures has been successfully flown under conditions which produce maximum surface temperatures of 525°F and average surface temperatures of about 350°F. The strength of this material, as shown in Figure 3, would not appear to be adequate upon first consideration; however, because of its low thermal conductivity and the short flight times, the temperature of the bulk of this material does not increase appreciably. Consequently, the radome performs satisfactorily.

Tests on radome materials have been carried out at many temperatures and the results are often difficult to compare. It is helpful in ranking materials to have a way of relating the rate r of thermal decomposition at a given temperature T to the rate r_o which would be obtained at another temperature T_o. The following equation may be derived from the well-known Arrhenius relation:

$$\frac{r}{r_o} = \exp\left[-\frac{E}{R}\left(\frac{1}{T} - \frac{1}{T_o}\right)\right] \qquad (1)$$

where the rates r and r_o may be expressed in percent decomposition per unit time, E is the activation energy of the reaction, R is the gas constant, and T and T_o are absolute temperatures. A rule of thumb is that the quantity E/R is about 30,000°K for the nonoxidative thermal decomposition of many plastic materials.[2] Expressed more specifically, a rise of 15°F in temperature causes a doubling of reaction rate in the region from 600 to 700°F.

B. Electrical and Mechanical Behavior

Investigations of the characteristics of materials at elevated temperatures have been concerned with evaluation of specific electrical and mechanical factors. Measurements of such electrical properties as dielectric constant and loss tangent at high temperatures are difficult, but progress is being made in obtaining reliable values. Figure 4 shows the reversible increase of dielectric constant with temperature for four fiberglass laminates.

Among the materials shown, the rate of increase is greatest for phenolic and least for silicone; epoxy and TAC-polyester show an intermediate rate. The dielectric constants for silicone and phenolic laminated panels held for various times at high temperatures are compared in Figure 5. The severe heating of the panels indicated on the figure brought about irreversible changes in the material which are reflected in the values of the dielectric constant obtained. The difference between the two types of laminates after exposure to 750°F for two hours can be seen easily (Figure 6*); almost all the resin has been burned from the phenolic panel but the silicone laminate appears to have suffered no permanent damage.

Partly because of the ease with which ultimate flexural strength can be measured, wide use has been made of it as a means for rating materials. A decrease in this quantity with increasing temperature may, like changes in the dielectric constant, be reversible or irreversible in character. It should be noted that room-temperature strength is no criterion of performance at high temperature. Thus a resin which shows extraordinarily high strength at room temperature may be considerably inferior to another resin at 500°F (see Figure 7). Oxidation may be important in the degradation of resins at high temperature. As shown in Figure 8, exposure of samples of phenolic laminates to 500°F for five hours in a nonoxidative environment caused only a slight decrease in room temperature flexural strength; the decrease was marked when oxygen was allowed access to the sample.

The aerodynamic heating which occurs when a missile radome is rapidly accelerated to supersonic speeds produces thermal shock, because the thermal gradients formed may give rise to severe stresses within the radome. Figure 9 shows the temperatures of the outer and inner surfaces of an alumina cone immersed in a bath of molten metal. By adjustment of the bath temperature and the time of immersion, a wide variety of flight conditions may be simulated. Laboratory results have been correlated to some degree with similar results obtained from actual flight tests. Hughes Aircraft Company is conducting a series of such tests from which considerable temperature data have been secured. (See "Temperature Data for the Falcon Radome," by J. H. Beno, R. W. Quint, and E. F. Smith, presented at this Symposium.)

III. NEW EXPERIMENTAL METHODS

Existing plastic materials are not in general suitable for the high-temperature requirements which are expected to be imposed by high-speed aircraft and missiles to be developed in the near future. The course of development of the new materials needed will be guided by investigations of relationships between composition and molecular structure on the one hand and physical and thermomechanical properties on the other. Several studies of these kinds involving the use of recently perfected instrumental methods have been undertaken at Hughes Aircraft Company.

In the study of plastic materials intended for use at high temperatures, infrared and ultraviolet spectrometers have a number of applications. It is possible, for example, to analyze resins of unknown composition, to detect the appearance or disappearance of functional groups as a result of oxidation, and to identify products of thermal degradation. Spectroscopic methods are particularly appropriate for thermosetting resins, whose insolubility in the

common solvents makes them difficult to analyze by ordinary chemical methods.

The usefulness of the X-ray diffractometer is fourfold. First, it provides a means of quantitative analysis of compounds. The principle of the analytical method is shown in Figure 10 in which the intensities of the characteristic scattering peaks of anatase and rutile are related to their abundances in titanium dioxide. Second, X-rays yield information concerning the distribution of intramolecular and intermolecular spacings in a material and serve as a measure of resin cure. In Figure 11 it can be seen that the peak of the scattering curve moves to longer distances with increasing cure time of a phenolic resin. Third, through small-angle X-ray scattering, information concerning molecular chain lengths is obtained. Fourth, X-rays establish degree of crystallinity[3] which affects elastic modulus and ultimate tensile strength.

The electron microscope yields structure in greater detail than X-ray scattering. In the electron micrographs of a phenolic resin shown in Figure 12, the spots of high density may be considered as polymerization nuclei of the plastic. These regions probably have higher cohesive strength than the relatively amorphous regions surrounding them. The spots are most readily visible near the edges of sections where they have apparently been left by the tearing action of the microtome blade, which separates them from the weaker matrix in which they are imbedded. In certain specimens polymerization nuclei can be observed in some regions but not in others. Prolonged heating apparently increases the number of the nuclei, as can be seen in Figure 12.*

In the measurement of elastic modulus with the usual physical testing machines, it is difficult to control the temperature of the sample; in addition, there is generally no provision for controlling the atmosphere surrounding the sample. As a result of these considerations an apparatus, shown in Figure 13, has been designed to measure at controlled temperature and atmosphere the natural frequency of the sample in the form of a vibrating reed. Young's modulus is given by the following expression:

$$E = K \rho \frac{L^4}{D^2} f^2 \qquad (2)$$

where E is the modulus, ρ is the density of the material, L and D are respectively the free length and the thickness of the reed, and f is the resonance frequency in cycles per second.[4] If metric units are used throughout, K has the value 38.24. The logarithmic decrement δ, which is a measure of the internal friction of the reed, is given by the equation

$$\delta = \frac{\pi}{\sqrt{3}} \frac{f_2 - f_1}{f} \qquad (3)$$

where f_2 and f_1 are the frequencies (just above and below the resonance frequency f) where the amplitude has one-half its maximum value.

IV. CONCLUSION

Much of the research and development activity discussed here has been undertaken only recently. Preliminary results, however, are encouraging, and it is hoped that some of the ideas presented will stimulate work elsewhere. At any one institution only limited contributions can be made to the store of knowledge. If present high interest in the field of radomes continues, further progress will undoubtedly be made in the development of materials for high temperature uses.

REFERENCES

1. G. D. Robertson and D. H. Baer, "An Analysis of the Aerodynamic Heating of a Solid-Wall Radome in Supersonic Flight and the Effect of Several Design Parameters on the Radome Behavior," Proceedings of the 1955 Radome Symposium, Vol. II (Confidential), pp. 55-74, Ohio State University.

2. S. L. Madorsky and S. Straus, "Thermal Degradation of Polychlorotrifluoroethylene, Poly-α, β, β Trifluorostyrene, and Poly-p-Xylylene in a Vacuum," Journal of Research of the National Bureau of Standards, Vol, 55, pp. 223-230 (October 1955).

3. S. Krimm and A. V. Tobolsky, "Quantitative X-ray Studies of Order in Amorphous and Crystalline Polymers," Journal of Polymer Science, Vol. 7, p. 57 (1951).

4. L. E. Nielsen, "Some Instruments for Measuring the Dynamic Mechanical Properties of Plastic Materials," ASTM Bulletin No. 165, pp. 48-52 (April 1950).

* Because of the format requirements of this publication, photographs can not be reproduced. Those figures not included here can be obtained by requesting them from the authors. A list of these figures and their captions follows.

Figure 6. Behavior of phenolic and silicone laminates on exposure to 750°F (Photo No. R 38778 - Phenolic, Photo No. R 38779 - Silicone)

Figure 12. Electron micrographs of phenolic resin panels (left)Postcure for 4 hours (right) Postcure for 428 hours (micrographs)

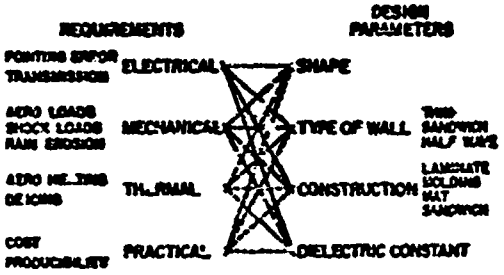

Figure 1. Interrelations of typical requirements and design parameters

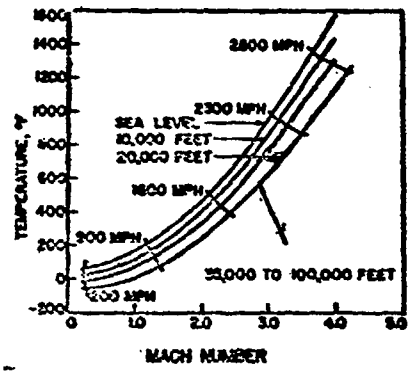

Figure 2A. Stagnation temperature as a function of Mach number for various altitudes

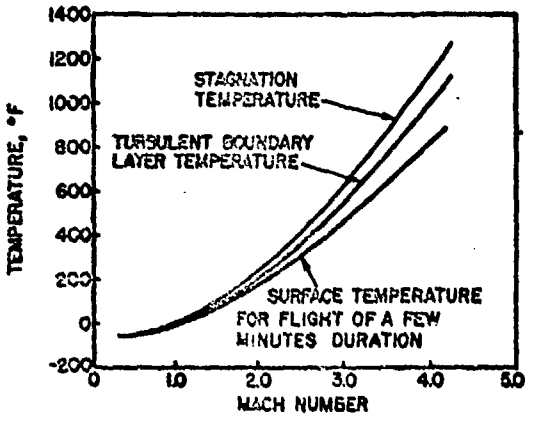

Figure 2B. Transient heating of a typical aircraft radome

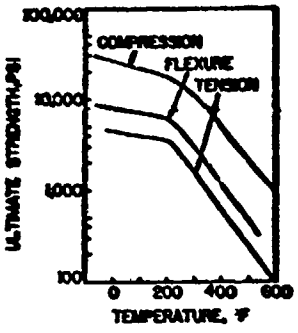

Figure 3. Effect of temperature on the strength of a radome material

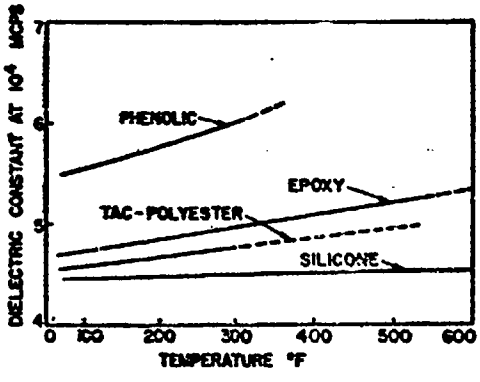

Figure 4. Reversible effect of temperature on the dielectric constants of fiberglass laminates

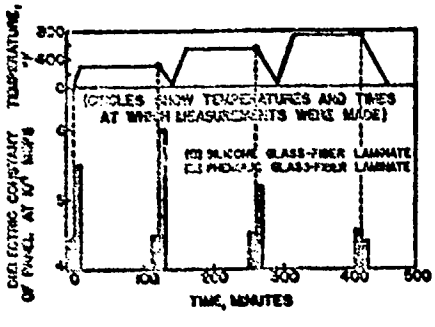

Figure 5. Irreversible effect of temperature on the dielectric constants of fiberglass laminates

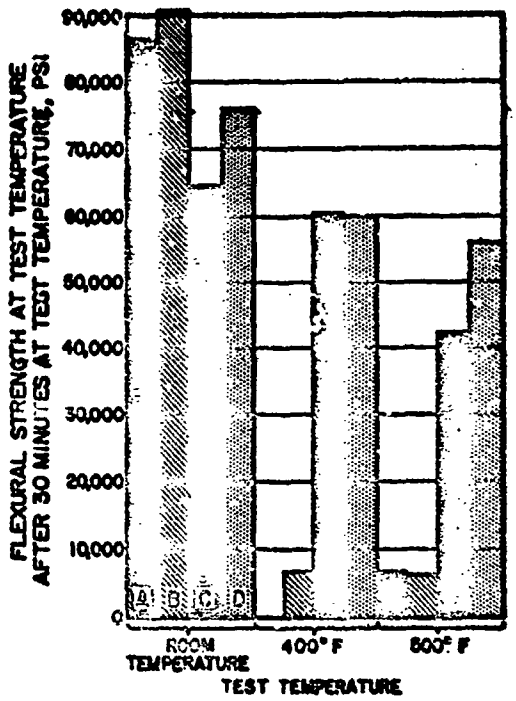

Figure 7. Comparison of the strengths of laminates containing various phenolic resins

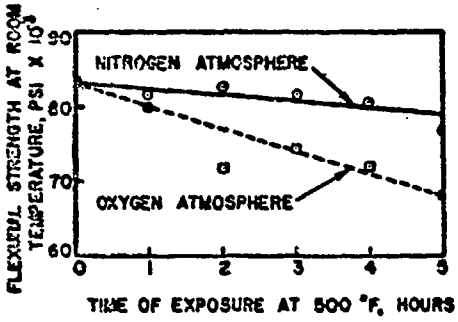

Figure 8. Effect of oxidation on the strength of a phenolic laminate

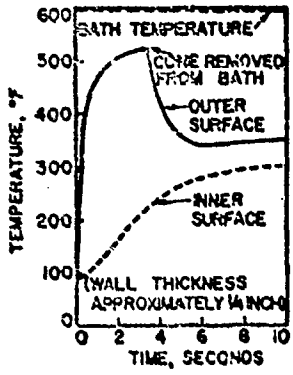

Figure 9. Rapid heating of a ceramic cone

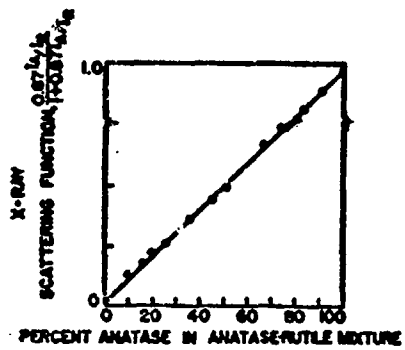

Figure 10. Analysis by X-ray scattering intensities of anatase-rutile mixture

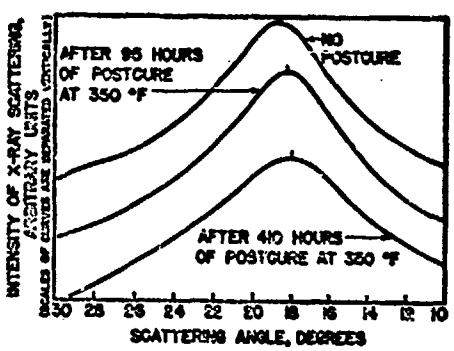

Figure 11. X-ray scattering for a phenolic resin

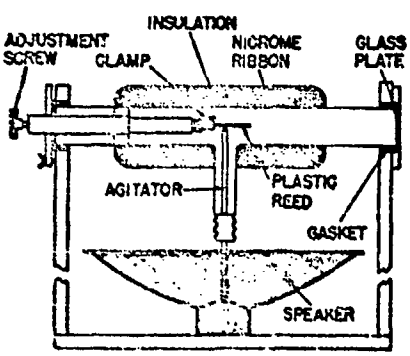

Figure 13. Elastometer

PROCESS SPECIFICATIONS

By

Fred T. Brewen

Zenith Aircraft
Gardena, Calif.

Today, radomes are used almost exclusively by the Military. This being the case, all requirements of the governing military specifications must be observed along with all those of the individual prime contractors -- the aircraft manufacturers. Occasionally, a potential fabricator may be awed by what may seem to him to be an overwhelming set of specification requirements. These requirements need not be merely burdensome, but may serve many useful purposes for the fabricator. We will discuss one requirement, that of preparing process specifications, and indicate some of the useful features which process specifications may possess.

Type and Scope:

Each of the specifications covering radomes and the materials which go into their manufacture requires of the radome fabricator a process specification which is to describe details of manufacture and control of process variables. Done properly, the preparation of specifications can be a time consuming job; however, again done properly, the specification is a very useful document. Thus, we have an alternative between a specification which serves only to comply with the required formalities or one which is well founded on sound engineering and manufacturing practice and, as such, is a ready reference for all phases of part design, planning, and production.

Once the course to be taken has been decided, a fabricator has the choice of preparing two types of specifications. First, he may prepare a specification for each part which is to be manufactured. In this case the task is simplified in that normally only one resin, one type of core material, one method of construction, etc. are employed. The disadvantage of the "part specification" is the large number of documents which will be required. The second choice is to prepare one set of specifications which can be assembled into a manual which will cover all phases of production for all types of parts. In this case, obviously, the specification for each phase must necessarily embrace all variations in the process which can be anticipated. Since the variations and combinations thereof are almost infinite, some degree of standardization must be employed.

Zenith has chosen the latter alternative of the large-scope specifications. Exhibit A, the index to Zenith's specifications, shows the field covered by these specifications. Each of the individual specifications normally contains several variations in procedures. In order to minimize the variations while maintaining the required quality levels, all processes have been established to provide optimum part characteristics. For example, the various cycles of postcure for certain of the high and intermediate temperature range resins could be all but innumerable, but the postcure which has been determined by test to provide maximum

properties is selected. Regardless of how low the stress levels of a part are with respect to the calculated allowables, the postcure which provides the maximum properties is selected. Carrying this standardization further, the designer and production planner will have only one resin and cure system to choose which will fulfill the requirements of the job at hand. Still further, with a given set of part requirements, tooling and production facilities, only one material or combination of materials and one process will be selected for the job. In this way the myriad material and process variations available in the reinforced plastics field are conveniently reduced so that the best combination for a job is chosen in much the same way as the metal working industry can call out a certain alloy or heat treatment.

Form and Usage:

If the specification is to accomplish the purposes previously set forth, there are definite requirements for the information it must contain. Exhibit B, which is extracted from the Introduction to Zenith's Manual of Specifications, establishes the general form for the specification and the information it is to contain. The materials and equipment call-outs are necessarily generalized since it often happens that a customer will supply his own tooling or at least he will specify the type of tooling to be used. Also, the customer will in many cases specify the materials to be used in his part. Obviously, in these cases the customer requirements take precedence over Zenith specifications. In the absence of such limitations, however, the call-outs of the specification are useful for planning. Certainly the detailed procedures section is useful to both Planning and to Manufacturing superintendents and leadmen.

The usage of the specifications is probably best described by discussing its use by different departments in the complete cycle of manufacture of a hypothetical part. Following the invitation to bid, the Estimating Department will prepare a cost estimate. Preparation of estimates can be assisted by reference to specifications for time estimates. Also, in those cases where the type of construction is left open, the estimator often obtains useful information by consultation with the specifications and with personnel of the Materials and Process Group, under whose jurisdiction the specifications are prepared at Zenith. Upon award of the contract the design engineers start their work. The drawing for the part will reference the Zenith Process Specification 1A-1000 (the Specification Manual code number) for all phases of fabrication, inspection, etc. By this reference the designer has tied down the job to certain processes and materials. It must only be decided then whether the part is to be void-free, which resin and glass are to be used, and so on. The Engineering Stress and Structures Group will determine what construction is optimum for a given set of requirements.

The next department concerned is the Manufacturing Planning Department. Working from blueprints, the planner prepares a detailed operation sheet or manufacturing outline. It is here that the Process Specification plays an important role, for the planner may call for an operation merely by referencing the appropriate specification code number. In this way, detailed procedures are not needed on the operation sheet. One significant step in the direction of eliminating planning detail at this level has been accomplished by establish-

ing catalytic systems for resins and assigning code numbers thereto. These catalytic systems have been worked out according to type of cure to be used, speed of gelation desired, and other such considerations. The appropriate catalytic system is entered on the manufacturing outline and the production personnel obtain the correctly catalyzed resin by requesting the listed code number. By this procedure, resin catalysis is completely standardized and we can be certain that the same mix is always used under the same conditions. To return to our following our part, after the manufacturing outline is completed and approved it is issued to the appropriate production departments where the part will be manufactured. Experienced leadmen and workers are normally capable of working from the manufacturing outline without referring to the process specifications for details of the procedure. The specifications are useful, however, for reference in cases of doubt and for training of new and less-experienced personnel. They are also useful when new procedures are specified and when standard procedures are revised.

The "police department" at Zenith which assures that the part will be manufactured according to blueprint and under approved processes is the Inspection or Quality Control Department. To this department the process specifications are of real value. In the absence of specifications, the task of inspecting for process and quality control is so arbitrary as to become completely unwieldy. Primarily at the request of the Inspection Department, Zenith Engineering has prepared a comprehensive manual on acceptance limits and rework procedures. This manual, The Acceptance and Rework Manual, defines in detail the nature and magnitude of defects and discrepancies which are: (1) acceptable without rework; (2) reworkable; and, (3) non-reworkable. In addition, standard procedures for all types of rework are established. The manual has been approved for use by Wright Field, but a great deal of work remains to be done to resolve the many questions arising from the large scope covered. The manual's significance lies in its being an approach toward the desired end of eliminating the primitive [illegible]ework procedures from quality control inspection of fiberglass laminate and [illegible]ch radomes.

Summarizing the progress of our hypothetical job, the process specification was used in varying degrees at each stage of its manufacture. Its most important role was played in Planning, Manufacturing, and Quality Control, and to lesser degrees elsewhere. At Zenith, the policy of basing specifications on engineering principles has gradually emerged. Zenith specifications are prepared to reflect procedures which have been proved to provide sound structural parts. It is in the collection and analysis of test data which are used as a basis for procedure specifications that the integration of the Engineering Department into the specification picture is accomplished.

Development of Process Data:

Radomes have been manufactured by Zenith for several years and certain basic processes used in normal(1) applications have evolved. Since the industry is a relatively young one, many of the engineering requirements currently in use are based upon test results obtained from the early radomes. For this reason, process data for the manufacture of the normal application radomes is now largely restricted to those problems which arise in production. These manu-

(1) In the context of this paper, "normal" radomes are considered as those which are to be used on subsonic aircraft.

facturing problems arise from time to time and usually involve short range investigations for immediate solutions. Typical of this is the problem which arose recently involving the need for a solvent to remove a residue from the flutes of a "lost-wax" construction. A program was set up to determine: first, which solvent or solvents would remove the residue; and second, what effects, if any, the selected solvents will have on the physical properties of fiberglass laminates. The data obtained indicated no deleterious effect, so process specifications were written stating: first, which solvent to use; second, what minimum temperature would provide the desired rapid dissolving of the residue; and third, the maximum exposure time which could be safely allowed.

Standard processes for the manufacture of radomes for supersonic aircraft and missiles have necessarily lagged somewhat behind the demand for these radomes. Since specifications for these radomes are needed probably even more than those for the more standard types, it is necessary to translate research data into process information almost as fast as it is produced. Research and development in this category must be designed to provide process data as well as design strength data. In many of these cases, speed is essential, and as soon as parts can consistently be fabricated to meet the required properties production commences. Obviously, the process used in the first attainment of the target is not always the best approach. For this reason process development often continues even when production radomes are coming off the line. While the process development continues, the writer of the process specification can contribute toward the ultimate usefulness of the information being obtained. Since, as was pointed out in the beginning, the radomes must be manufactured according to military specifications, it is important that the research being conducted be pointed toward the following. First, is the process being evolved in strict compliance with the military specifications? If not, what modifications are required to bring the process into compliance? Second, since at Zenith we are striving for generalized, large-scope specifications, how is the information to be formulated to provide this general coverage? To accomplish this second point, it is necessary to anticipate production problems which may be encountered should the process be adopted. By directing research along the above lines, a great deal of unnecessary and misdirected work may be avoided, and the net result should be a reliable process which will be acceptable to the Military.

Flexibility of Specifications:

The final significant feature of process specifications which we will discuss is their flexibility which will provide accuracy in reflecting trends in manufacturing practice and in materials. We have emphasized the importance of specifications in their ability to standardize production techniques and thereby lend themselves to the maintenance of quality. This function notwithstanding, the specifications would be targets of serious and valid criticism by production if they were allowed to become outmoded and obsolescent. It is vitally important, therefore, to provide "earphones" which can detect problems as they manifest themselves. At Zenith this flow of information has in the past come directly or indirectly from the Manufacturing Department, and corrective action has been taken accordingly. While this source is valuable and will remain in force, a hitherto untapped source is now being established.

The Inspection Department has undertaken to maintain a log of fabrication discrepancies referenced to the stage of the manufacturing process at which they occur. As the log is compiled it will provide a ready indication of repetitive trouble spots. When such trouble spots are detected the Materials and Process Group will be apprised of that fact and appropriate corrective action and revision of the specification accomplished, if the process is found to be the source. It is action of this sort which perhaps is the best insurance of the success of specifications. If the production people are convinced that the specifications are able to serve a useful purpose and that those responsible for the specifications are willing and able to aid in solving problems which arise, they are far less likely to regard the specifications as part of that scourge to production -- "paperwork." Once Production discovers that specifications need not hinder the work of moving radomes along the line, it will fully cooperate in their execution; and this, of course, is the ultimate aim of specifications -- to insure that parts emerging from the production line are indeed all they were originally engineered to be.

EXHIBIT A

INDEX TO ZENITH PROCESS SPECIFICATION MANUAL

Section VII - Preforming (600-699)

#600 - Technique of Preform Collection
#601 - Molding of Preform and Mat Laminates

Section VIII - Layup Procedures (700-799)

#700 - Layup Procedures for Void-Free Glass Fabric Laminates
#701 - Layup Procedures for Void-Free Glass Fabric Outside Skins for Sandwich Structures
#702 - Layup Procedures for Void-Free Glass Fabric Inside Skins for Sandwich Structures
#703 - Layup Procedures for Non-Void-Free Glass Fabric Laminates
#706 - Fabrication of Alkyd-Isocyanate Foam Sandwich Structures (Single and Multiple Layups)
#710 - Fabrication of Single Sandwich Honeycomb Structures with Void Free Outside and Inside Skins
#711 - Fabrication of Single Sandwich Honeycomb Structures with Void Free Outside and Non-Void-Free Inside Skins
#712 - Fabrication of Single Sandwich Honeycomb Structures with Non-Void-Free Outside and Inside Skins
#713 - Fabrication of Multiple Sandwich Honeycomb Structures with Void-Free Outside and Inside Skins
#714 - Fabrication of Multiple Sandwich Honeycomb Structures with Void-Free Outside and Non-Void-Free Inside Skins
#715 - Fabrication of Multiple Sandwich Honeycomb Structures with Non-Void-Free Outside and Non-Void-Free Inside Skins
#716 - Fabrication of Single Sandwich Wrapped Wax Structures with Void-Free Outside and Inside Skins
#717 - Fabrication of Sirgle Sandwich Wrapped Wax Structures with Void-Free Outside and Non-Void-Free Inside Skins
#718 - Fabrication of Single Sandwich Wrapped Wax Structures with Non-Void-Free Outside and Inside Skins
#719 - Fabrication of Multiple Sandwich Wrapped Wax Structures with Void-Free Outside and Inside Skins
#720 - Fabrication of Multiple Sandwich Wrapped Wax Structures with Void-Free Outside and Non-Void-Free Inside Skins
#721 - Fabrication of Multiple Sandwich Wrapped Wax Structures with Non-Void-Free Outside and Inside Skins

Section IX - Vacuum Bags (800-899)

#800 - Preparation of PVA and PVC Vacuum Bags
#801 - Installation of Vacuum Bag and Application of Pressure

Section X - Parting Agents (900-999)

#900 - Application of Parting Agents

Section XI - Curing (1000-1099)

#1000 - Techniques of Heat Lamp and Sun Lamp Curing
#1001 - Matched Die Press Molded Glass Fabric Laminates
#1002 - Techniques of Oven Curing

Section XII - Inspection and Repair (1100-1199)

#1100 - Acceptance and Rework Manual

Section XIII - Finished Part Fabrication (1200-1299)

#1200 - Riveting of Solid Glass Cloth Laminates
#1201 - Drilling of Solid Glass Cloth Laminates
#1202 - Drilling of Acrylic Plastic Parts
#1203 - Sawing of Laminates
#1204 - Grinding of Laminates
#1205 - Trimming of Laminates
#1206 - Routing of Laminates
#1207 - Milling of Laminates

Section XIV - Protective Coatings (1300-1399)

#1300 - Application of Zinc Chromate Primer
#1301 - Application of Rain Erosion Coating
#1302 - Application of Rain Erosion Anti-Static Coating
#1303 - Application of Lacquer and Enamel Surface Coatings
#1304 - Application of Rain Erosion Boot

Section XV - Storage and Handling of Plastic Parts (1400-1499)

#1400 - Packaging of Plastics Parts for Shipment
#1401 - Crate Fabrication

Section XVI - Quality Control of Raw Materials (1500-1599)

#1500 - Quality Control of Incoming Polyester Resins
#1501 - Quality Control of Incoming Glass Fabrics and Mats
#1502 - Quality Control of Incoming Adhesives
#1503 - Quality Control of Incoming Catalysts, Accelerators and Promoters
#1504 - Quality Control of Incoming Honeycomb
#1505 - Quality Control of Incoming Components for Foam
#1506 - Control of Resin Content of Machine-Impregnated Glass Fabric
#1507 - Quality Control of Incoming Preimpregnated Fiberglass Fabric

Section XVII - Storage of Raw Materials (1600-1699)

#1600 - Storage of Resins
#1601 - Storage of Glass Fabrics and Mats
#1602 - Storage of Foam Components
#1603 - Storage of Catalysts and Accelerators

EXHIBIT B

INTRODUCTION TO ZENITH PROCESS SPECIFICATION MANUAL

Purpose - It is the purpose of this Manual of Specifications to set forth the procedures and processes which are practiced in the production of reinforced plastics parts by Zenith.

Scope

This Manual of Specifications shall embrace all phases of production except those which are standard shop practice and of a nature so commonplace as to be not germane to a manual of this sort. The specifications included in this manual shall be acceptable to our customers, to the cognizant Government Agencies, or to both when both are concerned. Therefore, no specification shall be included in this manual until it has received written approval from the responsible authority. A copy of such written approval shall be attached to, and form a part of the specification.

This Manual of Specifications shall serve as a reference for all phases of planning for part production. As such, it shall be referenced in Engineering Drawings, Production Fabrication Outlines, and Process Bulletins and Specifications for specific parts. When the entire Manual of Specifications is to be referenced it shall be referenced as "1A-1000". When only one or a few sections are to be referenced the appropriate section numbers as listed in the Index shall be referenced.

Responsibility and Implementation

Responsibility - It shall be the duty of the Materials and Process Group to prepare all specifications. As part of this duty, that group shall be responsible for the compliance of all active Process Specifications to applicable Government and customer specifications and requirements. The Materials and Process Group shall conduct laboratory test programs for the purpose of obtaining information necessary to the preparation of specifications.

Implementation - It shall be the duty of Inspection Department to be thoroughly familiar with all Process Specifications and to insure Production compliance with the specifications. Difficulties in conforming to the Process Specifications shall be reported to Engineering Department which shall consider the problem for possible specification revision.

Form for Specifications - In general, the Process Specifications shall take the form to be described. In certain cases the nature of the subject will dictate the need for slightly modified forms.

Title - The title shall be listed.

Scope - The scope section shall specify precisely what the specification deals with, and coordinates with other specifications to place the subject in proper relation to the Process Manual as a whole.

Form for Specifications (cont)

Materials - This section shall specify all materials which are used in the particular process. Generally, very common materials which are normally used in the shop are not necessarily specified. In most cases a source of supply for the materials is listed.

Equipment - The equipment section shall call out equipment, tools, etc. which are peculiar to the operations with which the specification is concerned. Standard shop equipment will not necessarily be mentioned.

Procedures - Detailed descriptions of the various procedures of the process shall be specified in this section. All variations in the procedure which may be required to conform to the variations between customer requirements shall be included.

Process Control - This section specifies measures which must be taken to insure proper functioning of the process. In most cases this will consist of a list of those operations in the process which are of a critical nature and which, if improperly performed, can adversely affect the part and/or process.

QUALITY CONTROL OF REINFORCED PLASTICS STRUCTURES

By

Robert W. Matlock

Zenith Aircraft
Gardena, Calif.

The members of the engineering profession who become involved with the design or production of sandwich structures are invariably faced with the difficult problems of quality control. The word "difficult" is used because several years' search by many engineers has still failed to result in any solution which is either considered to be good, or has been adopted as standard practice.

The present methods of quality control consist of the control of the processes of fabrication and the fabrication and testing of sample test coupons. It is usually quite apparent to all concerned — the fabricator, the inspector, and the engineer — that these methods are no real solution to the problem, but are make-shift methods which are "better than nothing" or "a step in the right direction".

The author has no quarrel with process control, and in fact recognizes that this type of control is the foundation upon which the structural use of plastics must be built. If for no other reason, careful process control must be maintained to prevent ultimate rejection of fabricated parts. However, the nature of the steps followed in the fabrication of a sandwich structure are not of the type of which it can be said if steps a + b + c + ... n are correctly performed, then the part is correctly fabricated, and therefore, structurally sound. Although the reasoning may be correct in theory, it is simply not true in fact. There are too many variable factors. The limits of what is correct and not correct are too narrow and undefined. The biggest reason of all is, of course, the human element.

The attempt to achieve quality control by the fabrication and testing of sample panels or coupons is considered to be both impractical and dangerous. It is, furthermore, a great source of irritation to those involved in the fabrication of sandwich structures. Again, however, it is not proposed that sample panels and testing be eliminated as a method of quality control. It is an excellent method of checking process control, and should be used as such.

If the present methods of quality control are not satisfactory, then what is the solution? Is there a solution? To these questions can be added a third question. Is there a solution available now, today?

To answer the above questions let us first put our finger directly on the problem by deciding what we wish to accomplish by quality control. We want the part to have a nice appearance, we want it to fit properly, and we want it to perform satisfactorily in service. Since appearance and fit are matters for known and common inspection methods, this aspect will not be further considered here. In

the case of performance we must assume that if the part is structurally sound under the loading conditions for which it was designed, then it will perform in a satisfactory manner. To insure this, the actual part must be tested by either equivalent loads, or subjected to equivalent or greater stresses. This is the only sure method of proving that each and every sandwich structure will meet the above requirement of quality.

It appears, therefore, from all of the preceeding discussion that quality control should consist of process control, the fabrication and testing of sample coupons, and of final testing of the finished part. The use of testing as a method of insuring reliability is not common, probably because of the large anticipated costs. However, this is not necessarily true. New developments and new methods appear to be changing this situation. It is felt, therefore, that testing should be made full partner of the previously used methods, thus forming a team of great value and reliability. In the following sections, each method is discussed in greater detail.

Process Control

The term "process control" is used to include control over the basic materials entering the part, and the physical steps followed in its fabrication. This portion of quality control should never be relaxed, even though the finished parts are to be 100% proof loaded. The reason for this is obvious, in that only through adequate control during the fabrication stage can rejection, scrappage, or rework be avoided in the finished part. From an economic standpoint alone, process control during fabrication is a practical requirement

As an example of the quality control measures used by the Zenith Plastics Co. in the fabrication of reinforced plastics sandwiches for radomes and similar structural and semi-structural applications, the following measures are taken to control material quality:

1. Only certified materials are purchased.
2. Glass cloth is inspected for nominal thickness, contamination or dirt, broken fibers, or any other visual defects.
3. Each drum of resin is sampled and tested in the laboratory for gel time and viscosity.
4. Impregnated cloth is tested for resin content.
5. Sample laminates are made into standard tensile test specimens for a check on the combined materials.

In addition to the control for material quality, a rigorous inspection procedure of each step of the fabrication process is followed. As a final check on complete cure the Barcol hardness is taken.

A process similar to that above may easily be developed for other types of sandwich constructions. Although the materials and processes used in metal sandwich constructions, for example, are entirely different, it is quite clear that similar steps may be followed, and suitable controls established

Sample Panels

The extent to which materials and process engineers have relied on sample panel fabrication and testing as a quality control measure is disturbing. It is strongly suspected that the popularity of this method is largely due to the fact that it offers an obvious and palusible method of quality control, and that for the same reasons its defects have been disregarded. A little serious thought, however, will indicate at least three major faults.

The primary fault lies in the cost. Although the parts in themselves may be relatively small, it is a well known fact in the industry that the labor costs involved in making a small part are nearly as great as required for a large part. When one considers the general high cost of plastic sandwiches, it is apparent that the cost of sample panels is not inconsiderable. In addition to the cost of the sample itself must be added the cost of testing and the cost of recording and submitting the test results. In addition to all of these costs must be added one more item, and a very important item it is, the complication and interruption of regular production work. Although this last item is difficult to analyze, it is obviously one of considerable importance.

It may be concluded, therefore, that if sample panels and testing are used as a quality control measure, required by a specification, they do not come free. Although the charges for this work may not be listed as a separate and distinct item, it is quite apparent that the charges will be most probably buried in the cost of the parts.

The second point in the case against the test sample is its unreliability in determining whether the production part is sound. Even though the test sample be fabricated at exactly the same time by exactly the same personnel and of exactly the same materials as the finished part, let no one be so naive as to believe that human nature is such that identical care will always be given. Let it be remembered that if the production department makes the samples, and they should, it is the same department which is responsible for the prompt acceptance of the related parts. If anything is to be right, it will undoubtedly be the samples.

Probably the most annoying aspect of test samples is what happens when a test sample fails? Does this mean the part or parts are unsatisfactory? Not necessarily. It means only that the test sample was not good, and that the parts are suspect.

Perhaps the worst case is that in which the test panel passes with colors flying. In this case it might be concluded that the part is satisfactory, a very dangerous assumption indeed.

The third fault is very basic and goes directly to the heart of the matter. As the samples must necessarily be fabricated by the production personnel, it removes the function of quality control from the hands of the inspection department and places it where it should not be — in the production department. Although it may be logically argued that inspection could supervise the fabrication of the samples, this is not a practical solution. It places the inspector in the role of a policeman with the task of preventing dishonesty, rather than of maintaining quality control.

It is apparent from the previous discussion that the writer has little respect for the method of determining part quality by the fabrication and testing of sample panels. It is argued, however, that the use of sample panels should not be eliminated. It is suggested that their use be limited to a check and statistical control of the quality control process itself, and that they have no relation at all to a specific part. If for no other reason, it is good psychology to run a few test samples through the shop along with the day's production. If there is a gradual deterioration or a radical change in the processes used, it will most likely become apparent through the samples. As long as the results are not taken too seriously, good or bad, and the number of samples made is small, it is felt that only good can come from their use.

In connection with the use of test samples for quality control, it is a source of great wonder to the author that a very close source for good quality control measures has been overlooked. In every plastics shop may be found a considerable number of rejected parts or assemblies. Many of these are rejected for reasons other than structural faults, and provide a great source of test specimens which are not subject to the taint of special care in preparation. It is extremely helpful and advantageous for the structural laboratory to avail themselves to this source of free samples.

In addition to the rejects, it is suggested that consideration be given to removing an occasional production part for test purposes. It may be a surprising fact that a production part may be less expensive than a test sample. In the case of some of the extremely large radomes made by Zenith Plastics Co. this is obviously not the case, but it may be very true for a production run of small parts. In any event the value of a production part for test purposes will be greater than that of several test specimens.

Static Testing

Out of all the thought and discussion that has been expended on the effort to achieve quality control, it is amazing that there has been so little attention given to static testing. It is quite obvious that there is no other approach so direct as that of proof loading each and every part. From the standpoint of the stress engineer this is the ultimate in quality control, a method which proves without doubt that the structure will sustain the loads it was designed to carry. And it is, after all, the stress engineer who is most interested in quality control. It is he who assumes the responsibility for the structural integrity of the part, and it is he who must be satisfied.

Perhaps the reason that static testing has not received greater consideration is that the cost is expected to be high. This may or may not be true. If quality control is put on a dollar-and-cents basis, and it should be, then value is the function which should be considered the determining factor. A small amount of quality control for a small price is no greater value than a great amount of quality control for a larger price.

Furthermore, it is extremely doubtful that comparative cost studies of quality control methods have ever been made. Taking again the case of the sample panels, it is estimated that the cost of fabricating samples, preparing the specimens, and testing, will in many cases be greater than that of attaching a structure to a jig, applying load, and removing the structure. It is assumed, of course, that consideration has been given to the element of time in the design of the jig to facilitate mounting and removal, and in applying the load.

The Zenith Plastics Co. is currently static testing four separate radomes for one of its customers as a routine procedure. That the method of quality control by static testing is regarded as being practical and successful may be deduced from the facts that (1) these static tests began with one radome in 1948, which is still being tested on a statistical basis, and (2) none of these radomes has ever failed or given trouble in service except from accidental damage.

Of the four radomes mentioned above, two are tested on a statistical basis. On the remaining two, each unit is tested. The former two radomes may be described as being large. Of the latter two, one may be called very large and the other extremely large. It may be of considerable interest to show the cost of the static test in relation to the cost of the part. The table below is prepared for this purpose.

Radome No.	Size	Test Cost/Part Cost
1	8' x 9'	.067
2	8' x 9'	.050
3	9' x 15'	.031
4	30' x 20'	.005

The above tests are carried to yield (1.15 limit) load. The jigs were designed for destruction tests on the first units as well as for the proof testing. Consequently, the structure of the jigs is considerably stronger and more expensive than would be required for proof load only. In addition, approximately 95% of the equipment and jiggery used for Radome #3 is also used for Radome #4. It is also available for similar tests on other radomes if required, thus further reducing the cost of additional testing as its utility is increased.

It is sincerely believed that the test costs shown above are not really indicative of what can be done in this direction. Nearly all experience in the field of design of static test fixtures has been pointed toward an ultimate load test fixture. In these cases, speed of installation and removal, and the quick application of load are not problems to be given serious consideration. With an increase in experience in designing and using proof-testing jigs, it is quite apparent that methods of attachment for quick installation and removal of the part will be developed. This is also true of the problem of quickly applying and removing load. The bolt, the nut, and the shot bag can be made as obsolete as the Model "T".

(*Reprinted from* MECHANICAL ENGINEERING *for April, 1956, with permission of Copyright Owner*)

Ceramics as Basic Engineering Materials

By E. J. Smoke[1] and J. H. Koenig[2]

Rutgers University, New Brunswick, N. J.

Ceramic products are defined as those made of inorganic, nonmetallic material which are usually subjected to high temperatures during fabrication. This includes a wide range of products, but of more importance to the engineer, it embraces a wide range of unique and useful properties.

AMONG the unique properties of ceramic materials is refractoriness, that is, resistance to high temperatures. Fig. 1 shows the melting temperatures of some ceramic materials along with those of several metals. The melting temperatures of the basic crystalline phases of most ceramic materials are quite high starting in the range of 3000 F; iron melts at 2895 F. Glasses are ceramic materials also, but they cannot be considered as refractories. This is because they are not compounds but rather behave as supercooled liquids whose viscosity is extremely high at room temperature; thus they have softening ranges rather than melting temperatures.

Melting Temperatures

Ceramic products are being manufactured whose melting temperatures are lower than 3000 F, principally due to a high glass content. Ceramics made of clinoenstatite, titania, silica, mullite, forsterite, alumina, spinel, zircon, beryllia, zirconia, magnesia, and thoria are oxide-type ceramics. All but the first two are used as refractory materials where high-temperature processing is involved; that is, as furnace liners in heat-treating of metals, recovery of metals from their ores, alloying of metals, recovery of petroleum products from crude oil, nuclear applications, and the like. Thoria has a very high melting point, however; it is radioactive. Silicon carbide is used as a refractory and to a large extent as kiln furniture. Boron carbide has a high melting temperature but it is used only in special cases. Other carbides, sulphides, nitrides, and borides have still higher melting temperatures but have only been made experimentally or on a very limited scale because of the rarity of some of the elements involved and the protective atmosphere necessary in using these materials. They are being used experimentally in heat-engine parts such as jets, rockets, and so on.

The highest melting metal is tungsten which melts at approximately 6100 F. Zirconium, tantalum, and hafnium carbides, and graphite have melting temperatures above this with hafnium carbide having the highest melting temperature known of approximately 7520 F.

Ceramic products are generally a mixture of one or more crystalline phases with glass, the latter material varying up to approximately 45 per cent. This glass content affects the refractory properties. Included in Fig. 1 is a graph of the "safe continuous operating temperature" of some of these ceramics. The best glasses can be used continuously only up to approximately 900 F. Steatite and forsterite can be used continuously to 1830 F without distortion when used as technical ware such as high-frequency insulation, or whenever dimensional tolerances in the range of ±1 per cent are prerequisite. However, forsterite, when used as furnace parts, operates successfully up to 3000 F. Normal porcelains have been used up to 2185 F. Zircon, whether used as technical ceramics or as a refractory, operates very well up to 2650 F. Silicon carbide, which is used as furnace parts, stands up very well to approximately 2750 F in air. Silica is used principally as a refractory in open-hearth furnaces where the temperature approaches 3000 F. Mullite refractories are used continuously up to 3200 F.

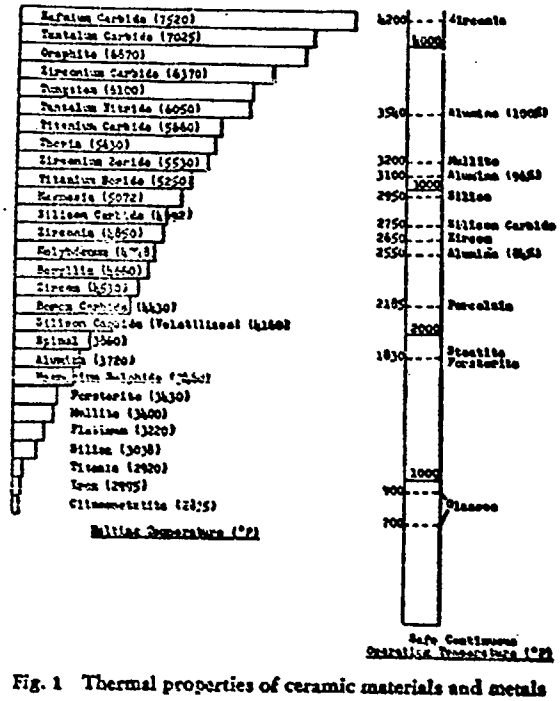

Fig. 1 Thermal properties of ceramic materials and metals

The effect of glass content and/or an additional crystalline phase or phases is illustrated by the safe continuous operating temperatures of several alumina bodies. A body containing 86 per cent alumina can be used continuously up to 2550 F; another containing 96

[1] Research Professor, School of Ceramics.

[2] Professor and Director, School of Ceramics.

Contributed by the Process Industries Division and presented at the Diamond Jubilee Annual Meeting, Chicago, Ill., November 13–18, 1955, of THE AMERICAN SOCIETY OF MECHANICAL ENGINEERS. Condensed from ASME Paper No. 55—A-160.

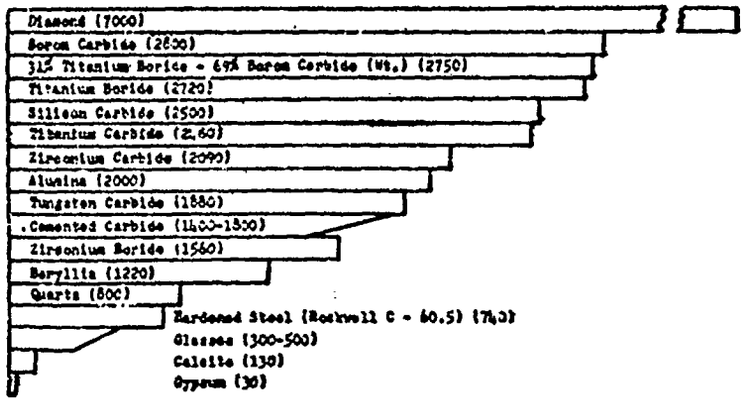

Fig. 2 Hardness (Knoop scale) of ceramic materials ranging from 30 to 7000

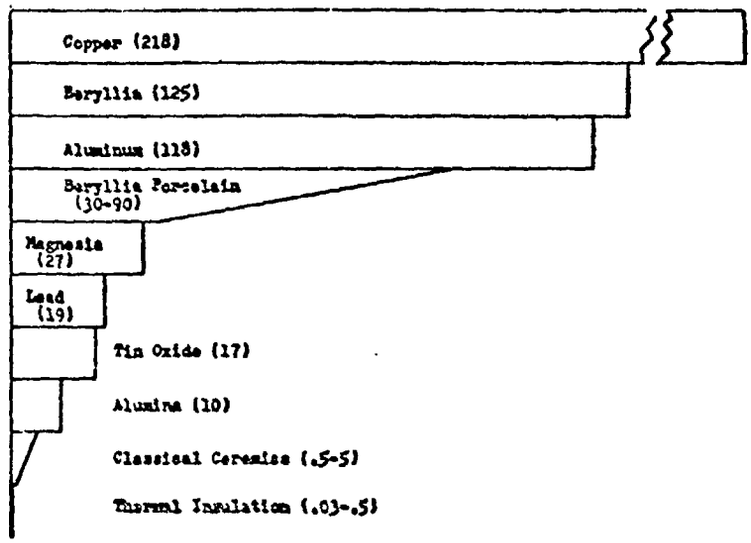

Fig. 3 Thermal conductivity of ceramic products Btu/hr sq ft/(deg F/ft), at 140 deg

per cent, up to 3050 F; while pure recrystallized alumina, that is, containing no glass, can be used continuously up to 3520 F. These are used as furnace parts and technical ceramics of close dimensional tolerance and for high-temperature vacuum applications.

Zirconia provides a very high safe continuous operating temperature (circa 4200 F) and in the fused stabilized form is used as furnace parts.

Alumina and zirconia are applied to metals in thicknesses up to 0.010 in. by the flame-spray process. This type coating shows promise for heat-engine parts, abrasion-resistant coatings, and erosion-resistant parts.

Thus ceramics provide a wide selection of refractory materials for use as furnace parts or as technical ware and the choice depends upon end use and economics.

Hardness

Hardness is another property unique to ceramics covering the range from 30 on the Knoop scale for the mineral gypsum to 7000 for the diamond as shown in Fig. 2. Glasses range from 300 to 500. The hardest metals are hardened steel at Rockwell C 60.5 which is approximately 750 on the Knoop scale. Several ceramic materials fall in this range also but the majority possess greater hardness. The cemented carbides are made of synthetic ceramic materials such as tungsten, titanium, and tantalum carbides whose Knoop hardness numbers range from 1400 to 1800. They are used as tools for machining metals to close dimensional tolerance.

Alumina has a value of 2000 and is used as a grinding and lapping compound, and as the abrading media in grinding wheels for machining steel. A relatively new application is as tool bits for machining metals. This extreme hardness and the fact that this type ceramic can be fabricated to extremely close dimensional tolerance lends itself as wear-resistant parts such as gages, bearings, thread guides, nozzles, and technical ware in general.

Silicon carbide, with a Knoop hardness of 2500, is one of the most important abrasives in terms of lapping and grinding, and as grinding wheels. It lends itself best for fabricating very hard dense materials such as ceramics, including cemented carbides, cast and chilled iron, and nonferrous metals.

Titanium boride has a value of 2720 and boron carbide of 2800; this latter was the hardest synthetic material until quite recently. However, in the past year man has made the first synthetic diamonds. Diamond is the hardest known material. It is marketed in many grain sizes and in many type grinding wheels. Its extreme hardness and durability make this material of economic significance even though the initial cost is quite high.

The property of extreme hardness has made ceramic abrasives actually indispensable in the fabrication of metals and other materials. There are no substitutes for ceramic abrasives.

Thermal Conductivity

Another engineering property of extreme importance is thermal conductivity. Again, ceramic products cover a wide range from near zero up to 125 Btu as shown in Fig. 3. In the very low range of thermal conductivity a variety of thermal-insulating materials are manufactured from mineral products such as asbestos, magnesia, diatomaceous silica, refractory clays, mineral and glass wools, and synthetic fibers; these are used from below room temperature to above 3000 F as drier, oven and furnace liners and backings, pipe covering, and numerous other applications.

Ceramic products in general are characterized by low thermal conductivity and approximately 98 per cent of all products manufactured have thermal-conductivity values no higher than 5 Btu. This is due not only to the property being inherently low but also to the large per cent of pore space or voids which are present in some of these materials. It has been noted in the foregoing that magnesia is an excellent thermal insulator yet Fig. 3 shows that it has a value of 27. The former value is for a very porous material while the latter value is for one containing no more than 1 per cent pore volume. Thus all ceramics possessing thermal-conductivity values above 5 Btu are nonporous materials. Alumina ceramics have thermal-conductivity values up to 10 Btu.

Tin oxide has a value of 17 but has not been used industrially to any extent in ceramic bodies. The metal lead has a value of 19. Magnesia's conductivity as a dense ceramic, as mentioned, is 27 and has been used as electrical insulation in vacuum tubes. Above this range the only ceramic material is beryllia and its value is 125 Btu as compared to aluminum at 118 and copper at 218. By combining beryllia with other ceramic materials a range of porcelains can be made whose thermal conductivity ranges from 90 to 30 Btu. Some sparkplug and high-frequency insulators, where high thermal conductivity is of importance, have been made from beryllia and beryllia porcelains. However, because of the toxic effect of this material, its use has been limited. It is now considered that this material can be used safely when the proper precautions are taken.

Thus ceramic products can be made which cover the wide range of thermal conductivity from values of 0.05 to 125 Btu, which is from the best thermal insulators to conductivities exceeding that of the metal aluminum.

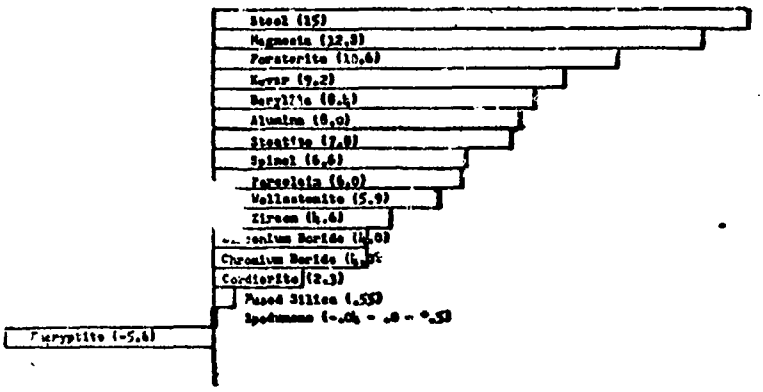

Fig. 4 Coefficient of linear thermal expansion of ceramic materials; room temperature, 700C (1292 F)

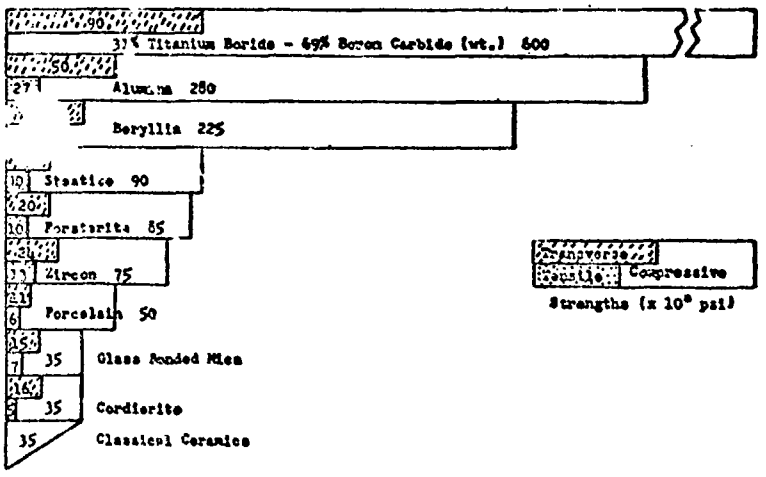

Fig. 5 Tensile, transverse, and compressive strengths of ceramic materials

Thermal Expansion

Ceramic materials are manufactured which cover the range of linear thermal expansion from 0.5-13 $\times 10^{-6}$ in/in/deg C between room temperature and 700 C as shown in Fig. 4. Magnesia has the highest thermal expansion at 12.8. Low-carbon steels have values in the range of 15 over the same temperature range while copper is approximately 17. One of the prime applications of a desired high thermal expansion in ceramics is in glass-to-metal and ceramic-to-metal seals for electron tubes and other vacuum-tight, strong, high-temperature seals. There are two types of seals. The compression type is exemplified by copper and forsterite or alumina, and Kovar and alumina. In this case a metal of higher thermal expansion surrounds the ceramic of lower thermal expansion which, when soldered together, results in a strong vacuum-tight compression seal. The other type is the matched seal in which the thermal expansion of metal and ceramic is approximately the same. Glass-to-Kovar is a glass-to-metal seal of this type. The iron-nickel series of alloys covers a wide range of thermal expansion and a thermal-expansion match can be found for most ceramics; however, only over a limited temperature range.

Invar is a low-expanding material at relatively low temperatures but tends to increase quite rapidly as the temperature is increased. In the realm of ceramics, much lower thermal expansions are possible. In fact, there are two types which actually contract on heating. Both are lithium aluminosilicates. The one type exhibiting the low positive to low negative values (Fig. 4) is the crystalline phase beta-spodumene. It can be made to have no contraction or expansion up to 600 C. Beta-eucryptite is the other crystalline phase and its coefficient of linear thermal expansion is -5.6×10^{-6}. This latter material has not been made in the nonporous state and because of its very high degree of contraction,

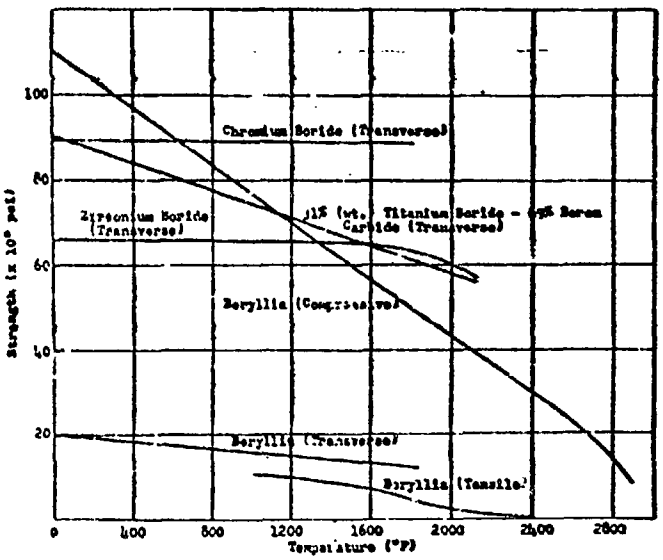

Fig. 6 Strength versus temperature curves of some ceramic materials

pressive strength varies from 8 to 10 times the tensile strength. One commercial alumina body has a tensile strength of 27,000 psi, its transverse strength is 50,000 psi, while its compressive strength is 290,000 psi. Alumina bodies with compressive strengths as high as 400,000 psi have been reported.

The values given in Fig. 5 are optimum values and these tend to decrease either with a decrease in the basic crystalline phase or with increase in pore volume. As an illustration, alumina ceramics are manufactured as special refractories with compressive strengths of the order of 11,000 psi while that of the completely nonporous material used as wear-resistant parts and electrical insulation has a compressive strength of 290,000 psi. This extremely strong material is being used as extrusion and pressing die parts, precision gages, plungers for reciprocating pumps, mechanical-seal parts, bearing sleeves, liners for pumps and impeller-wear parts, thread guides, and as high-frequency insulation particularly for vacuum-tight ceramic-to-metal seals.

has found little use. However, the beta-spodumene is quite important as a refractory material (to 2200 F) of high thermal-shock resistance. Some uses include trays on which dental products are rapidly fired; tubes through which billets are heated to forging temperature by induction heating; and in the firing of certain white wares. It is being used as either zero or low-expanding tubes in dilatometers for determining thermal expansion of ceramics and metals at higher temperatures. It is being evaluated as a base material for precision electrical resistors and capacitors where dimensional variation with temperature is detrimental.

Thermal-shock resistance is relatively high in most porous ceramics because of inherent structure. However, where strong ceramics are desired porosity must be minimized. In dense ceramics the thermal-shock resistance is dependent to a marked degree on thermal expansion; the lower the thermal expansion the higher the thermal-shock resistance. Similar specimens of an alumina ceramic whose coefficient of linear thermal expansion is 8.0, crack when quenched into water at room temperature from 400 F. Beta-spodumene bodies, whose thermal expansion approaches zero, have resisted failure when quenched from 2200 F to water at room temperature.

Thus ceramic products cover the coefficient of linear thermal-expansion range from $+12.8$ to -5.6×10^{-6} in/in/deg C from 25–700 C, and ceramic products are being produced or can be designed to any specific value in this range.

Strength

The compressive strength of ceramic materials covers a very wide range from materials so weak that they can be crushed between the fingers in the case of some heat insulators, to values as high as 600,000 psi for a mixture of 31 per cent (by weight) titanium boride and 69 per cent boron carbide. In general, for more or less conventional ceramics, with tensile strength at unity, the transverse strength is approximately 2 times and the compressive strength 10 times.

Beryllia is another extremely strong ceramic with a compressive strength of 188,000 psi and transverse strength of 35,000 psi. Steatite, forsterite, and zircon ceramics have compressive-strength values between 75,000 and 90,000 psi. Steatite is the most economical of the group to manufacture. It is used extensively as electrical insulation especially for high-frequency applications and at moderately elevated temperatures because of its high strength, excellent electrical insulating properties, and the ability to fabricate this material to close dimensional tolerance. Porcelain, glass-bonded mica, and cordierite have lower compressive strengths in the range of 35,000 to 50,000 psi. Porcelain, because of its strength, ease of manufacture, and general durability, is used extensively for domestic and technical ceramics.

Fig. 6 shows the effect of temperature on the strength of some ceramic materials. A beryllia ceramic, whose tensile strength is approximately 14,000 psi at room temperature, is still 5000 psi at 1800 F; its transverse strength at room temperature is 20,000 psi and still 11,500 psi at 1800 F; while its compressive strength at the lower temperature is 110,000 psi, 50,000 psi at 1800 F, and 7000 psi at 2912 F. Chromium boride, whose room temperature transverse strength is 88,000 psi, remains constant to 1700 F. Zirconium boride exhibits the same effect over the same temperature range with a value of 66,000 psi, and at 2200 F this value only drops to 55,000 psi.

The titanium boride-boron carbide material mentioned previously has a transverse strength of 90,000 psi at room temperature and drops steadily to 55,000 psi at 2200 F. It is these high-strength properties at high temperatures that are of extreme interest for high-temperature engines and air frames. Radomes which house radar equipment are being made of ceramic materials because of these properties. One laboratory is experimenting with actual missiles made entirely of ceramic materials, the reason being that as the speed increases, the temperature also increases and it appears that only ceramic materials can withstand the extreme conditions of temperature and pressure encountered.

DEVELOPMENT OF TOOLING AND PROCESSES FOR FABRICATING LARGE HIGH-ACCURACY RADOMES

by

R. H. Vreeland, Head, Engineering Projects Group
Plastics Department
Research Laboratories
Hughes Aircraft Company
Culver City, California

I. INTRODUCTION

Radomes that are under development for use with certain fire control systems must meet critical boresighting requirements, and they must maintain this required accuracy under the high temperatures and aerodynamic loads encountered during operation of the high-velocity interceptor aircraft on which they will be mounted. Although radomes of the large size necessary for these systems can be fabricated commercially, radomes so produced do not meet these requirements. Therefore, a die-development program, initiated in 1952, was pursued concurrently with the development of radome-molding procedures and processes.

Theory and past experience both indicate that a radome of streamlined shape achieves the best electrical performance if it is of half-wave-wall configuration. In this type of radome, undesirable reflections from the radome surfaces can be almost completely cancelled if very close tolerances on the thickness and dielectric properties of the radome wall are carefully maintained. Experience with smaller radomes has shown that close tolerances can best be met by radomes that are molded under high pressure between matched, hardened steel dies. Although this method of radome fabrication requires a relatively high initial expenditure for equipment and tooling, the exceptional quality and reproducibility of the product more than offset these costs.

A program that was undertaken to develop such a set of matched dies is described in this paper. Early in this program it became apparent that no dies for plastics molding that even approached the required size and tolerances had ever been built before and that the accuracy necessary between surfaces had, in the past, been limited to dies that were only a fraction of the size required. Because of this lack of experience it was therefore decided that the final set of dies would be designed from the data obtained by the design, fabrication, and tryout of a scale model of these dies. The die-development program that resulted is discussed herein.

II. PURCHASE OF EQUIPMENT

After the first rough sketches of the dies were completed, it was necessary to initiate the purchase of the equipment required in using these dies. This seemingly premature action was necessary because of the long time needed to approve funds, to design and fabricate the equipment, and to ship, assemble, and test it. Among the equipment purchased were the following large items.

1. Hydraulic Press

After calculations had established that a rigid and very accurate press having a 2500-ton capacity was required for use with the final dies, the standard presses of this size available from various commercial press builders were studied. Although none of the standard presses had the rigidity and accuracy of movement desired, several companies thought these qualities could be attained. Rigidity could be achieved by housing the four press posts in built-up slab sides and then bracing these sides with cross-rails. The daylight and stroke of the available presses were much too short for the anticipated application but to increase them would be to sacrifice accuracy and rigidity. It was therefore decided to purchase a press with 10-foot daylight and to move the die in and out of the press after each molding cycle. This was possible because of the developmental nature of the program.

The press that was purchased (see Figure 1*) was built by Williams White and Company.

Its specifications are as follows:

Capacity:	100 to 2500 tons adjustable compression, moving down
Platen area:	78 inches by 66 inches
Bed-face size:	88 inches by 66 inches
Daylight:	120 inches maximum
Stroke:	72 inches maximum
Stripping:	140 tons with "kicker" cylinders only 750 tons with stripper cylinders included
Stripper-ram stroke:	18 inches maximum
Total weight:	363,000 pounds (supported by twelve 20-ton piles)
Height above floor:	29-1/2 feet
Total height:	35 feet, 3 inches
Size of pit:	11 feet by 20 feet by 5-3/4 feet deep

After the press was installed and the gibs adjusted, the following characteristics were measured and found to be within the stipulated tolerances:

Parallelism between the face of the moving platen and the face of the base is within 0.0015 inch over the entire stroke.
Change of parallelism is 0.002 inch over the entire stroke.
Horizontal movement of the moving platen through the entire stroke is 0.001 inch with smooth travel and 0.002 inch with jogging.
Deflection of the base under a uniformly distributed load of 2500 tons is 0.006 inch in a span of 64 inches.

2. Vertical Boring and Turning Mill

A survey of facilities throughout this country revealed that there was no lathe or vertical boring mill that could be made available for machining the mold surfaces of these large dies to the accuracies demanded. As a consequence, it was necessary to purchase such a machine tool. Conferences with those using this kind of equipment revealed that a vertical boring mill with an electronic tracer was the most accurate machine for the purpose.

Accordingly, a modified, 6-foot, heavy Cincinnati Hypro vertical boring and turning mill was purchased (see Figure 2*). This machine includes a General Electric electronic duplicating attachment on the left rail head.

Specifications for this machine are as follows:

One right-hand turret head, one left-hand ram-type swiveling rail head, one right-hand side head	
Swing:	76 inches
Height under rail:	101 inches
Travel of left-hand ram:	72 inches
Vertical travel of rail:	90-1/2 inches
Speed of table:	0.96 rpm to 75 rpm
Diameter of table:	72 inches
Feeds:	0.004 inch to 0.750 inch per revolution
Weight:	91,500 pounds
Support:	Nine 20-ton piles under a concrete pad 17 inches thick
Accuracy of duplicating:	$\pm$0.002 inch
Finish of work:	27 micro-inches possible under favorable conditions; 50 to 60 micro-inches expected under normal conditions.

A series of measurements made while machining various dies on this mill show that the accuracy in duplicating a large die can be within $\pm$0.0003 inch. The finish on forged tool steels has been in the region of 100 micro-inches, but this finish can be improved to a finish as fine as one micro-inch by using a grinder on the ram and then polishing the surface.

3. Curing Oven

A large oven is required for postcure of the radome after its removal from the die. A suitable oven was purchased.

Its specifications are as follows:

Gas-fired, floor-type, vented; equipped with Partlow temperature programming and control	
Heating capacity:	600,000 Btu
Maximum operating temperature:	550°F
Exhaust fan:	675 cubic feet per minute
Circulating fan:	6000 cubic feet per minute
Outside dimensions:	9 feet wide, 9 feet long, 14-1/2 feet high
Inside working area:	6-1/2 feet wide, 8 feet long, 10 feet high
Door opening:	6-1/2 feet by 10 feet.

The oven was installed in such a position relative to the large press that either the layup fixture or the dies could be rolled into the oven for precuring or postcuring on the tooling, thus eliminating a considerable amount of distortion in the part.

4. Fifteen-Ton Crane

A crane was necessary to assist in the erection of equipment and to move the tooling and finished products. Although a larger crane would have provided more lifting power, one having a 15-ton capacity was decided upon in order to obtain the greatest coverage of floor area. This crane has a 30-foot span and an 80-foot craneway. It is mounted on separated columns, which are supported by 35,000-pound capacity piles. The maximum distance from the bottom of the hook to the floor is 32 feet; the floor area covered by this crane, measured from the center of the hook, is 22 by 69 feet.

5. Housing for Equipment and Facilities

The equipment already mentioned is installed in a building having a high bay area approximately 32 by 80 feet. This building is supplied with steam, water, electric power, gas, telephone, and air. The steam line is a 6-inch insulated pipe carrying saturated steam at 140 psi with a temperature of 360°F; a 3-inch condensate return line is parallel to it. There is a flash tank in the building for condensing the spent steam and a pump to return the condensate to the boilers of the central heating plant.

Cold water is piped in from a nearby building; hot water is provided by a heater within the building. Hot water at various temperatures for layup-fixture heating is obtained from a steam-and-water mixer. Two towers mounted on the roof of the building furnish a cooling system for the dies in the presses and for the heat exchangers in the press hydraulic systems. Vacuum is obtained by the use of vacuum pumps that are located in the building.

III. DESCRIPTION OF THE DIES

Five sets of large, matched dies for the high-pressure molding of laminated fiberglass radomes have been completely designed and have the characteristics shown in Table I. All are designed for use in the 2500-ton hydraulic press, and the molding surfaces are to be contoured in the vertical boring mill.

The designs were completed in the order shown in the table; the "D" dies were the first to be fabricated. Equipment was purchased on the basis of a rough design of the "C" dies. The main parts of each set of dies are the punch (hereafter called the male die) and the cavity (referred to as the female die). Each male die includes a ring around its base that is used for stripping the part from the male die. Also, each male die is mounted on a base that holds it to the bottom platen of the press. The four guide pins and bushings are standard items in most dies. In the first four sets of dies, the lower (wide) end of the female die is divided and has a collar that serves as the guidance area for the female die.

IV. DESIGN PARAMETERS AND LIMITATIONS

These five sets of dies can be divided into two groups according to their design parameters, which were determined by the intended application. The first three sets ("A," "B," and "C" dies) were to be used under most extreme molding conditions — the use of very high and rapidly applied pressures, with preforms of relatively poor quality made from many types of

materials having a large bulk factor when preformed, and with a rapid increase of molding temperature. The "D" and "E" dies were to be used under more controlled conditions – a maximum of 1000 psi uniform molding pressure, a slow increase of molding pressure, carefully made preforms from only one kind of material with minor variations, a very low bulk factor on the preform, and gradual, controlled die heating.

In addition to these parameters there were the limitations imposed by the size of the existing equipment; these were:

1. The weight of any component could not exceed approximately 20 tons.
2. The total height of the assembled die could not exceed 110 inches.
3. The outside diameter of any die part could not exceed 75 inches.
4. The height of any part (including the clamping device) could not exceed 102 inches unless the part cleared the boring-mill rail.
5. The maximum depth of contour that could be accurately cut in the female die was 66 inches.
6. The amount of saturated steam available at 360°F and 140 psi was about 60,000 pounds per hour, which was available only for short periods.
7. The crane hook was 32 feet from the floor.

V. DIE DESIGN

The drawings of the dies were made by a small group of die designers, each of whom contributed a certain amount of basic knowledge to the program. One designer had several years of experience in the design of small plastics dies, another had machine-design experience with various job shops, while a third had a little shop experience, and so on. The basic die design, however, was done by the writer, with the help of many others, as discussed in a later section.

As soon as a drawing of the largest radome (the "C" radome configuration) was available, a rough die design was made for this configuration, which was to be molded under fairly severe conditions. With this basic design in mind, the required equipment was purchased.

The first set of dies to reach the final design stage was the smallest set, designated the "A" dies in Table I. In addition to molding finished radomes 24 inches in diameter and 37 inches long, these dies were to serve in testing several mechanisms and in measuring several molding conditions.

An automatic stripping device was incorporated into the design of this set of dies so that the molded part could be easily removed when the dies were opened. This device consisted of a set of cams in the male die that operated a set of fingers in the female die; the fingers protruded under a stripper ring and moved it up with the female die. The stripper ring then lifted the part from the male die. In order to ensure that the part stayed on the male die and separated from the female die when the dies were opened, two grooves were machined in the male die.

The design of the first set of dies included three types of guidance between the male and female for accurate alignment; each type could be

removed so that the usefulness of the others could be tested. The types of guidance were:

1. Four standard die guide pins and bushings
2. A guide pin through the nose of the part
3. Guidance between the base of the male die and the open end of the female die.

These guidance devices were considered very necessary because the use of preforms of poor quality imposed severe eccentric loading conditions on this set of dies.

This set of dies also incorporated a device for clamping the nose of the preform to the male die. Such clamping is necessary because of the shape of the finished part and the bulk factor. As the dies close, the first contact between them, through the part, is at the open end of the radome. The movement of the dies is then almost normal to the thickness of the part so that the force exerted by the press may tear the cloth or pull the preform down the nose of the male die. The nose clamp is intended to eliminate the latter problem.

It was expected that the first three sets of dies ("A," "B," and "C" in Table I) would be nitrided on the molding and wear surfaces and then chrome-plated. (These operations are discussed in detail in another section.) A check-out of the equipment for performing these operations was to be accomplished by nitriding and chrome-plating the "A" dies; these dies would also be used in testing the heating system that would be employed with the first three sets of dies.

The second and third sets of dies were to incorporate almost the same features as the first set. They would have an automatic stripping device, the three guidance systems, the nose clamp, nitrided and chrome-plated molding and wear surfaces, and a high-velocity-steam heating system. In addition, the female die in each set was to be made in two pieces, with a joint along the mold surface.

The fourth set of dies ("D" in the Table) was to follow in general the design of the first set. It would include the automatic stripping device and the three guidance systems. However, the nose clamp to be used was of a different type. The clamping plug had a larger diameter and fitted the flat part of the nose in addition to a portion of the conical part of the radome. This plug fitted into the female die in such a manner that, as the female closed under pressure and molded the nose of the part, the shear pin started to fail in shear. When the dies opened and the part was stripped from the male die, very little stripping force was necessary to shear the pin in the opposite direction.

In addition, this fourth set of dies was to have much softer molding and wear surfaces than the first three sets. The heat treatment was not as severe as that used for the first three sets, and the nitriding and chrome-plating were eliminated. Also, the high-velocity-steam heating system was replaced by a chambered-steam system.

The fifth set of dies ("E" in the Table) closely resembled the fourth set in general construction except that a simple stripping mechanism with manually operated fingers replaced the automatic stripping device.

VI. PROBLEMS CONNECTED WITH THE DIE DESIGNS

In designing each of the five sets of dies, the first problem encountered was the scarcity of experienced die designers. It was soon realized that the design of plastics dies is a field quite different from other types of design. Since no designers with experience in designing large plastics dies were available, it was decided to design the dies to be like some smaller ones (with which we have had considerable experience), except that all dimensions had to be larger; the tolerances, however, had to be held as close as those found in very small dies.

In "blowing up" the design of a small die, the problem of weight had to be considered because only limited space and handling equipment were available. It was definitely necessary to analyze the dies structurally in order that excessive weight could be reduced. In fact, for the largest dies, (called "C" in the Table), the stress analysis resembled that for a major airplane component, with even more consideration given to rigidity and deflections. The services of several experienced aircraft stress engineers were used in making these analyses.

The problem of heating the dies came up next. The usual practice of heating dies by means of a chamber around the female die and a hollow male die was acceptable for the last two ("D" and "E") sets and was adapted from the small die design. However, in heating by this method, uniform wall thickness was much more important on the molding surfaces of the large dies than on those of smaller dies.

To obtain the fast heating rate required with the first three sets, the chamber method of heating was inadequate because the transfer of heat from practically quiet steam through a water film into a steel surface is very slow. In the design of these dies, then, a system of high-velocity steam was used. Saturated steam was introduced into tubes wrapped around the female die and into grooves cored into the male die. To reduce the accumulation of condensed water, a specially developed water trap was installed along the walls, every ten or twelve feet of tube length. For the calculation of the quantity, pressure, and temperature of the steam in these heating systems, the services of a thermodynamicist were employed.

In order to obtain hard molding surfaces on the first three dies, a form of surface treatment was necessary. The common methods of case hardening (pack carburizing, gas carburizing, cyaniding, and carbo-nitriding) require a quench from 1375°F or higher, which produces considerable distortion. Since a large amount of contour grinding would be required to clean up this distortion, these methods were eliminated from further consideration. Contour grinding was not desirable because:

1. Wheel wear would make it difficult to obtain the necessary accuracy.
2. Grinding would not result in uniform surface hardness due to the varying depths of stock to be removed.

3. A considerable amount of grinding in the boring mill would tend to wear the ways of the mill and thereby reduce its accuracy.

Flame-hardening was another method of surface hardening considered. However, this method, which is essentially a two-dimensional process, could not be easily adapted for use with dies of the shape required. To design a flame-hardening fixture for each die would be costly and the result would not be satisfactory. Hard chrome-plating was eliminated because it is porous and uneven in thickness.

The metallurgists that were consulted agreed that a form of heat treating known as nitriding would be the most suitable method. Because only a relatively low temperature (usually 975°F) is required for this process and no quench is needed, the amount of distortion would be minimum. By the use of the Floe process, the thickness of the white layer could be controlled to less than 0.0005 inch and could be removed by only a hand polish. With nitriding, the steel dies could be heat treated, finish machined, and case hardened, so that only a small amount of polishing would then be necessary.

The nitriding operation, especially the Floe process, is relatively new; therefore, the advice of an expert in this field was obtained, and a nitriding facility was designed under his direction. This facility has yet to be built and tested, and the exact process required for specific die parts to be determined. It is definitely needed because none of the heat-treating companies in this area has a furnace large enough to nitride the largest parts.

After the required strength of the die steel had been determined by structural analysis and the method of surface treating was decided upon, the proper material for making the dies was selected. After it was decided that the male and female die parts for high-pressure plastics molding should be fabricated of forged steel, a modified 3-1/2 percent chrome, air-hardening, tool steel was selected for the two smaller sets ("A" and "D" in Table I). This steel is in common use in England, but does not have an SAE designation. For the last die ("E" in Table I), SAE 4140 steel was chosen because no nitriding was necessary nor was the desired core strength unusually high.

The choice of material for several smaller die parts also presented problems. For instance, the steel selected for the nose guide pin of each die had to allow considerable bending deflection without breaking and yet retain a high resistance to bending and wear as well as good hardenability. For the smaller dies ("A," "B," and "D"), SAE 1095 bar stock was the material selected for the nose guide pin. For the larger dies, this part was too thick to respond to the heat treatment suitable for SAE 1095 so it was made of Gordon tool steel.

Deep hardenability, toughness, and resistance to wear were also required for the die guide pins. For the smaller dies, these guide pins were made of SAE 4340 bar stock and were heat treated to a hardness of 55 to 56 on the Rockwell C scale. For the larger dies, the material specified was ASM class II-B-1, air-hardened and drawn to Rockwell C 58 to 61.

The guide bushings and nose clamp for all the dies were made of Carpenter's Super Samson bar and were gas carburized to give a wear-resistant surface. The stripper rings, stripper cams, and stripper slides were

fabricated of ASM class II-B-2, heat treated to Rockwell C 57 to 59. Most of the other parts were made of materials that are in relatively common use for these applications.

In order to ensure that the dies would undergo little or no distortion during the nitriding process, metallurgists recommended that a stress-relieving operation in a controlled atmosphere be carried out after each contour-turning cut. Since there seemed to be no controlled-atmosphere furnace of sufficient size available and since the limited use to which such a furnace could be put did not warrant building one, the nitriding furnace was to be used for stress-relieving operations. The design of the nitriding furnace, therefore, made provisions for these operations.

The three dies that were to be nitrided were also to be polished to a high luster and then flash chrome-plated with 0.0003 to 0.0005 inch of chromium. Past experience had shown that a flash chrome-plating acts as a lubricant on the molding surfaces, a desirable feature on these dies that were to be used under severe molding conditions. However, very few platers will try to plate over nitrided steel because all of the "white layer" must first be removed from the nitrided surfaces.

Although no facility for plating a piece of steel as large as the "C" female die was available in the Los Angeles area, a concern was found that was planning just such a facility, which would be completed in time to handle this job.

The selection of suitable machine shops in which to fabricate these dies was not too difficult. An investigation of forging facilities in this country revealed that only two companies had electric furnaces, ingot molds, and forging presses that were sufficiently large to process the larger dies ("C" and "E"). A slight modification in the design of the "E" dies made it possible for a local company to pour and forge this set. By a fortunate coincidence this was the only local company that also had machine tools sufficiently large for machining these dies. Thus, it was possible to place just one order with a local concern for the complete manufacture of the "E" dies (except for the contouring of the mold surfaces).

A thermodynamicist determined the requirements of the steam for heating the dies; an outside consulting firm designed the heating-control system. These controls were necessary in order to maintain the temperature of the dies at the desired value until the preform was loaded, to raise the temperature at a specified rate until the molding temperature was reached, and then to maintain this temperature during the curing cycle. The controls also included the necessary plumbing and valves for cooling.

A safety engineer checked these dies in relation to safety, insurance, and health. His approval of the design of all the dies as well as of many of the items of auxiliary equipment was obtained before fabrication was started. Among the reasons for this concern were the following:

1. The resin in the material of which the part is made contains a certain amount of volatiles.
2. The preform is made on a fixture that is heated to 190°F, and the material is heated to a temperature as high as 130°F during the

layup operation.

3. The female-cavity detail part of one of the dies weighs over 14 tons, and the female die assembly weighs over 24 tons.
4. Three sets of dies were to be loaded into the press at temperatures of 190°F to 200°F.
5. The steam temperature is 360°F, and molding temperature is as high as 310°F.
6. The glass cloth used in making the radome is irritating to the skin of most people and some are allergic to it. Fine particles of the material can be carried in the air.

To design the auxiliary equipment needed in connection with the dies, a small machine-design group was set up. The results of their efforts are discussed in the following section.

VII. DESIGN OF DIE-HANDLING EQUIPMENT

The excessive weight of the main parts of these dies as well as the large number of different handling operations required adequate handling equipment. The design and fabrication of proper equipment was accomplished concurrently with that of the dies, so that it was available when these large pieces of steel were to be moved to a particular area in preparation for a certain operation.

To minimize repetition, the handling procedure followed for one set of dies will be explained here, and any additional items not typical will be added as the discussion proceeds. For various reasons it will be most convenient to describe the equipment that is to be used with the last set of dies ("E" in the Table); however, the illustrations will be those of the equipment for the "D" dies.

The large forging for the male die contained a cylindrical knob on the smaller end. This knob allowed adequate handling in the machine shop and also served as a means of chucking the male die into lathes and vertical boring mills for turning the face at the large end and boring the inside.

The first handling fixture (see Figure 3*) designed for the male plug served several purposes. The base was fastened to the male die so that it could be clamped into the vertical boring mill for contour machining. After the male form had been lifted onto the mill by the knob, which was then machined off, the nose-pin hole was drilled, counterbored, and tapped. An eyebolt fitting this hole was used for lifting the part from the mill, although the handling fixture also could have performed this operation. The eyebolt was primarily designed to be shipped with the male die when it was sent out for nitriding and chrome-plating (as in the case of the first three sets of dies). It provided a means of handling the detail part during these processes. The male handling fixture had two other uses: it provided a means for handling the detail male form for the layup fixture (which was either similar to, or the same as, the male die detail), and for moving the entire layup fixture after assembly. This is a desirable feature, because it is necessary to get the layup fixture out of the way when the die is moved into the oven.

The female die also had a large knob on its smaller end that facilitated handling in the machine shop and provided a means of attaching the die

to the face plate of the lathes and boring mills. After heat treating and rough machining, the female cavity had a wide flange welded to this knob, and the holes for attaching the collar were drilled in the other end of this part. To handle the die after this stage of fabrication, a fixture was designed to grasp it at the nose end, and a set of eyebolts was purchased for the open end. A set of equalizing slings was also purchased so that the die could be moved in a level position. Because the female die required a large amount of handling in various positions (this was particularly true of the first three female dies), a rotation fixture was designed for turning it over. With this fixture the various shops could contour-machine with the open end up, nitride with the open end down, and then chrome-plate with the open end up again.

A simple, table-type fixture that could be used with all five female die assemblies was built to serve as a storage fixture as well as for the assembly of details into the die and the inspection and cleaning of the die assembly after use.

Additional equipment suitable for use with all five sets of dies is needed for the molding cycle. With each molding cycle, the "C" and "E" dies have to be moved into the press and then out again. A die-transfer truck that moves on roller skids is used for this purpose. Due to the limited height inside the press, it is only five inches high.

A pair of tracks was laid to guide the truck to the press, and a winch was installed to move it. A series of pulleys enables the operator to move the truck down the track in either direction. A turntable is used to turn the die and head it into the oven. The track from the press to the turntable constitutes the die-loading area; a track perpendicular to the first track and running from the turntable to the oven forms the layup area. Directly in front of the press is a steel plate covering the pit. Reinforcement was placed in the pit under this plate, and a temporary track was installed over it. The bed of the press has a bed plate with machined grooves that correspond to the track. This plate serves as a track inside the press and can be left in the press during the molding cycle.

The molding cycle is as follows: A preform (layup) is made on a layup fixture. It is then stripped from the fixture and loaded onto the heated male die, which rests on the transfer truck. The heated female die is lifted from the storage table by the use of the handling fixture, the equalizing slings, and the crane; it is leveled and then lowered over the male die until it bottoms. The handling equipment is uncoupled, and the assembly on the truck is pulled into the press by the winch. The truck is positioned on the grooved bed plate with pins provided for this purpose.

The dies are then rejoined with the control panel; the upper platen of the press is lowered until it contacts the die, and bolts are inserted to tie the die to the upper platen. After the male and female dies are joined, the upper platen is raised, and the truck is removed from the press. The bed plate can also be removed, but this is not necessary. The die assembly is then lowered until it contacts the press base platen (or bed plate). The lower bolts are inserted, the tie blocks removed, and the dies are closed under pressure as the controls are adjusted.

After the part is cured and the dies have cooled, the press is opened

to break the part from the female; the part is then stripped from the male. The dies are then closed, the tie blocks are inserted, the lower bolts are removed, and the die assembly is raised. The truck is then moved in, the die is lowered to the truck, the upper bolts are removed, and finally the die is moved out in front of the press. The handling fixture is installed on the female die, the tie blocks are removed, and the female is lifted from the male with the crane and slings and is set on the storage table; the finished part is then removed from the male die.

For the "A," "B," and "D" dies, the procedure for loading the dies into the press needs to be followed only once; the dies can be opened after the mold cycle, and, because of the smaller size of the part, it can be removed from the open dies while they are still in the press.

VIII. DESIGN OF OTHER MISCELLANEOUS EQUIPMENT

In addition to the matched steel dies and their handling fixtures, various other items of tooling and equipment are necessary for the high-pressure molding of large radomes. The more important items are discussed below.

The layup fixture (see Figure 4*) mentioned previously is a very necessary piece of equipment in the molding of any laminated part. This fixture, on which are built up the preforms that go into the dies, is essentially a male die with a stripping mechanism and is mounted on a base having casters. It enables the technicians to build up pieces of impregnated glass cloth into the rough radome shape. This form must be steam-heated and the fixture must provide easy access to all parts of the form for ironing, trimming, pressing, etc.

Due to the thickness of the part (approximately one quarter of an inch), it becomes increasingly difficult to heat each successive layer of cloth in the preform because of the insulation offered by the previous layers. Proper heating of these layers is accomplished with unit electric heaters. To ensure that the temperature is uniform and stable, an enclosure was built around the layup area. It consists of a metal framework covered with canvas and has lights and an exhaust fan on the ceiling. The entire assembly is suspended from one column of the building; it can be raised out of the way, or it can be lifted by the crane and stored in another area.

To handle the largest preforms (those for the "C" and "E" radomes weigh over 100 pounds each) a clutch device is used to reach inside the molded-in insert, grasp it, and lift the preform over to the male die.

A set of adapter plates was built for mounting the "B" dies in the press. These plates contain bolt holes that match the bolt pattern in the press platens as well as those in the base and upper flange of this set of dies. The plates also contain bolt patterns for other dies that were used in molding parts other than the large radomes.

Stripper posts of various lengths and designed to fit the ways of the press were used for breaking the dies apart. These posts are used in pairs and fit vertically between the stripper cylinders in the press base and the upper platen.

It was necessary to machine some of the radomes molded on the "D" dies to various thicknesses for electrical testing. The initial machining was accomplished on the male die before stripping. The radome, still on the male die, was removed from the press and, by means of the handling fixture, was mounted on the boring mill for contour machining. It was then stripped from the die by means of a special fixture. The main advantage of machining a part on the male die is the accuracy that can be obtained.

For additional machining of the above parts, for machining parts already stripped from the male, and for trimming the radomes to length (both ends), a machining mandrel was built (see Figure 5*). In order to duplicate the male die as closely as possible, the contour of the mandrel was turned on the boring mill using the same template that had been used for turning the contour of the male die. An abrasive-wheel cutoff mechanism was used to trim the radomes to length.

A template and template mount were other necessary items of tooling. The template mount was used for locating and holding the template on the boring mill during the contour-machining operation. With the use of a compensating tracer stylus and a micrometer-adjustment device on the tracer head, both of which were designed by the development group, it was possible to machine both the male and female dies of each set with only one template, a unique accomplishment.

A gage was developed to check the thickness of the "D" radome as it was being machined on the mandrel. This gage, which fits over either the male die or the machining mandrel, gives the thickness reading directly for any point on the radome. It also serves to check tool wear during the machining operation and indicates if the radome has slipped from the die or mandrel (see Figure 5*).

The thickness of the finished radomes is measured by a mechanical thickness gage. The radome is suspended by its nose and the instrument enables a direct reading to be made of the thickness at any point by raising (or lowering) and rotating the radome. Although considerable work was done on electronic thickness gages, a satisfactory gage has not yet been developed.

The "E" radome has a metal ring assembly spliced to the aft end for mounting the radome on an airplane. To machine this splice joint in the radome, an automatic thickness router is used in connection with simple jig that holds the work. Then the radome and ring are loaded on an assembly fixture for locating the parts and drilling rivet holes and for riveting the parts together.

Several other items of tooling were designed for this program, such as test fixtures, inspection tools, and a bulk-reducing fixture, however, they will not be discussed since they have little direct bearing on the actual die program.

IX. FABRICATION OF TOOLING

The "D" dies were the first set to go to the shop for fabrication and are the only dies that have been completed (see Figures 6 and 7*). The following discussion of fabrication problems will therefore be concerned with this set.

The most difficult problem, in the opinion of the writer, was that involving the use of the boring mill in machining the contour of the molding surface of the dies. Because of the accuracy which can obviously be obtained by the use of only one template for contour-machining both male and female dies, our engineering group developed a method that would make this possible. This operation involved the design and tryout of the micrometer adjustment and compensating tracer stylus mentioned previously. The method is an improvement over the tried-and-true method of using matched templates to machine matched dies — a male template for the male die and a female template for the female die, the set varying by the thickness of the finished part.

Another problem that came up in connection with the "D" dies was the alignment of holes for the automatic stripping mechanism in the female collar. It was found that jig boring was the only sure way of attaining the alignment between the horizontal and vertical holes for the 12 sets of cams and slides. This was an expensive and difficult operation because of the hardness of the heat-treated forging.

Hardening the wear surface of the female collar was also difficult. The drawing stated merely that it should be of a certain hardness and the procedure was left to the machine shop. The choice of flame-hardening was eventually made because the machine shop that was building the dies had developed that process to a high quality. There was considerable reservation in this choice because of the possibility of cracking around the jig-bored holes. However, the final results justified the decision.

Another problem encountered was that of sampling from the forging. Several tensile-test specimens cut from the excess stock of the female die were tested to determine core strength and hardness. In addition, specimens were cut from the knob of the male die for hardness measurements. These two areas were not truly typical of the forging, but they were the only ones from which specimens could be taken.

One of the hardness specimens showed a banded structure, with bands about 0.040 inch apart, and its hardness varied as much as 11 points on the Rockwell C scale. The boring-mill operator had complained of "hard spots" while contouring, so additional samples were cut. Since it was not possible to obtain this banded structure elsewhere, it was written off as only a local characteristic at the most-necked-down area of this particular forging.

To seal the steam chambers, a material was required that would repeatedly withstand the temperature and pressure of the molding cycle. However, because seals of teflon were used, great difficulty was encountered in compressing a large area of this material when assembling the steam chambers.

Delivery dates proved a serious handicap. As a policy, most machine shops underestimate the time necessary to fabricate a piece of tooling. This practice makes it difficult to schedule an entire project.

X. CONCLUSIONS

The tool-development program discussed in this paper is only partially complete but progressing very rapidly. However, many months will pass before

it is completed and a final report can be written. The results obtained thus far are available for the advancement of the art of large-radome development.

The experience gained from the molding and testing of these radomes, as well as similar smaller ones, has provided data that will be useful to others who are working on similar parts.

The large press, the very accurate boring mill, and the other equipment have contributed significantly to the successful development of large, highly accurate radomes. It was fortunate that procurement of this equipment was initiated early in the program, because it takes about a year to build machine tools the size of the press and mill, and it requires almost another year to put them into good running order in a particular plant.

The development of reliable sources for engineering, materials, machine work, and testing is another result of this program. The search for these services is very time-consuming when they are not readily available, and they are very often necessary before even the planning can be started.

The finished designs for five different sets of matched dies and their auxiliary tooling have provided the designers engaged in this program with a vast amount of information on which to base future designs. These five designs have been completely engineered and are ready for fabrication. In fact, much of the tooling has been fabricated and has been checked in actual operation.

Finally, the results obtained by the use of the tooling that has been fabricated and data on the parts that have been manufactured and tested, as well as on the equipment that has been proven by actual use, are contained in reports readily available to those interested. In addition, there are many other reports on the engineering studies that accompanied the design of this large tooling; all are available from the writer.

TABLE I

GENERAL CHARACTERISTICS OF FIVE SETS OF MATCHED DIES

DESCRIPTION	"A" DIES	"B" DIES	"C" DIES	"D" DIES	"E" DIES
Radome Diameter in Inches (Approximate)	24	23	38	24	37
Radome Length in Inches (Approximate)	37	50	83	37	78
Maximum Press Load (Tons)	500	900	2500	225	530
Maximum Average Molding Pressure (psi)	2200	4300	4300	1000	1000
Total Weight of Dies (Tons)	6	8	37	5	13

* Because of the format requirements of this publication, photographs can not be reproduced. Those figures not included here can be obtained by requesting them from the author. A list of these figures and their captions follows:

Figure 1.	2500-ton press	HAC Photo No. S11423
Figure 2.	Vertical boring and turning mill	HAC Photo No. S13336
Figure 3.	Male die detail in handling fixture	HAC Photo No. R34755
Figure 4.	Layup fixture with preform	HAC Photo No. R36157
Figure 5.	Thickness gage on machining mandrel	HAC Photo No. R38527
Figure 6.	Male die assembly	HAC Photo No. R38699
Figure 7.	Female die assembly	HAC Photo No. R38697

THE MEASUREMENT OF PHASE DELAY
OR
DIELECTRICS AT MICROWAVE FREQUENCIES

by

EMANUEL H. GROSS
EINO J. LUCHA

Wright Air Development Center

For the past several years, Airborne Fire Control Radars have been improved considerably and have become a necessary part of USAF aircraft.

To utilize the full potential of the Weapon Systems, the radome has to be designed, built, checked and corrected in vast quantities. In an attempt to meet this demand, large scale construction of facilities has begun.

Interferometers, boresight measuring equipments, transmission and reflection test ranges and dielectric measuring equipments have been and are being constructed in an attempt to design and produce the required radomes.

Even at best, the testing, evaluation and correction of fire control radomes are time consuming and costly. One of the many attempts to reduce the cost and time involved has been directed to the improvement of test equipment.

Wright-Field looking for a simple go or no-go gage for production testing had in mind a single horn, induction or perhaps a capacitive type device to detect the electrical phase variation in all types of radome walls. This device had to be small, easily carried, accurate and simple to use. The main objective was to be able to use this device on all shapes and sizes of radomes regardless of the material used in its basic construction.

A device was conceived, by the Radome Branch, Wright Air Development Center, whereby the reflection coefficient could be used to determine the equivalent electrical thickness of a radome under investigation, with a single horn at normal incidence.

One of the prospective advantages of this new instrument lies in the fact that it not only indicates a rejected radome but can tell the operator where and to what extent, either positive or negative, the radome is out of tolerance "electrically". Another advantage lies in its simplicity of design and operation which reduces testing time and cost.

Figure one (1) shows the basic diagram. A Klystron is used to supply energy at a 1000cps modulated X band frequency. The forward sensing

directional coupler (D_1) is used to detect the forward energy from the Klystron. The other directional coupler (D_2) is used to detect reflected energy from a sample when placed at the antenna aperture. A precision constant phase attenuator (A) is placed in the forward sensing arm of directional coupler (D1), and a constant amplitude phase shifter (ϕ) is placed in the reflected energy arm of (D_2). Energy is fed from (A) and (ϕ) to the hybrid arms of a magic tee. A crystal detector on one of the coplaner arms of the magic tee is connected directly to a V.T.V.M. The other coplaner arm is terminated by the use of an E-H tuner and a resistance load.

By adjusting the attenuator in the forward energy arm, it is possible to obtain the exact magnitude of forward energy to balance the reflected energy at the magic tee thereby giving a null. Further, by adjusting the phase shifter, either automatically or manually, it is possible to get a very sharp null in amplitude and in phase. The calibrating of this device is accomplished by a metal panel placed at the antenna aperture.

THEORY

Electrical thickness, effective dielectric constant and phase delay and their variations can be determined by measuring the reflection coefficient of a dielectric test panel, or radome. In obtaining the reflection coefficient, a known reference is required against which the signal reflected from a panel can be compared. When a metal calibration panel is used, the reflection is 100% and the phase reversal is π .

If $|P|^2$ is the power reflected from the radome panel, comparing this with the 100% metal panel reflection means that the $|P|^2$ is $|R|^2$, the absolute value of the complex reflection coefficient of the radome panel. If P' is the measured phase indication of the signal returned from the panel, using 0° as a calibration point, which was obtained by use of the metal panel, then $\pi + P' = R'$ will be the argument of the reflection coefficient of the radome panel.

The electrical thickness, effective dielectric constant, and phase delay, and their variations can all be computed from R and R'. A solid wall, at normal incidence for the lossless case

$$R' = \frac{3\pi}{2} + T' \quad (1)$$

where T' is the argument of the complex transmission coefficient. Since phase delay is expressed as,

$$\psi = T' - \frac{2\pi d}{2} \quad (2)$$

where d is panel thickness and the wavelength, we have

$$\psi = R' - \frac{3\pi}{2} - \frac{2\pi d}{\lambda} \quad (3)$$

Thus we have expressed phase delay in terms of measurable quantities. Since,

$$R' = -\frac{3\pi}{2} - \arctan \frac{1+r^2}{1-r^2} \tan \phi \quad (4)$$

where $r = \frac{1-\sqrt{\epsilon}}{1+\sqrt{\epsilon}}$

and $\phi = \frac{2\pi d}{\lambda}\sqrt{\epsilon}$ (electrical thickness)

then $|R|^2 = 1-|T|^2 = \frac{4r^2 \sin^2\phi}{(1-r^2)^2 + 4r^2 \sin^2\phi}$ (5)

now we have two equations expressing the measured R' and $|R|^2$ in terms of and ϕ. These two equations can be solved simultaneously to give ϕ in terms of R' and $|R|^2$. Since dielectric constant is

$$\epsilon = \frac{\phi^2\lambda^2}{4\pi^2 d^2} = \left(\frac{1-r}{1+r}\right)^2 \quad (6)$$

we have the dielectric constant in terms of known quantities. Similarly the equivalent formulas for the more complex cases such as sandwiches and lossy radome walls can be devised utilizing normal incidence.

The Dalmo-Victor Company was awarded the development Contract AF33(616)-3092 to completely develop such an instrument. The final instrument will feature automatic null seeking, recording, be small and light weight, and will be exceptionally easy to operate. It is expected that the accuracy will be ± 1 electrical degree. Delivery should be withing the next few months.

CONCLUSION

If such a device as this meets all expectations, fabrication of fire control radomes including monopulse can be checked accurately and quickly. This device is not expected to replace all the other large equipments, but certainly will expedite the production testing, correcting and final approval of guidance type radomes.

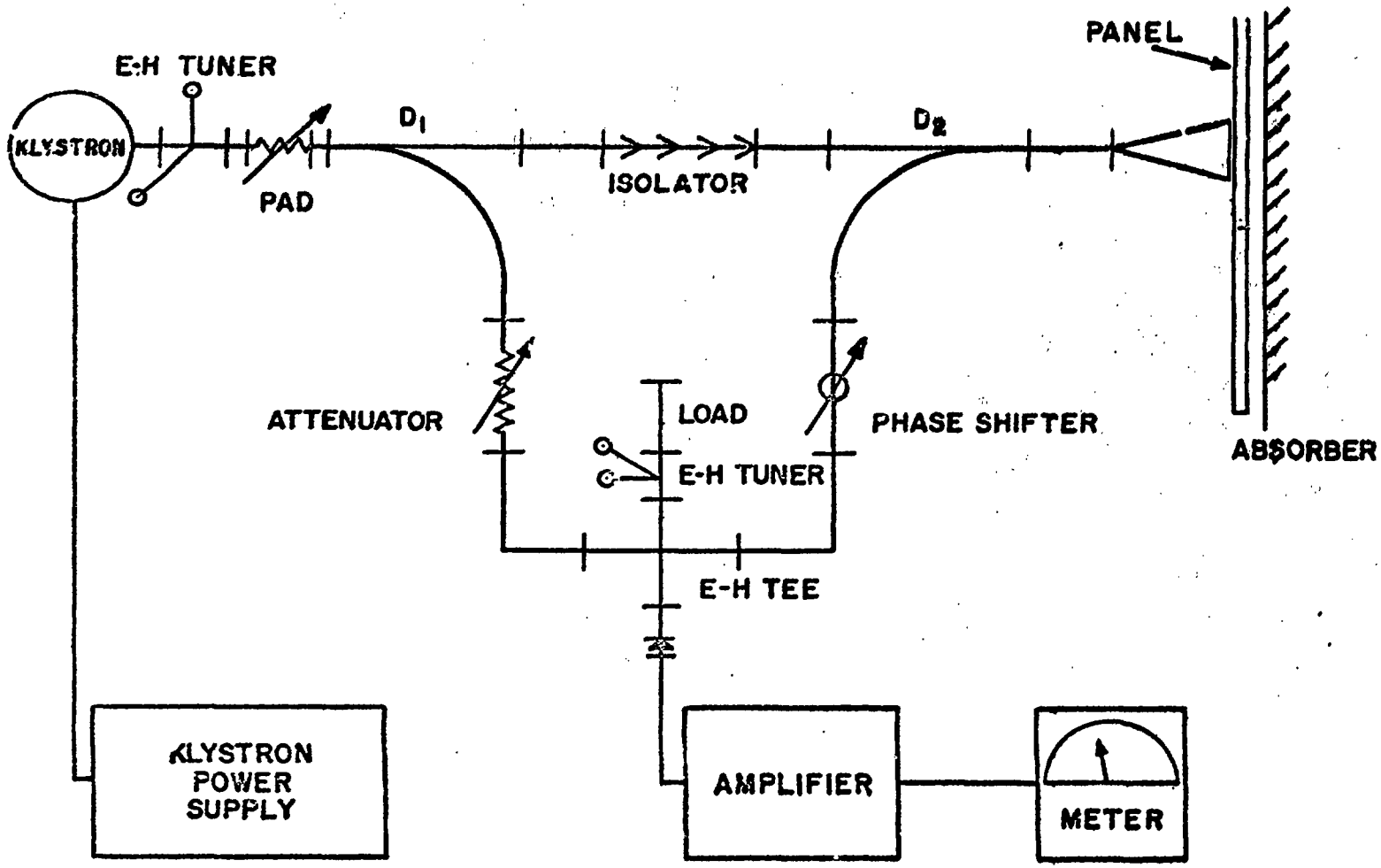

FIG. 1 ELECTRICAL THICKNESS GAGE

HUGHES AIRCRAFT COMPANY
RESEARCH LABORATORIES

Culver City, California

ELECTRICAL THICKNESS MEASUREMENT BY A SINGLE-HORN METHOD

by

H. R. Hope

In order to correct the boresight error of a radome, it is necessary to start with a radome whose walls are uniform in electrical thickness over any given cross section taken perpendicular to the radome axis. It is a difficult problem to manufacture radomes of uniform electrical thickness; therefore, it is desirable to be able to measure the electrical thickness of the radome wall. This measurement may then be used in a control procedure in the manufacture or subsequent correction of the radome. The most common method of making this measurement is by means of a two-horn interferometer. This method is in general satisfactory; however, particularly for large radome of a high fineness ratio, the mechanical problems of maintaining the separation of two horns, one inside and one outside the radome, to close tolerance becomes very difficult. Thus, it would be desirable to obtain the electrical thickness of the radome wall by means of a reflection measurement using only a single horn placed outside the radome. Such an apparatus has been designed and constructed at Hughes Aircraft Company and is the subject of this paper.

The electrical thickness, ϕ, of a dielectric panel is defined by the equation

$$\phi = \frac{2\pi d}{\lambda} \sqrt{\epsilon} \qquad (1)$$

at normal incidence. The reflection from the panel has minimum amplitude when $\phi = \eta\pi$. Then, if λ_m is the wavelength for minimum reflection, for $\eta = 1$,

$$\pi = \frac{2\pi d}{\lambda_m} \sqrt{\epsilon} \qquad (2)$$

Dividing (1) by (2), we obtain

$$\phi = \frac{\lambda_m}{\lambda} \pi = \frac{f}{f_m} \pi \qquad (3)$$

ϕ is the electrical thickness at the operating frequency or design frequency of the panel. If dielectric constant is desired, it may be computed from

$$\epsilon = \left(\frac{\lambda_m}{2d}\right)^2 = \left(\frac{c}{2 f_m d}\right)^2 \qquad (4)$$

$$\text{I.P.D.} = \phi = \frac{2\pi d}{\lambda} \qquad (5)$$

Another term in common use is insertion phase delay, defined, for normal incidence by equation (5). The above is valid only in the far field of the horn, which is not strictly the case with the present apparatus.

A block diagram of the apparatus used to measure the reflection from the panel is shown in Figure 2. As may be seen, it is basically a reflectometer setup terminated in an E-plane rectangular horn. The frequency is swept by means of a tracking klystron, the frequency of which is varied with a hand crank. The reflection is measured with a directional coupler and crystal detector and is displayed on a recorder. The recorder table is servo-driven along with the klystron frequency. Thus, a graph with reflected power on the vertical axis and frequency on the horizontal axis is obtained.

The measurement of the frequency at which minimum reflection occurs is complicated by the fact that interactions between the horn and the dielectric panel occur, thus causing minima to appear at many frequencies. As shown by R. M. Redheffer,[1] this interaction is due to two causes. First, the reflection from the panel adds vectorially to the reflection at the mouth of the horn due to the mismatch of the horn to space. When these two reflections are out of phase, a minimum will occur, even though the reflection from the panel is not a minimum. This effect has been reduced by the design and construction of an extremely well-matched horn. The horn is flared to an E-plane aperture of approximately 1 1/2 inches. The transition from the waveguide to the horn is a curved section tangent to two walls of the waveguide, thus minimizing throat reflections. A ground plane 3 inches by 5 inches is located at the mouth of the horn. The remaining mismatch is minimized by the insertion of a teflon strip and a block of polyfoam in the mouth of the horn. The horn match is shown in Figure 3. A second cause of interaction is the backscattering of reflected energy by the horn and the resultant multiple reflections between the panel and the horn. This effect is naturally aggravated by the ground plane used for matching. However, probably due to rapid inverse - square attenuation of these multiple reflections, they have been found experimentally not to interfere with the measurements as did the interactions due to mismatch of the horn.

---

1. R. M. Redheffer, "The Interaction of Microwave Antennas with Dielectric Sheets", M.I.T., Rad. Lab., Report R - 423 - 18

In order to test the operation of the equipment, three 12 inch by 6 inch panels of plexiglass ground to thicknesses of 0.437 inch, 0.414 inch, and 0.392 inch were made. Curves of reflection versus frequency are shown in Figures 4, 5, and 6. The dielectric constant of the plexiglass was then computed and compared with the dielectric constant as computed from a measurement made on a small sample of each sheet in a cavity dielectrometer. As may be seen, the measurements by any one method agree with each other within ± 2 percent. However, the reflectometer measurements are considerably lower in value than those made with the interferometer and cavity. It is felt that this is due to the fact that spherical rather then plane waves are incident on the panel, thus increasing the apparent angle of incidence. This effect becomes smaller as the dielectric constant is increased and the panel becomes thinner. A sheet of epoxy - Shell 1001 12 inches by 12 inches of thickness 0.278 inches was measured with the reflectometer as shown in Figure 7. Its dielectric constant was computed and compared with a measurement made on the panel with an interferometer. The measurements all agree to within 2 percent.

Many measurements were made on radomes, since this was the primary purpose of the instrument. A typical measurement is shown in Figure 8. This radome has previously been found to be electrically uniform with respect to rotation with the Hughes Aircraft Company boresighting equipment. The dielectric constant and electrical thickness at 9000 mcs. are shown and compared with results obtained from an interferometer. No change in electrical thickness with radome rotation was observed. Both measurements were taken at a point where the radome was about 5 inches in diameter. No effect due to the opposite wall of the radome was observed. A second radome, found to be asymmetrical with respect to rotation with the boresighting equipment, was measured. This radome has a variation in physical thickness with rotation of 0.004 inch in addition to a variation in dielectric constant of the wall. Electrical thickness and dielectric constant measurements at various rotational positions were computed and compared with measurements made on an interferometer. The electric thickness varies about 8° from the thin to the thick portions of the dome.

All of the measurements were made at an optimum distance of 3/4 inch from the horn to the panel. Variations of ± 1/8 inch cause no appreciable shift in the frequency of minimum reflection. At distances much smaller than 3/4 inch, the reflection from the front interface of the panel becomes large with respect to that from the rear interface of the panel due to inverse - square attenuation, and the minimum almost disappears. At distances much larger than 3/4 inch the magnitude of the reflection from the panel picked up by the horn becomes too small for satisfactory measurement. The range of the tracking klystron and of the horn match is 8000 to 10,000 mcs; thus the instrument is limited to a range of ± 20 percent in dielectric constant or ± 20 degrees in electrical thickness if the panel or radome is designed to be a half-wave thick at normal incidence at the center frequency of 9000 mcs. Obstacles such as panel edges in the field of the horn do not seem to affect the readings of the reflectometer greatly. Panels as small as 6 inches by 6 inches

give satisfactory results and it is felt that 3 inch by 3 inch panels will also be satisfactory, although this has not yet been tried. The measurements made by the reflectometer are consistently too low especially for panels of low dielectric constant. Thus the instrument in its present form must be calibrated for such measurements. However, the relative measurements at various points of a radome wall are sufficiently accurate and are still very useful. It may be possible to apply a theoretical correction to account for the fact that the panel is in the near field rather than the far field of the horn. It may also be possible to construct a lens in the mouth of the horn to produce more nearly plane waves at the panel.

The reflectometer is being modified for normalization with a ratio meter to eliminate errors due to variations in klystron output with frequency. For rapid measurement, the tracking klystron will be replaced by a traveling-wave tube electrically swept through the 8000 to 10,000 mcs. range several times a second. The reflection versus frequency may then be displayed on the face of an oscilloscope. An attempt is being made to construct a matched horn without the use of a ground plane.

It is felt that the present instrument is capable of a relative measurement of dielectric constant with an accuracy of $\pm$ 2 percent, electrical thickness with an accuracy of $\pm$ 1 percent, and a resolving power of one electrical degree.

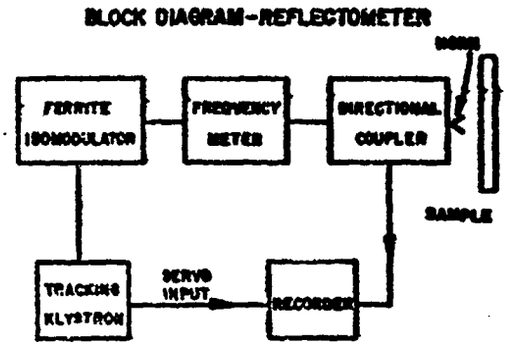

Figure 1

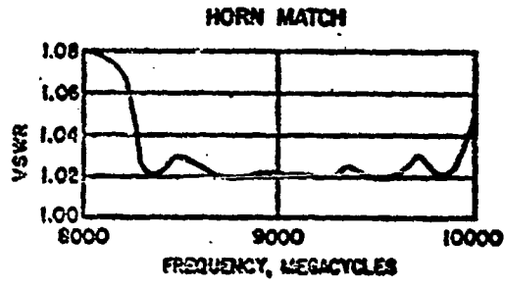

Figure 2

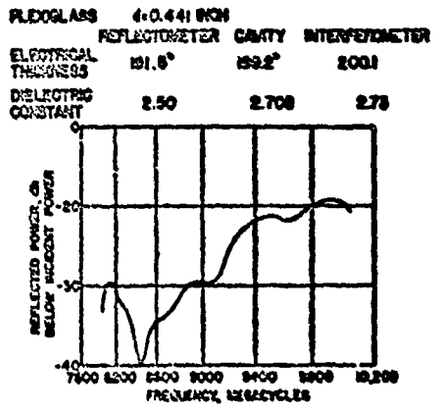

Figure 3

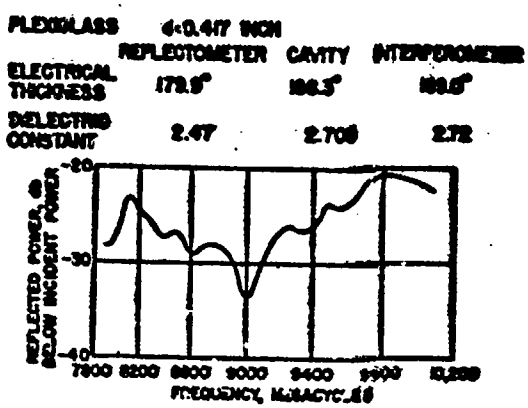

Figure 4

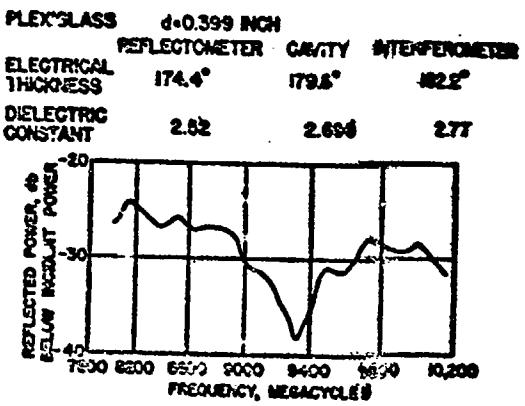

Figure 5

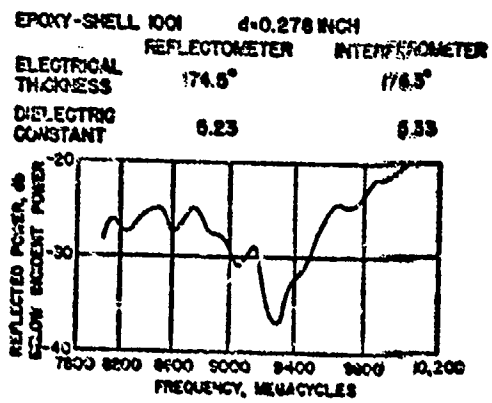

Figure 6

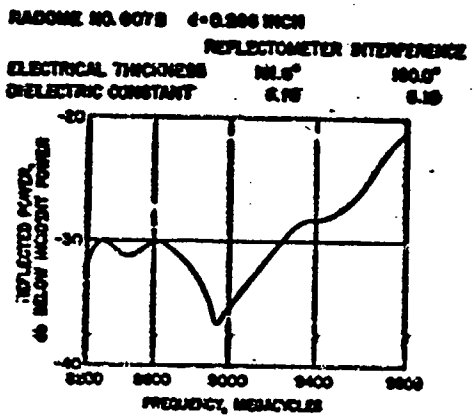

Figure 7

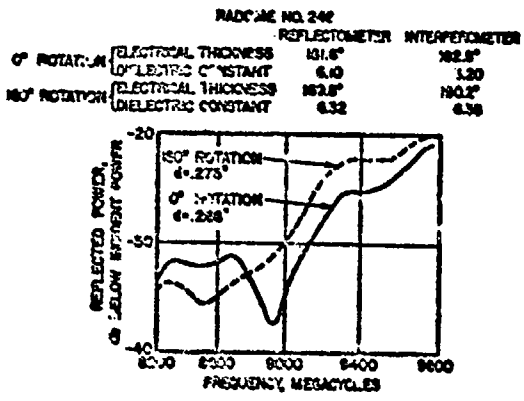

Figure 8

A NON-DESTRUCTIVE TEST METHOD FOR SANDWICH STRUCTURES

By

Robert W. Matlock

Zenith Aircraft
Gardena, Calif.

Early radomes were usually overstrength due to the electrical requirements for sandwich thickness, the double contoured shape of the parts, and the slow speed of the aircraft on which they were installed. This condition of overstrength is gradually being eliminated by more critical weight requirements, by higher speeds and related higher loads, and by higher temperatures which reduce the physical properties of the materials. It is apparent that the "fat" of overstrength radomes is in the fire, and high margins of safety of sandwich structures belong to the past.

The high margins of safety of early radomes was an essential factor of their design. It was known that bonds were weak and inconsistent. Parts were tested by tapping with a coin to detect unbonded areas. Quality control was limited by lack of knowledge of the factors which influenced part strength. Radomes fabricated to early standards would be entirely unacceptable today, primarily because of low and inconsistent bond strength.

The use of sandwich construction in aircraft is increasing, both for radomes and other structural components. The radome itself is fast becoming a primary structural component whose failure would endanger or cause the loss of the aircraft. The radome may be necessary to the shape of the aircraft for controlability, may carry cabin pressure loads, airframe loads, or perform other vital functions. There can be no compromises with quality and no inconsistencies of strength with these primary structures.

Because fabrication methods are complex, consist of many variables, each of which is subject to human error, positive knowledge of quality and strength is needed. In particular, proof of adequate bond strength is required. This paper presents a device and a method which has been successfully used since 1948 for the detection of weak bonds in sandwich structures.

Method of Operation:

Any engineer is familiar with a punch press and the method used in punching holes in a sheet of metal. Referring to Figure I, it can be seen that when the load "P" on the punch exceeds the shear resistance of the material around the periphery of the punch, a plug will be sheared out of the plate. The shear stress at failure is:

$$f_s = \frac{P}{A} = \frac{P}{\pi d t} \qquad (1) \quad \text{(Ref. Figure I)}$$

If the supporting collar be increased in diameter, the plate will be subjected to a bending stress as well as a shear stress. However, the shear stress around the perimeter of the punch will be unchanged. (Ref. Figure II). Furthermore, if the plate be changed to a sandwich, the conditions of equilibrium must still be satisfied. In this case the shear stress will exist principally in the sandwich core material (Ref. Figure III) and will have the following value:

$$f_s = \frac{P}{A} = \frac{P}{\pi d(n-t)} \qquad (2)$$

The shear stress so imposed in the sandwich core material is identical to that produced in the standard flexural test specimen. (Ref. Figure IV). The shear stress in both cases is transferred across the bond between the core and the skin. The bond strength is thus measured by the failing load. It is noted that the shear stress induced by the tester is a maximum at the exact periphery of the foot, and decreases in proportion to the diameters of the concentric circles.

In the beginning the simple device shown in Figure V was used. The weight "W" was lowered onto the panel at the prescribed intervals. Because of the clumsy nature of this device, its constant load, lack of portability, and difficulty of applying it to redcue shapes, a better method of applying the load was needed. This better method was found in the vacuum cup. (Ref. Figure VI).

The principal of operation of the cup is obvious on inspection. When the cup is evacuated, load is applied between the foot and the sandwich, thus creating the shear stress in the core. The load on the foot may be calculated as follows:

$$P = \Delta p\, A = \Delta p\, \pi \left(\frac{D}{2}\right)^2 \qquad (3)$$

where p is the vacuum, psi, and other symbols are as noted in Figure VI. Note that this equation neglects the area under the foot.

The shear stress in the core material is approximately equal to the following value:

$$f_s = \frac{\pi D^2 \Delta p}{4 \pi d(n-t)} = \frac{D^2 \Delta p}{4(n-t)d} \qquad (4)$$

A prototype vacuum cup device was delivered to the Forest Products Laboratory in 1950 for evaluation. Report 1832-B was published as a result of this work and reports the following conclusions:

1. Poor bonds in sandwich panels having cores of aluminum foil honeycomb, glass cloth honeycomb, or balsa, can be detected by proper use of the tester.

2. It makes no difference on which side of the panel the poor bond occurs.

3. Cores which fail without sudden failure, such as CCA or cotton honeycomb, cannot be detected.

4. The instrument is approximately as effective as a flexural shear test in detecting poor bonds, but not as sensitive as a flatwise tensile test.

Since publishing the above report, Forest Products Laboratory has fabricated and demonstrated a tester using a large vacuum area and a large number of feet. This variation may be useful if a large number of like parts are to be tested. It is apparent that Forest Products Laboratory feels the device will successfully test the bond strength of sandwich panels. In addition, the author has used the device for approximately five years on various radomes fabricated by Zenith Plastics Company and has shown the tester to be a valuable instrument for quality control or Material Review Disposition work.

Comparative Tests:

In order to compare the results obtained by use of the tester with flexural shear and flatwise tension values, a series of five panels representing typical radome configurations were fabricated and tested. The panels were 36" x 51", and constructed as shown below with glass cloth faces and glass honeycomb core.

Panel Number	1	2	3	4	5
Face Thickness	.025	.035	.036	.025	.035
Panel Thickness	.534	.300	.352	.298	.739
Core Material	¼PE x 6.0	¼PE x 6.0	¼PE x 6.0	¼NP x 4.0	3/16PE x 4.5

Test specimens were cut from the panels as shown on Figure VII. Results from this series of tests are shown in Table I. The ratios of the minimum and maximum to the averages are also shown.

It is noted from a study of the values that the sensitivity of the tester is of the same order as that of the flexural shear tests performed on samples. It may also be noted that in both cases the actual scatter of data is large.

Recommended Method of Use:

If a large number of like parts are to be checked, it is suggested that a flat panel typical of the cross-sectional configuration of the part be made and tested as outlined in this paper. The test value recommended for use in checking the part should be approximately 70% of the failing value for the test panel. If the flexural samples and flatwise tensile samples indicate the panel is considerably weaker or stronger than can be expected of the part, the test value may be adjusted accordingly.

If only a limited number of parts are to be tested, the equations presented may be used to calculate the test values. The value of shear stress to be developed may be taken as the expected value of bond strength or the design values of shear stress in the core. Standard practice at Zenith is to use 70% of the average value of the ultimate shear strength of the core in the TL and TW plane. This value is well below that which will damage the core material, but will show up any large deficiencies in the bond.

TABLE I - RESULTS OF TESTS FROM THE TESTER, SHORT SPAN FLEXURAL, AND FLATWISE TENSION FOR THE FIVE PANELS TESTED

			Panel 1		Panel 2		Panel 3		Panel 4		Panel 5	
			f_s	Ratio	f_s	Ratio	f_s	Ratio	f_s	Ratio	f_s	Ratio
Flexural Test	TW Plane	Min	119	.915	172	.905	209	.95	140	.91	96	.89
		Max	159	1.22	209	1.07	236	1.07	171	1.12	119	1.10
		Avg	130		190		220		153		108	
	TL Plane	Min	234	.96	248	.79	314	.91	285	.95	173	.77
		Max	258	1.02	344	1.10	376	1.09	312	1.04	258	1.15
		Avg	248		312		345		300		258	
Tester		Min	246	.91	397	.915	387	.93	232	.75	224	.90
		Max	305	1.13	470	1.08	447	1.07	386	1.26	260	1.05
		Avg	270		437		417		308		248	
Flatwise Tensile Average			307		390		387		189		420	

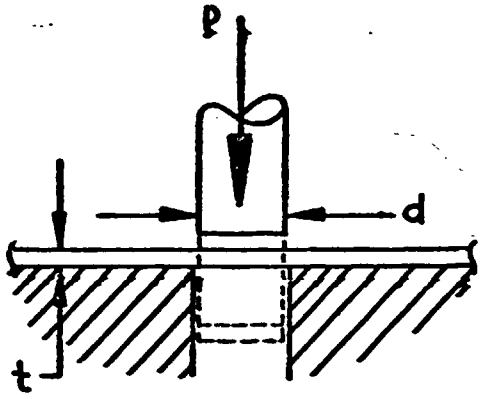

FIGURE I

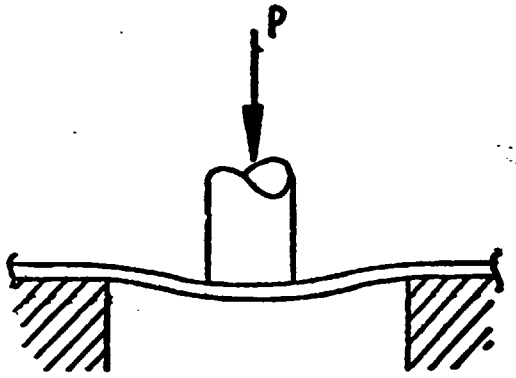

FIGURE II

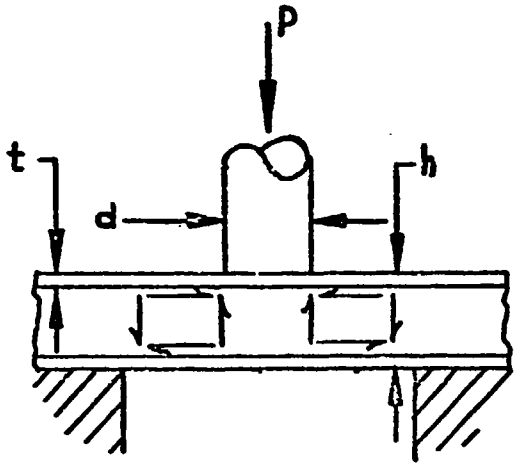

FIGURE III

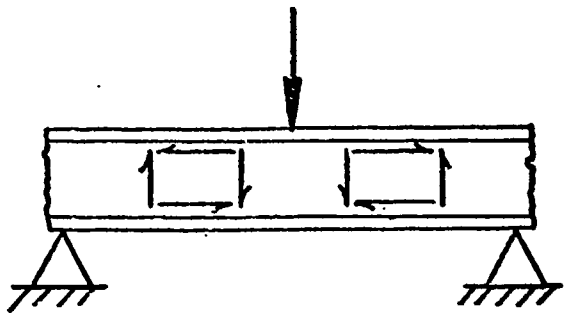

FIGURE IV

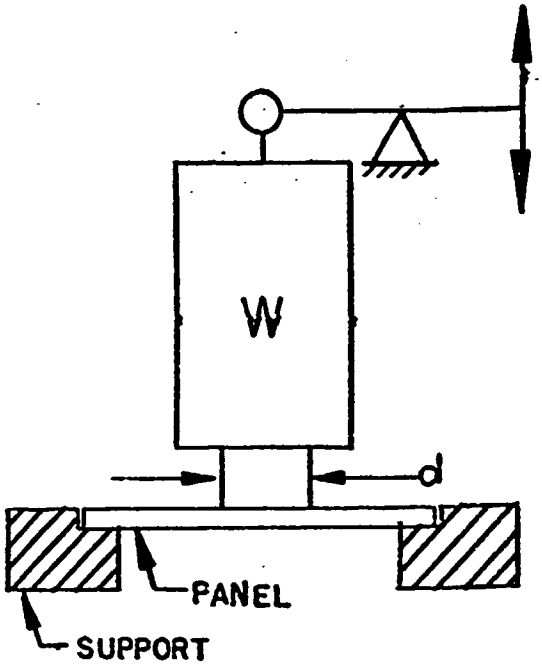

FIGURE V

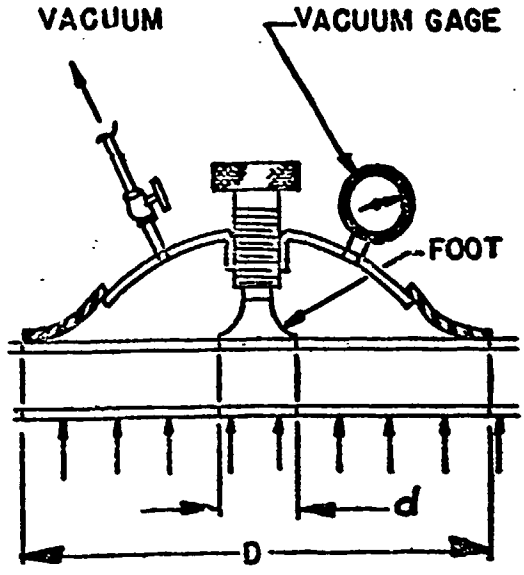

FIGURE VI

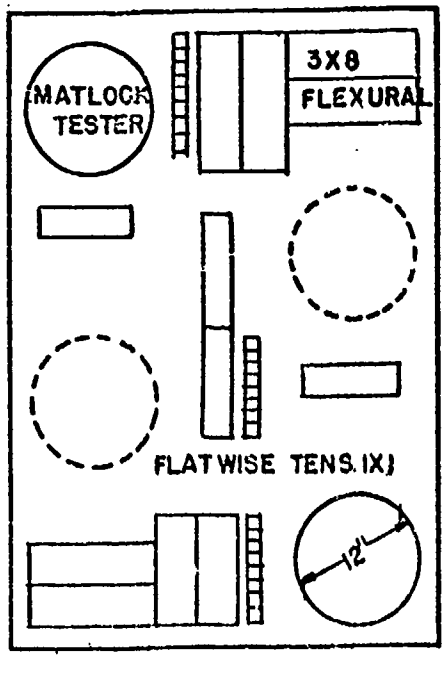

FIGURE VII

DEVELOPMENT OF A NONDESTRUCTIVE TEST FOR GLASS-REINFORCED PLASTIC LAMINATES

by

A. J. Schwarber, Jr.

Nondestructive Testing Research, Battelle Memorial Institute

For a number of years the Bureau of Ships has been sponsoring research for the purpose of developing instrumentation and procedures for nondestructively testing glass-reinforced plastic laminates. Original application of glass-reinforced laminates by the Navy was for construction of small boats. At present, however, the use of these materials has extended to many other structural and semistructural uses. The ever-increasing volume of the materials being procured and the structural requirements involved have necessarily increased the need for improved inspection techniques. Current inspection techniques involve visual inspection with strong white light, and/or tapping of the laminate. It would be highly desirable to furnish the inspector with instrumentation to augment the tests he currently uses.

An "idealized" nondestructive-test instrument for polyester-glass laminate should have as many of the following characteristics as possible:

(1) Portability and ruggedness
(2) Economy and ease of operation
(3) Capability of detection of:
    (a) Delamination
    (b) Porosity
    (c) Dry spot
    (d) Resin segregation
    (e) Incomplete cure
(4) Ability to measure laminate thickness
(5) Ability to measure resin or glass content of laminate
(6) Ability to penetrate at least 1/2 inch of laminate
(7) Must be a "one-side" inspection tool.

Early in the research program, a comprehensive survey was made of existing equipment and procedures, and the various energy forms used by this equipment were reviewed for possible application to laminate inspection.

LAMINATE SAMPLES USED FOR EVALUATING INSTRUMENTS AND TEST PROCEDURES

Samples of laminates containing dry spot, delamination, porosity, and resin segregation were obtained from various manufacturers. In most cases the samples were flat panels 6 inches square, with thicknesses ranging from 0.10 to 0.50 inch. Several samples of glass-reinforced tubing were also obtained for testing. Several laminate panels 1/4 inch thick were made in the laboratory with small cellophane inserts between the two central layers of reinforcement. These panels thus contain typical delamination defects. A group of special panels were fabricated by the Material Laboratory of the New York Naval Shipyard.

The resin employed was modified with styrene to a viscosity of approximately 600 centipoises. The laminates were made in a press with platens heated at 200 F. Polished ferrotype plates were used as the mold, and the curing time was 1/2 hour.

In one group of samples, an attempt was made to hold the resin content of the panels constant, with panel thickness being varied. Table 1 described this group of samples.

In another group of samples, an attempt was made to hold the panel thickness constant at 1/4 inch, while the resin content of the panels was varied. Table 2 describes this group of samples. The maximum deviation of these samples from the 1/4-inch nominal thickness is about 4 per cent.

MISCELLANEOUS TESTS

Inspection with Light

The most effective nondestructive tests currently in use on laminates involve visual inspection by transmitted or reflected white light.

Many tests were made with ultraviolet and infrared light, to determine whether another portion of the light spectrum might prove more efficient than the white range, but white light proved to be superior. The visual inspection of laminates is effective since most serious defects cause discoloration in the material. Obviously the method is limited to translucent material, and some other means must be used where opaque laminates are concerned.

TABLE 1. CONSTANT-RESIN-CONTENT, VARYING-THICKNESS SAMPLES

Panel	Nominal Thickness, inch	Number of Plies	Resin Content, per cent	Specific Gravity
7	1/8	10	38.5	1.79
8	3/16	15	39.1	1.76
9	1/4	20	37.1	1.80
10	5/16	25	39.6	1.77
11	3/8	30	38.9	1.76
12	1/2	40	38.1	1.78

Note: Reinforcement -- Style 1,000 glass cloth.

TABLE 2. CONSTANT-THICKNESS, VARIABLE-RESIN-CONTENT SAMPLES

Panel	Reinforcement	Number of Plies	Resin Content, per cent	Specific Gravity
1	Cloth(1)	21	36.8	1.79
2	Cloth(1)	24	32.1	1.86
3	Cloth(1)	19	41.1	1.71
4	Polyester mat(2)	6	75.4	1.40
5	Polyester mat(2)	9	62.5	1.48
6	Polyester mat(2)	8	67.3	1.45
13	Polyester mat(2)	4	82.3	1.35
14	Polyester mat(2)	10	57.8	1.51
15	Cloth(3)	14	48.8	1.63

(1) Style 1000--114 cloth

(2) 1-1/2 ounce Polyester Mat (Treatment 17)

(3) Equivalent to Style 1000 cloth.

All samples nominally 1/4 inch think.

Tapping Tests

Tapping laminates with a blunt object is often an effective means for locating laminar-type defects, due to the difference in sound generated when the material above a delamination is vibrated. This test method is currently used to evaluate the extent of questionable areas of laminates. Since the results of this test method depend completely upon the skill of the inspector, instrumentation to verify his judgment would be very desirable. Experiments were performed with an electromechanical tapping device, in an attempt to develop such an instrument. The instrument uses a variable-frequency relaxation oscillator to control the tapping rate, and another control allows the force of impact of the tapper to be varied. A crystal detector is used to pick up the vibrations from the laminate. The vibrations can be listened to with earphones, and their waveform may be monitored with an oscilloscope.

The electromechanical tapper used on glass-reinforced laminates did not disclose any more information than routine tapping and listening techniques. However, a device of this type may have a possible application for inspecting "honeycomb" sandwich material, where bonding of the outer skin to the honeycomb reinforcement must be inspected.

Dye-Penetrant Tests

A number of tests were made with liquid dye penetrants, to evaluate the application of the test method to laminate inspection. For a penetrant inspection to be effective, defects must necessarily be open to the surface. Surface crazing and porosity show up very well under penetrant inspection. Where penetrant can be applied to the edge of a panel, delaminations at the edge may be readily located. The method has been very useful for laboratory evaluation of laminate samples.

Radiography Tests

Radiographs were taken of a number of laminate test panels. The panels were 1/4 inch thick, made with Vibrin 112 resin reinforced with 184-114 glass cloth. Exposures were made for 5 minutes at 40 KVP and 8 milliamperes, at a distance of 30 inches. Type M film was used. The radiographs clearly show areas of obvious density variation, such as gross porosity and resin concentrations. Delaminations were not detected. This method is costly and time consuming, and involves a relatively large amount of equipment, so it has been used only for laboratory tests.

ULTRASONIC TESTS

Ultrasonic tests have been used successfully for a number of years to locate internal discontinuities in metals. The method is effective on most metals since they have relatively good ultrasound-propagation qualities. Most reinforced plastic materials have poorer acoustic propagation qualities. Therefore, using ultrasonics to inspect reinforced laminates involves much more than a direct "applications" problem.

Pulse Echo

A pulse-echo-type instrument uses a quartz crystal to transmit pulses of ultrasonic energy into the material under test. The time required for a pulse of energy to be reflected back to the crystal from an interface is measured electronically and is displayed as an indication on a cathode-ray screen. This screen may be calibrated so that the thickness of a material, or the distance to a discontinuity in the material, can be determined directly.

Laboratory tests with pulse-echo equipment were made at frequencies of 1, 2-1/4, and 5 megacycles per second. No useful results could be obtained.

Through Transmission

Through-transmission inspection is usually accomplished by using an instrument with two crystals, one for transmitting, the other for receiving. The crystals are mounted directly in line with each other, and the work piece is placed between them. An inspection of this type must be conducted in a suitable sound-transmitting fluid such as water or oil. The fluid provides acoustic coupling between the crystals and the work piece. The receiving, or detecting crystal, produces an electrical signal proportional to the amount of ultrasonic energy impinging upon it. The signal is usually amplified and displayed on an oscilloscope screen. Since defects or discontinuities in the work piece attenuate the beam of ultrasound, a sudden decrease in amplitude of the received signal as the work piece is being scanned is indicative of some defect in the material.

While this test method is not a "one-sided" test, it was found to be quite effective for laboratory evaluation of the internal quality of small laminate test panels. Delamination-type defects could readily be

located in laminates up to 1/2 inch thick. The extent of the delaminated area could be determined, and the panel surface could be marked accordingly. Dry-spot and gross-porosity defects also could be located. Frequencies of 1, 2-1/4, and 5 megacycles were used for the tests, with the best results obtained at 1 megacycle.

Resonant Frequency

A resonant-frequency ultrasonic instrument uses a transducer to transmit the energy into the work piece. Suitable coupling fluid (water, oil, or glycerin) is necessary between the transducer and the work piece. Electronic circuitry in the instrument is provided to furnish a means of sweeping a prescribed range of frequencies. If the material being tested is in the thickness range corresponding to the frequency range being covered, it will resonate at a frequency characteristic of its thickness. The transducer registers this frequency as a change in the electrical circuit. This change may be detected by means of a change in tone of a signal in earphones, by an increase in the reading of a sensitive meter, or as a "pip" on an oscilloscope trace. The oscilloscope trace may be calibrated so that the location of the "pip" indicates thickness of the work piece directly. If a defect or discontinuity in the work piece presents a large enough reflecting surface to the ultrasonic energy, a "pip" indicating the depth of the defect below the surface will be seen on the oscilloscope screen.

Audigage Tests

A number of commercial resonant-frequency ultrasonic instruments were tested on various laminates. One of these instruments, the Audigage, is manufactured by Branson Instruments, Incorporated, Stamford, Connecticut. The Model FMSS-5 Audigage has a frequency range of 0.65 to 2.00 megacycles. Using a special Type B transducer with this instrument, delaminations could be located in samples 1/4-inch thick. This 1.30 megacycle transducer is made by sandwiching barium titanate between two layers of quartz. Thickness measurements were made on laminates in the thickness range of 1/8 to 1/2 inch, with accuracies within 6 per cent. Thickness measurements could be made within 3 per cent when high-quality laminates were being tested.

Sonizon Tests

Another commercially available resonant-frequency instrument tested on laminates was the Sonizon, manufactured by the Magnaflux Corporation, Chicago, Illinois. The standard Sonizon instrument is equipped with five quartz transducers that cover the frequency range of 0.25 to 5.00 megacycles per second. In operation, a coupling fluid such as oil or glycerin must be placed between the transducer and the work piece. Resonance indications are observed on a cathode-ray screen. The screen can be calibrated to indicate thickness directly.

The instrument is designed primarily for the inspection of metals. The quartz transducers furnished with the equipment will not produce useful resonance indications from glass-laminate materials. Work is currently in progress to adapt barium titanate transducers to the instrument.

Barium titanate is basically an electrostrictive material which, when polarized, assumes properties similar to piezoelectric materials such as quartz. Higher amplitude vibrations can be obtained from barium titanate than from quartz.

If the barium titanate transducers can be used effectively with the instrument, the cathode-ray screen will then produce visual indication of the internal quality of the laminate under test.

DIELECTRIC TESTS

Audio-Frequency Tests

Early evaluation of various energy forms applicable to glass-laminate inspection indicated that dielectric tests might be developed to the point where they could furnish useful information about the material. Initial tests at audio frequencies were performed with probes having planar contact surfaces, applied to flat laminate specimens. An audio-oscillator was used to supply energy to the probes, and a vacuum-tube voltmeter was used to measure voltage changes in the system. These early tests indicated that penetration was achieved to a depth of at least 1/4 inch in laminate, and the method appeared feasible for laminate thickness measurement from one side of the work piece.

Crystal-Oscillator Probe Development

Investigation of existing patents on dielectric-testing equipment disclosed that United States Patent 2,601,649 describes an electronic thickness gage for dielectric materials. This patent is issued to Mr. H. A. Wadman, and is assigned to the Emhart Manufacturing Company, Hartford, Connecticut. It was considered that some modification of this gage might be developed into an inspection instrument for glass-laminate material.

Description

The instrument is designed to detect variations in dielectric materials. It does this by using the dielectric properties of the material under test to vary the capacitance of a condenser in a critically tuned resonant circuit. As the dielectric between two plates of a condenser is varied, the capacitance of the condenser is also varied. The contact electrode of the instrument forms one side of this condenser, while the grounded shell of the probe forms the other side. When the contact electrode is placed against a laminate test piece, the capacitance between the electrode and ground is changed. This change in capacitance causes a change in the amount of plate current being drawn by the crystal-controlled oscillator circuit. A vacuum-tube voltmeter is incorporated in the instrument to furnish meter indications proportional to the amount of plate current being drawn by the oscillator. The instrument may be calibrated so that the meter readings indicate laminate thickness (when resin content of the sample is not a variable), or resin content (when thickness is not a variable). A gross defect in the laminate, such as a dry spot or resin concentration, will cause a sudden meter deflection as the probe passes from normal laminate to a position over the defective area.

Three models of the instrument have been built; the first was battery operated, the second used either batteries or regular line voltage, while the Model 3 instrument operates from 110 volts alternating current. The oscillator circuit is contained in the hand-held probe, which is a stainless steel cylinder about 8 inches long and 2-1/4 inches in diameter. The contact electrode, which is placed against the surface to be inspected, consists of a 1-inch-diameter brass roller, mounted on a brass shaft several inches long. The contact electrode is insulated from the stainless steel shell of the probe by a polystyrene bushing.

Thickness Measurements

The Model 3 instrument functions well as a laminate thickness gage. Applying the instrument to the group of samples described in Table 1, a plot of meter reading as a function of laminate thickness was obtained. This plot is shown in Figure 1. Since the samples all contain about 38.5 per cent resin content, thickness of the samples is the critical variable.

To see if the probe would be functional on laminates with considerable curvature, the following experiment was performed. A thickness-measurement test

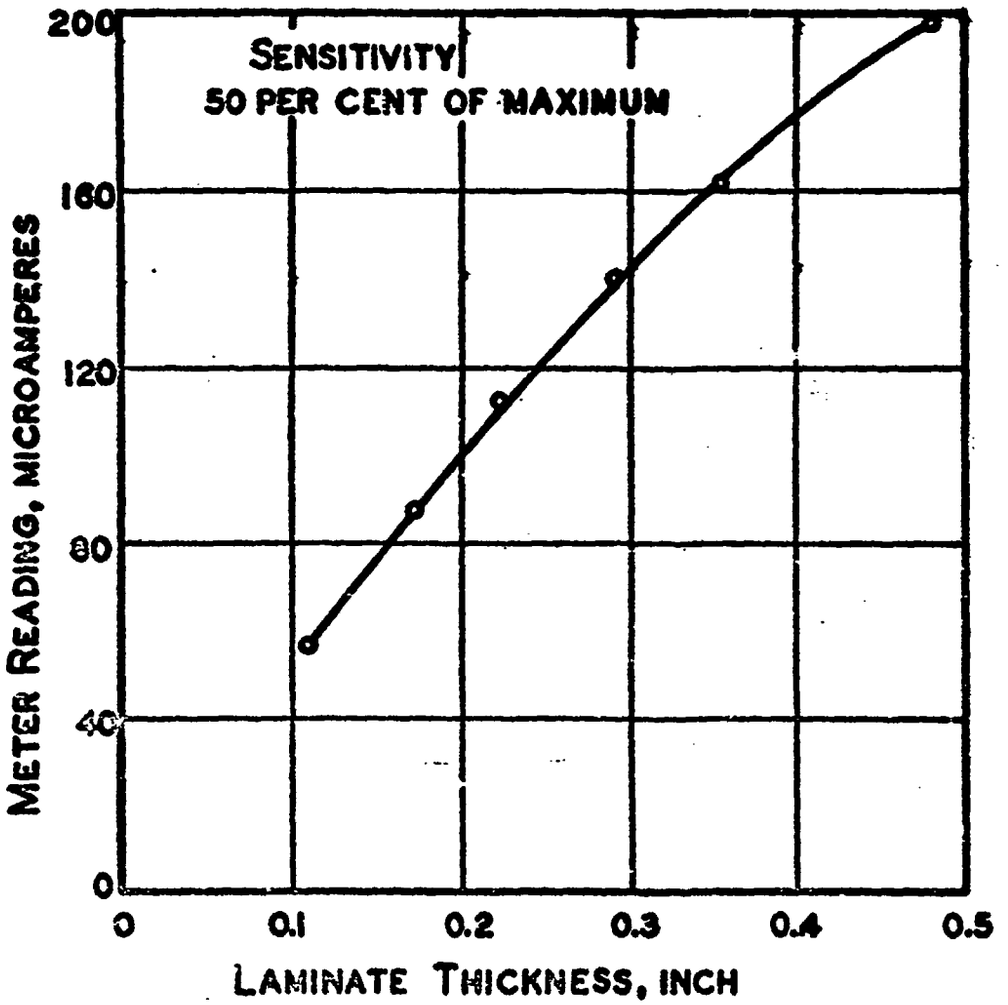

FIGURE 1. METER READING AS A FUNCTION OF LAMINATE THICKNESS

was made on a section of glass-reinforced plastic oil-well tubing. The 3-1/2-inch-OD tubing is made with glass-mat reinforcement and is centrifugally cast. The roller electrode was placed against the outer surface of the tubing, and readings were taken at 45-degree intervals around the circumference. A tubing micrometer was used to obtain actual thickness readings for correlation with the meter values. This relationship is shown in Figure 2. The maximum wall thickness variation is about 0.025 inch, and is readily indicated by the probe.

Resin-Content Measurements

Resin content as well as thickness of laminates affect the plate current readings of the Model 3 probe. Although thickness appears to have the greater effect, it is possible to use the instrument as a resin-content gage.

For resin-content measurement tests, panels of the same thickness (1/4 inch) were chosen. Table 2 describes these samples. The resin-content range covered by these samples extends from about 30 to 80 per cent. Mat and cloth type reinforcement is used in the samples, although no sample contains both types. The curves in Figure 3 show plate current plotted as a function of the resin content of the samples. Note that the curve from the cloth-reinforced samples differs distinctly from the mat-samples curve. Evidently the type of reinforcement affects the measurements.

CONCLUSIONS

(1) Visual inspection is still the best nondestructive test for laminate quality, when the materials concerned are not opaque.

(2) A skilled inspector, using "tapping" tests, can locate suspicious areas in opaque laminates by noting the duller sound obtained when tapping these areas. An electromechanical tapping device may be effective for checking the bond of the outer skin to honeycomb reinforcement.

(3) Dye penetrants will detect laminar defects occuring at the edges of a panel, and will also show surface porosity and crazing.

(4) Radiography will detect internal density variations, porosity, and cloth folds, but is usually ineffective for locating delaminations.

(5) At present, pulse-echo ultrasonic techniques are ineffective for laminate inspection.

(6) Through-transmission ultrasonic tests are quite effective for locating internal defects such as delaminations, dry spots, and gross porosity, in small laminate panels. One megacycle operation is superior to 5 megacycles.

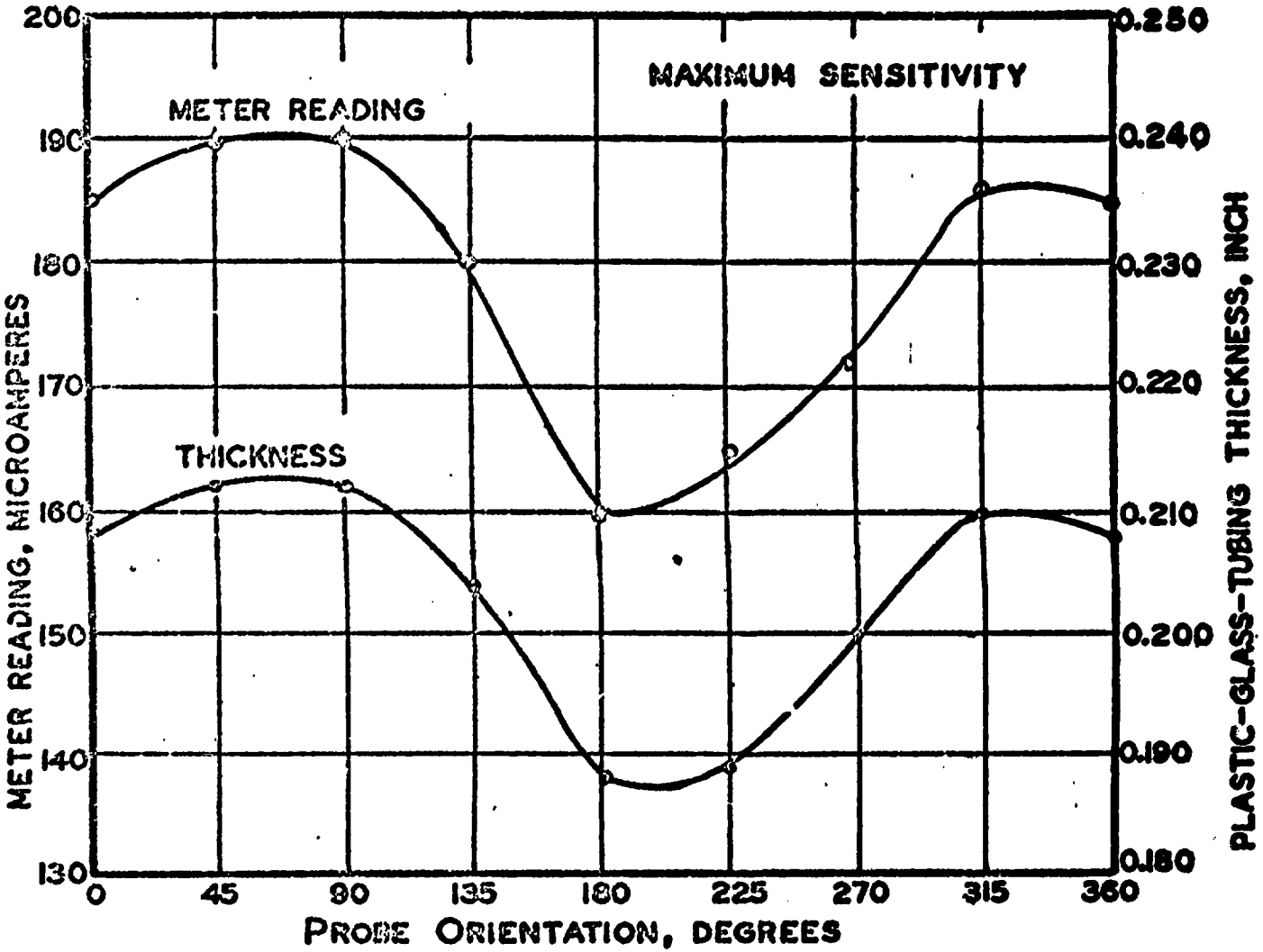

FIGURE 2. COMPARISON OF METER-READING AND THICKNESS CURVES

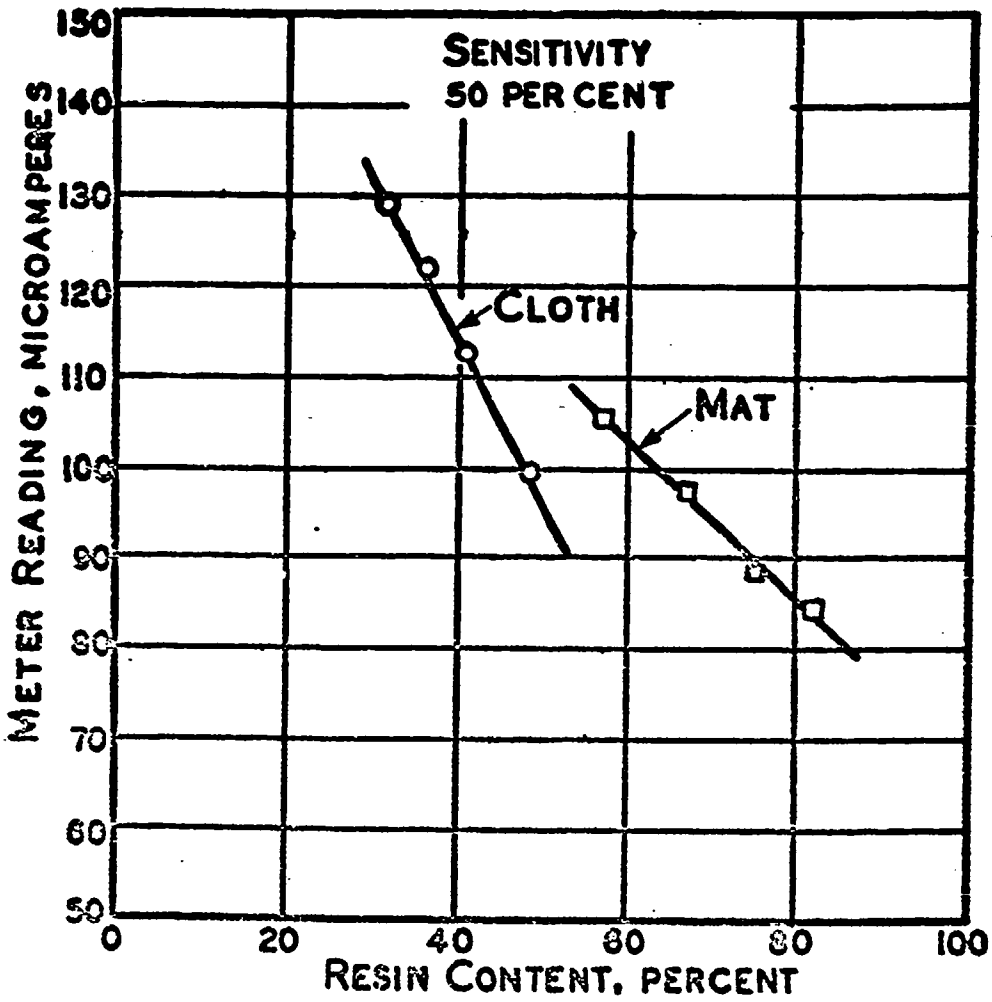

FIGURE 3. METER READING AS A FUNCTION OF RESIN CONTENT

(7) One resonant-frequency instrument, the FMSS-5 Audigage, used with a Type B transducer, will effectively measure laminate thickness with accuracy within 8 per cent. It will also determine the depth of delamination defect with the same degree of accuracy.

(8) Work is in progress on adapting barium titanate transducers to the Magnaflux Sonizon, which may enable it to effectively measure laminate thickness and locate delaminations.

(9) Dielectric tests can effectively measure laminate thickness from one side of the work piece. They can also be used to quickly determine resin content of laminates, if the thickness variable is relatively constant. Detection of resin concentrations or dry spots are possible under certain conditions.

(10) The current research program may result in improved dielectric-testing equipment, and modified resonant-frequency ultrasonic instruments.

ACKNOWLEDGMENT

The work described is part of a study "Nondestructive Testing of Reinforced Plastic Parts for Naval Application". The author is grateful to the bureau of Ships, U.S. Navy, for permission to publish this work, which was conducted at Battelle Memorial Institute under Contract No. NObs-61761.

AUTOMATIC BORESIGHT MEASURING EQUIPMENT

John B. Damonte and Al Gaetano
Dalmo Victor Company, San Carlos, California

ABSTRACT

The high fineness ratio required by modern boresight radomes has reduced present day radome design to an art rather than a science. The radome designer must have at his disposal some means of rapidly collecting boresight shift data, which he can employ to improve or control a given radome design.

This paper describes an automatic boresight measuring system, consisting of a radome mounting fixture, a radar tracking antenna and a null seeking mechanism, which can be employed to provide such data. The automatic boresight measuring equipment is able to automatically collect and record boresight data, cross talk data, and the vector sum of these two as a function of the angle of look. The accuracy of these measurements is better than 0.25 mils.

This particular set of automatic boresight measuring equipment can also be employed as a radiation pattern measuring device.

INTRODUCTION

"A chain is no stronger than its weakest link." Two links of particular importance to the aeronautical electronics engineer are the radar antenna and the radome. The tracking radar antenna is responsible for detecting the target of interest and then accurately determining its relative angular position and range. The radome is responsible for enclosing and protecting the radar antenna during flight, introducing little or no error in the location of the target of interest (boresight error).

With the advent of supersonic aircraft, nose radomes have assumed conical shapes with high-fineness ratios, rather than the hemispherical radomes formerly used with subsonic aircraft. This change to high-fineness ratio conical radomes has greatly increased the radome designer's problem, especially in connection with boresight shift for various angles of look. Radome design is presently at a state where it is more of an art than a science, and therefore the radome designer must have some tool that will allow him to evaluate just how good a radome may be, and just how its characteristics vary as small changes are made in radome construction.

The purpose of this paper is to describe such a tool -- an automatic boresight measuring instrument. This particular set of boresight equipment consists of:

a) a radar tracking antenna and a beam shift recording mechanism which together establish a radar line of sight, and

b) a radome mounting fixture which supports the test radome associated with the tracking antenna and rotates in such a manner that all points on the radome may be explored.

Basically, the equipment is capable of simultaneously measuring and recording the boresight error, the cross talk error, and the vector sum of these two, over angular cuts of 100° with a measurement accuracy of the order of 0.2 milliradians.

MECHANICAL DESIGN

The problem of designing a radome mounting fixture such that we may conveniently explore any desired portion of a given radome, at first sounds like a straightforward design procedure. However, we must be careful that whatever scanning motion is employed truly reproduces the scanning motion that takes place in the actual installation. Consider, for example, an aircraft installation of a tracking antenna and a radome where the antenna executes an azimuth sweep for an elevation angle of -10°. The intersection of the radar line of sight with the radome is a curve, parabolic in form, that lies in a plane parallel to the axis of the radome. If we were to install the radome about the tracking antenna on the pattern range, and if we were to take an azimuth cut by rotating the radome for the radome tilted relative to the fixed tracking antenna to simulate -10° in elevation at dead ahead, the intersection of the line of sight with the radome in this case is a curve parabolic in form, but lying in a plane that intersects the axis of the radome. These two cuts are not equivalent. Figure 1 indicates just how the various azimuth and elevation sweeps intersect the radome. It can be shown that if we wish to accurately duplicate the boresight errors encountered in an actual installation, that the test radome must be mounted with its azimuth and elevation axes interchanged. The mechanical design philosophy of the radome mounting fixture is based on this premise. Briefly, it may be described as follows:

The positioning mechanism shown in Figure 2 consists of a "vertical axis" turntable on which is mounted the half-yoke support for the "horizontal axis" scanning mechanism. The "horizontal axis" scanning mechanism is mounted on the half-yoke with large diameter bearings and supports the radome ring bearings. It is

motor driven throughout its operating range. The radome support ring is mounted on roller bearings to permit rotation of the radome on its own axis through 360°. A suitable clamp is provided to lock the radome support ring at any desired setting. The support ring inside diameter is 46" and will accomodate radomes up to 42" in diameter. The equipment can be modified to accomodate larger radomes. Maximum great circle angular motion permitted by the 46" ring is approximately 100°. A mounting plate is provided at the upper end of the antenna support bracket for mounting the particular radar tracking antenna associated with the radome under test. A boresight telescope bracket is mounted on the "horizontal axis" scanning mechanism parallel to the radome axis and normal to the radome support ring. This boresight telescope mounting enables the operator to calibrate the test equipment and to check its accuracy. The antenna support bracket is rigidly attached to the base of the radome mounting fixture for boresight error measurements. It can be employed in conjunction with the turntable for radiation pattern measurements.

The other end of the boresight measuring equipment consists of a null seeking system. This system includes a microwave shaping device and a positioning mechanism mounted on a pedestal which utilizes a biplaner parallelogram linkage to position the microwave shaping device. This particular piece of automatic boresight measuring equipment was designed for a 1,000" boresight range and the null seeking mechanism is designed to search a 30 x 30 milliradian sector.

ELECTRICAL DESIGN

Electrically, the automatic boresight measuring equipment operates somewhat as follows: a microwave source of energy supplies energy via a flexible coaxial cable to a parabolic antenna mounted on the null seeking mechanism. This antenna transmits a pencil beam in the direction of the radome and radar tracking antenna mounted at the other end of the 1,000" boresight range. The radar tracking antenna receives this energy as modified by the radome and develops a tracking error signal proportional to the apparent location of the null seeker source of energy. These tracking error signals are resolved into azimuth and elevation components and are fed back to motors that control the null seeker, which in turn drives the null seeker in such a manner as to reduce the tracking error signal to zero. As the radome is rotated through some desired cut, the effect of the radome changes and the apparent location of the null changes, thereby changing the relative position of the null seeker. The position of the null seeker is transmitted to a graphic recorder where boresight error, cross talk error and the vector sum of these two are available for analysis.

A block diagram of the boresight servo amplifier is shown in Figure 3, and its operation may be described as follows:

Energy is accepted by the tracking radar antenna system which, in this particular case, is a conical scanning antenna operating at a spin rate of 35 cycles per second. This signal is detected by a crystal video detector and is applied to a two-stage video amplifier. The output of this amplifier is detected by means of a simple "box-car" type of detector using a keyed detection scheme. This method of detection is useful in reducing the 1,000 cycle noise in the amplifier and it also helps to alleviate certain overloading and blocking conditions that might exist under extreme transient errors. This detector extracts the spin frequency modulation and amplifies it. The I,000 cycle carrier frequency is rejected by a series filter arrangement and the smoothed output is applied to a narrow band, 35 cycle amplifier filter, which discriminates against spin frequency second harmonic noise. The resulting signal is phase detected, using as a reference two voltages derived from the scanner spin generator which are indicative of the azimuth and elevation beam position. The two DC outputs of the phase sensitive detectors are fed through servo compensated networks, and then chopped at 60 cycles before being applied to their respective motor drive amplifiers. Two feed back loops are provided around the motor drive amplifiers. The first loop is employed to reduce the output impedance to prevent single phasing of the servo motors. The second loop employs tachometer feed back to reduce the motor time constant and therefore allows a higher loop gain with a resulting improved static accuracy. Tachometer feed back also improves the high frequency response thereby reducing the effects of wind loading.

Typical response curves for such a system are shown in Figure 4. These curves indicate that the dynamic error, as limited by servo response, for a ramp boresight shift pattern with a slope of 3 mils per degree, is somewhat less than 0.3 mils for a rotational rate of 180° per 10 minutes. If tachometer feed back is employed, the maximum error can be reduced to less than 0.2 mils for a rotational rate of 180° per 5 minutes, and to less than 0.1 mil for a rotational rate of 180° per 10 minutes.

The factors which ultimately determine the accuracy of the boresight measurement can be conveniently divided into static and dynamic system accuracies. The static errors include such factors as motor sensitivity, noise due to spin frequency second harmonic and carrier demodulation, drift of balance, wind loading, mechanical stiction and magnetron instabilities. The sum total of these errors is relatively small, probably of the order of 0.075 milliradians.

The dynamic inaccuracies include such factors as servo system response, reference generator phasing and wind loading. As described above, the servo response depends somewhat on the slope of the boresight error; for an extremely poor radome (boresight shift

rate of 3 milliradians per degree) with a 3 minute data collection period, the maximum error due to servo response was less than 0.2 mils. The proper adjustment of the reference generator phasing is important in reducing cross talk. Experiments to date indicate that small inaccuracies in spin generator phasing do not materially affect the overall accuracy. Wind loading is a problem that must be considered on an individual site basis. The frequency spectrum of most wind gusts is sufficiently high to cause jitter in the tracking system unless extremely high servo frequency response is obtained. The use of a high gain, rapid response tachometer feed back loop immediately around the motor and its driving amplifier has been instrumental in reducing wind gust effects to a tolerable minimum. On an overall basis, the boresight measurement equipment is able to operatewith an accuracy of better than ± 0.25 mils. On the average, the accuracy of the system is probably better than 0.2 mils. Obviously, the accuracy of the system will depend in a large measure on the boresight rate of the radome and the speed with which the boresight data is collected.

DATA COLLECTION RATES

The automatic boresight measuring equipment described above provides the radome designer with a tool that will quickly and accurately determine the boresight shift characteristics of a given radome. The various points on the radome may be explored by taking azimuth cuts, elevation cuts and/or circumferential (roll) cuts. The data collection rates depend on the maximum boresight shift slope likely to be encountered and the required measurement accuracy. For a rather poor boresight radome (maximum shift slope of 3 mils/degree) and a measurement accuracy of ± 0.25 mils, a 100° azimuth or elevation cut would require 2.8 minutes. For a reasonably good boresight radome (maximum shift slope of 0.5 mils/degree) and a measurement accuracy of ± 0.25 mils, a 100° azimuth and elevation cut would require 0.5 minutes. For radomes with small boresight shift rates, one can employ a long data collection period and possibly realize boresight accuracies of 0.1 mil.

CONCLUSIONS

1) The high-fineness ratio required by modern boresight radomes reduces present day radome design to an art rather than a science.

2) A radome designer must have at his disposal some means of rapidly collecting boresight shift data which he can employ to improve or control a given radome design.

3) An automatic boresight measuring system consisting of a radome mounting fixture, a radar tracking antenna, and a null seeking mechanism, can be employed to provide such data.

4) The automatic boresight measuring equipment is able to automatically collect and record boresight data, cross talk data, and the vector sum of these two as a function of angle of look. The accuracy of these measurements is better than 0.25 mils.

5) The automatic boresight measuring equipment can also be employed as a radiation pattern measuring device.

ACKNOWLEDGEMENT

The authors would like to acknowledge the contributions of Gordon L. Shepherd (Mechanical Engineer) and Sanford Evans Jr (Systems Engineer) to the design of the automatic boresight measuring equipment, and Glenn A. Walters (Director of Research) who was instrumental in the development of a working model.

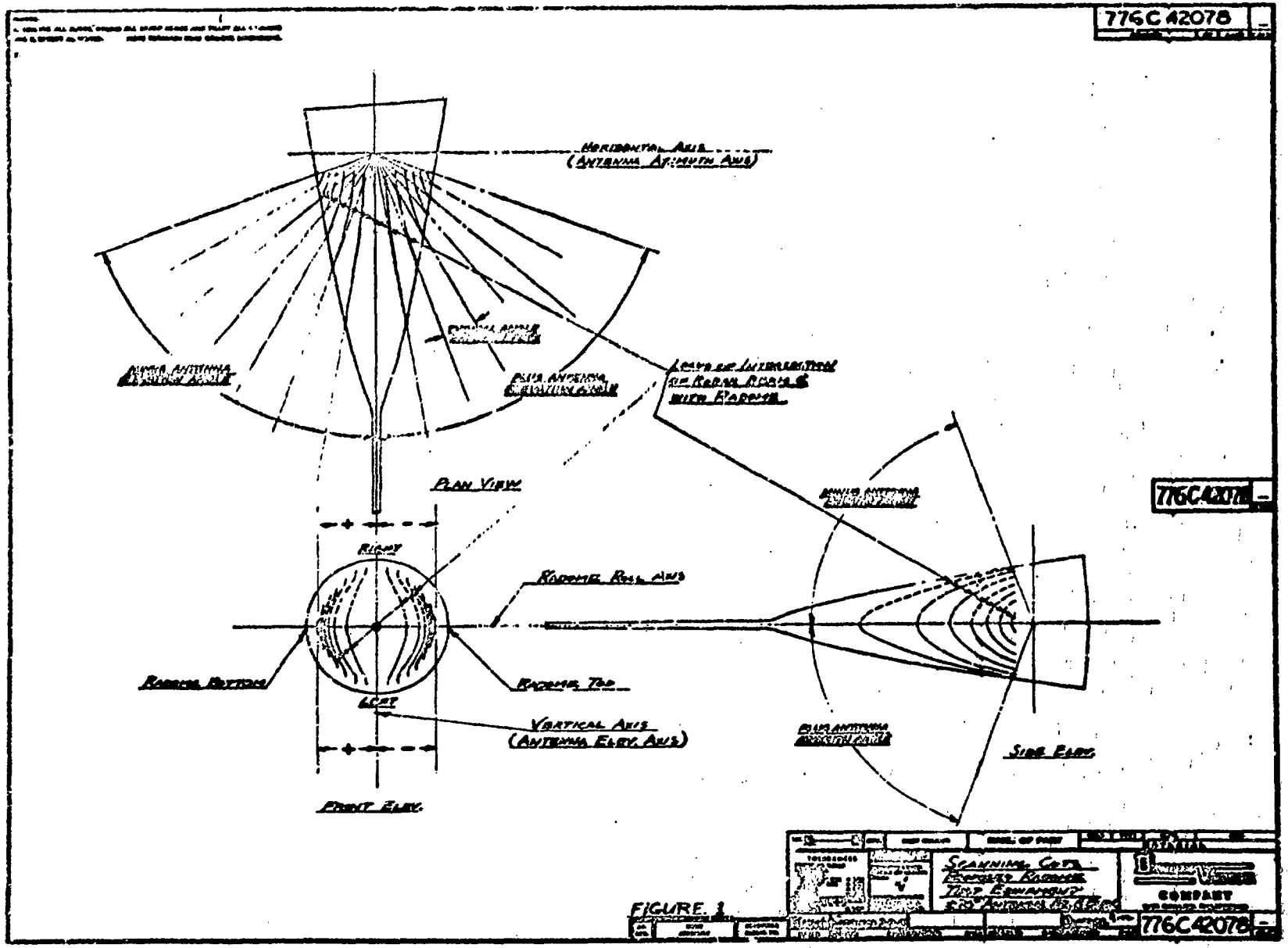
776C 42078
HORIZONTAL AXIS
(ANTENNA AZIMUTH AXIS)
PLAN VIEW
RIGHT
RADOME ROLL AXIS
RADOME BOTTOM
RADOME TOP
LEFT
VERTICAL AXIS
(ANTENNA ELEV. AXIS)
FRONT ELEV.
SIDE ELEV.
776C42078
776C42078

FIGURE 1

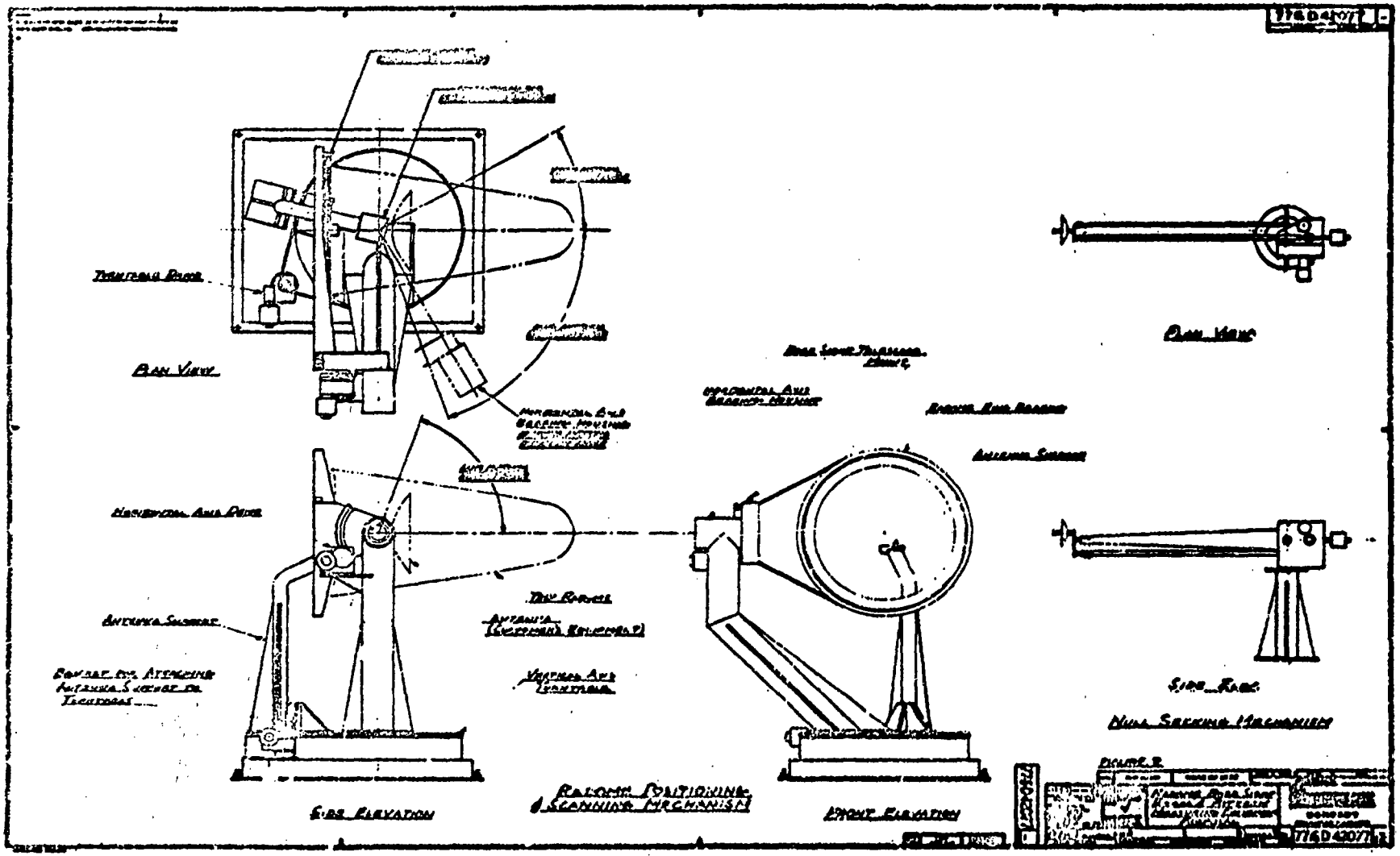
Plan View
Plan View
Side Elevation
Rotary Positioning & Scanning Mechanism
Front Elevation
Side View
Horn Scanning Mechanism

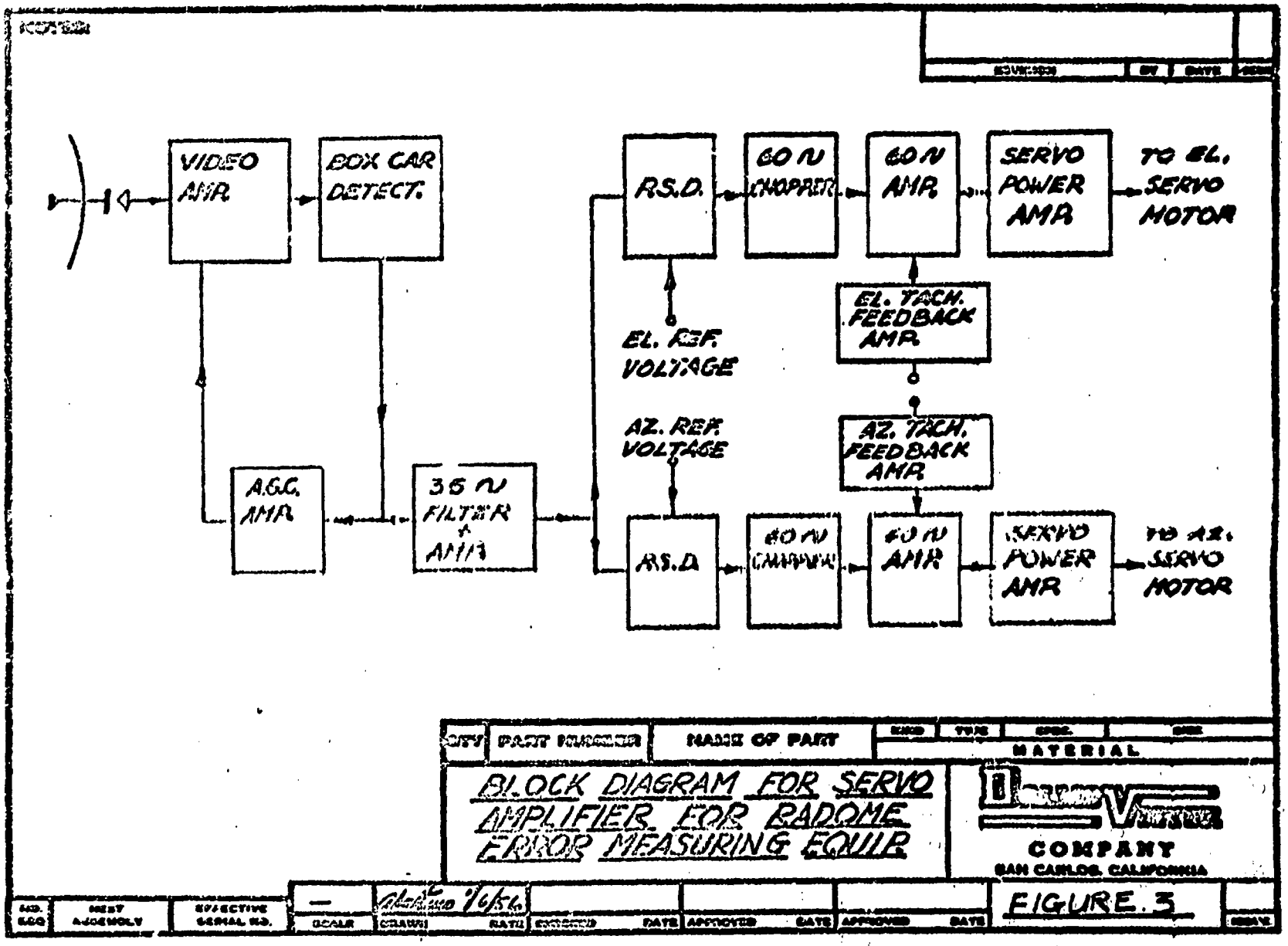
VIDEO AMP.
BOX CAR DETECT.
R.S.D.
60 N CHOPPER
60 N AMP.
SERVO POWER AMP.
TO EL. SERVO MOTOR
EL. TACH. FEEDBACK AMP.
EL. REF. VOLTAGE
AZ. REF. VOLTAGE
AZ. TACH. FEEDBACK AMP.
A.G.C. AMP.
35 N FILTER & AMP.
R.S.D.
60 N CHOPPER
60 N AMP.
SERVO POWER AMP.
TO AZ. SERVO MOTOR
BLOCK DIAGRAM FOR SERVO AMPLIFIER FOR RADOME ERROR MEASURING EQUIP.
COMPANY
SAN CARLOS, CALIFORNIA
FIGURE 3

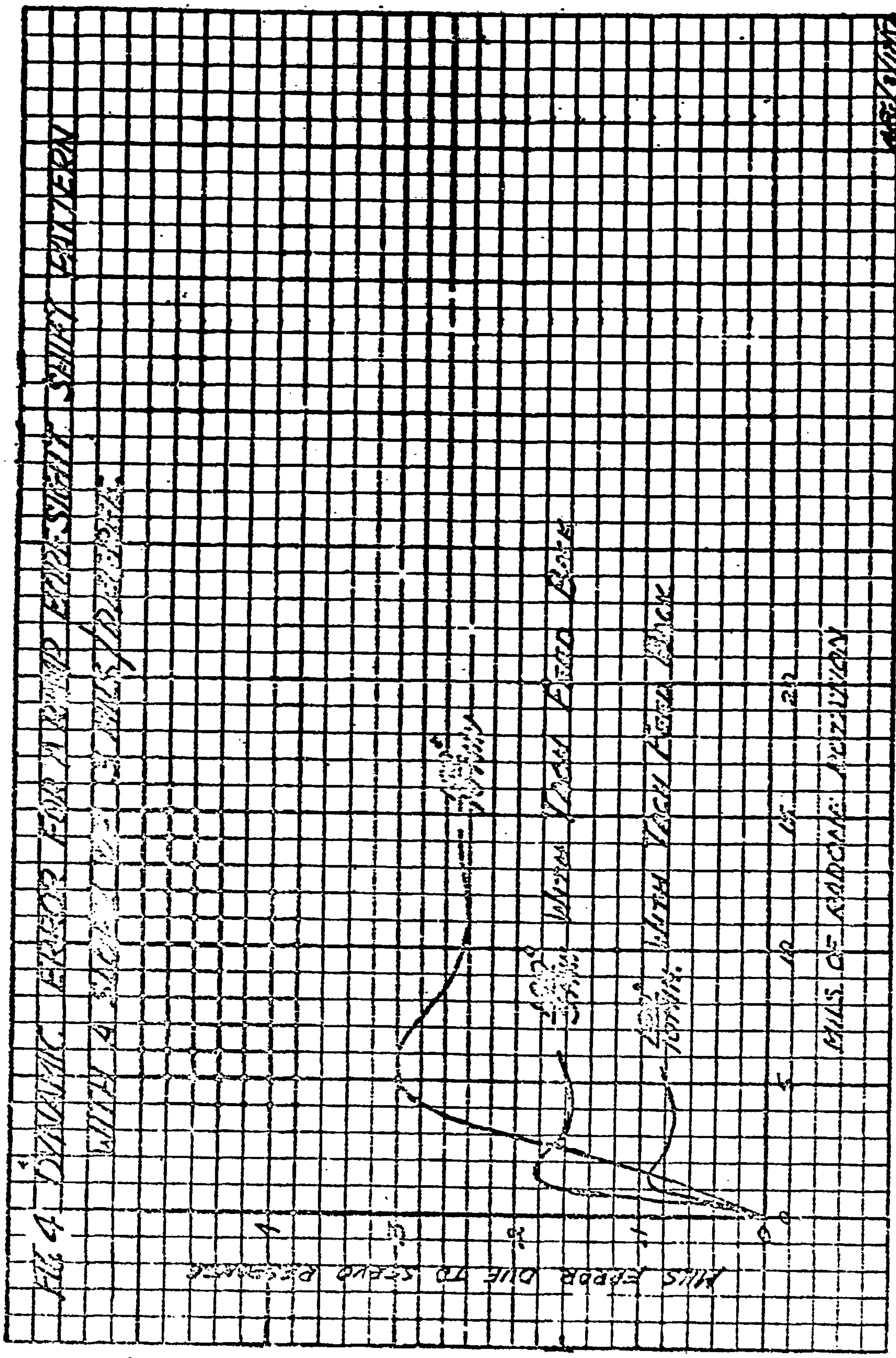

FIG 4 DYNAMIC ERROR
SIGHT SHIFT PATTERN
WITH A
WITH TACH FEED BACK
WITH TACH FEED BACK
0
5
10
15
20
1
.2
.3
MILS OF RADOME

30 April 1956

RADOME SURVEY

OFFICE OF NAVAL RESEARCH

1. Bjorksten Research Laboratories Nonr-1464(00)-analyses in connection with the optimum design of the metal screen radome (under investigation per NBSs-93247) ONR Project Engineer H. E. Sorrows

2. Hughes Aircraft Company Nonr-1466(00(- analysis of uniform, systematic and random radome deviation with the objective of establishing radome tolerances
ONR Project Engineer H. E. Sorrows

3. National Bureau of Standards NAonr-132-52 study of inorganic fluorosilicates in connection with radome materials requirements
ONR Project Engineer W. Arsem

4. Rutgers University Nonr-404(03) -development of ceramic materials and ceramic techniques for radome applications ONR Project Engineer W. Arsem

BUREAU OF AERONAUTICS

1. Emerson and Cuming, Inc. NOas 491-c - development of a low density (10-12lb/cuft) inorganic foamed-in-place structural material to withstand temperatures up to 900°F BuAer Project Engineer P.M. Goodwin

2. Forest Products Laboratory NAer 01683 - joint USAF-Navy program-development of crite ia for the more efficient design of reinforced plastic structures includin publication of ANC-17 Bulletin "Plastics for Aircraft - Part I Reinforced Plastics" June 1955 BuAer Project Engineer P.M. Goodwin

3. Imperial Glass Corporation NOas 55-213-c - development of a higher modulus (stiffer) glass fiber for use in reinforced plastics
BuAer Project Engineer P.M. Goodwin

4. Vitro Laboratories NOas 56-382-c - investigation of the feasibility of elect ro-phoretic deposition of uniformly thick bonded solids onto plastic radomes for rain erosion protection BuAer Project Engineer I. B. Galane

5. Westinghouse Electric Corporation NOas 51-884-c - development of KelF irdomes including an investigation of the effect on KelF properties of irradiation, high temperatures, and special fabrication techniques.
BuAer Project Engineer I. B. Galane

NAVAL AIR DEVELOPMENT CENTER

1. Bjorksten Research Laboratories NBSs-93247 - investigation of the applicability to radome design of metal screens to be embedded in the radome wall to minimize insertion phase and reflection and to maximize transmission efficiency
NADC Project Engineer J. Ambrogi, Jr.

2. Virginia Polytechnic Institute Department of Ceramic Engineering N00(62269)23378A - development of lightweight medium dielectric (4-6 range) foamed ceramic core with dense ceramic skins having the same dielectric and thermal expansion as the core (to utilize electrical superiority of half-wave wall construction and structural advantage of A sandwich)

NADC Project Engineer J. Ambrogi, Jr.

3. NADC current developments include

a. aerodynamic heating investigation
b. unity dielectric wall development
c. lightweight medium dielectric ceramic development
d. deicing systems
e. development of dielectric insert theory
f. near field instrumentation
g. materials for use at elevated temperature

NADC Project Engineer J. Ambrogi, Jr.

RADOME SURVEY

HUGHES AIRCRAFT COMPANY, CULVER CITY, CALIFORNIA
ANTENNA DEPARTMENT

A. **Current Research and Development Projects**

1. Design and development of radomes for use in missiles and interceptors.
2. Measurement of dielectric constant and loss tangent of dielectric materials at elevated temperatures.
3. Development of equipment for the measurement of insertion phase delay of dielectric walls.
4. Development of microwave antennas for use in missiles which require a radome as an integral part.
5. Theoretical and experimental investigations of the various types of obstacles which affect radome pointing errors.
6. Investigation of the various techniques of radome error prediction.
7. Study of the electromagnetic transmission characteristics of doubly curved dielectric walls.
8. Measurement of the near-field of antennas with and without radomes.
9. Investigation to compare the error produced by a radome when mounted in front of a monopulse type antenna and when the same radome is mounted in front of a conical scanning antenna.

B. Additional work is required on the following subjects:

1. Near-field measurement accuracy required for the prediction of radome pointing errors.
2. The accuracy of the presently known techniques of measuring near-fields.
3. The permissible electrical non-uniformity in a fabricated radome resulting in a so-called "uniform radome" as determined by measurements made on pointing error measuring facilities.
4. Investigation of the electromagnetic effect of the nose of a streamlined radome in producing radome pointing errors.

C. The chief investigators are:

D. E. Adler	V. Galindo	H. A. Schetne
J. S. Ajioka	F. T. Hata	C. B. Shaw, Jr.
M. Bar	H. R. Hope	G. I. Tsuda
C. B. Barker	V. J. Jenkins	B. L. Walsh
S. R. Boyd	S. Kaspin	L. W. Wilson
J. E. Fromn.	L. L. Philipson	J. Zorzy

PLASTICS DEPARTMENT

A. Current Research and Development Projects

1. Investigation of heat-resistant polymers, directed toward the development of materials capable of withstanding flight at high Mach numbers, including a study of the mechanisms of thermal degradation, the prevention of loss of strength at elevated temperatures, and the development of new and improved polymers for high temperature applications.

2. Development of radome materials of uniform and controlled dielectric constant, by the use of combinations of high dielectric constant fillers.

3. Investigation of alternate techniques and tooling for economical production of high quality radomes, particularly for interceptor aircraft.

4. Investigation of materials, configurations, protective devices, etc., for missile radomes to render them capable of flight at tactical velocities in rain and after prolonged exposure to adverse climatic conditions.

B. Suggestions for Future Programs

Investigation and development of dielectric materials adequate for use on missiles and aircraft at supersonic speeds. Some required characteristics are listed below:

1. Maintenance of dielectric constant within acceptable limits over the operating range of temperatures.

2. Mechanical strength at operating temperatures sufficient to withstand acceleration and aerodynamic loads.

3. Ability to withstand thermal shock caused by aerodynamic heating.

4. Resistance to rain erosion at tactical velocities.

C. The Chief Investigators are:

Dr. E. L. Armi, Head of Plastics Department
Mr. J. H. Beno, Assistant Head of Plastics Department
Mr. W. Crofut, Staff Consultant
Mr. M. D. Hudson, Head of Components Development Section
Mr. G. D. Robertson, Head of Materials Application Section
Mr. E. F. Smith, Head of Applied Physics Group
Mr. R. H. Vreeland, Head of Engineering Projects Group
Dr. R. A. Spurr, Senior Staff Chemist
Mr. J. B. Rust, Senior Staff Chemist